NORTHWESTERN UNIVERSITY

# The Kinesin-1 Motor Domain is Regulated by a Direct Interaction of its Head and Tail

A DISSERTATION

SUBMITTED TO THE GRADUATE SCHOOL
IN PARTIAL FULFILLMENT OF THE REQUIREMENTS

for the degree

DOCTOR OF PHILOSOPHY

Field of Cell and Molecular Biology
Integrated Graduate Program in the Life Sciences

By

Kristen Ann Dietrich

EVANSTON, ILLINOIS

December 2008

ABSTRACT

# The Kinesin-1 Motor Domain is Regulated by a Direct Interaction of its Head and Tail

Kristen A. Dietrich

Kinesin-1 is a motor protein that transports cargo along microtubules. Inside cells, the majority of kinesin-1 is regulated to conserve ATP and ensure its proper intracellular distribution and coordination with other motors. Regulated kinesin-1 is folded in half, and interactions between coiled-coil regions near the N-terminal enzymatically active heads and the C-terminal regulatory tails bring these globular elements in close proximity to stabilize the folded conformation. However, it has remained a mystery how the kinesin-1 tail inhibits ADP release and thus catalytic activity in this folded conformation.

To test whether the tail regulates the head by directly interacting with it, my collaborators and I performed photochemical cross-linking experiments on head and tail domains *in trans* and analyzed these results using mass spectrometry. These techniques provided the first evidence of a direct contact between the head and tail domain and allowed for mapping of the inhibitory interaction; the regulatory QIAKPIRP motif of the tail interacts with Switch I and the nucleotide pocket of the motor domain. Cryo-electron microscopy on a head-tail crosslink confirmed this finding and provided a possible mechanism for regulation, as Switch I was observed for the first time in an "open" position, a conformation with high ADP affinity. A new state for kinesin-1 was also seen, in which the tail simultaneously interacts with Switch I and the microtubule. In this state the motor is regulated through the interaction of the QIAKPIRP motif of the tail with

Switch I, but remains microtubule-bound through stabilizing interactions between the tail and tubulin. The physiological relevance of this state remains unknown.

Electron paramagnetic resonance and fluorescence assays were used to examine how the tail, specifically the K922 residue, inhibits ADP release. The tail-induced conformational restriction of the nucleotide pocket is distinct from the conformational changes caused by microtubule binding and occurs independent of the regulatory K922 residue. While the exact mechanism of inhibition could not be determined, structural and biochemical homology with G-proteins suggests that the tail may be acting in a manner similar to guanine nucleotide dissociation inhibitors; this mode of regulation may be a common feature among kinesin family members.

**Scientific Acknowledgements**

I would like to thank Chuck Sindelar for performing and analyzing the cryo-EM reconstruction; Christine Cremo and Paul Brewer for the MALDI mass spectrometry analysis and gracious gift of Mant-ADP; Nariman Naber and Roger Cooke for teaching me EPR and analyzing the spectra; Yao Wong for the fluorescence assays and preparing the EPR manuscript; Mark Seeger for helping with protein purification; and finally Sarah Rice, for guidance in data analysis and experimental procedures, teaching me so much about kinesin as well as biochemistry and cell biology and overall mentorship. She made me the scientist that I am today. Thank you.

This study was carried out with the financial support of a National Institutes of Health Training Grant in Molecular Biophysics.

**Acknowledgements**

Many people have made the work of this thesis possible. Throughout this project I learned invaluable lessons about perseverance, dedication, and importantly science. The achievements I have made would not have been without the help of so many important people in my life.

I would like to thank my parents, Steven and Marcia Dietrich, and my brothers, Jeff and Jon, who have been forever supportive of my education and career path, encouraging me to achieve my potential.

I would also like to thank my thesis advisor, Sarah Rice, one of the most enthusiastic scientists I have met, with a great love for what she does and a strong willpower to achieve it. As her first graduate student we both learned invaluable lessons, coming out better mentors, scientists, and people. I couldn't have asked for a better lab environment; discussions were enthusiastic, stimulating, and we had a lot of fun together. She has collected a wonderful group of people who do great science, and I wish them all the best of luck in their pursuits. I will never forget the weekends we had at her parent's house in Wisconsin (and I probably won't go waterskiing again either!). Thank you; you have made science not only rewarding, but also enjoyable. I have learned so much about science and life from you. Keep it up, we really appreciate and need it!

Doug Freymann and Pam Focia have been an important part of my time here at Northwestern. From day one, they have considered their students as family, and I am very grateful for that. They have always been people I could turn to, with rational, yet understanding advice. As faculty members they provided us with thought-provoking discussions, yet in a relaxed environment. Our small, yet intellectually and socially active group is a delight to get together with for science, or just beers. I look forward to Doug and Pam parties for years to come!

I would like to thank my collaborators, whom without their help and expertise this project would not have been possible. Chuck Sindelar, who graciously spent many hours analyzing cryo-EM images and providing his input on things, making this project his own. Christine Cremo, for performing and analyzing the mass spec data, even with the very unfortunate and frustrating labeling of C13, and also for the kind gift of Mant-ADP, making the fluorescence assays possible. And to Nariman Naber and Roger Cooke, who made me feel at home while performing EPR experiments at UCSF.

Thanks to my classmates, the Gelfand lab, and other members of the structure-function group, for providing a stimulating environment in which to do science, yet a great social outlet.

I would also like to thank the members of the Rice lab. Adam Larson, Kari Barlan, and Peggy McMahon who all made the lab run smoothly. Mark Seeger, who not only helped with many of the experiments, but also has a desire to learn what I have to say about kinesin and especially the tail. And I would like to thank Yao Wong, who gave me nothing but patience, understanding and adoration. He was my rock through all of this, providing a wonderful balance between work and play and opened my eyes to so many wonderful things. Thank you.

**Original Publications**

This thesis is based on the following articles:

Dietrich KA, Sindelar CV, Brewer PD, Downing KH, Cremo CR, Rice SE (2008) The kinesin-1 motor protein is regulated by a direct interaction of its head and tail. *Proc Natl Acad Sci U S A*. 105(26):8938-43.

Wong YL, Dietrich KA, Naber N, Cooke R, Rice SE. Kinesin's tail Restricts its ATP Pocket. Manuscript submitted, *Biophys J*.

TABLE OF CONTENTS

**Chapter IV**

LIST OF FIGURES

# Chapter I

## Introduction to kinesin-1 regulation

**Introduction**

Conventional kinesin is a microtubule-based molecular motor that is capable of fast processive movement toward the microtubule (MT) plus-end (1-4). Kinesin was first identified in 1985 as a cytosolic protein capable of *in vitro* MT-stimulated ATPase activity, and was shown to be responsible for the movement of vesicles along microtubules in squid axons (5). Kinesins participate in the directed transport of a wide variety of cargoes along the microtubule cytoskeleton, including neuronal vesicles, membranous organelles such as mitochondria, peroxisomes, and lysosomes, as well as protein complexes and mRNA (7). Kinesin family members also play a major role in cell division, including the formation of the bipolar mitotic spindle, and the transport and segregation of chromosomes. They have also been shown to regulate the structure of the microtubule cytoskeleton (8) and to modulate MT stability (9). Loss of function of many of the kinesin family members in humans and other organisms results in a variety of different diseases (10), and viruses have also been known to hijack the cytoskeletal transport systems (11).

Conventional kinesin (also known as kinesin-1 or KIF5, and hereafter referred to as kinesin) is the prototypical member of the kinesin superfamily. The human genome contains three genes for conventional kinesin, KIFs 5A, 5B, and 5C (12), which differ in their expression profiles and cargo binding regions (6). KIF5B is ubiquitously expressed and functions as a transporter for cargoes associated with the ER, mitochondria, Golgi complex, lysosomes, and endosomes (11). Our work focuses on the universally expressed KIF5B gene.

Kinesin anatomy

Native kinesin exists as a heterotetramer containing a homodimer of the kinesin heavy chain (KHC, α chain, 110-120 kDa) with two light chains (KLC, β chain, 60-70 kDa) bound to the C-terminal ends of the heavy chains. The kinesin heavy chain is relatively well conserved across the fungi and animal kingdoms, while light chains have only been found in animals. Thorough sequence analysis of kinesin superfamily members has revealed that all kinesin heavy chains share a homologous catalytic motor domain that both hydrolyzes ATP and binds to microtubules in a nucleotide-dependent manner. Beyond the motor domain, the sequences of kinesin family members diverge, resulting in motor proteins with different oligomerization, motile properities, and thus cellular function (16). Research on the kinetic and motile properties of kinesin has focused mainly on conventional kinesin, with the human and drosophila proteins as the model conventional kinesin family members for studying intra-molecular regulation.

The N-terminus of the kinesin heavy chain contains the highly conserved motor, or head domain of the molecule. This domain is roughly ~330 amino acids and is the catalytic core of the motor, containing both the ATP binding motif as well as the microtubule-binding interface. The three dimensional solution-state structure of the motor domain has been solved by x-ray crystallography (17-19), while cryo electron microscopy (cyro-EM) has captured the structure of the head while bound to microtubules (20-23). Following the catalytic core of the motor is the neck, consisting of the neck-linker region, a small 10 amino acid β-sheet that is the mechanical element, undergoing nucleotide-dependent conformational changes that are thought to drive kinesin motility and specify directionality (24-27), and the neck coiled-coil region. This short coiled-coil segment of ~40 amino acids is of relatively unknown function, but most likely confers dimerization of the head domains and therefore be involved in processivity of the motor.

Following the catalytic core is a long, rod-like extended coiled-coil stalk of ~560 amino acids and 60 nm in length (28). This stalk is broken into two coiled-coil segments by a flexible hinge, termed Hinge II. This hinge is thought to allow the heavy chain to fold over onto itself, as discussed below.

The C-terminus of the molecule consists of a roughly 150 amino acid tail domain that is essential for kinesin-1's function as an intracellular transporter. The tail domain is predicted to be globular in shape and is thought to be involved in two key processes for intracellular transport: cargo binding (29, 30) and self-inhibition. Cargo binding regions have been found on both the kinesin light chains and heavy chains, allowing for the attachment of cargo for directed transport along the microtubule cytoskeleton. Near the extreme C-terminus of the tail domain lies a short sequence conserved regulatory motif termed the IAK region (IAKP(L/I/V)RxG) (QIAKPIRP in human kinesin-1) (29). The ability of kinesin-1 to be auto-regulated by an element in its C-terminus is necessary for efficient and directed transport, yet the mechanism of tail-mediated regulation, and how this inhibition is turned on and off is not well understood.

Cell fractionation and immunolocalization studies have shown that a majority of kinesin found in cells is neither bound to microtubules nor to organelles, but is rather in a soluble cytoplasmic form (5, 31, 48, 49). The existence of a large cytoplasmic pool of kinesin-1 led to the idea that cells may have a mechanism that keeps kinesin in an inactive, non-microtubule-bound state until it is needed to transport cargo (50). This mechanism would prevent the futile movement of kinesin along microtubules, resulting in an economic use of cellular ATP and kinesin, as well as preventing the accumulation of kinesin at the plus ends of microtubules in the cell periphery, where it is unable to load cargo and transport it to its destination (31).

Inhibited kinesin exists in a folded conformation

Early work on native kinesin using electron microscopy discovered a novel characteristic of full-length kinesin. It was shown that the molecule could bend at a hinge-like region in the middle of the molecule, Hinge II, to produce a folded over conformation in which the N- and C-termini were close to each other. The ability to form this state was dependent on the ionic strength of the solution. Almost all molecules were folded over in low salt concentrations, while the ratio of extended molecules increased as the salt concentration rose (51-53). It was later shown using sucrose gradient centrifugation that kinesin was also able to undergo large conformational changes in solution as a function of ionic strength (50). This direct hydrodynamic evidence for a folded 9 S conformation at low ionic strength which can reversibly unfold to an extended 6 S form at high ionic strength (50) strongly agreed with what had been observed by electron microscopy. A majority of kinesin-1 is likely to be folded *in vivo*, as it was observed to be in the compact conformation at 150 mM potassium aspartate (50), a solution that mimics physiological salt concentrations. This folding is inherent to the heavy chains, as the light chains and eukaryotic modifications are not required (50, 54).

As further kinetic studies became available it was found that kinesin purified from natural sources had substantially lower MT-stimulated ATPase activity than truncated or partially proteolyzed protein (55). The ATPase rate of the native species is stimulated 1000-fold by the interaction with tubulin (37), and measurements on both the heterotetrameric and the homodimeric forms were consistent with each other, having low rates of microtubule-stimulated ATPase activity (56-57). Surprisingly, these rates were in striking contrast to the high MT-stimulated ATPase rates measured for truncated constructs (39, 58). It quickly became apparent that the ATPase rate of native kinesin was too slow to fully account for the observed *in vitro*

motility and the *in vivo* rates of organelle transport. Truncated kinesins, on the other hand, were in very good agreement with the expected kinetics. This allowed for the speculation that kinesin purified from natural sources was trapped in an inhibited state (36, 50, 56). The kinetic disparity combined with evidence from electron microscopy and sedimentation assays suggested a possible explanation for the difference between the observed behavior of full-length kinesin and that necessary to support intracellular motion. It was postulated that the tail of the kinesin heavy chain was in some way inhibiting the microtubule-stimulated ATPase activity of the motor. This inhibition was relieved when kinesin was absorbed onto glass surfaces or beads, which may mimic cargo binding, suggesting a means for the timely relief of tail-mediated inhibition *in vivo* (59).

If inhibition of ATPase activity was occurring through an interaction between the tail and motor domains, then it is expected that mutations that disrupt kinesins ability to fold would have ATPase rates comparable to tail-less constructs. Deletion of the flexible Hinge II does in fact eliminate the ability of kinesin to adopt the folded state, and restores microtubule-stimulated ATPase activity and single molecule motility to that of fully-active constructs (59-61). Importantly, the ability of the molecule to adopt a folded conformation has *in vivo* consequences, as the deletion of Hinge II also displays an unregulated phenotype in Neurospora in which kinesin is found accumulated at the hyphae tips (61). Thus, kinesin must contain this flexible Hinge II in the stalk region to be able to adopt the compact conformation, and loss of the ability to fold over results in a constitutively active molecule. However, despite the strong evidence that now pointed to an interaction between the N-terminal motor domain and the C-terminal tail domain that is formed in this folded state, little work was done on investigating whether an interaction between these two domains truly existed, as there was no direct evidence for an

interaction. Despite the evidence pointing towards the tail as a crucial means of regulation, the kinesin-1 field focused on mechanisms for tail-mediated inhibition that dealt with allosteric interactions involving the neck coiled-coil without the development of a working model for regulation, rather than examining the possible role of the tail itself in inhibition.

The observation that full-length kinesin has a substantially lower ATPase activity combined with the requirement of folding for inhibition, suggested to us that the inhibition of full-length kinesin is due to interaction of the heads with tail domains in the compact conformation. Truncation studies showed that formation of the compact state requires the C-terminal ~50 amino acids (54, 59). The interaction stabilizing the compact conformation was narrowed down to the head region from residue ~1-365, extending into the neck coiled-coil (Drosophila numbering) and the tail from amino acid 893-960. Mutational studies in Neurospora confirm the importance of the tail coiled-coil region of the C-terminus for folding (65). Conclusive evidence that the head domain and the C-terminal tail domain interact gave further support to the idea that either the tail itself or the formation of the compact conformation inhibited the ATPase activity of the motor.

The tail inhibits ADP release

Knowledge from the truncation studies above allowed for a direct comparison of the ATPase activities of the folded full-length molecule and an unfolded, minimally truncated motor (DKH894, residues 1-894 in drosophila) (54). The extended DKH894 was found to have similar microtubule-stimulated ATPase activities to that of shorter truncated head constructs, meaning that either the loss of the ability to fold or elements in the tail that were deleted are necessary for inhibition, while the kinetics of the full-length protein (DKH975) was at least 10-fold lower and

indicative of a motor with inhibited catalytic activity. It was also found that much of the previous observed ATPase activity of full-length kinesin was due to contamination with proteolysis products that can still fold, but retain full enzymatic activity, suggesting that regulation had more of an inhibitory effect than previously thought (62).

*Drosophila* constructs of more than 935 residues and equivalent human kinesin constructs are able to adopt a compact conformation (54). Both the full-length DKH975 and the slightly truncated DKH960 proteins were shown to be inhibited in their microtubule-stimulated ATPase activity, but further truncation into the conserved IAK-homology region to residue 945 in drosophila resulted in a motor that is no longer inhibited, but instead constitutively active, displaying kinetics more akin to fully active motors (62). These results imply that the ability to form the compact conformation is necessary, but not sufficient for inhibition of ATPase activity, and suggests that inhibition requires residues between 945 and 960.

The affinity of full-length DKH975 or the slightly truncated DKH960 for microtubules is too weak to detect saturation in ATPase conditions, so the direct measurement of $k_{cat}$ and $K_{0.5(MT)}$ of regulated motors was not possible. However, use of the apparent second-order rate constant, also known as the bimolecular ATPase rate constant, $k_{bi(ATPase)} \approx k_{cat}/K_{0.5(MT)}$, allows for a direct comparison of the kinetics between inhibited and active motors. Comparison of the regulated DKH960 to the apparent second-order rate constant of active kinesin constructs shows that the MT-stimulated ATPase activity of DKH960 is inhibited over ~130-fold (54). Further analysis by comparison of the rates of microtubule-stimulated ADP release upon initial productive association with the microtubule determined that the step in the ATPase cycle that was inhibited in DKH960 was the release of ADP (~80-fold) (62). The rate of ADP dissociation from the motor domain is the rate limiting step both in solution and while on microtubules (37, 43),

meaning that in the absence of microtubules Mg-ADP is trapped in each active site of kinesin with an off rate ($k_{off}$) of ~0.002 $s^{-1}$ (37). The kinetic evidence that this is the inhibited step in tail regulation is consistent with the tail's important role of regulating intracellular transport, as the most efficient step to inhibit is that that is rate limiting.

Consistent with the ability of the tail to inhibit the microtubule-stimulated ADP release activity of the motor, it was also shown to have an effect on motility. Single molecule fluorescence assays demonstrated that full-length kinesin had a 90-99% decrease in the frequency of motility events (59). Full-length kinesin was able to move processively once it became bound to a microtubule, but this movement was discontinuous with pauses and then bursts of unidirectional motion (59).

The ability of the tail to inhibit the motor domain's MT-stimulated ATPase activity was further confirmed recently using sets of short tail peptides (63). These experiments found that peptides containing the IAK sequence motif were able to significantly inhibit the microtubule-stimulated ATPase activity of the motor as well as reduce microtubule motility in a gliding assay. Although the Yonekura experiment (63) was able to show the inhibitory effect of the IAK region, in general, multiple attempts to titrate in tail fragments during microtubule-stimulated ATPase assays and motility assays have had limited success. The tail does seem to inhibit the ATPase and motility properties of tail-less kinesin constructs, but this inhibition is not complete (60-61, 63). Tail fragments have also been shown to bind strongly to microtubules (62), and it is thought that this is the major cause of the observed reduction of ATPase activity and motility, making the analysis of tail-mediated regulatory effects difficult.

Direct comparison of the kinetic parameters for inhibited versus active constructs indicated that tail mostly inhibits the microtubule-stimulated ADP release step in kinesins

enzymatic cycle. The effect of folding therefore appears to be inhibition of the initial productive association of the motor-ADP complex with the microtubule. This may either be from the inability of inhibited motor to release its bound ADP to form a productive kinesin-microtubule interaction, or it may be due to the direct blockage of microtubule binding. It appears that once the kinesin dimer is bound to the microtubule, it has only a mild 2-fold inhibition of processivity. Recent results have shown that the tail is also able to inhibit the basal release of bound ADP (64, 114), indicating that inhibition is most likely not through direct competition with microtubule binding.

The overlooked necessity of a Head-Tail interaction

It was widely accepted that the tail is playing a role in inhibiting the MT-stimulated ATPase activity of the motor, specifically by inhibiting both basal and microtubule-stimulated ADP release (62, 64). The mechanism by which the tail inhibited this step was unknown. It was also not known where the tail was interacting to exert its effect on the catalytic cycle. What was known was that the neck coiled-coil, as well as the residues in the tail coiled-coil N-terminal to the conserved IAK region must be present in order for kinesin in fold over on itself (59), however, additional residues C-terminal to this in the tail, specifically the region including the IAK motif are absolutely necessary for inhibition. Therefore, folding is required but not sufficient for regulation. The IAK region itself may be important for inhibition, as truncation in the middle of this region destroys regulation (DKH945) (54). Additionally, single and double point mutations to the IAK show an unregulated phenotype in Neurospora (61). However, the necessity for the IAK for inhibition could be due to either a role in the stabilization of the compact state, or this region could itself be acting in an inhibitory manner. The C-terminal ~15

residues are not absolutely required for inhibition, as DKH960 still retains full regulatory function (61-62). Yeast two-hybrid screens in Neurospora suggest that the neck coiled-coil is required for interaction with the tail (65); the neck coiled-coil has also been implicated in tail binding by other groups (54, 59). Together, these results suggest that an interaction between the neck coiled-coil and the tail coiled-coil region just N-terminal to the IAK (DKH927-937) mediate folding of the full-length molecule, but additional residues C-terminal to this in the tail are necessary for inhibition.

Although it is fairly well documented that an interaction between the neck coiled-coil and the tail coiled-coil occurs, it is likely that this interaction is not the cause of inhibition, but rather acts to stabilize the compact conformation so that additional interactions between the tail and motor can take place. Several lines of evidence exist for the necessity of additional interactions for inhibition. Extensive mutagenesis (66) and cross-linking experiments (67) have shown that the neck coiled-coil sequence in not critical for MT-stimulated ATPase activity. Additionally, as noted above, the ability to adopt the compact conformation is not sufficient for inhibition. Although the kinetic evidence appears to demand an additional direct interaction between the kinesin-1 tail and motor domain, no evidence for this interaction has been found, even in experiments using extensive mutagenesis and screening approaches (61, 65).

Four plausible mechanisms for tail-mediated inhibition existed: It was possible that an allosteric interaction involving the coiled-coil regions of the neck and tail resulted in retention of ADP, however as described above, the kinetic evidence seemed to instead demand a direct interaction between the head and QIAKPIRP motif of the tail. If there was a specific interaction between the head and tail, this interaction could directly act to stabilize bound ADP, or instead could allosterically affect nucleotide binding. Along with the allosteric interaction described

above, the tail could have interactions with the motor domain far from the nucleotide pocket that cause conformational changes that are translated by the protein into stabilization of ADP. Thirdly, the tail could be directly competing with microtubule binding, however the recently found ability of the tail to inhibit basal ADP release in the absence of microtubules suggests otherwise. Lastly, the tail instead could be acting to directly stabilize bound ADP.

Surprisingly, given the importance of kinesin-1 regulation in the cell, little work had been accomplished on identifying how the tail inhibited the motor domain. Despite the fact that to us the data required a direct interaction between the two domains, it was not an accepted belief in the field as there was no direct evidence for this interaction; very little was known and few groups were working on the problem. While the lack of knowledge most likely stemmed from difficulties working with the full-length protein (described in Appendix I), we were able to make a major breakthrough using biochemical and biophysical techniques on head and tail domains *in trans*.

The present work: Finding the elusive direct interaction between the head and tail; How does the tail inhibit ADP release from the motor domain?

Progress in the kinesin field has allowed us to gain a better picture of how kinesin-1 is self-regulated, however much remained to be accomplished, as nothing was previously understood about how the tail was acting to inhibit the motor domains activity. As regulation of the plus-end directed motor is essential for proper intracellular transport, understanding the mechanism of auto-regulation would provide a more complete view of the intricate workings within the cell and allow for perturbation of the system.

Multiple lines of evidence led us to believe that kinesin-1 was regulated through a direct interaction between the head and tail domains, however there was no evidence of this interaction. Kinetic evidence had shown that full-length kinesin is inhibited in its microtubule-stimulated ATPase activity compared to truncated or tail-less constructs. Hydrodynamic studies and electron microscopy revealed that the kinesin-1 heavy chain underwent conformational changes that were dependent on the ionic strength of the solution, and intriguingly, adopted a folded conformation in which the N- and C-termini of the motor are in close proximity at physiological salt concentrations. These pieces of data suggested that the tail domain of the kinesin heavy chain is able to inhibit the catalytic activity of the motor domain and that this regulation may have physiological consequences. These data, together with the notion that a majority of kinesin in cells is in a soluble form and not microtubule-bound, indicated that the kinesin motor protein was able to self-regulate itself by an interaction between the head and tail domain. This interaction would prevent the futile consumption of ATP, as well as strategically place the motor where it is most valuable, in the interior of the cell, where it can pick-up and transport cargo towards the cell periphery in conjunction with other molecular motor proteins. Later mutagenesis work found that the enzymatic inhibition of the motor is dependent on the molecule's ability to adopt the compact conformation, and mutagenesis and genetic screens were able to identify an interaction between the neck coiled-coil and the tail coiled-coil that stabilizes this state. Inhibition is unlikely to be due to the interaction between the coiled-coil regions of the neck and tail domain, as either mutation, stabilization, or deletion of the neck coiled-coil have no effect on the enzymatic activity of isolated motor domains. Biochemical assays have shown that the tail inhibits both the intrinsic and microtubule-stimulated release of ADP from the motor domain. The tail has also been shown to inhibit microtubule binding, most likely by locking the

kinesin head in an ADP-bound state that has a low affinity for microtubules. Importantly, it was found recently that this inhibition could be recapitulated with the use of tail peptides containing the conserved IAK sequence motif.

Many of the details of tail-mediated inhibition are unknown, including the inhibitory interactions and mechanism by which it occurs. Although the kinetic data seem to necessitate an additional interaction between the head and tail domains of kinesin to account for the inhibitory ability of the tail, no direct evidence for this interaction has been found. We sought to elucidate the mechanism by which the tail domain inhibits the motor domain's activity, specifically, to find a direct interaction between the kinesin-1 head and tail, and to use this information to better understand how the IAK motif is able to hold kinesin-1 in an inactive ADP-bound state. This would be the first data for a direct interaction between the head and tail domain. We have approached the question of tail regulation using several techniques, including photochemical cross-linking, mass spectrometry, cryo-EM microscopy, EPR spectroscopy, and fluorescence assays in order to gain structural information on the inhibitory interaction between the head and tail domain. These techniques not only allowed us to produce the first evidence for a direct interaction between the head and tail domains, but also allowed us to map the interaction surface between these two domains. Our findings that the regulatory portion of the tail interacts with Switch I of the motor domain not only imply a mechanism for the tail's action, but the combination of the cross-linking mapping and cryo-EM reconstruction suggest another state for kinesin that may be possible in the cell, a conformation in which the kinesin-1 head is microtubule-bound, however the tail both inhibits the enzymatic activity of the motor by retaining ADP in the nucleotide pocket and further stabilizes the interaction between the weakly-bound head and the microtubule by additionally interacting with tubulin. These results allowed

us to design further experiments in an attempt to get at the exact mechanism of tail inhibition, as well as have spawned additional thesis proposals. Interestingly, this mode of kinesin regulation is strongly reminiscent to how the G-protein superfamily is regulated, suggesting that this inhibitory mechanism may be applicable to other kinesin family members as well. Experiments testing this hypothesis have been attempted with the kinesin-2 family member OSM-3.

# Chapter II

## The Kinesin-1 Motor Domain is Regulated by a Direct Interaction of its Head and Tail

**Foreword**

Kinesin-1 is a molecular motor protein that transports cargo along microtubules. Inside cells, the vast majority of kinesin-1 is regulated to conserve ATP and to ensure its proper intracellular distribution and coordination with other molecular motors. This regulation has also been shown to occur *in vitro*. Regulated kinesin-1 folds in half at the flexible hinge II region in its coiled-coil stalk. Interactions between coiled-coil regions near the enzymatically active heads at the N-terminus and the regulatory tails at the C terminus bring these globular elements in close proximity and stabilize the folded conformation. However, it has remained a mystery how kinesin-1's microtubule-stimulated ATPase activity is regulated in this folded conformation. We proposed that the observed neck coiled-coil- tail coiled-coil interaction is a stabilizing interaction that allows for a direct inhibitory interaction between the motor domain and the QIAKPIRP regulatory sequence motif in the tail to occur. In this chapter I present the first evidence for a direct interaction between the kinesin-1 head and tail. To achieve this we photochemically cross-linked heads and tails *in trans*, analyzed the products by mass spectrometry, and produced an 8-Å cryo-EM reconstruction of the cross-linked head–tail complex on microtubules. These data demonstrate that a conserved essential regulatory element in the kinesin-1 tail interacts directly and specifically with the enzymatically critical Switch I region of the head. This interaction suggests a mechanism for tail-mediated regulation of the ATPase activity of kinesin-1. Interestingly, in our structure, the tail makes simultaneous contacts with the kinesin-1 head and the microtubule, suggesting the tail may both regulate kinesin-1 in solution and hold it in a paused state with high ADP affinity on microtubules. The interaction of the Switch I region of the kinesin-1 head with the tail is strikingly similar to the interactions of small GTPases with their regulators, indicating that other kinesin motors may share similar regulatory mechanisms.

The mechanism of the tails action and prospects for similar regulatory interactions in other kinesin family members is further investigated in Chapter III and Appendix II of this thesis. In this chapter I will provide the background data that led us to propose that the known interaction between the coiled-coil regions of the neck and tail is not inhibitory, instead occurring to stabilize a direct inhibitory interaction between the motor and tail domains. In Section I, I discuss the experimental rationale behind the project, while Section II contains the material and methods. The experimental results are examined in Section III. The work done on this project resulted in publication in the Proceedings of the National Academy of Sciences (PNAS), 2008 Jul 1;105(26):8938-43. The published PNAS manuscript and supplemental information available online for this publication comprise Section IV.

## Section I: Introduction and Experimental Design

### Introduction

The motor protein kinesin-1 uses energy from ATP hydrolysis to move intracellular cargo from the interior of the cell towards the microtubule plus end, usually located towards the cell periphery. Kinesin-1 is either regulated or activated for cargo movement in response to various cues, ensuring its proper localization within the cell, preventing futile consumption of ATP, and facilitating cargo transport to the right destination. The mechanism by which active kinesin-1 converts ATP hydrolysis into movement is fairly well established, as much work has been done using isolated motor domains that are fully active. However, little is known about how full-length kinesin-1 is regulated when it is not needed for cargo transport.

Regulated kinesin-1 heavy chain adopts a folded conformation in which it remains very tightly bound to ADP and does not bind strongly to microtubules (33, 62). This folding can

occur in the absence of kinesin light chains, although the light chains confer additional regulatory function that will not be discussed here (31, 33). Regulation of the full-length protein has been shown to require a flexible Hinge II region within the long coiled-coiled stalk of the molecule, where it is thought that the molecule can fold over onto itself, resulting in a compact conformation that has been seen both hydrodynamically using sucrose gradient centrifugation and by rotary shadowing EM. In this folded conformation an interaction occurs between the neck coiled-coil and the tail coiled-coil (54, 59, 65). This interaction stabilizes the compact conformation and positions the C-terminal globular tail domain near the N-terminal enzymatically active heads (Figure 1) (50, 51).

Kinetic data on tail-mediated regulation have shown that the folded conformation of kinesin-1 is not strictly necessary, nor is it sufficient for inhibition of ADP release by the heads. Furthermore, the neck coiled-coil region seems to play no role in the motor's catalytic activity. Isolated motor domains truncated before the neck coiled-coil (K349 for example) retain full enzymatic activity except for processivity, which is lost due to the lack of dimerization of the motor domains without this neck coiled-coil. Additionally, mutation or replacement of the neck coiled-coil in longer constructs seems to have no effect on the motor's activity. These data suggest that the known interaction between the neck coiled-coil and the tail coiled-coil is not inhibitory.

Importantly, it is also known that short deletions from the C-terminus of the protein do not affect the motor's regulation; however if more than about thirty amino acids are removed the molecule loses its inhibitory properties even when folding into the compact conformation is not compromised. The regulation of the motor domain's enzymatic activity has been shown to require a sequence conserved QIAKPIRP regulatory motif found in the extreme C-terminus of

the tail domain (residues 919–926 in human kinesin-1). This conserved QIAKPIRP sequence in the C-terminal globular portion of the tail is not required for kinesin-1 to fold, but deletion or mutation of this sequence abolishes regulation both *in vitro* and *in vivo* (33, 61, 62). These motors are no longer inhibited in their microtubule-stimulated ATPase activity in *in vitro* kinetic assays, and *in vivo* in Neurospora are found accumulated at the microtubule plus end rather than diffuse throughout the cytoplasm (61). The QIAKPIRP sequence specifically inhibits kinesin-1's initial microtubule-stimulated ADP release step, when it first engages on the microtubule (62). Specifically, the tail has been shown to inhibit both the basal and microtubule-stimulated release of bound ADP (64). Short peptides containing the QIAKPIRP sequence but lacking any tail coiled-coil elements have also been shown to inhibit ADP release by truncated kinesin-1 heads (63). Oddly enough, a direct head–tail interaction has never been identified for kinesin-1, even in experiments using extensive mutagenesis and screening approaches, despite the fact that the kinetic data appear to demand it (61, 65).

Together, the known data suggests that the interaction between the neck coiled-coil and tail coiled-coil elements is not in itself inhibitory, but instead could provide structural support for a relatively weak but direct head–tail interaction involving the critical QIAKPIRP sequence. The proposed direct head–tail interaction would then perform the critical regulatory function of preventing microtubule-stimulated ADP release and subsequent movement by kinesin-1. The goal of our work was to detect and identify this unknown direct interaction between the kinesin-1 motor and tail domains.

The QIAKPIRP sequence of the tail inhibits kinesin-1's initial microtubule-stimulated ADP release step, while a region of the tail roughly 15 residues N-terminal to this sequence binds to microtubules (54, 62). If these two activities occurred simultaneously, kinesin-1 could

pause in a state that is tightly bound to microtubules but inhibited in its ATPase activity and thus movement. Consistent with this idea, pauses have been observed in processive runs by single molecules of full-length but not truncated kinesin-1 (59). While regulation primarily prevents the heads from productively engaging with microtubules, it is intriguing to suggest that a second regulatory mechanism of the kinesin-1 tail may affect its movement on microtubules by enabling it to pause its enzymatic activity but remain microtubule-bound.

In this Chapter I will show that a direct interaction occurs between the inhibitory QIAKPIRP sequence of the tail domain and the Switch I region in the head of kinesin-1 (residues 190–205). For kinesin motors and for small GTPases, Switch I plays a critical role in nucleotide binding and/or release (21, 68, 69, 70). Thus, a Switch I–tail interaction is consistent with the known kinetic mechanism of tail-mediated regulation (62) and is analogous to the mechanisms by which GDP dissociation inhibitor proteins (GDIs) inhibit small GTPases (63, 71). The mechanism of tail-mediated inhibition is further examined in Chapter III of this thesis. Additionally, our results also show that the tail can, at least in principle, bind to the heads and microtubule at the same time. This may create a parked state for kinesin-1 on microtubules that can be modulated by other factors for additional regulation of the motors activity. Future experiments will be necessary to test this hypothesis.

**Figure 1. Description of kinesin-1 regulation**

Head residues of the kinesin-1 heavy chain are colored cyan, coiled-coil residues gray, and predicted globular tail residues are orange (73). The kinesin-1 light chains and/or the light chain-binding region of the heavy chain are shown in green.

A. Model of active kinesin-1 carrying cargo along a microtubule and regulated kinesin-1 in solution.

B. Model of kinesin-1 heavy chain showing regions of head, stalk, and tail involved in tail-mediated regulation. The monomeric K349 and dimeric K420 constructs are truncated as indicated. The K349 fragment does not contain significant portions of the neck coiled-coil interacting region. The 6x-histidine tail constructs Tail 823-963 and Tail 823-944 contain the tail coiled-coil interacting region as well as the regulatory QIAKPIRP sequence motif. The 27-mer tail peptide contains only the QIAKPIRP motif. See Figure 2A for further details on the constructs used.

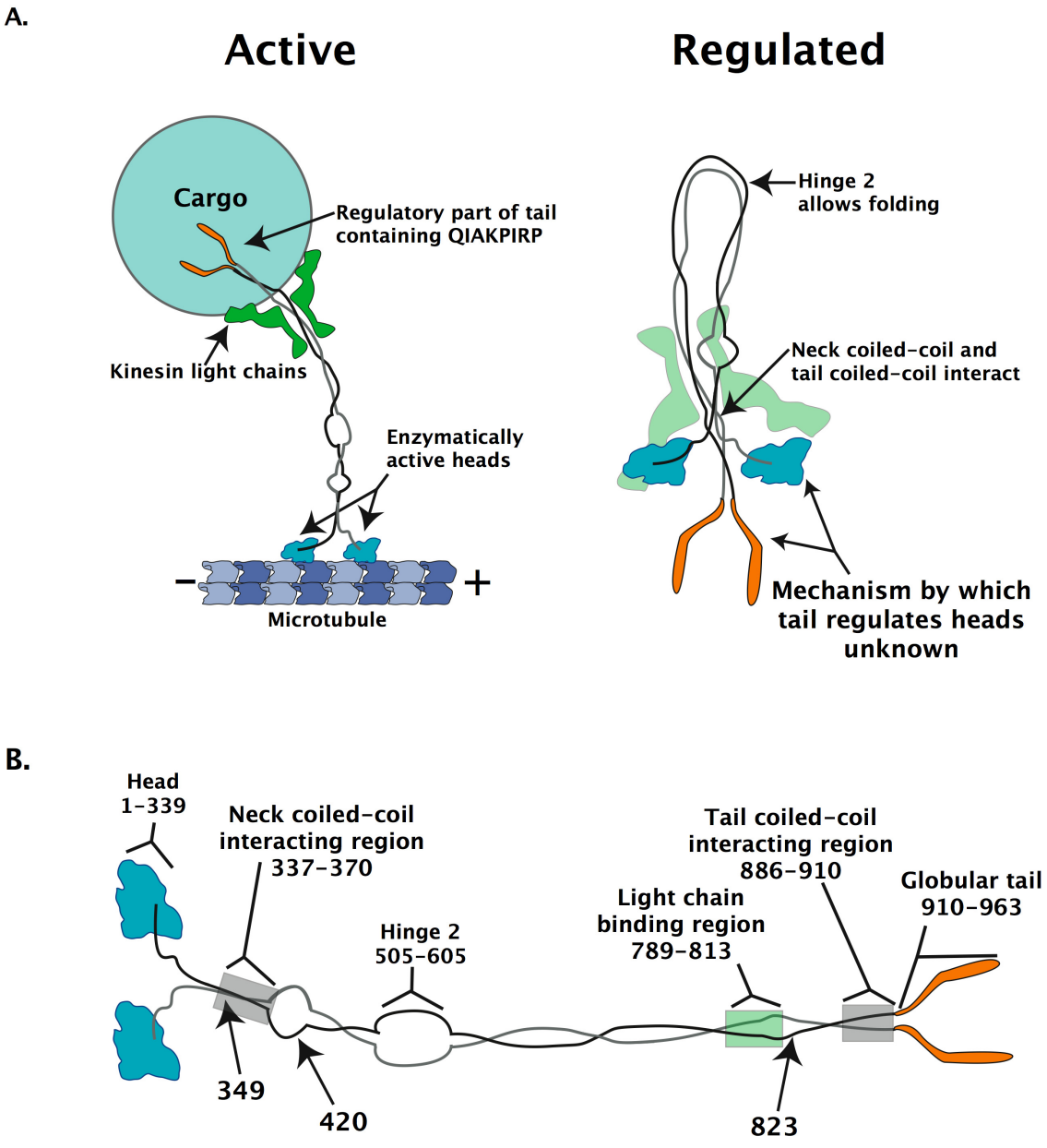
A.
Active
Regulated
Cargo
Regulatory part of tail
containing QIAKPIRP
Kinesin light chains
Enzymatically
active heads
Microtubule
Hinge 2
allows folding
Neck coiled-coil and
tail coiled-coil interact
Mechanism by which
tail regulates heads
unknown
B.
Head
1-339
Neck coiled-coil
interacting region
337-370
Hinge 2
505-605
Light chain
binding region
789-813
Tail coiled-coil
interacting region
886-910
Globular tail
910-963
349
420
823

Experimental Design

In an effort to address the mechanism of kinesin-1 regulation we sought to use kinesin-1 head and tail constructs *in trans*, as we had previously tried using full-length protein but were unable to achieve the amount of purified full-length protein necessary to perform biochemical assays to test enzymatic inhibition (detailed in Appendix I). Our experimental plan was to crosslink separate head and tail domains together in order to determine how they are interacting (see Figure 2A for constructs). The experiments center on the use of a heterobifunctional photoactivatable crosslinker benzophenone-4-maleimide (B4M, Invitrogen Corporation, Carlsbad, CA). The maleimide moiety of the crosslinker specifically labels reactive cysteines and was attached site-specifically to the motor domain on a single engineered cysteine residue added back to a motor domain that has had all of its surface cysteines removed (cysteine-light mutant, or CLM). Labeled head and separately expressed tail proteins were mixed together under conditions that have been determined to promote their association. The sample was then irradiated with short wavelength UV light to activate the benzophenone moiety of the crosslinker. Upon photoactivation, this group reacts with nucleophiles or creates C-H bond insertion products within proteins. If the tail protein was interacting with the motor domain within the 9 Å reach of where the B4M crosslinker is attached, the head and tail will be covalently cross-linked together (experimental scheme outlined in Figure 2B). The success of this reaction was analyzed simply by Coomassie staining of SDS-PAGE gels, looking for the emergence of a band on the gel of the apparent molecular weight of the head protein + tail protein. Upon a successful cross-link, the product can be further analyzed using mass spectrometry to determine which region of the tail protein is interacting with the motor domain in the near vicinity of the attached B4M. The data from several successful head mutants will

allow us to map the head-tail interaction surface, possibly allowing for a proposed mechanism of tail-mediated inhibition of the kinesin-1 motor domain.

In order to carry out the experiments as planned we first created and purified separate head and tail constructs. The head constructs contain single cysteine add-backs at locations we thought may be involved in a head-tail interaction, while the tail constructs contain the conserved QIAKPIRP regulatory motif. After the protein preparation, conditions in which the head and tail domains associate together were determined, as association is necessary for efficient crosslinking. Next, efficient labeling conditions were found in which the single cysteine add-backs on the motor domain reacted with the benzophenone-4-maleimide crosslinker. After labeling, head and tail proteins were then dialyzed into conditions in which they were found to associate, and crosslinking was initiated using UV light. After irradiation cross-linking samples were analyzed using Coomassie-stained SDS-PAGE gels. A negative crosslinking result implied that the tail is not interacting with the head in the region assayed, however before this conclusion could be reached it first had to be shown that the particular cysteine was efficiently labeled with B4M.

It seemed logical to start our project using head constructs that were readily available to us in the lab. These single cysteine add-backs were located in varying regions of the motor domain and had already been shown to label well using maleimide groups (72). Once a specific cross-link between the head and tail domains was found, we could then design further cysteine add-backs to map the interaction surface. Several successful cross-linking reactions between the head and tail allowed us to map the interaction surface between the proteins using mass spectrometry.

To further examine the head-tail interaction we performed cryo-Electron Microscopy (cryo-EM) on a head-tail cross-link bound to microtubules in order to get a structural view of inhibition. Cryo-EM of kinesin heads bound to microtubules is a technique widely used in the field that would allow us to get a low to medium resolution of our protein complex due to symmetry imposed on the system by microtubule binding. In order to use this technique we first had to work around a very important problem. Kinesin-1 motor domains do not bind well to microtubules when ADP is bound in their nucleotide pocket. Upon a successful encounter with a microtubule filament, ADP is released from the nucleotide pocket, resulting in a nucleotide-free motor that has a high affinity for microtubules. The affinity is also high when AMPPNP, a triphosphate analog, is bound to the motor. The tail domain has been shown to inhibit this first microtubule-stimulated ADP release step, resulting in a motor that remains bound to ADP with low microtubule affinity. It would therefore be quite difficult to achieve sufficient decoration of a head-tail complex on microtubules, as the head would remain in a state with low microtubule affinity. To solve this problem we turned to a Switch II mutant, G234A, in which microtubule binding and the nature of the bound nucleotide are uncoupled. This mutant binds tightly to microtubules and ADP at the same time, thus potentially allowing us to bind our head-tail cross-linked product to microtubules. We therefore took advantage of this mutation and technique and sent our cross-linked protein to Dr. Charles V. Sindelar at Lawrence Berkeley National Labs in order to get a structural view of our head-tail complex.

Below I detail the constructs and the methods used throughout this project. Overall, this technique turned out to be a large success for us. Not only were we able to get the first evidence for a direct head-tail contact, but also we were able to map the regulatory QIAKPIRP portion of the tail domain interacting with the Switch I region of the motor domain. A Switch I–tail

interaction is consistent with the known kinetic mechanism of tail-mediated regulation (62) and is strikingly similar to the mechanisms by which GDP dissociation inhibitor proteins (GDIs) inhibit small GTPases. These data indicate that kinesin-1 and G-proteins may share more than just structural similarity, as they may be regulated by similar mechanisms. These data also bring to question whether other kinesin motors may share similar regulatory mechanisms as that found for kinesin-1. The work on this project was followed by further investigation on these two topics, discussed in Chapter III and Appendix II, respectively.

## Section II: Materials and Methods

### A. Constructs

#### Head and Tail Constructs & Purification in Brief

Successful head constructs that produced specific cross-links to the tail domain used in the cross-linking portion of this project were dimeric K420CLM with single cysteine residues added back at residues S188C, A193C, and M197C. The monomeric K349CLM with a G234A mutation and single cysteine add-back at S188C were used for cryo-EM. These constructs are described in further detail below. Upon protein expression using the Novagen Overnight Express Autoinduction media (Novagen (EMB Chemicals, Merck KgaA), Darmstadt, Germany) soluble protein was purified essentially as previously described (79). Briefly, protein was bound to Whatman P11 phosphocellulose resin and eluted with increasing ionic strength. Following dilution to decrease the salt concentration, the protein was run over a ReSource 15S cation exchange column, with kinesin remaining in the flow-through. After an overnight dialysis step and pH change if a K349 construct was being purified, the protein was bound to a ReSource 15Q anion exchange column and eluted with increasing salt. Upon pooling, the purified protein was

given a hard spin at 100,000 x g for 10 minutes and frozen as a 20% (w/v) sucrose solution in liquid nitrogen. A variety of head constructs as well as the construction of single cysteine add-backs and a more detailed purification scheme are outlined more thoroughly below.

Tail constructs used for this project are described in more detail below under the tail constructs heading. Briefly, the longest tail construct encodes for residues 823-963 of the human kinesin-1 tail domain, referred to as Tail 823-963. A slightly shorter construct containing residues 823-944 (Tail 823-944) that still retains regulatory activity was also used. These two constructs were engineered with a N-terminal 6x-histidine tag for purification purposes. A 27-mer tail peptide of residues 901-927 was purchased from GenScript (Piscataway, NJ). This short peptide contains the conserved regulatory QIAKPIRP motif of the tail. After overnight expression at 24°C, soluble tail protein was then purified using Talon resin (Clontech, Mountain View, CA). A more detailed purification protocol is below, but briefly the purification was performed following the manufacturers guidelines, eluting with 500 mM Imidazole, however, I found that reducing the salt concentration to 300 mM NaCl before elution was key in maintaining protein solubility. After elution, 20% (w/v) sucrose was added and the protein was subject to a high speed spin at 100,000 x g for 10 minutes to remove any precipitation and frozen in liquid nitrogen.

Head constructs: Mutants and Purification

The kinesin-1 motor domain, also referred to as the head, has been extensively worked with in many labs. Our lab had a variety of human kinesin-1 head constructs to start this project with. In addition to the wild-type monomeric K349 (containing residues 1-349) and dimeric K420 (residues 1-420) (Figure 2A), we also had cysteine-light versions of these proteins, created

by Sarah Rice and given to us from the laboratory of Ron Vale at UCSF, for discerning the movement of the kinesin-1 neck linker region. All of the surface cysteines, as determined using the crystal structure of the motor domain (PDB 1mkj or 1bg2), have been mutated to either serine or alanine depending on their environment. This background allows for site-specific labeling of the motor domain by adding back a single cysteine residue at ones desired location using site-directed mutagenesis. Sarah Rice had created and successfully labeled a number of these mutants in her work, including E103C, S149C, S188C, T328C, C330 (natural cysteine), V333C, and E349C (see Figure 5A, 5C, 7A for some mutant locations). E103C is located in the loop 5 region of the motor domain. This structurally conserved loop is located 11 Å from the nucleotide pocket of kinesin, and is the binding site for monastrol, a potent inhibitor of the mitotic kinesin Eg5. Interestingly, monastrol inhibits the same enzymatic step in Eg5 as the tail does in kinesin-1. S188C is located near the nucleotide pocket at the end of the negatively charged alpha 3 helix. Located in the structural element immediately following this residue is Switch I, a conserved element within the G protein, myosin, and kinesin superfamilies that is intimately involved in nucleotide binding and release. T328C, C330, V333C, and E349C are located within the neck linker region of the motor domain that undergoes conformational changes dependent on the identity of the bound nucleotide.

These mutants were in three separate regions of the protein where an interaction with the tail seemed plausible: the L5 loop analogous to the monastrol binding site, the Switch I region, and the neck linker region. These available mutants thus provided a starting point for determining where on the motor domain the tail was interacting. Their use to start probing the location of the interaction greatly cut down on the amount of cloning initially required. If we were able to verify a specific cross-link in the crosslinking reaction by the emergence of a sharp

band on a Coomassie-stained gel at the appropriate molecular weight for a head + tail complex, we could focus our efforts by making additional mutants to verify and map the interaction, but in the beginning we took advantage of the constructs we already had available to us.

Once we had identified a successful and specific crosslink between the tail and the head domain with a single cysteine residue added back at position S188C (discussed below) we created additional mutants within the cysteine-light background to map the interaction surface. Mutants were created using the Quikchange II site-directed mutagenesis kit (Stratagene, La Jolla, CA) and all constructs were verified by DNA sequencing. These included D181C, located on the bottom of the alpha 3 helix, on the opposite end as S188C, and residues A193C, M197C, and N198C, which are located within the Switch I region (Figure 5A). Additional mutations made for this project, but not tested included L99C, Q113C, I119C, M180C, N255C, and K341C.

In addition to the single cysteine add-backs we also created a G234A mutant in the K349CLM S188C background. G234 is involved in the γ-phosphate sensing mechanism of the protein. Mutation of this residue to alanine results in a catalytically incompetent motor that uncouples microtubule binding from the identity of the bound nucleotide. This G234A mutation thus allows the motor to bind strongly to microtubules while ADP-bound. This mutant was then used in microtubule-binding experiments involving cross-linking, as well as necessary in order to obtain the cryo-EM reconstruction of the head-tail cross-linked complex.

Head constructs were expressed and purified without the use of affinity tags using our labs established protocols, although some modifications were made to increase the yield and purity of the protein. All mutants expressed and purified as expected, except for the E103C mutant, which was far less stable than other cysteines in previous studies (72). This protein does

not remain soluble during the overnight dialysis step and the protein therefore requires the purification to be performed as quickly as possible. This was not performed for this project, however would be possible if desired. The purification scheme for the remaining head constructs are as follows: BL21-CodonPlus (DE3)-RP competent cells (Stratagene, La Jolla, CA) were transformed and allowed to grow at 37°C on carb/chlor plates. Our initial expression conditions were to inoculate 2L of TPM media with an overnight culture and allow the cells to grow at 37°C until the optical density reached between 0.6 and 1.0. Cells were then transferred to a 4°C refrigerated shaker to cool for 30 minutes. Expression of protein was induced by adding 200 μM IPTG and allowing cells to shake at 20°C overnight. However, I found that head constructs expressed well using Novagen's Overnight Express AutoInduction media (Novagen (EMB Chemicals, Merck KGaA, Darmstadt, Germany)), allowing for a high yield of soluble protein with minimal work. 500 ml of autoinduction media in Thompson flasks were inoculated with 10-15 colonies of transformed cells. Cells were shaken at 37°C, 400 rpm for 24 hours before harvesting. The autoinduction media works by limiting the carbon sources available to the growing cells. Once the cells use the other available carbon sources found in the media, they resort to using lactose, inducing the expression of protein with continued cell growth at high density.

Following expression cells are pelleted and resuspended in Head Lysis Buffer containing 25 mM Hepes pH 6.8, 100 mM NaCl, 2 mM $MgCl_2$, 1 mM EGTA, 0.02% Tween-20, 1 mM DTT, and 40 μM ADP or ATP supplemented with protease inhibitors (500 μM PMSF (phenylmethylsulphonyl fluoride), 1 μM E-64 (trans-Epoxysuccinyl-L-Leucylamido-(4-Guanidino) Butane), 10 μg/ml Leupeptin, and 1 μg/ml each of Pepstatin A and Aprotinin). Upon freezing in liquid nitrogen, cell pellets were thawed and lysed with a French Pressure Cell.

Lysate was spun at 33,100 rpm for 35 minutes in the Ti 50.2 rotor (Beckman Coulter, Inc., Fullerton, CA) to clear cellular debris. K349 and K420 constructs behave identically in the purification scheme except for the last step in the purification, an anion exchange column, in which there is a pH change for K349.

The high speed supernatant is first loaded onto a 30-ml phosphocellulose (PC) (P11 Resin, Whatman Inc. (GE Healthcare), Florham Park, NJ) column equilibrated in Head Lysis Buffer. Nonspecific binding was reduced by washing the column at this salt concentration until the absorbance at 280 nm decreased to baseline. Bound protein was eluted with a 100-700 mM NaCl linear gradient, in which kinesin-1 elutes at roughly 350-400 mM NaCl. Fractions containing protein, as measured by reaction with Bradford reagent, are pooled together and the sample is diluted with PC Buffer A until the conductivity is equal to 150 mM NaCl. Protein is then run over a 20 ml ReSource 15S column (Amersham Biosciences (GE Healthcare), Piscataway, NJ) equilibrated in PC Buffer A + 150 mM NaCl. Kinesin-1 constructs do not stick to this column under these conditions; therefore the column flow through is collected. Protein is then dialyzed overnight into Q Buffer A + 80 mM NaCl. The Q buffer for K420 constructs is identical to the PC buffer, however for K349 constructs the pH is raised to 8.0. After dialysis, the pH of the K349 constructs were adjusted as necessary, and protein was loaded onto a ReSource 15Q anion exchange column (Amersham Biosciences (GE Healthcare), Piscataway, NJ) equilibrated in 80 mM NaCl at the appropriate pH. The column is washed to remove unbound protein, and kinesin-1 is eluted using an 80-800 mM NaCl linear gradient. The protein elutes from the column at roughly 150-200 mM NaCl. Fractions containing protein are pooled and can be frozen at this point after the addition of 20% (w/v) sucrose. However, I have found that rebinding and eluting the protein to the Q column under the same conditions results in a

much cleaner and more concentrated preparation. This additional step can also be performed after sample thawing.

Tail constructs: Construction and Purification

We next needed to decide what tail constructs would be ideal for use in our experiments. We required something that would be stable enough to express and purify, and ideally did not suffer from large amounts of proteolysis. However, protein degradation is not as much of a concern for the experiments planned, as any protein that has been substantially proteolyzed will not cross-link in our assay. In addition, it was desirable to engineer the constructs with a 6x-histidine tag for purification purposes. Conflicting data is found in the literature as to whether C-terminal tags, even small ones like a 6x-histidine, interfere with the regulatory mechanism of the tail domain. As this is what we are investigating we wanted to be sure that our purification tag does not affect regulation. We therefore chose to engineer a 6x-histidine tag located at the fragment's N-termini as far as possible from the regulatory end of the protein. David Hackney had created a drosophila tail construct consisting of residues 864-975 with a N-terminal GST tag in his work determining the location of the neck coiled-coil and tail coiled-coil interaction (54). We decided to construct the equivalent construct of the human kinesin-1 tail with the exception of the purification tag used. This corresponds to residues 823-963 of human kinesin-1, referred to as Tail 823-963. We also created a slightly shorter tail protein that still retains regulatory activity, but does not suffer from as severe proteolysis. This construct is identical to that above except ends at residue 944 (Tail 823-944), equivalent to drosophila residue 960.

Once we were able to determine that a region just N-terminal to the conserved QIAKPIRP sequence of the tail is interacting with a cysteine located at the end of the alpha 3

helix (S188C) (discussed in Section III below) we wanted to examine whether a peptide of this sequence could interact with the head. A 27-mer peptide encoding residues 901-927 of the human kinesin-1 heavy chain was purchased from GenScript (Piscataway, NJ) and contained an N-terminal biotin tag that was not used for the purposes of these experiments (Figure 2A).

Tail constructs were created by PCR. The forward primer introduced a unique EcoRI site, followed by an N-terminal methionine and a 6x-histidine tag before residue 823. The reverse primer for the tail construct containing residues 823–963 introduced a unique XhoI site after the stop codon. The reverse primer for the tail construct containing residues 823–944 introduced a stop codon after residue 944 followed by a unique XhoI site. These constructs were ligated into a pET17B vector (Novagen (EMB Chemicals, Merck KGaA, Darmstadt, Germany)) that was modified to remove a N-terminal T7 tag. Both constructs were verified by DNA sequencing.

Expression conditions were tested to maximize the amount of soluble protein. Ideal expression conditions were to grow transformed BL21(DE3)RP cells from an overnight starter culture in LB at 37°C until the $OD_{600}$ ranged from 0.6-1.0. Cells were then cooled for 30 minutes at 4°C, 0.1 mM IPTG was added to induce protein expression, and cells were allowed to induce at 24°C overnight. After induction, cells were collected by centrifugation. Cell pellets were then resuspended in Tail Lysis Buffer consisting of 50 mM $NaPO_4$ buffer pH 8.0, 300 mM NaCl, 20 mM Imidazole, 10% glycerol, and 5 mM βME with the addition of protease inhibitors (500 μM PMSF, 1 μM E-64, 10 μg/ml Leupeptin, and 1 μg/ml each of Pepstatin A and Aprotinin) and cell paste was frozen directly in liquid nitrogen and stored at -80°C.

We originally attempted to purify the tail constructs using Nickel-NTA resin (Invitrogen, EMB Biosciences, Carlsbad, CA). While this media was able to bind and elute our 6x-histidine

tagged tail protein, the eluted protein was rather unstable in solution as it quickly started precipitating after elution, and the sample contained large amounts of contaminating proteins. These contaminants will not only make analysis of the crosslinking reaction more difficult, but may be affecting the solubility of our protein; the contaminants dramatically increase the total protein concentration and crowd our already unstable protein, causing additional precipitation. We then tried Talon resin (Clontech, Mountain View, CA) in our 6x-histidine purification instead of the Ni-NTA resin in order to increase the purity of our sample. Talon resin employs the use of cobalt ions instead of the normally used nickel. This resin has been touted as providing cleaner preparations under identical conditions, as well as works better for some ill-behaved proteins (John Ceislak, personal communication, Talon Metal Affinity Resin Brochure, Clontech Product #635503 manufacture's brochure). The tail constructs did indeed bind to Talon resin, and the resin provided superior purification of our construct compared to the Ni-NTA resin as many of the contaminating proteins are removed.

The protein purification scheme that worked best for the tail protein was an affinity purification using the Talon resin. Additional purification techniques, described below, were attempted for the tail, however, none proved to be useful. For the Talon preparation frozen cell pellets of expressed tail protein were lysed using a French Pressure Cell and the lysate was cleared with a 100,000 x g spin. Protein in the high-speed supernatant was batch bound to Talon resin equilibrated in lysis buffer for 1 hour at 4°C with rotation and resin was poured into a 5-ml disposable column. Resin was washed with roughly 25 column volumes of High Salt Wash buffer containing 50 mM $NaPO_4$ pH 7.0, 1 M NaCl, 20 mM Imidazole, and 5 mM βME. Washing was continued as long as protein continued to leach off the column as measured by a Bradford assay. When the washes no longer appeared blue upon addition to Bradford reagent,

the salt concentration of the sample was dropped to 300 mM NaCl by washing with Tail Low Salt Wash Buffer (50 mM $NaPO_4$ pH 7.0, 300 mM NaCl, 20 mM Imidazole, and 5 mM βME). I found this step to be helpful in maintaining the amount of soluble tail. Bound protein was then eluted using Tail Elution Buffer containing 50 mM $NaPO_4$ pH 7.0, 300 mM NaCl, 500 mM Imidazole, and 5 mM βME. Fractions that contain protein as measured by reaction with Bradford reagent were pooled together and 20% (w/v) sucrose is added to the protein. The sample was then given a hard spin at 100,000 rpm for 10 minutes at 4°C in a TLA110 rotor to clear any aggregating or precipitating protein. I found this hard spin step key to reducing protein precipitation in subsequent uses. Protein was then frozen directly in liquid nitrogen and stored in liquid nitrogen until future use.

A myriad of degradation products are present in the Tail 823-963 protein purifications (visible in the left gel of Figure 2C), which was expected given the susceptibility of the full-length protein to proteolysis from the C-terminus (62). This degradation was substantially reduced in the Tail 823-944 purifications (Center gel Figure 2C), as found previously using drosophila constructs (62). Additionally, I found the following points helpful in reducing contaminates and maintaining tail protein solubility. Washing the resin with the High Salt Wash buffer until protein is no longer detected in a Bradford assay was helpful in removing a vast majority of contaminating proteins. I also found that adding a wash step using a Low Salt Wash buffer to reduce the NaCl concentration before elution was helpful in maintaining protein solubility. Elution fractions, especially from the beginning fractions containing high concentrations of protein, seem to precipitate quite quickly. Pooling desired fractions as soon as possible was advantageous in reducing the amount of immediate precipitation, as total protein concentration is reduced. The addition of 20% sucrose to the eluted protein helps maintain

protein solubility upon thawing, however I recommend giving the protein sample a 100,000 x g spin for 10 minutes both before freezing in liquid nitrogen and upon sample thawing. This single step greatly decreased the amount of protein that precipitated during subsequent dialysis or concentration steps.

Another point of interest to a researcher using these tail constructs is that the tail does not react very strongly to the Bradford reagent, especially on short time scales. We thus use a Vanilla-Lowry method for accurately determining the protein concentration of our tail constructs. Protein pooling though, can be done relying on the Bradford method, however the reaction will not turn as blue as one would expect for peak fractions. Amido black stain also is a quick method for determining the presence or absence of protein in the sample. The tail seems to react well with this reagent after absorption onto nitrocellulose.

Attempts were made to clean-up tail preparations after elution from the Ni-NTA or Talon resin, as some contamination still remained. Two different techniques were tested based on previous experiences with the tail-containing full-length DKH975 and the physiochemical characteristics of our constructs, a hydrophobic Phenyl HP column, and a HiTrap S cation exchange column.

The Phenyl HP hydrophobic column (Amersham Biosciences (GE Healthcare), Piscataway, NJ) was selected because the full-length DKH975 protein binds to this column better than shorter C-terminal proteolysis fragments, suggesting that elements in the tail are affecting the affinity of the molecule for the media; therefore the tail itself may stick to this column quite well. The Tail 823-963 protein was tested for binding to this column under conditions that were found to work well for DKH975. Ammonium sulfate was added to a final concentration of 750 mM and the sample was spun at 100,000 x g for 10 minutes to remove any precipitation formed

during the addition of ammonium sulfate. A majority of the tail remained in solution after the ammonium sulfate addition, suggesting that the concentration could be raised if necessary to promote column binding. Tail protein was injected onto the Phenyl HP column, however it was found that neither the Tail 823-963 protein nor a majority of the contaminants bind to this column under the conditions tested. The ammonium sulfate concentration could be raised to promote protein binding, however bound protein would most likely elute early in the reverse linear gradient, at high salt concentration. This was not ideal, as reducing the salt concentration in the tail samples without causing precipitation has been difficult. We therefore turned to the use of the S ion exchange column in an attempt to further purify our protein.

The cation exchanging methyl sulfonate (S) column was selected based on the calculated isoelectric point of the tail proteins. Tail 823-963 has a calculated pI = 10.83, while Tail 823-944 has a pI = 10.64. These proteins contain an excess of positive charges, and therefore should bind well to the negatively charged medium of a strong cation exchanger when the pH of the solution is below the isoelectric point. The use of the HiTrap S column (Amersham Biosciences (GE Healthcare), Piscataway, NJ) after elution from the Ni-NTA or Talon resin necessitated that the conductivity of the protein solution be reduced to about 100 mM NaCl to promote protein binding. Unfortunately, decreasing the salt concentration of our tail samples had been problematic, particularly at high total protein concentrations. I therefore tried to dialyze the solution into buffer containing 300 mM NaCl with low amounts of Imidazole to maintain protein solubility. Once a majority of the salt was removed by this method the sample was quickly diluted down to 100 mM NaCl, hopefully keeping the protein happier with the quick change in salt concentration rather than the gradual shift during dialysis. Despite our efforts, the protein quickly precipitated during the dialysis step, most likely stemming from high total protein

concentration and unseen precipitates that act as nucleators for further protein precipitation. This column has been tested for its use in further purifying tail constructs. As expected, the tail binds well to the media, however the column does not result in either the concentration or further purification of the sample (Mark Seeger, personal communication).

Overall, the use of the Talon resin provided enough purification of the Tail 823-963 and Tail 823-944 constructs for our uses with this project. David Hackney had used a GST-tagged tail protein in his work, ensuring formation of a tail dimer, similar to that in the homodimer of the full-length molecule. We next set out to determine whether our shorter Tail 823-944 protein containing only a 6x-histidine tag is monomeric or dimeric in solution.

Tail proteins containing residues 823-944 would be expected to be dimeric, as they contain a significant portion of the predicted tail coiled-coil (residues 823-911) (73). To determine if our protein was indeed dimeric we performed gel filtration chromatography on the protein under conditions similar to those found physiologically. Tail 823-944 protein purified using Talon resin was thawed, given a hard spin to remove precipitates, and spin concentrated four-fold. Protein was then injected onto the Superose6 gel filtration column (Amersham Biosciences (GE Healthcare), Piscataway, NJ) equilibrated in buffer containing 50 mM $NaPO_4$ pH 7.0, 200 mM NaCl, and 20 mM Imidazole. The peak in the tail elution from this column, as determined using Coomassie-stained 15% SDS-PAGE gels, was found to be 17.5 ml. Three low molecular weight standards in the appropriate range of the tail, Ribonuclease A (mw 13,700, peak 19.8 ml), Chymotrypsinogen A (mw 25,000, peak 19.0 ml), and Ovalbumin (mw 43,000, peak 18.0 ml), were also injected onto the column in order to analyze the oligomeric state of the tail. Blue dextran was used to determine the void volume of the column. Calculating the $K_{av}$ of each protein by subtracting the void volume determined using blue dextran from the elution

volume of the protein divided by the void volume subtracted from the total volume of the column (24 ml), and plotting this number versus the log of the protein molecular weight in daltons gives a linear standard curve for the low molecular weight standards. These proteins are globular in shape, therefore plotting the $K_{av}$ versus the molecular weight of the Tail 823-944 protein if it were a monomer (14561.52 daltons) or a dimer (29123.04 daltons) will give us an idea of whether our protein in monomeric or dimeric in solution, keeping in mind that our protein is most likely not completely globular, especially for the dimer, as the coiled-coil region will most likely be in a rod-like conformation, causing the protein to appear bigger than it actually is by gel filtration. Thus we would expect our protein to fall below the standard curve for wholly globular proteins. As expected, the Tail 823-944 protein data fits best when the molecular weight of the dimeric protein is used as this point falls slightly below the standard curve for globular proteins (Figure 3). These data suggest that the Tail 823-944 is indeed a dimeric protein in solution. The Tail 823-963 protein would also be expected to be a dimer in solution based on these results.

**Figure 2. Photocross-linking of kinesin-1 head and tail domains**

A. Head and tail constructs. Color scheme as in Figure 1. Cysteine-light monomeric and dimeric human kinesin-1 heavy chain head constructs have been described (24, 79). Dimeric tail constructs contain N-terminal 6x-histidine tags and residues 823–963 or 823–944. The 27-mer tail peptide (residues 901–927 with an N-terminal biotin tag) corresponds to the bracketed region of the dimeric tail constructs and is shown with the conserved QIAKPIRP underlined.

B. Photocross-linking scheme. Heads and tails are colored as in *A* with blue outlining on the neck coiled-coil and orange outlining on the predicted tail coiled-coil. The head in the foreground is positioned as if it were docked on a microtubule with the plus end up, the same orientation as the head in Figure 6*A*. Cysteine 188 (S188C) and bound ADP (blue ellipse) are shown. After conjugation to the maleimide moiety of the benzophenone-4-maleimide, the structure of which is shown below (*Center*), heads were associated with tails, then irradiated to initiate photocross-linking as described in the text. A red star marks the cross-linked site (*Right*). Dimeric heads and tails are shown, but cross-linking was observed at position S188C using any combination of the head and tail constructs shown in part *A*. We cannot determine whether one or both heads of a kinesin-1 dimer interact with the dimeric tail. This diagram model is consistent with our observed <50% cross-linking efficiencies. An interaction between the neck coiled-coil and tail coiled-coil is shown, based on previous studies (59, 61).

C. Coomassie-stained 4-20% SDS-PAGE gradient gels showing photocross-linking. For the photocross-linking experiment shown in the left gel, the heads contained both the S188C and the G234A mutation, whereas in the others, the heads contain only the S188C mutation. The tail constructs used for these experiments are indicated on each gel. Lanes for all gels are as follows: SeeBlue Plus2 Prestained Standard (Invitrogen), tail, head + S188C, head + tail before UV exposure, head + tail after a 5 minute UV exposure with 254 nm light. The emergence of a band of the approximate molecular weight of a head + tail cross-link can be seen after irradiation, indicating that the tail fragment used in each of the experiments interacts in the vicinity of the cysteine added-back at position S188C. Protein bands marked with arrows contained both head and tail sequences, as verified by MALDI-MS. The Tail 823-963 construct showed considerable amounts of proteolysis (*Left gel*), while the degradation was significantly reduced in the Tail 823-944 construct (*Center gel*), and eliminated in the 27-mer peptide (*Right gel*). The neck coiled-coil—tail coiled-coil interaction is not necessary for this direct head-tail interaction to occur, as crosslinking was efficient between the K349 monomer and the 27-mer peptide, neither of which contain the coiled-coil interacting region.

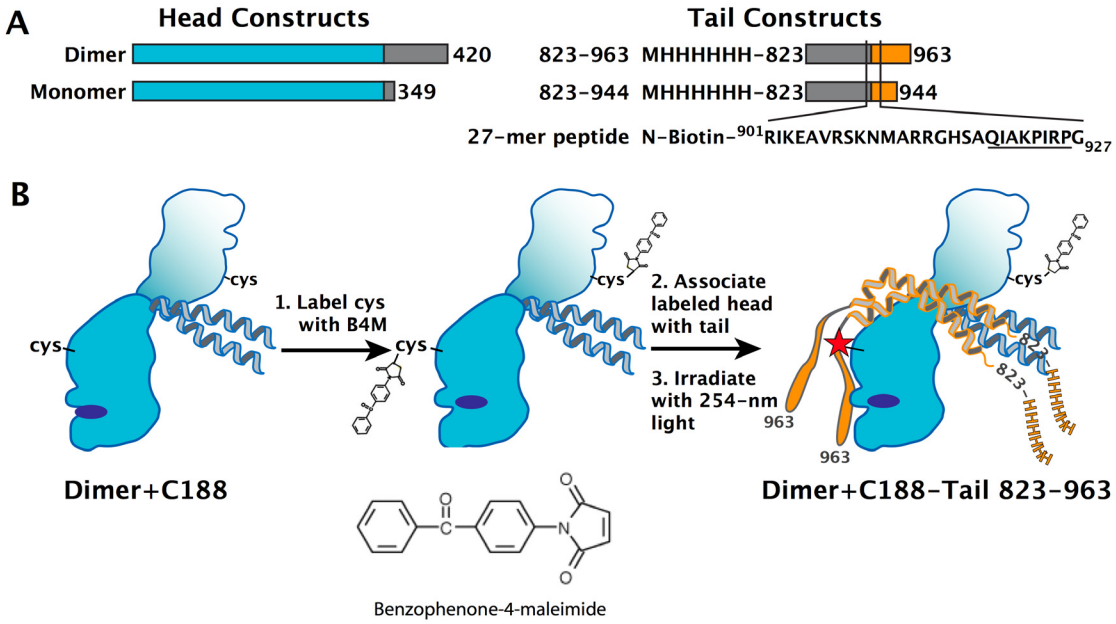
A
Head Constructs
Tail Constructs
Dimer
420
Monomer
349
823-963 MHHHHHH-823
963
823-944 MHHHHHH-823
944
27-mer peptide N-Biotin-901RIKEAVRSKNMARRGHSAQIAKPIRPG927
B
cys
1. Label cys with B4M
2. Associate labeled head with tail
3. Irradiate with 254-nm light
963
Dimer+C188
Dimer+C188-Tail 823-963
Benzophenone-4-maleimide
C
Ladder
Tail (823-963)
Dimeric head
No UV
Cross-link
Tail (823-944)
27-mer peptide
Monomeric head
250
148
78
64
50
36
22
16
6

**Figure 3. The Tail 823-944 protein is dimeric in solution**

Plot of the calculated $K_{av}$ from the elution data versus the molecular weight (log scale) for globular protein standards and the Tail 823-944 protein from the Superose6 gel filtration column (Amersham Biosciences (GE Healthcare), Piscataway, NJ). Three low molecular weight standards in the appropriate range of the tail, Ribonuclease A (mw 13,700), Chymotrypsinogen A (mw 25,000), and Ovalbumin (mw 43,000), were used in order to analyze the oligomeric state of the tail. The calculated $K_{av}$ of the tail (shown as a green line) is plotted using the molecular weight of both the monomer (14561.52 daltons) and the dimer (29123.04 daltons), colored blue and red respectively. Both theoretical oligomeric states fall below the curve created by the globular molecular weight standards, appearing larger than predicted. This is expected, as the Tail 823-944 protein contains a significant portion of the tail coiled-coil that should exist in a more extended and rod-like state, elongating the molecule. The experimental data is most consistent with a dimeric state of the tail and could be confirmed using analytical ultracentrifugation.

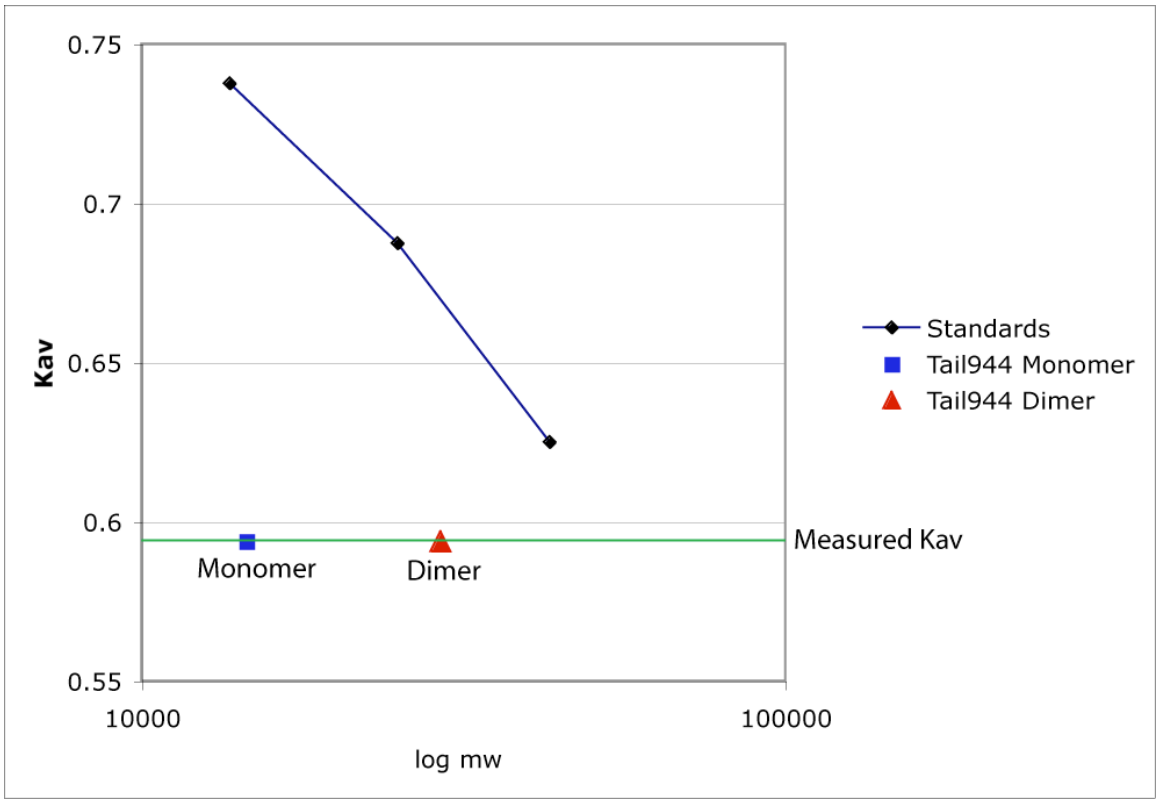
0.75
0.7
0.65
0.6
0.55
Kav
10000
100000
log mw
Monomer
Dimer
Measured Kav
Standards
Tail944 Monomer
Tail944 Dimer

B. Methods

Association of the head and tail *in trans*

Through our efforts, described below, we found that both purified monomeric and dimeric head constructs could be retained by Talon resin only in the presence of one of the dimeric tail constructs. Ideal association conditions to limit nonspecific interactions were found to consist of 50 mM K-Acetate, 10 mM Tris-Acetate pH 7.0, 4 mM $MgSO_4$, 20 mM Imidazole, 50 mM NaCl, 0.05% Tween-20, 5 mM βME, and 40 μM ADP. Importantly, the 27-mer peptide was able to successfully compete with the tail for head binding. Details on the experimental design and procedure are detailed in the following paragraphs.

Once we were able to express and purify our head and tail constructs, we wanted to develop an assay to assess whether our head and tail proteins were able to interact *in trans*. We first tested whether the 6x-His Tail 823-963 construct could associate with the K420CLM dimer, as these proteins both contain the coiled-coil interacting regions. To do this we turned to the presence of the 6x-histidine tag engineered on the tail domain.

The experiment was designed as follows: Tail proteins will bind specifically to Talon resin through the 6x-hisitidine tag found on their N-terminus, while the head alone should not bind to the resin, as it does not contain an appropriate affinity tag. The head, however, should be retained on the column by the bound tail under conditions in which the head and tail are able to associate, eluting with the tail after the addition of high concentrations of imidazole.

To determine conditions in which the head and tail are likely to associate we compared data regarding the salt concentrations necessary to induce the compact conformation of the kinesin-1 heavy chain with that used in tail peptide experiments (50, 54, 63). In addition to promoting association we also needed to ensure that the tail proteins remained soluble and that

the resin under these conditions did not nonspecifically retain the head protein. The tail had proven problem-some under the low ionic strength conditions thought required in order to get association, however, the protein seemed to be more stable when heads were added before the dialysis into low salt. Initial efforts also found that the tail protein behaved more predictably under low ionic strength in an acetate buffer compared to phosphate solutions.

After dialysis together to allow for association, the head-tail complex were batch bound to Talon resin before washing with the same buffer to remove unbound protein. Bound tail protein was then eluted using excess imidazole. Heads alone served as a negative control to ensure that nonspecific binding was not occurring. We expected that if the head and tail constructs were specifically associating under our conditions that the head would be retained on the Talon resin and elute with the tail upon the addition of imidazole.

The ideal conditions determined to promote the association of the complex while limiting nonspecific interactions between the head and the resin were in buffer containing 50 mM K-Acetate, 10 mM Tris-Acetate pH 7.0, 4 mM $MgSO_4$, 20 mM Imidazole, 50 mM NaCl, 0.05% Tween-20, 5 mM βME, and 40 μM ADP. Under these conditions K420CLM was not present in the elution fractions from the Talon resin when the tail is not present, however when the head and tail are allowed to associate before column binding, the head is mildly retained, and could be seen in elution fractions by Coomassie staining or western blotting using the Suk4 monoclonal antibody (113) (Figure 4A). The buffer conditions used in our crosslinking assay (see below, Binding buffer) were also tested for their ability to promote association between the head and tail using this assay. While heads were retained by the presence of tail protein, some nonspecific interactions were occurring between the head and the resin under these conditions. These

conditions were thus suitable for our crosslinking reaction, however could not solely be used to determine if our constructs are able to interact.

The association experiment was also used to assess if a specific interaction between the Tail 823-963 and the monomeric K349CLM head could occur. We expected the K349CLM protein to have a much lower affinity for the tail protein, as this head construct lacks the neck coiled-coil region known to interact with the tail coiled-coil. Similar to the K420CLM construct, K349CLM was retained on the Talon column by the presence of the Tail 823-963 protein, as it is visible in the imidazole elutions of a Coomassie-stained 4-20% SDS-PAGE gradient gel (Figure 4B). This result suggests that there is a weak interaction between the head and tail domains that is not mediated by the neck coiled-coil—tail coiled-coil interaction, as the K349CLM construct does not contain this region. Western blot analysis was not performed, as K349 does not react with the Suk4 monoclonal antibody that is used to detect K420.

As expected, K420CLM and K349CLM were also found to associate with the shorter Tail 823-944 protein. We reasoned that if the head-tail interaction was specific, our 27-mer peptide should be able to compete with tail binding, given our ability to crosslink the tail and the peptide to identical locations on the motor domain, as discussed below in Section II. The experiment was performed as above, except that before the elution of bound tail protein using excess imidazole, two peptide elutions were performed, using 10 and 100 μM of the 27-mer peptide. As reasoned, the peptide was indeed able to compete with the Tail 823-944 protein for binding to K420CLM, as head protein is visible in both the peptide elution fractions as well as additionally found in the imidazole elution, as assayed by Coomassie staining (Figure 4C). It was also found that the 27-mer peptide was able to compete with the tail for binding to the monomeric K349CLM construct, however, as the affinity of the monomer for the tail is weaker,

protein is barely visible in the elution fractions, not strong enough to be seen well in a scanned image. The weak competition of the tail peptide may also be due to additional interactions not found in the 27-mer tail peptide that may be necessary for a tight interaction between the head and tail. Future experiments, including x-ray crystallography, will be necessary in order to map the entire head-tail interaction surfaces.

Photocross-linking of the head and tail *in trans* with B4M

Briefly, heads containing a single cysteine add-back were dialyzed into labeling buffer (25 mM Hepes pH 7.5, 100 mM NaCl, 2 mM $MgCl_2$, 1 mM EGTA, 200 μM Tris(2-carboxyethyl) phosphine hydrochloride, 50 μM ADP) at 4°C. A 5-fold molar excess of benzophenone-4-maleimide, B4M (Invitrogen, EMB Biosciences, Carlsbad, CA), was added to 1–2 mg/ml head and reacted for 12 hours at 4°C in the dark. The labeling reaction was quenched with 25 mM 3-mercaptoethanol (βME) and excess label removed by repeated spin concentration in centrifugal filter devices (Millipore Corporation, Billerica, MA) into binding buffer (50 mM K-acetate, 10 mM Tris-acetate pH 7.0, 4 mM $MgSO_4$, 20 mM imidazole, 5 mM βME, 40 μM ADP) plus 300 mM NaCl. Approximately 90% of kinesin-1 heads reacted with B4M under these conditions, as measured by a 5,5%-dithiobis 2-nitrobenzoic acid (DTNB, Pierce, Thermo Scientific, Rockford, IL) assay. Purified tails were added to yield an approximate ratio of five tails:one head. The combined proteins were dialyzed into binding buffer for 3 hours, spun 10 min at 355,000 x *g* to remove any aggregates, and then irradiated for 5 minutes with 254-nm UV light. Approximately 25% of monomeric heads or 35% of dimeric heads cross-linked to either the dimeric tail protein or the 27-mer peptide. Experimental design and detailed methods of the labeling and crosslinking procedure are described in the paragraphs immediately below.

**Figure 4. Specific association of the head and tail constructs using Talon resin**

Binding of dimeric and monomeric head constructs to kinesin-1 tails using Talon resin (Clontech, Mountain View, CA) shows that our head and tail constructs described in Figure 2A are able to associate and the 27-mer tail peptide can compete with the dimeric tail for binding to the head. See text for further experimental details.

A. A western blot using the monoclonal antibody Suk4 to detect the K420 head protein. In the absence of the 6x-histidine Tail 823-963 protein, the dimeric K420 protein does not bind to Talon resin nonspecifically, as it is not seen in the elution fractions (*Left*). However, when dimeric heads and tails were mixed in a roughly 1:2 molar ratio under conditions in which they associate and batch-bound to Talon resin significant amounts of K420 head protein co-eluted with the tail fragments upon the addition of excess imidazole (*Right*). For the left blot, lanes are as follows: SeeBlue Plus2 Prestained molecular ladder (Invitrogen Corporation, Carlsbad, CA) (not visible), K420 positive western control, K420 starting sample, flow through from Talon resin, wash fractions #1-3 of 8, elution fractions #1-7. No K420 band is detectable in the elution fractions indicating that the head is not nonspecifically retained by the Talon resin under our conditions. For the right blot, lanes are as follows: K420 positive western control, SeeBlue Plus2 Prestained molecular ladder (not visible), K420 + Tail 823-963 starting sample, flow through from Talon resin, wash fractions #1-3 of 8, elution fractions #1-7. K420 is retained on the Talon resin only when the tail protein is present, indicating that these two domains can functionally interact.

B. A Coomassie-stained SDS-PAGE gel of a monomeric K349-Tail 823-963 association assay. The experiment was performed as in A, however the monomeric K349 protein does not react with the Suk4 mAb. Lanes are as follows: SeeBlue Plus2 Prestained molecular ladder, K349 positive control, K349 + Tail 823-963 starting sample, flow through from Talon resin, wash fractions #1-6 of 8, elution fractions #1-5. K349 is retained by the Talon resin in the presence of the tail, co-eluting with the addition of excess imidazole to the resin. While binding between the monomeric K349 head and dimeric Tail 823-963 proteins seems weaker than that seen for the dimeric K420 heads (Figure 4C), this is not unexpected, as the K349 construct lacks the neck coiled-coil region that interacts with the tail coiled-coil. These results indicate that our head and tail constructs can associate in the absence of this stabilizing interaction.

C. A Coomassie-stained 4-20% gradient SDS-PAGE gel of the association of the dimeric K420 head and Tail 823-944 tail constructs and competition elution with the 27-mer tail peptide. As in A, the K420 head protein is not retained by the Talon resin in the absence of the 6x-histidine tagged tail protein. Similarly, the presence of the dimeric Tail 823-944 protein allows for retention of the head on the resin. The 27-mer tail peptide was able to successfully compete with the dimeric tail construct for interactions with the head, as some head can be seen in the 10 μM and 100 μM peptide elution fractions. Additional bound head co-elutes with the dimeric tail protein upon the addition of excess imidazole. For the left gel, lanes are as follows: SeeBlue Plus2 Prestained molecular weight standard, 5 μl of the K420 heads loaded onto resin, 20 μl of the column flow through, 20 μl of the first and second wash, 30 μl of the eighth wash, 30 μl

of the first and second imidazole elution fractions. For the right gel, the lanes are as follows: SeeBlue Plus2 Prestained Standard, 5 μl of the K420 heads and Tail 823-944 mixture loaded onto resin, 20 μl of the column flow-through, 20 μl of the first and second washes, 30 μl of the eighth wash, 30 μl of the 10 μM peptide elution, 30 μl of the 100 μM peptide elution, 30 μl of the first and second imidazole elution fractions.

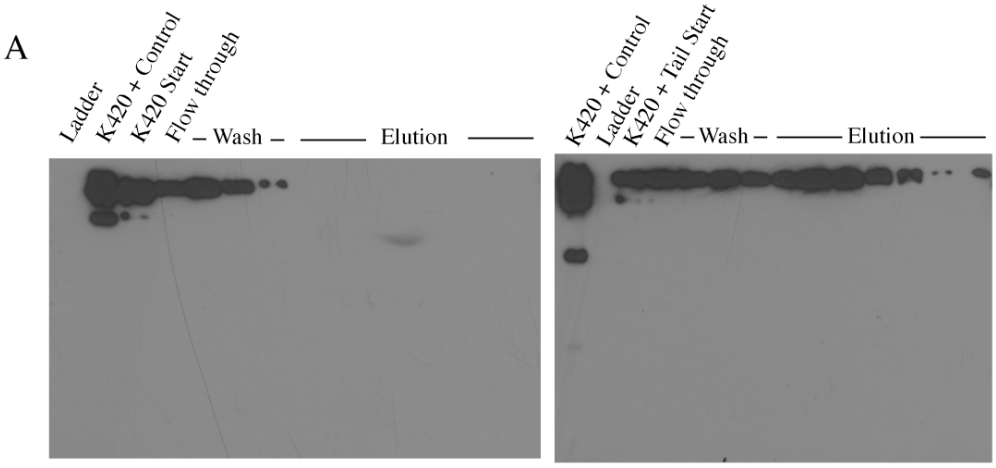
A
Ladder
K420 + Control
K420 Start
Flow through
Wash
Elution
K420 + Control
Ladder
K420 + Tail Start
Flow through
Wash
Elution

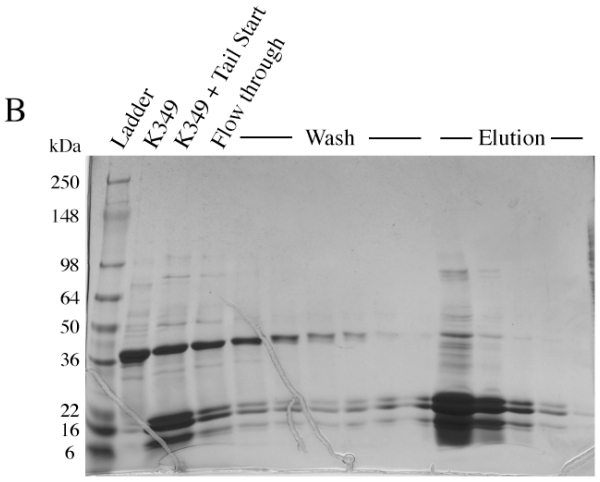
B
kDa
Ladder
K349
K349 + Tail Start
Flow through
Wash
Elution
250
148
98
64
50
36
22
16
6

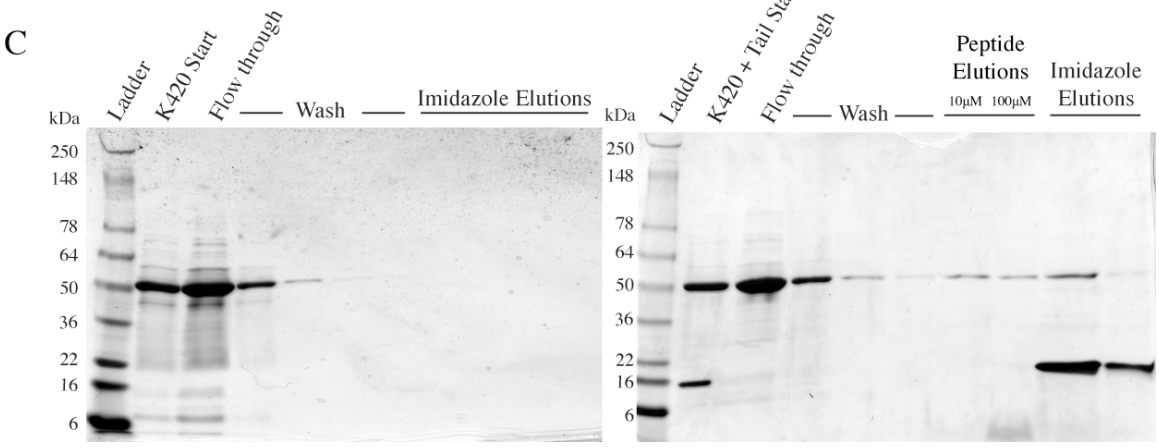
C
kDa
Ladder
K420 Start
Flow through
Wash
Imidazole Elutions
250
148
78
64
50
36
22
16
6
kDa
Ladder
K420 + Tail Start
Flow through
Wash
Peptide Elutions
10μM 100μM
Imidazole Elutions
250
148
78
64
50
36
22
16
6

*Crosslinking experimental design*

Once we were assured our two constructs were able to interact under low salt conditions we attempted to crosslink the two proteins together using the heterobifunctional photoreactive crosslinker benzophenone-4-maleimide (B4M, Invitrogen, EMB Biosciences, Carlsbad, CA) attached to various locations on the motor domain. The maleimide moiety specifically labels reactive cysteines, while the benzophenone group reacts with nucleophiles or creates C-H bond insertion products upon irradiation with 254 nm UV light. We could site-specifically label our head proteins by adding a single cysteine residue using site-directed mutagenesis to our cysteine-light head constructs (dimeric K420CLM or monomeric K349CLM). This cysteine could be placed anywhere we wish to probe for a head-tail interaction. Once the crosslinker is attached to the motor domain we then add tail protein back under the conditions determined above, in which the head and tail associate, and irradiate the sample with UV light to activate the benzophenone reaction. We expected that if the tail protein is interacting with the motor domain within the 9 Å reach of the crosslinker, a cross-link will form. Analysis of the crosslinking reaction can be done using SDS-PAGE, looking for the emergence of a molecular weight band equal to that of the head + tail, as well as depletion of the head and tail in the sample. In order to carry out this experiment, we first needed to determine conditions in which our single reactive cysteines engineered onto the head protein label with the maleimide moiety of the B4M crosslinker.

*Labeling single cysteine add-backs on the motor domain with B4M*

Several considerations were necessary for the success of the maleimide labeling reaction, specifically the accessibility and local environment of the added-back cysteine, and the labeling conditions. First, the location of the cysteine must make it accessible to labeling under the

experimental conditions. This was accomplished by designing mutants based on the crystal structure of the motor domain (PDB ID code 1mkj). Locations were selected to be surface exposed as well as in sites plausible for a tail interaction. Additionally, the cysteine will not react well if surrounded by acidic groups, such as aspartic or glutamic acid residues, as the local pH is perturbed. This situation was most likely the reason for our lack of crosslinking at position D181C described in Section III below, as a plethora of negative charges surround this residue, making it very hard to label efficiently.

Reaction conditions were also considered. Reducing agents such as DTT (dithiothreitol) or βME (beta-mercaptoethanol) cannot be used in the labeling reaction, as they contain sulfhydryl groups and thus will react strongly with the maleimide group of the crosslinker. However the use of non-sulfhydryl reducing agents, such as TCEP (tris(2-carboxyethyl)phosphine), at low concentrations (100-500 μM) is acceptable. While TCEP has been shown to inhibit maleimide reactions when used at high concentrations (81), the low concentrations used here do not interfere with the cysteine labeling reaction but are sufficient to keep reactive cysteines from crosslinking to one another (72). Maleimides react well in the pH range around 7.0, which is good for protein stability. We did consider the use of a benzophenone-4-isothiocyanate crosslinker (Invitrogen Corporation, Carlsbad, CA); however, its optimal reaction pH is 9.0 and is not site-specific, as it reacts with any amine group. We would therefore need to modify our experimental layout for use of this crosslinker, as it would be more advantageous to label the tail protein first with the isothiocyanate, as there are less reactive groups, then try to crosslink the head to the labeled tail. This is plausible, but work would need to be done to ensure the tail's stability at pH 9.0. As maleimide reactive groups have previously been shown to label the kinesin-1 motor domain quite well, and the reaction conditions are less

extreme, we decided to work with the B4M crosslinker. Therefore, preparations of the head constructs required purification or dialysis into an appropriate buffer for labeling. This buffer should contain TCEP instead of DTT or βME, and the pH should ideally be between 7.0 and 7.5. We opted for a buffer containing 25 mM Na-Hepes pH 7.5, 2 mM $MgCl_2$, 1 mM EGTA, 100 mM NaCl, 200 μM TCEP, and 40 μM ADP for our labeling reactions.

The first cysteine on the head that we tried to label was S188C in the K420CLM background. This cysteine reacts well with maleimide probes under our labeling conditions, and protocols for efficiently labeling this site were available to us. An accurate measurement of the protein concentration is needed after dialysis into labeling buffer, therefore a standard curve using known amounts of BSA was created using Bradford reagent using the manufacturer's protocol (Pierce, Thermo Scientific, Rockford, IL). Our reactions typically contained about 20 μM head protein, although were occasionally three-times as concentrated. A variety of labeling conditions and ratios were examined for their ability to efficiently label the single reactive cysteine. These included the use of equal molar, three- and five-times molar excess of B4M over protein. However, no difference was seen between the labeling ratios as to their ability to crosslink the tail protein. A five-fold molar excess of B4M was therefore frequently used, however equal molar amounts of the crosslinker were used for some of the less stable Switch I constructs. In addition to the ratio of label to protein, two reaction conditions were tested for their ability to label cysteine S188C: an overnight labeling at 4°C, and a harsher labeling condition of 4 hours at room temperature. Again, no difference could be detected in the crosslinking reaction between the two labeling conditions, however, as labeling the Switch I mutants A193C, M197C, and N198C made them slightly more susceptible to precipitation, these reactions were performed using the more gentle overnight labeling protocol.

Overall, a typical reaction scheme for single cysteine add-backs in the head is thus: after dialysis into labeling buffer to remove excess salt and DTT head concentration is accurately measured. A 100 mM stock of B4M was made by dissolving the powder in DMSO (dimethyl sulfoxide) and stored at -20°C protected from light. The maleimide moiety of the crosslinker is not sensitive to light, and the benzophenone should only be activated under shorter wavelength UV, not the fluorescent light found within the lab. However, it can be activated by sunlight, and therefore extra caution was taken when working with the crosslinker or labeled protein, including working under dark conditions as much as possible. The concentrated B4M crosslinker stock was then added to the protein at a 5-times molar excess and the reaction sample was mixed well by pipeting up and down. Frequently white precipitate was seen when the crosslinker is first added to the protein solution. This was most likely B4M that is unable to stay in solution, as the crosslinker itself is not soluble in aqueous environments. This precipitate clears upon mixing and did not seem to be problematic. The reaction was allowed to go overnight at 4°C wrapped in foil. It is then quenched by the addition of excess βME (25 mM), and unreacted B4M is removed from the sample by buffer exchange and sample concentration using 10,000 mwco spin concentrators. Approximately 90% of kinesin-1 heads reacted with B4M under these conditions, as measured by 5,5'-dithiobis 2-nitrobenzoic acid (DTNB) assay performed by Sam McBrayer, a rotating graduate student.

*Crosslinking reaction*

The crosslinking reaction between the head and tail was first attempted using a single cysteine added-back at position S188C in the motor domain (K420CLM S188C), and the longer Tail 823-963 protein. Once the head was efficiently labeled with the B4M crosslinker, tail

protein was added to the sample. This mixture was then dialyzed into Binding buffer containing 50 mM K-Acetate, 10 mM Tris-Acetate pH 7.0, 4 mM $MgSO_4$, 20 mM Imidazole, 5 mM βME, and 40 μM ADP for three hours. Frequently, tail precipitation was a problem during this dialysis step. A variety of buffer pH's and dialysis times were tried. The buffer pH seemed to have no effect on tail stability, while shorter dialysis times with frequent buffer changes reduced precipitation. The addition of 5% sucrose in the buffer also did not alleviate precipitation. I did find several steps that seemed to ameliorate the problem. First, I found that buffer exchanging the labeled head into Binding buffer + 300 mM NaCl during the removal of excess label eliminated the immediate precipitation of the tail in solution due to the low salt concentration. This was also significantly helped by giving the tail protein a hard spin at 100,000 x g for 10 minutes after thawing to remove any unseen precipitates. Quickly changing the salt concentration during the dialysis also seemed to improve tail solubility. Ideally for a 3 hour dialysis the buffer is changed every 20-30 minutes for the first 3 L, and the remaining buffer is allowed to dialyze longer. The presence of the head protein in the solution seemed to have a positive effect on the stability of the tail. I found that having an excess of heads over tails during the dialysis step helped with keeping the tail protein soluble. This is most likely a stabilizing effect from association with the head domain.

Despite all of our efforts, small amounts of precipitation were still seen after protein association. This is very likely excess tail protein and was removed by another spin at 100,000 x g. The benzophenone moiety of the crosslinker is activated by UV light, with the greatest crosslinking efficiency peaking at 260 nm. Reaction time, ranging from minutes to hours, must be determined experimentally for ones sample. I found that irradiation of the sample with 254 nm UV light in a quartz cuvette equipped with a magnetic stir bar at either 4°C or room

temperature for either 5, 10, or 20 minutes resulted in nearly identical cross-linking efficiencies. No difference was seen between the two temperatures or with longer irradiation, suggesting that the reaction was essentially complete after 5 minutes. Analysis of the cross-linking reaction was performed by comparing the protein sample before and after irradiation on a Coomassie-stained 4-20% gradient SDS-PAGE gel, looking for the emergence of a cross-linked product in the irradiated sample equal to the molecular weight of the head + tail proteins (Figure 2B, 2C). Cross-linked products were then confirmed and analyzed using mass spectrometry.

Mass spectrometry analysis of photocross-linked products

In order to determine what region of the tail domain were interacting with the alpha 3/Switch I region of the motor domain we initiated a collaboration with Dr. Christine Cremo at the University of Nevada School of Medicine in Reno, Nevada in order to perform mass spectrometry on our cross-linked products. With the help of her technician, Paul Brewer, we were able to map the interaction surface between the head and the tail domains.

Samples of both protein mixtures before exposure to UV and after crosslinking were run on SDS-PAGE gels and stained with Coomassie brilliant blue G-250 dye to visualize protein bands. These gels were then sent to Dr. Cremo, where the cross-linked band was excised from the gel and subject to tryptic digestion to form peptides. The resulting tryptic peptides were analyzed by MALDI-MS. Sample preparation, trypsin digestion procedures, and mass spectral data analysis were performed in Dr. Cremo's lab essentially as described (74). Some of the digests were applied to a C18 PepMap 100 column (Dionex Corporation, Sunnyvale, CA) and chromatographed using a gradient from 2% acetonitrile, 0.1% formic acid, to 80% acetonitrile, 0.08% formic acid on an UltiMate 3000 Nano LC System (Dionex, Sunnyvale, CA) attached to a

Probot microfraction collector (LC Packings, Dionex, Sunnyvale, CA) spotting sample directly to a MALDI plate in 7 mg/ml α-cyano-4-hydroxy-cinnamic acid supplemented with 2% (wt/wt) ammonium citrate in 75% acetonitrile. Internal standards were insulin B-chain and angiotensin 1–7 clip. The sequence of the dimeric head K420CLM G234A S188C cross-linked to the tail construct containing residues 823–944 was confirmed by tandem mass spectrometry as described (74). The non-irradiated protein sample served as a control to eliminate background contaminants in the mass analysis. Peptides that were found to contain both head and tail sequences were used to map the interaction surface. The identity of the head peptide was known, as the tryptic pattern surrounding the single added-back cysteine can be predicted using the head sequence. Mass analysis of the tail portion thus allowed for identification of the short tryptic tail peptide cross-linked using the B4M at the indicated cysteine in the head. For all reactions except the K420CLM G234A S188C—Tail 823-944 crosslink, cross-linked products were found in "families", that is, several similar masses were identified that result from slight variations in the tryptic digest pattern. The existence of these families serves as positive identification of a cross-link. The K420CLM G234A S188C—Tail 823-944 tryptic product was confirmed by sequencing using tandem mass spectrometry (74).

Purification of the cross-linked product

We desired a structural view of how the head and tail were interacting in our cross-linked complex. To do this we turned to a collaboration with Dr. Chuck Sindelar at Lawrence Berkeley National Laboratories in order to perform Cryo-Electron Microscopy (cryo-EM) of monomeric K349CLM G234A cross-linked to Tail 823-944 through the added-back cysteine at residue S188C.

In order to average cryo-EM images for a structural view of the head-tail crosslink, described below, we required an abundance of cross-linked protein over free head in our sample. The final purification scheme using Talon resin is described in detail in the last paragraph under this heading. Our first attempt at removing free head from the K349CLM G234A S188C—Tail 823-944 crosslinked sample relied on the 6x-histidine tag present on the N-terminus of the tail. We expected that both the tail and the head-tail crosslink would bind to the Talon resin, while free head would not be retained. As expected, free tail and head-tail cross-links were indeed retained by the column. However, some free head remained in the sample, therefore we also examined the use of gel filtration and anion exchange chromatography as well as the use of phosphocellulose resin for purifying the head-tail cross-link.

We reasoned that the head-tail cross-linked product would elute before either the free head or free tail from the Super6 gel filtration column. However, under the conditions used, Binding buffer + 150 mM NaCl, all of the major proteins in the sample eluted in overlapping fractions without sufficient resolution to separate the head-tail crosslink from other proteins. This indicates that we are still getting association between the monomeric head and the tail protein under these conditions, and that the salt concentration would need to be raised in order to better separate proteins within the sample. This technique remains feasible for purification of the cross-link, however, we opted not to continue, as protein was diluted by the column. Eluting protein required concentration by precipitation in order for visualization by Coomassie staining, which is not an option in our purification for downstream uses. Western blotting would not only be time-expensive, but cannot be carried out for monomeric head proteins, as they do not react with Suk4, and the Tail constructs do not react well with a handful of commercially available antibodies raised against a 6x-histidine tag.

The MonoQ anion exchange column was also tested for its ability to separate head-tail cross-links from free head and tail. Again, we found that we got no separation of the cross-link from the other proteins in the sample. Additionally, the pH change to 8.0 thought to be useful for crosslink binding, as the K349 head requires this raise in pH, resulted in a fair amount of protein precipitation.

We also investigated how the Tail 823-963 protein behaved independently on phosphocellulose (PC) resin and the MonoQ anion exchange column (Bio-Rad, Hercules, CA). We found that while some of the tail was unable to bind to the PC resin, much of it remained bound until elution with high salt. This is very similar to the head alone and therefore would not be useful in removing any of our contaminants. It was also found that the Q column did not bind the tail particularly well either. Interestingly, we also had difficulty getting the K349CLM S188C protein to bind to either the PC resin or the MonoQ column under the binding buffer conditions. These are two columns routinely used to purify head constructs, so it was surprising that the head did not bind well to the resins under these conditions. This data in combination with the tail binding data makes the use of either of these columns less than ideal for the purification of the head-tail crosslink.

Overall none of these techniques seemed very useful for purifying the cross-linked product from the free head and tail proteins. The tail itself was problematic, as it was frequently found in some amounts in the column flow through, however still was able to bind to all of the columns under varying degrees. All in all, the combined results reveal that the use of binding buffer with a variety of our chromatographic procedures was problematic. The only option for purifying the cross-linked protein by these means would be to change the buffer conditions after the crosslinking reaction to those more suitable for our procedures. This would no doubt be a

difficult task as one must first buffer exchange while keeping the cross-linked protein soluble, then find a chromatographic procedure in which that buffer works to separate the proteins. If unsuccessful, one would have to change buffers again and repeat the experiments. This will be both time and protein expensive with no guaranteed results. With this in mind, the Talon purification scheme provided us with enough enrichment of the cross-linked protein and was therefore employed as our purification technique, detailed in the paragraph below.

After the K349CLM G234A S188C—Tail 823-944 crosslinking reaction was performed as described above, the protein sample was batch bound to Talon resin for 1 hour at 4°C with rotation. Resin was then poured into a Zebra spin concentrator (Pierce, Thermo Scientific, Rockford, IL) and washed using buffer containing 50 mM $NaPO_4$ buffer pH 7.0, 300 mM NaCl, 20 mM Imidazole, 2 mM $MgCl_2$, 5 mM βME, and 40 μM ADP. Protein bound to Talon resin was then eluted using buffer containing 50 mM $NaPO_4$ buffer pH 7.0, 300 mM NaCl, 500 mM Imidazole, 2 mM $MgCl_2$, 5 mM βME, and 40 μM ADP. Fractions containing significant amounts of protein as determined using Bradford reagent, were pooled together and spin concentrated roughly 4-fold in a 10,000 mwco spin concentrator spun at 10,000 rpm at 4°C. This sample was not buffer exchanged to prevent protein sticking to the membrane under lower salt conditions. Protein was then inserted into three separate 20 μl dialysis buttons, fitted with 6,000-8,000 mwco dialysis membrane and dialyzed for 1 hour 30 minutes into buffer containing 2.5 mM PIPES pH 6.8, 10 mM NaCl, 2 mM $MgCl_2$, 1 mM EGTA, 10 mM Imidazole, 5 mM βME, and 40 μM ADP. No precipitation was visible, therefore the salt concentration was further lowered by dialysis for an additional 1.5 hours into 2.5 mM PIPES pH 6.8, 5 mM NaCl, 2 mM $MgCl_2$, 1 mM EGTA, 5 mM Imidazole, 5 mM βME, and 40 μM ADP. Protein was removed from dialysis buttons using a G27 needle and stored in cryo vials for shipment on ice to Dr.

Chuck Sindelar for cryo-EM experiments. This technique resulted in the enrichment of the cross-linked head-tail product 3-fold, so that 65% of the heads in the sample were cross-linked to tails. While not ideal, the head-tail cross-link was abundant enough for Dr. Sindelar to obtain a sub-8 Å cryo-EM reconstruction of the head-tail interaction while bound to microtubules.

Cryo-EM of a head-tail cross-link

Photocross-linked protein partially purified and concentrated as detailed above was shipped overnight on ice for cryo-EM. The remaining cryo-EM experimental aspects were performed by Dr. Chuck Sindelar. Detailed methods can be found in reference 84. Briefly, partially purified head-tail cross-linked product was bound to microtubules. Images were averaged to improve the resolution of the reconstruction, yielding a nominal resolution of 8 Å as reported by the program RMEASURE (82).

**Section III: Experimental Results and Discussion**

A. Single cysteine add-backs in the Switch I region cross-link the tail

A specific cross-link between the head and tail *in trans* is formed with a single cysteine add-back at position S188C

Our K420CLM S188C + Tail 823-963 crosslinking sample dialyzed into binding buffer to promote head-tail association was transferred to a quartz cuvette equipped with a small stir bar, allowing for mixing on a magnetic stir plate. Cross-linking was initiated by irradiation with 254 nm UV light. Non-irradiated and irradiated samples were analyzed by Coomassie staining of 4-20% gradient gels, looking for the emergence of a cross-linked product in the irradiated sample equal to the molecular weight of the head plus tail proteins. After 5 minutes of

irradiation one can see the clear emergence of a sharp cross-linked band on the gel, along with selective loss of both the head and tail proteins (Figure 2C, left gel). This reaction was repeated with the same results using the shorter Tail 823-44 protein (Figure 2C, center gel). Crosslinking between the monomeric K349CLM S188C head construct and the shorter Tail 823-944 protein as well as with the added G234A mutation in the head discussed below (K349CLM G234A S188C) gave identical results. Importantly, the reaction was still successful using the monomeric head and the 27-mer tail peptide (Figure 2C, right gel). Both of these constructs lack the coiled-coil interacting regions, and are evidence that this direct interaction between the head and the tail can occur in the absence of additional stabilizing interactions. Approximately 25% of monomeric heads or 35% of dimeric heads cross-linked to tails or the 27-mer peptide. The crosslinking at position S188C was also independent of nucleotide state, as the emergence of cross-linked products was identical with ADP or the triphosphate analog AMPPNP.

The tail does not cross-link to the neck linker region

Crosslinking reactions between the tail and single cysteine add-backs in the neck linker region of the dimeric K420CLM protein (T328C, C330, V333C, E349C) were not successful. This reaction was performed in the presence of both ADP and ATP in the nucleotide pocket, to induce both the docked and undocked conformation of the neck-linker. Crosslinking at these locations was not found to be dependent on the nucleotide state. These residues had previously been shown to label well for others using maleimide probes (72), and labeled well with fluorescein-5-maleimide under identical conditions, however this percentage was never quantified. The lack of crosslinking thereby does not seem to be due to insufficient labeling of

these residues. The results therefore imply that the tail is not interacting with the neck linker region in either nucleotide state.

Additional cysteine add-backs in Switch I map the head-tail interaction

These results indicated that the tail domain was interacting specifically with the head very near to Switch I and the nucleotide pocket, as the S188C mutation is located at the end of the alpha 3 helix. As expected, this interaction did not require the presence of the extreme C-terminus of the tail domain (residues 945-963), as the shorter Tail 823-944 construct cross-linked with the same efficiency as the entire Tail 823-963 protein. The Tail 823-944 protein was therefore used for additional experiments, as it does not suffer from the proteolysis issues seen with the longer tail. With this data in hand we created additional single cysteine add-backs in the head in order to map the tail interaction. Crosslinking reactions were performed for single cysteine residues added back to the dimeric protein at positions S149C, D181C, A193C, M197C, and N198C.

Cross-linking reactions were successful between A193C, M197C, and N198C with both the Tail 823-944 protein and the 27-mer peptide. These residues are located in the conserved Switch I region of the motor, thus indicating that the tail was directly interacting with Switch I to inhibit nucleotide release. Unlike at position S188C, labeling and crosslinking at these positions resulted in proteins that were more susceptible to precipitation. This was not unexpected, as Switch I is an important mechanical element of the motor domain and misbehavior is most likely due to unnatural conformations of Switch I, resulting in the inability of the motor to bind nucleotide efficiently and thus precipitating. Increasing the nucleotide concentration and reducing the amount of B4M to an equal-molar ratio seemed to alleviate some of the solubility

problems. However, the amount of cross-linked protein remaining in solution for the A193C and M197C reactions was sufficient for both analyzing the success of the crosslinking reaction by Coomassie staining as well as mass spectrometry to determine the interacting region of the tail (discussed below).

K420CLM N198C cross-linked to the Tail 823-944 protein precipitated quite strongly upon crosslinking. The instability of this mutant is most likely attributed to the loss of a critical salt bridge that is formed though residue N198 (Chuck Sindelar, personal communication). This precipitation proved problematic in obtaining enough soluble protein to be loaded onto the gel without smearing of the bands. A successful cross-link could be seen, however the sample required concentration of the cross-link in order to be analyzed by MS. As native protein is not required, we attempted to purify the A193C cross-linked protein under denaturing conditions using the 6x-histidine tag found on the tail. After determining and adjusting for a pH change from the addition of 6 M guanidine hydrochloride to the sample in order to keep the pH around 8.0, the protein was denatured overnight at 4°C and then allowed to batch bind to Talon resin. After washing, bound protein was eluted from the column with 250 mM Imidazole, the highest concentration obtainable under our buffer conditions. Unfortunately it was found that a vast majority of our cross-linked protein was found in the column flow through under these conditions. Additional elution using 500 mM Imidazole in a lower concentration of guanidine did elute some of the cross-linked protein. The flow through and final elution fractions containing cross-linked product were sent for MS analysis as described below, however the protein was not well suited for mass spectrometry analysis and no results were obtained.

Residue D181C in the alpha 3 helix

Residue D181 is located on the opposite end of the negatively charged alpha3 helix as S188 (see Figure 5). Given the highly charged character of this helix and the plethora of positive charges found in the tail domain, we reasoned that the tail is very likely interacting electrostatically with the alpha 3 helix of the motor domain. We therefore selected to mutate residue D181 to a cysteine to perform our crosslinking experiment and confirm our proposal. However, we were not able to form a cross-link between the tail and K420CLM D181C. On hindsight, this is most likely due to lack of efficient labeling of this cysteine due to the local environment surrounding this residue. The high number of negative charges found on this face of the helix makes this cysteine highly unreactive to maleimide probes. DTNB assays were not performed to assess labeling efficiency, however a more properly placed mutant may successfully crosslink to the tail N-terminal to the region found to interact with S188C. Unfortunately mutagenesis attempts on this helix have been unable to produce an effect on regulation (Yao Wong, personal communication).

Residue S149C

The crosslinking reaction was also performed using the Tail 823-944 protein and the 27-mer peptide with a cysteine located at residue S149C in the motor domain (K420CLM S149C). This residue is located on the surface of the protein about 13 Å from residue S188 in the opposite direction of the nucleotide pocket (Figure 5C). While the peptide was able to rarely crosslink to the head labeled at this position, Tail 823-944 did crosslink with decent efficiency about 50% of the time. The experiment was repeated four times. On one occasion the 27-mer tail peptide efficiently cross-linked to the head at positions S149C. The success of these cross-linking

reactions seemed to be highly dependent on the amount of excess tail or tail peptide in the reactions. Results from the mass spectrometry analysis of this protein, discussed below, indicated that S149C was crosslinking to very similar regions of the tail peptide as residue S188C (Figure 5C). The Tail 823-944 protein, however, was found to cross-link with the head in two different positions, both N-terminal to the known tail coiled-coil region that interacts with the neck coiled-coil. Both of these sequence stretches are found nearer to the N-termini of the protein (Figure 5C). These results were at first confusing to us, but upon looking at the problem from a structural perspective one can attempt to make sense of the data. The 27-mer tail peptide results can easily be explained by the structure. Residue S149 is in roughly the same position as residue S188, just shifted to the side of the molecule, away from the nucleotide pocket. If positive charges in the tail are interacting electrostatically with the negative charges found on the outside face of the alpha 3 helix, one could imagine that if N-terminal regions of the tail were anchored at the bottom of alpha 3 (on the opposite end of the helix as S188), and if the C-terminal regions of the tail were somewhat disordered or flexible, a similar region of the tail that would crosslink to position S188C would be also be within the reach of the crosslinker attached to position S149C. The cross-linking results obtained with the Tail 823-944 protein are not as easily explained. As the ability to form a successful cross-link appeared dependent on the concentration of tail in the sample, it can be argued that the vast excess of protein in the sample allowed for rather “nonspecific” interactions to occur due to molecular crowding. It may be the case that the N-terminus of our tail proteins is flexible in solution, as they are N-terminal to the site thought to interact with the neck coiled-coil region of K420. When the tail is anchored to the neck coiled-coil and in the region around residue S188 through interactions with the head, the remaining N-terminal portions of the tail may be flexible and floppy enough to be in reach of a

crosslinker attached to residue S149C. The combined results therefore suggest that the head-tail interaction is fairly dynamic, however the crosslinking reaction involving residue S149C was only found to occur less than half of the time with an apparent dependence on the concentration of the tail in the sample, which suggests to me that it is possibly an experimental artifact, while on the other hand crosslinking at position S188C was robust for both the tail constructs the 27-mer tail peptide regardless of the amount of tail present in the crosslinking reaction.

B. Analysis of head-tail crosslinks using mass spectrometry

Residue C13 labels with B4M

During the mapping of the head-tail interaction, described below, mass spectrometry analysis of some of the cross-linked products revealed that we still contained another reactive cysteine in our sample. This cysteine was determined to be C13 by comparing the tryptic digest patterns of the three remaining cysteines in the CLM constructs with the mass spec results. This cysteine was left intact in the cysteine-light constructs, as it should be completely buried and not surface exposed. Previous work done labeling S188C within the same CLM background using fluorescent and gold labels did not indicate that this cysteine was reactive. However, as the mass spectrometry analysis can pick up even small amounts of this product, it is likely that the cysteine, while buried, can react slightly due to molecular breathing of the protein. To test how much of this cysteine is actually crosslinking, we repeated our crosslinking experiment using K420CLM with no additional cysteine residues added. We expected that if C13 is labeling and crosslinking significantly, this can be picked up by SDS-PAGE analysis of the crosslinking reaction. Analysis of Coomassie-stained SDS-PAGE gels did not indicate that appreciable amounts of C13 are crosslinking to the Tail 823-944 protein. As C13 cross-links were more

likely to be seen in the Switch I mutants it is possible that structural instability created by mutation of these conserved residues increases the structural dynamicity of the motor domain, exposing residue C13 for labeling more frequently than in stable constructs. Although the mass of the C13 trypsin products were similar to those of S188C, the presence of C13 in our crosslinking reactions did not affect the quality of data obtained by the mass spectrometer and did not compromise our results.

The regulatory QIAKPIRP motif of the tail cross-links to Switch I

The mass spectrometry analysis revealed that the monomeric K349 and dimeric K420 constructs containing S188C cross-linked to similar locations in the dimeric Tail 823-944 tail protein and the 27-mer peptide (Figure 5B). These data show that our head and tail constructs can associate specifically, regardless of whether the interaction of the neck coiled-coil and tail coiled-coil is intact. The presence of the additional G234A mutation had no effect on the region of the tail cross-linked to position S188C, demonstrating that the cross-linked product used for cryo-EM structural analysis described below is cross-linked at the same position. The locations of the single cysteine add-backs at residues S188C, A193C, and M197C on the kinesin-1 structure roughly form a line on the side of kinesin-1 leading from alpha 3 (S188C) into Switch I (A193C and M197C) (Figure 5A). The cross-links follow a pattern such that the region of the tail that cross-links to S188C is immediately N-terminal to the A193C and M197C cross-links (Figure 5B). Notably, A193C and M197C in Switch I cross-link directly to the conserved QIAKPIRP sequence of the tail, placing the absolutely necessary K922 in Switch I, near the nucleotide pocket. Because Switch I controls the rate of microtubule-stimulated ADP release by kinesin motors (70), an interaction of the QIAKPIRP sequence with Switch I is consistent with

the fact that this sequence inhibits microtubule-stimulated ADP release approximately 80-fold (62). The mechanism in which the tail is acting to inhibit the release of bound ADP was further examined using electron paramagnetic spectroscopy, or EPR. The work on this project was done in collaboration with Yao Wong, a graduate student in our lab, and can be found detailed in Chapter III of this thesis.

C. Cryo-EM of a head-tail cross-link

We desired a structural view of how the head and tail were interacting in our cross-linked complex. We thus set-up a collaboration with Dr. Chuck Sindelar at Lawrence Berkeley National Laboratories in order to perform Cryo-Electron Microscopy (cryo-EM) of monomeric K349CLM G234A cross-linked to Tail 823-944 through the added-back cysteine at residue S188C and partially purified using Talon resin as described in the methods section. The symmetry imposed by the microtubule filaments enables averaging of the MT-bound head-tail images, greatly improving the resolution of the cryo-EM reconstruction; full decoration of microtubules thus also increases the resolution. The G234A mutation in the head will allow for tight binding of the motor domain to microtubules in the presence of ADP and has been shown to have no effect on how the head and tail interact within the region surrounding S188C. In order to perform these experiments though, we first needed to ensure that the presence of the tail does not interfere with microtubule binding. To do this, we developed a reciprocal microtubule-binding/cross-linking assay described in the next section.

**Figure 5. Mass spectrometry analysis of cross-linked products**

A. Diagram model and partial sequences of kinesin-1 head and tail. Coloring and relative positions of head and tail elements are as in Figure 2*B*, except that positions of cysteine mutations used for cross-linking (S188C, A193C, and M197C) in the head are indicated, alpha 3/Switch I are in purple, and the β6 sheet immediately after Switch I is in green. Below, sequences of head (residues 172–212) and tail (residues 894–933) near the identified benzophenone-4-maleimide cross-links are shown. In the head sequence, residues 188, 193, and 197 of the head sequence are in bold, Switch I residues are bracketed, and the kinesin superfamily conserved SSRSH sequence in Switch I is underlined. In the tail sequence, the predicted break between the tail coiled-coil and globular tail is shown in the tail sequence (73). The 27-mer peptide sequence is bracketed, and the conserved regulatory QIAKPIRP sequence is underlined.

B. Cross-linked products in the Switch I region of the heads and tails identified by MALDI-MS. The cysteine mutation in the head and the constructs used for benzophenone-4-maleimide photocross-linking reactions are identified in the left column. Specific head-tail cross-links found in each reaction are shown in the two right columns, with a line connecting the head and tail peptide fragments found within each cross-linked product.

C. Structure of the kinesin-1 motor domain (PDB 1mkj) indicating the location of the S149C mutation. Coloring as in A, with positions S188C and S149C shown as yellow

and red spheres, respectively. The relative position of the head is rotated ~90° to the right from part A. Residue S188 lies roughly halfway between the bound ADP (blue) and residue S149.

D. Cross-linked products identified by MALDI-MS for the K420CLM S149C mutant and the Tail 823-944 and 27-mer tail peptide. A portion of the tail sequence (residues 843-933) is shown. The 27-mer peptide sequence is bracketed, and the conserved regulatory QIAKPIRP sequence is in bold. Portions of the Tail 823-944 protein that cross-linked to position S149C are in solid underline, while the fragment of the 27-mer peptide that cross-linked in this same location is indicated by a dashed line.

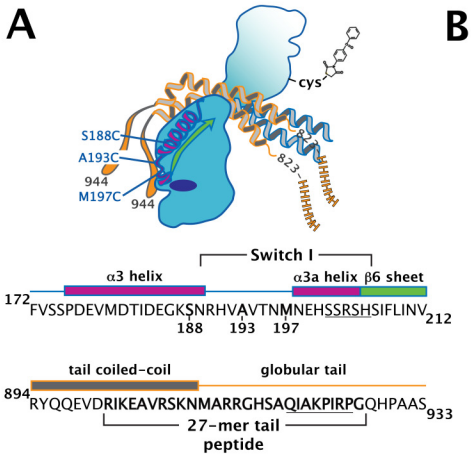
A
cys
S188C
A193C
944
M197C
944
823
Switch I
α3 helix
α3a helix β6 sheet
172 FVSSPDEVMDTIDEGKSNRHVAVTNMNEHSSRSHSIFLINV 212
188 193 197
tail coiled-coil
globular tail
894 RYQQEVDRIKEAVRSKNMARRGHSAQIAKPIRPGQHPAAS 933
27-mer tail peptide

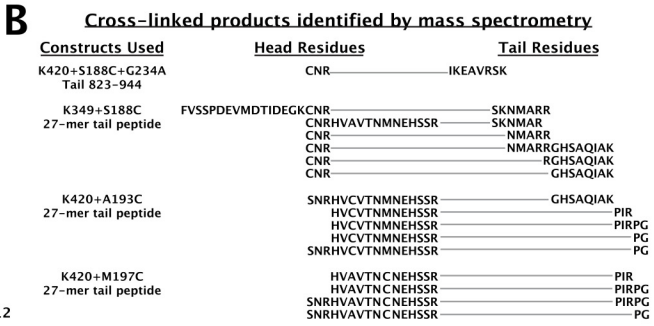
B
Cross-linked products identified by mass spectrometry
Constructs Used
Head Residues
Tail Residues
K420+S188C+G234A Tail 823-944
CNR IKEAVRSK
K349+S188C 27-mer tail peptide
FVSSPDEVMDTIDEGKCNR SKNMARR
CNRHVAVTNMNEHSSR SKNMAR
CNR NMARR
CNR NMARRGHSAQIAK
CNR RGHSAQIAK
CNR GHSAQIAK
K420+A193C 27-mer tail peptide
SNRHVCVTNMNEHSSR GHSAQIAK
HVCVTNMNEHSSR PIR
HVCVTNMNEHSSR PIRPG
HVCVTNMNEHSSR PG
SNRHVCVTNMNEHSSR PG
K420+M197C 27-mer tail peptide
HVAVTNCNEHSSR PIR
HVAVTNCNEHSSR PIRPG
SNRHVAVTNCNEHSSR PIRPG
SNRHVAVTNCNEHSSR PG

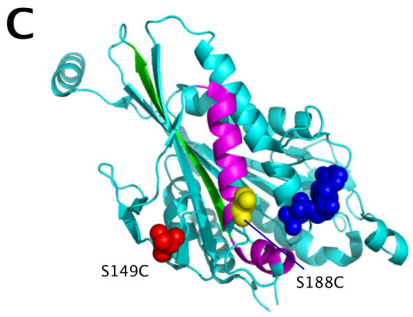
C
S149C
S188C

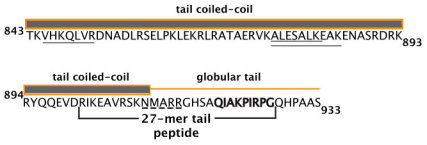
D
tail coiled-coil
843 TKVHKQLVRDNADLRSELPKLEKRLRATAERVKALESALKEAKENASRDRK 893
tail coiled-coil
globular tail
894 RYQQEVDRIKEAVRSKNMARRGHSAQIAKPIRPGQHPAAS 933
27-mer tail peptide

Reciprocal microtubule-binding/crosslinking assay

To ensure that the cross-linked product will bind strongly enough to microtubules in order to get the decoration necessary for cryo-EM averaging we investigated whether microtubule binding and cross-linking are mutually exclusive in a reciprocal experiment. As the K420 dimer can bind to microtubules with one head, leaving the other head in solution, we needed to use the monomeric K349 protein to ensure that we were directly analyzing microtubule binding.

We wanted to test whether the product from our K349CLM G234A S188C and Tail 823-944 crosslinking reaction could bind to microtubules as well as if crosslinking could occur on a microtubule-bound head. In order to do this, K349CLM G234A S188C was labeled with B4M as above. After removal of excess label and precipitates, Tail 823-944 was added to the sample and the mixture was allowed to dialyze into binding buffer as in the crosslinking reactions. Microtubules were prepared following our standard polymerization protocol from porcine tubulin purified in our lab. Final stock concentrations of microtubules were around 100 μM, and were stored at room temperature. After dialysis the head and tail mixture was given a hard spin to remove any precipitation and protein concentration was determined using Bradford reagent. The 13 μM solution was assumed to be mostly from the K349 head protein, as the Tail 823-944 does not react strongly with Bradford reagent. The experiment as designed was somewhat difficult to analyze, entirely due to the fact that tubulin and K349 are very close in molecular weight. Caution was therefore taken to ensure that the tubulin band is not too heavy, as a thick band makes visualization of the head-tail cross-linked product on a Coomassie-stained gel difficult.

The experimental design, diagramed in Figure 6A, was to divide the head + tail sample after dialysis into binding buffer into three parts: Part A contained 2/5$^{ths}$ of the head + tail sample. Polymerized microtubules were first added to this sample at 50% of the concentration of the head + tail sample. The K349CLM G234A S188C head labeled with B4M will bind strongly to microtubules under these conditions due to the G234A mutation. This sample containing MT-bound head was then divided into two. One half was then irradiated with 254 nm UV light to initiate the cross-linking reaction, while the other serves as a control. The experiment in Part A tested whether a MT-bound head could crosslink the tail.

Part B of the experiment contained 2/5$^{ths}$ of the head + tail sample. This sample was first irradiated to induce cross-linking between the head and tail. After crosslinking the sample was divided into two. One half had 50% microtubules added to it, while the other did not, serving as a crosslinking control. The samples in this part of the experiment were designed to test whether the cross-linked protein can still bind to microtubules. Part C contained 1/3$^{rd}$ of the sample had nothing more done to it, serving as a control. It was neither irradiated nor were microtubules added.

All samples from this experiment were spun over a 60% glycerol cushion in order to separate microtubule-bound protein from protein remaining in the supernatant. The acetone-precipitated supernatant and pellet fractions were resuspended in equal volumes of sample buffer and samples were run on an 8% SDS-PAGE gel in order to maximally separate the K349 and K349-Tail crosslink from the large tubulin band. Analysis of Coomassie-stained gels indicated that both the cross-linked head-tail product as well as the tail can bind to microtubules, and that microtubules do not inhibit crosslinking, as the tail can be efficiently cross-linked to MT-bound head (Figure 6B). Visualization of the K349 band is difficult as the microtubule concentration is

still quite high, however, the cross-linked band can easily be seen in comparison to the sample that was not irradiated.

This experiment was also repeated using the K420CLM G234A S188C dimer and the Tail 823-963 proteins yielding similar results. Additionally, identical results were obtained using K420CLM S188C bound to microtubules through the use of the triphosphate analog AMPPNP rather than the G234A mutation. However, as mentioned above, the use of the dimer prohibits us from distinguishing whether the cross-link is found on the microtubule-bound head or the head suspended in solution.

The results of these experiments confirmed that the head-tail cross-linked product could bind to microtubules. This important feature was necessary in order to obtain a cryo-EM reconstruction of the head-tail interaction and now allowed us to continue with our cryo-EM efforts. In order to achieve the efficient decoration of microtubules necessary for image averaging of the cryo-EM structure we needed to purify the cross-linked product to the best of our abilities. The main concerning contaminant is the uncross-linked head, as it will bind with similar efficiency to the microtubule lattice and images of the head alone and the head-tail cross-link will be averaged together. Therefore reducing the amount of free head in the sample was our main concern before sample analysis. The partial purification scheme developed for the cross-linked protein is detailed in the Section II methods.

**Figure 6. Microtubule-binding and cross-linking are not mutually exclusive**

A reciprocal microtubule-binding and cross-linking experiment. This experiment shows that cross-linked products of monomeric K349 heads with the G234A and S188C mutations and dimeric tails containing residues 822-944 bind to microtubules and, reciprocally, microtubule-bound monomeric heads can crosslink to tails. The same is true for the dimeric K420 head using the triphosphate nucleotide analog AMPPNP to bind tightly to microtubules rather than the G234A mutation.

A. Flow diagram describing the experiment for the monomeric K349CLM G234A S188C head with Tail 823-944. Letters A-E identifying samples in both the schematic and the gels. After labeling of the motor domain with benzophenone-4-maleimide, tails are added to sample and the mixture is dialyzed into binding buffer to induce association between the two domains. Head protein concentration after dialysis is roughly 13 μM by Bradford reagent (Pierce, Thermo Scientific, Rockford, IL). The experiment was then divided into three parts. Part 1 tests whether cross-linking can occur while the head is bound to microtubules. The G234A mutation, used for the monomeric K349 head, or AMPPNP, used in the dimeric K420 head, can be used to induce tight microtubule binding. Part 2 of the experiment tests whether cross-linked head-tail can bind to microtubules, and part 3 serves as a control. Part 1: +MT +/-XL: Two-fifths of the protein was incubated with microtubules (final concentration roughly 50% that of heads = 6.6 μM) + 10 μM taxol (Sigma) + 1 mM ADP. This reaction was split into two halves. One half was irradiated with 254 nm UV light for five minutes to

initiate cross-linking. These constitute the +MT +XL (A) and +MT –XL (B) samples. Part 2 XL +/- MT: Two-fifths of the protein was first irradiated with 254 nm UV light for five minutes. This sample was then divided into two, half of which was bound to microtubules as in part 1. These constitute the XL + MT (C) and XL –MT (D) samples. Part 3: One-fifth of the protein was left as a control. This is the –XL –MT (E) sample. All samples were then spun over a 60% glycerol cushion at 80,000 rpm in a TLA120.1 rotor (Beckman Coulter, Inc., Fullerton, CA) for 20 minutes at 25°C to separate the supernatant from the microtubule-bound pellet. Supernatants were acetone precipitated overnight and all pellets were resuspended in 50 μl of 1x sample buffer.

B. Coomassie-stained SDS-PAGE gel of a reciprocal microtubule binding and cross-linking experiment using monomeric K349CLM G234A S188C head protein and Tail 823-944 tail protein. The G234A mutation allows for tight microtubule binding in the presence of ADP, while the S188C mutation allows for labeling of the motor domain with benzophenone-4-maleimide. Experimental procedure as described in A. Lanes are as follows: SeeBlue Plus2 Prestained marker (Invitrogen), Tail 823-944 control, supernatant of A (+MT +XL), supernatant of B (+MT –XL), supernatant of C (XL + MT), supernatant of D (XL –MT), supernatant of E (-XL –MT), pellet of A (+MT +XL), pellet of B (+MT –XL), pellet of C (XL + MT), pellet of D (XL –MT), pellet of E (-XL –MT). The cross-linked band is indicated by the arrow and can clearly be seen in the microtubule pellet of part A (+MT +XL) and part C (XL + MT), indicating that crosslinking can occur while the head is bound to microtubules and the cross-linked head and tail are still able to efficiently be bound to microtubules. Below is a black-and-white image of the section

containing the cross-linked band from the same gel, in which the cross-linked bands are more discernable.

C. Coomassie-stained SDS-PAGE gel of a reciprocal microtubule binding and cross-linking experiment using dimeric K420CLM S188C head protein and Tail 823-963 tail protein. The triphosphate analog AMPPNP is used to induce tight microtubule binding of the motor domain. The experiment was performed as in A, B. Lanes are as follows: SeeBlue Plus2 Prestained marker, K420CLM S188C, K420CLM S188C-Tail 823-963 cross-linked product, supernatant and pellet of part A (+MT +XL), supernatant and pellet of part B (+MT –XL), supernatant and pellet of part C (XL + MT), supernatant and pellet of part D (XL –MT), supernatant of part E (-XL –MT). The cross-linked band is indicated by the arrow. As above, cross-linked protein is clearly visible in the microtubule pellet of part A (+MT +XL) and part C (XL + MT). However, due to the nature of the dimeric protein, it is not known whether the cross-linked head is the one bound to microtubules or the head in solution.

A

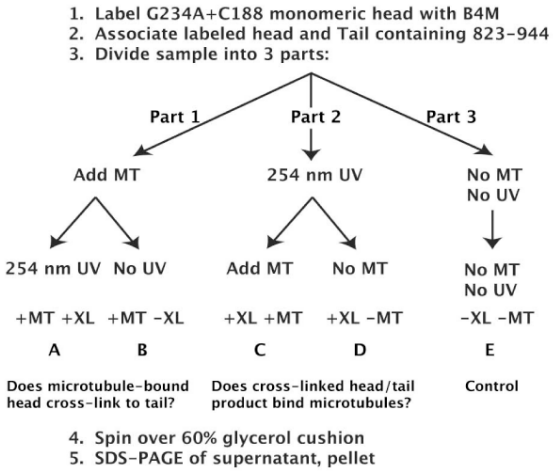
1. Label G234A+C188 monomeric head with B4M
2. Associate labeled head and Tail containing 823-944
3. Divide sample into 3 parts:
Part 1
Part 2
Part 3
Add MT
254 nm UV
No MT
No UV
254 nm UV
No UV
Add MT
No MT
No MT
No UV
+MT +XL
+MT -XL
+XL +MT
+XL -MT
-XL -MT
A
B
C
D
E
Does microtubule-bound head cross-link to tail?
Does cross-linked head/tail product bind microtubules?
Control
4. Spin over 60% glycerol cushion
5. SDS-PAGE of supernatant, pellet

B

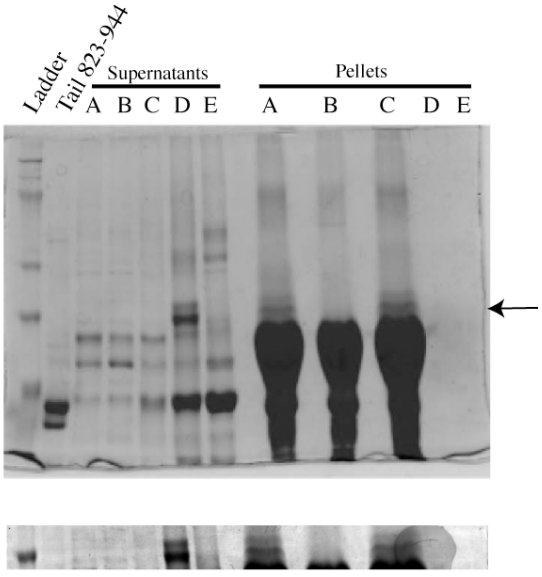
Ladder
Tail 823-944
Supernatants
Pellets
A B C D E
A B C D E

C

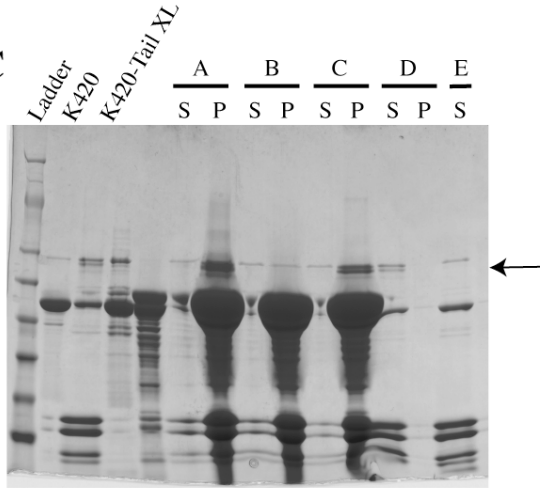
Ladder
K420
K420-Tail XL
A
B
C
D
E
S P S P S P S P S

Analysis of an 8 Å Cryo-EM Reconstruction of Cross-linked Head and Tail Bound to Microtubules

The purification of the cross-linked K349CLM G234A S188C—Tail 823-944 complex using Talon resin allowed for us to obtain a sub-8 Å structure of the head-tail interaction while bound to microtubules. This structure not only allows us to visualize the tail where it is cross-linked to the head at residue S188C on the end of the alpha 3 helix, but also contains an extensive contact between the tail and the Switch I region of the motor domain. Interestingly, the tail seems to hold the Switch I region of the head in a "solution-like" conformation in which the head has a high affinity for ADP. This conformation of Switch I has never before been seen for a microtubule-bound motor domain in any nucleotide state, suggesting that the tail is inducing this conformation to inhibit ADP release. Additionally, the tail makes simultaneous contacts with both the kinesin-1 head and the microtubule filament, suggesting that the tail may both regulate kinesin-1 in solution through the interaction of the QIAKPIRP tail motif with Switch I of the motor domain, and hold it in a parked state with high ADP affinity on microtubules. This structure has allowed us to gain insight into the inhibitory mechanism in which the tail is acting to hold ADP in the nucleotide pocket.

In our cryo-EM map, density for tubulin and the kinesin-1 head closely resembles that reported for the 8 Å nucleotide-free kinesin-1—microtubule complex (21) (Figure 7). We are also able to visualize considerable additional density corresponding to the cross-linked Tail 823-944 (yellow density). The tail appears as an elongated density parallel to the microtubule axis making simultaneous contacts with both the kinesin-1 head (Figure 7A) and the microtubule (Figure 7B). The precise structure of the tail cannot be determined from our map, however direct and specific head-tail contacts are readily apparent.

*The Tail contacts Switch I*

The crystal structures of monomeric human kinesin-1 (75) and bovine tubulin (76) were fitted into our cryo-EM density in order to identify specific residues in the head and microtubule that are involved in tail interactions. The most significant contact between the head and tail in our map encloses Switch I, including residues 193 and 197 (Figure 7A, magenta). Residue S188C is within 5 Å of density attributed to the tail, which is accordant with the fact that the head and tails used for this reconstruction were cross-linked at this location using our benzophenone-4-maleimide crosslinker. That residue S188C, A193, and M197 all appear either in or very near the tail density is consistent with our ability to specifically cross-link the tail to these residues in solution. In line with this, residues 328, 330, and 333 of the motor domain that we were unable to cross-link the tail to appear on the opposite side of the kinesin-1 head as the tail density in our reconstruction. (Figure 7A). In our map, a distinct gap can be seen between two adjacent head-tail complexes on the side of the motor domain where residues 328, 330, and 333 are located and the tail density of the other head (Figure 7C). This visual conformation and the cross-linking data allow us to conclude that the tail is not interacting with the neck linker region or on that face of the kinesin-1 head.

*The Tail-Switch I contact is specific*

The most prominent tail contact in our map is with Switch I of the kinesin-1 head. This interaction is extensive, as it is maintained when the reconstruction is rendered at isocontour levels in which no other head-tail or head-microtubule interactions are evident. In order to demonstrate that this tail-Switch I contact is specific, as opposed to the tail finding a convenient groove on the microtubule surface, as propositioned by one of our reviewers of the PNAS

publication, we produced an asymmetric microtubule density map (Figure 8). Normally data is reconstructed by averaging the thirteen microtubule protofilaments together, allowing for a large increase in the resolution of the map. However, in the asymmetric microtubule density map, data was reconstructed without averaging of the microtubule protofilaments. This 16 Å map, although of lower resolution compared to our fully averaged 8 Å density, preserves the specific geometry of the 13-protofilament microtubule, including the microtubule seam. Due to the geometry of 13-protofilament microtubules, there is a 40 Å offset of α and β tubulin subunits at the seam. This offset disrupts the usual position of the kinesin-1 heads immediately to the right side of the seam relative to the tubulin subunits immediately to the left side of the seam as viewed from above with the microtubule plus end located at the top of the image (Figure 8B). This disruption in the positioning of the heads relative to the adjacent protofilament allows us to determine whether the tail-Switch I contact is specific, or rather reflects a convenient crevice in the kinesin-1—microtubule interface of the tail to dock into. If the latter was true then the tail-Switch I contact would be absent at the microtubule seam, because this "convenient crevice" is altered in this location; the crevice formed by the kinesin-1 heads to the right of the seam and tubulin subunits to the left of the seam is different from everywhere else on the microtubule (Figure 8A). However, our asymmetric reconstruction of the head-tail cross-link clearly shows that the tail-Switch I contact is specific, as this contact is clearly and strongly preserved at the microtubule seam (Figure 8C), and would not be seen without specific interactions occurring between Switch I and the tail domain.

*The Tail holds Switch I in a "solution-like" conformation*

Not only does our 8 Å cryo-EM reconstruction show a strong and specific interaction between the tail and Switch I of the motor domain, but it also illuminates additional structural features about the head-tail interaction. The presence of the tail in our cryo-EM reconstruction confers unique structural attributes to the head that are consistent with the tail's regulatory function. These features can be easily seen if one compares our cryo-EM reconstruction of the head-tail complex on microtubules to the microtubule-bound nucleotide-free kinesin-1 cryo-EM structure (21) (Figure 7D-E). Fitting the x-ray crystal structure of ADP-bound kinesin-1 in solution (PDB 1mkj, 75, shown in dark blue) into the two cryo-EM reconstructions shows a distinct conformational change occurring in Switch I in the presence of the tail. The entire Switch I element from the solution-state crystal structure fits into the electron density assigned to Switch I in our cryo-EM reconstruction of the tail-bound kinesin-1 head on microtubules (Figure 7E, magenta). This is in stark contrast to the cryo-EM reconstruction of the nucleotide-free kinesin-1, in which the majority of the Switch I element of the solution-state structure is well outside the cryo-EM density (Figure 7D). Not surprisingly, the Switch I conformations seen in x-ray crystal structures of ADP-bound kinesin-1 representing the solution-state structure of the molecule (references 75, 77) are different from those found in cryo-EM reconstructions of microtubule-bound kinesin-1 in various nucleotide states (21, C.V.S and K.H.D., unpublished data, personal communication). This is consistent with the hypothesis that Switch I undergoes a conformational change upon microtubule binding in kinesin-1. Using the known movement of Switch I in myosin motors upon actin binding, the analogous movement of Switch I in kinesin-1 may weaken the ADP affinity of the motor, allowing for microtubule-stimulated ADP release (70). Conversely, as the conformation of Switch I found in x-ray crystal structures of ADP

bound kinesin-1 fit into the Switch I density in our cryo-EM reconstruction of the tail-bound kinesin-1—microtubule complex (Figure 7E), we propose that the tail inhibits ADP release by binding to Switch I and locking the head into a "solution-like" conformation with very high ADP affinity. This mechanism of inhibition is consistent with the known regulatory functions of the tail as well as explains tail-mediated inhibition of both microtubule-stimulated and basal ADP release.

*The Tail simultaneously interacts with Switch I and the microtubule*

The ability of the tail to hold the kinesin-1 head in a "solution-like" conformation with high ADP affinity is not the only regulatory information gleaned from our cryo-EM reconstruction. In addition to the Switch I contact, it is also visible in our map that the tail also makes simultaneous contact with the microtubule filament. Through these two contacts the tail could potentially park the tail-bound kinesin-1 head on the microtubule; the tail-microtubule contact allows the ADP-bound head, with a low affinity for microtubules, to remain bound to the microtubule, while the QIAKPIRP sequence of the tail simultaneously shuts down the enzymatic activity of the head by interacting with Switch I, inhibiting ADP release. Consistent with this idea, pauses have been observed in processive runs by single molecules of full-length but not truncated kinesin-1 (59). Tail-microtubule contacts are observed between the tail and the H10/S9 loop of both the α and β tubulin subunits (Figure 7B). The region of the tail contacting the β-tubulin subunit is near the location of the cross-link with S188 C in the head (Figure 5, approximately residues 913-915). This visualization is compatible with previous data demonstrating that residues 901-911 of the tail have nucleotide-independent microtubule-binding activity (62). Interestingly, residues 907-916 also constitute a portion of the binding site for Fez-

1, a protein that has been shown to activate kinesin-1 cargo transport (78). At first glance our hypothesized "parked state" appears to contradict the main function of tail-mediated regulation, which is to prevent kinesin-1 from productively engaging with and binding to microtubules, achieved by maintaining an ADP-bound state for the motor domain, in which the affinity for microtubule binding is quite low. However, the C-terminal residues not present in our truncated dimeric tail construct (residues 945-963), the Fez-1 protein, or other factors, may reversibly mask the tail-microtubule interaction seen here. This would enable regulatory partners of kinesin-1 to fully control the motile properties of the motor by inducing transitions between the regulated state in solution, our hypothesized paused state on microtubules, and the actively moving state on microtubules. The ability of kinesin-1 to remain microtubule-bound but still inhibited would allow for fine-tuning of the motor, affecting its movement while on microtubules by enabling it to pause its enzymatic activity but remain microtubule-bound. Kinesin-1 can thus be ideally positioned on the microtubule for effective molecular transport without futile consumption of ATP or mislocalization of the motor.

**Figure 7. Cryo-EM map of cross-linked head and tail bound to microtubules at 8 Å resolution**

A. View from outside the microtubule, with the plus end pointing up. Cyan head density, magenta Switch I density, white microtubule density, and yellow tail density were rendered by using the ‘‘Color Zone’’ function of University of California, San Francisco (UCSF) Chimera (80), by coloring the isosurface based on proximity to fitted crystal structures of tubulin and kinesin-1 (21). Atomic models of bovine tubulin (76) and human kinesin-1 (75) (dark blue ribbon) were fit into map density using the real-space docking function ‘‘Fit Model in Map’’ from UCSF Chimera. Sites for photocross-linking experiments are rendered in colored van-derWaals (VDW) spheres, where red indicates that specific cross-links were found, and green indicates they were not. ADP is rendered in VDW spheres. The head–tail contact at Switch I, where a magenta–yellow boundary occurs on the isosurface, is circled.

B. Side view, similar to *A* but rotated 90° about the vertical axis, with tail–microtubule contacts visible.

C. Reconstruction of head-tail complex showing tail contacting the head near Switch I and not near the neck linker. Coloring and kinesin-1 position are as in part A. The tail makes a contact with the left side of the kinesin-1 head near Switch I, and there is a visible gap between the right side of the kinesin-1 head near the neck linker and any tail density in the reconstruction.

D. Reconstruction of nucleotide-free kinesin-1 bound to microtubules, from reference 21. View, rendering, and color scheme are matched to *A* and *B*, and view orientation is intermediate between those of *A* and *B*. Switch I is out of density in this structure, as it is for several others at this resolution.

E. Kinesin-1 head–tail reconstruction with the same orientation, view, rendering, and color scheme. Switch I from the x-ray crystal structure (PDB ID code 1mkj) is within the cryo-EM density in this reconstruction, consistent with the tail holding Switch I in a ‘‘solution-like’’ state. See text for discussion.

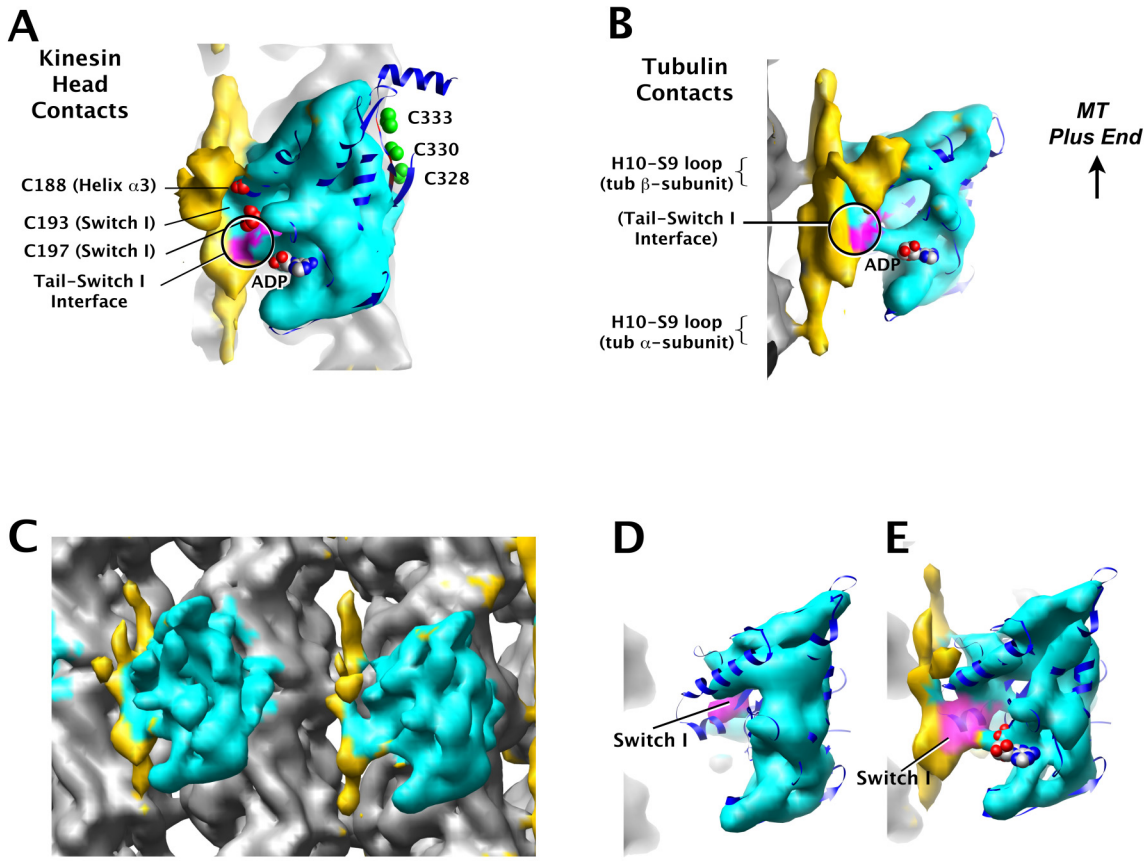
A
Kinesin
Head
Contacts
C333
C330
C328
C188 (Helix α3)
C193 (Switch I)
C197 (Switch I)
Tail-Switch I
Interface
ADP
B
Tubulin
Contacts
H10-S9 loop
(tub β-subunit)
(Tail-Switch I
Interface)
ADP
H10-S9 loop
(tub α-subunit)
MT
Plus End
C
D
Switch I
E
Switch I

**Figure 8. Asymmetric 13-protofilament microtubule map of kinesin-1 head-tail complex showing a specific Switch I/Tail contact at the microtubule seam**

A. Diagram models showing expected geometry of specific vs. nonspecific Switch I-tail contacts for tails at the microtubule seam versus elsewhere. Coloring is as in Figure 7. Microtubule plus end is up. To the left of the microtubule seam as with elsewhere on the microtubule (*Left*), the observed contacts from top to bottom are between the tail and β-tubulin, then Switch I, then α-tubulin. On the microtubule seam, the expected contacts depend on whether the tail-Switch I contact is specific or not because of the unique 40-Å shift in the lateral contacts between tubulin monomers at the seam. If the tail/Switch I contact is specific, then it will be preserved, occurring between the tail at the seam and the kinesin-1 head to the right side of the seam, at the expense of α- and β-tubulin contacts with the tail (*Center*). These tubulin contacts will be switched so that α-tubulin occurs at the top (where β-tubulin was in the *Left*), the preserved Switch I/tail contact is in the center, and the β-tubulin-tail contact occurs at the bottom. If the Switch I/tail contact is nonspecific, tubulin/tail contacts will be preserved at the seam while the Switch I/tail contact with the head to the right will be absent (*Right*). This is expected because the position of the heads on the right of the seam is shifted by 40 Å.

B. Section of an asymmetric map, colored as in *A*, microtubule plus end is up. The Switch I/tail contact is magenta, and the microtubule seam is denoted with a dashed line.

C. Side view (as in Figure 7*B*) of kinesin-1 head/tail complexes located one protofilament to the left of the seam (*Left*) and at the seam (*Right*). To the left of the seam, contacts are as expected in the *Left* of (*A*) above. At the seam, the Switch I/tail contact is preserved while tubulin/tail contacts are switched, as expected for a specific Switch I/tail contact.

# A. Expected Results of Asymmetric Map for Specific and Non-specific Head-Tail Contacts

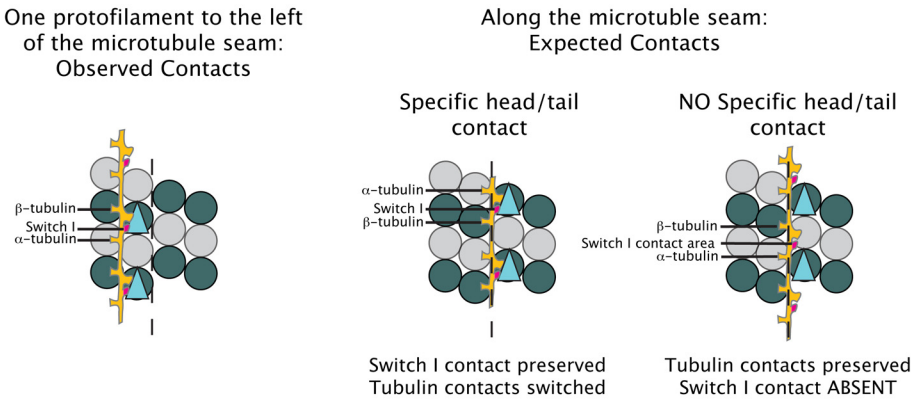


B.

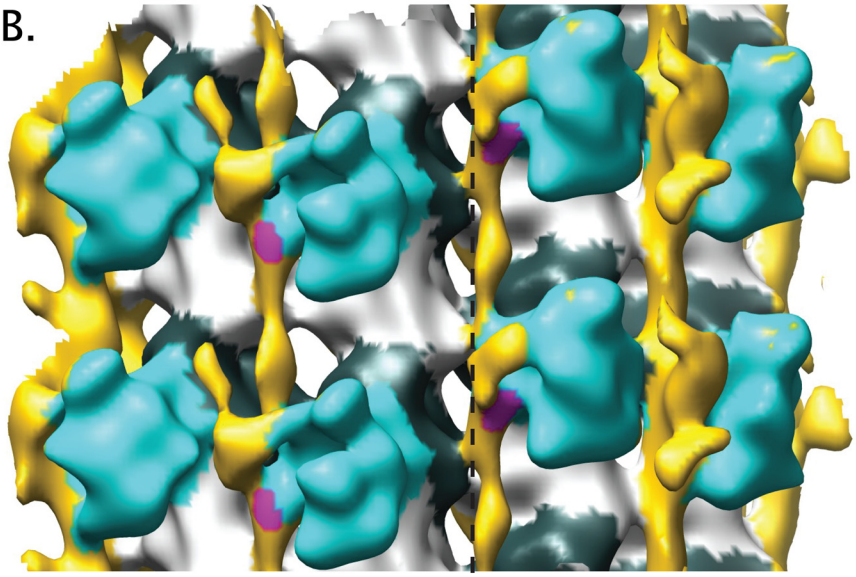

C.

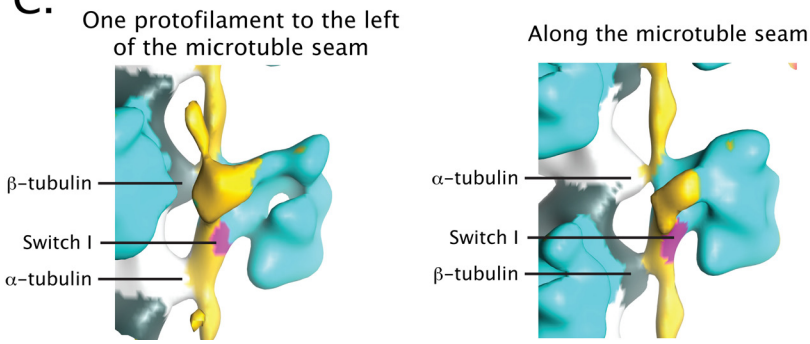

**Conclusions**

*In trans* cross-linking reactions between the head and tail domains of kinesin-1 using the heterobifunctional, photoreactive crosslinker benzophenone-4-maleimide have allowed us to obtain the first evidence for a direct interaction between the motor and tail domain. Importantly, this interaction does not require the stabilizing neck coiled-coil—tail coiled-coil interaction to occur, as cross-linking was efficient and specific using a monomeric K349 head and the 27-mer tail peptide, two constructs that both lack these coiled-coil interacting regions. In addition to proving that the kinesin-1 head and tail domains directly interact we were also able to map the location of this interaction. We found using MALDI mass spectrometry that the conserved regulatory QIAKPIRP sequence motif of the tail domain interacts directly with Switch I of the motor domain. This interaction not only seems to stabilize kinesin-1 in a solution-like conformation of Switch I, in which the motor's affinity for ADP is quite high, as visualized in our 8 Å cryo-EM reconstruction of the head-tail crosslink, but also places the absolutely necessary lysine 922 residue in close proximity to the nucleotide pocket. The role this regulatory lysine plays in the inhibitory mechanism as well as the tails in general, were investigated using spin-labeled nucleotides with electron paramagnetic resonance spectroscopy. While it was found that this lysine residue was not essential for formation of the head-tail interaction, it did play an important role in stabilizing bound-ADP in the nucleotide pocket. The work on this aspect of the project in collaboration with Yao Wong in our laboratory, has resulted in a manuscript is in preparation, and is presented in Chapter III.

Our ability to visualize the head-tail interaction while kinesin-1 was microtubule-bound using cryo-EM also allowed for us to hypothesize the existence of a parked state for kinesin-1 on microtubules, as simultaneous contacts between the tail and both Switch I of the motor domain

and the microtubule are visible. This "parked" state for kinesin-1 would allow for fine-tuning of the motors movement, as the existence of this state would allow for an inhibited, yet microtubule-bound, motor protein. Another graduate student in our lab, Mark Seeger is attempting to determine the specific interaction(s) between the kinesin-1 tail and the microtubule filament.

Kinesins and small GTPases share a common core structure and mechanism by which nucleotide binding and hydrolysis result in enzyme activation. It is therefore intriguing that the interaction of the conserved QIAKPIRP sequence in the kinesin-1 tail with Switch I of the motor domain is analogous to the manner in which several small GTPases are regulated. In light of the structural, enzymatic, and now regulatory, similarities between small GTPases and kinesin-1 it is tempting to suggest that targeting Switch I may be a common means of regulation for other members of the kinesin superfamily. This proposition was further investigated in the course of my graduate work using OSM-3, a Kinesin-2 family member that is also enyzmatically regulated by its C-terminal tail domain. While the project has not given us a definitive answer as to whether there is indeed a regulatory interaction between the OSM-3 tail and Switch I of the motor domain, the groundwork is set for future work on this project and the experimental tools are in place to test the hypothesis with this and other proteins. Details regarding this aspect of the project are found in Appendix II of this thesis.

**Section IV: Published Manuscript and Supplemental Information**

# The kinesin-1 motor protein is regulated by a direct interaction of its head and tail

Kristen A. Dietrich*, Charles V. Sindelar†, Paul D. Brewer‡, Kenneth H. Downing†, Christine R. Cremo‡, and Sarah E. Rice*§

*Department of Cell and Molecular Biology, Northwestern University, Chicago, IL 60611; †Life Sciences Division, Lawrence Berkeley National Laboratory, Berkeley, CA 94720; and ‡Department of Biochemistry and Molecular Biology, University of Nevada School of Medicine, Reno, NV 89557

Communicated by Edwin W. Taylor, Northwestern University Feinberg School of Medicine, Chicago, IL, April 15, 2008 (received for review December 12, 2007)

**Kinesin-1 is a molecular motor protein that transports cargo along microtubules. Inside cells, the vast majority of kinesin-1 is regulated to conserve ATP and to ensure its proper intracellular distribution and coordination with other molecular motors. Regulated kinesin-1 folds in half at a hinge in its coiled-coil stalk. Interactions between coiled-coil regions near the enzymatically active heads at the N terminus and the regulatory tails at the C terminus bring these globular elements in proximity and stabilize the folded conformation. However, it has remained a mystery how kinesin-1's microtubule-stimulated ATPase activity is regulated in this folded conformation. Here, we present evidence for a direct interaction between the kinesin-1 head and tail. We photochemically cross-linked heads and tails and produced an 8-Å cryoEM reconstruction of the cross-linked head–tail complex on microtubules. These data demonstrate that a conserved essential regulatory element in the kinesin-1 tail interacts directly and specifically with the enzymatically critical Switch I region of the head. This interaction suggests a mechanism for tail-mediated regulation of the ATPase activity of kinesin-1. In our structure, the tail makes simultaneous contacts with the kinesin-1 head and the microtubule, suggesting the tail may both regulate kinesin-1 in solution and hold it in a paused state with high ADP affinity on microtubules. The interaction of the Switch I region of the kinesin-1 head with the tail is strikingly similar to the interactions of small GTPases with their regulators, indicating that other kinesin motors may share similar regulatory mechanisms.**

cross-linking electron microscopy regulation switch

The motor protein kinesin-1 uses energy from ATP hydrolysis to move intracellular cargo to the microtubule plus end. Kinesin-1 is either regulated or activated for cargo movement in response to various cues, ensuring its proper localization and facilitating cargo transport to the right destination. The mechanism by which active kinesin-1 converts ATP hydrolysis into movement is fairly well established, but little is known about how kinesin-1 is regulated when it is not needed for cargo transport.

Regulated kinesin-1 adopts a folded conformation in which it remains very tightly bound to ADP and does not bind strongly to microtubules (1, 2). This folding can occur in the absence of kinesin light chains, although the light chains confer additional regulatory function (1, 3). In the folded conformation, the hinge II region of kinesin-1's coiled-coil stalk bends, and an interaction occurs between the neck coiled-coil and the tail coiled-coil (4–6). This interaction stabilizes the folded conformation, positioning the C-terminal globular tail domain near the enzymatically active heads [supporting information (SI) Fig. S1] (7, 8).

Kinetic data on tail-mediated regulation have shown that the folded conformation of kinesin-1 is not strictly necessary, nor is it sufficient for inhibition of ADP release by the heads. The conserved QIAKPIRP sequence in the C-terminal globular portion of the tail (residues 919–926 in human kinesin-1) is not required for kinesin-1 to fold, but deletion or mutation of this sequence abolishes regulation (1, 2, 9). The QIAKPIRP sequence specifically inhibits kinesin-1's initial microtubule-stimulated ADP release step, when it first engages on the microtubule (2). Short peptides containing the QIAKPIRP sequence but lacking any tail coiled-coil elements have also been shown to inhibit ADP release by truncated kinesin-1 heads (10). Oddly enough, a direct head–tail interaction has never been identified for kinesin-1, even in experiments using extensive mutagenesis and screening approaches, despite the fact that the kinetic data appear to demand it (6, 9). The interaction between the neck coiled-coil and tail coiled-coil elements could provide structural support for a relatively weak but direct head–tail interaction involving the critical QIAKPIRP sequence. The proposed direct head–tail interaction would then perform the critical regulatory function of preventing microtubule-stimulated ADP release and subsequent movement by kinesin-1.

The QIAKPIRP sequence of the tail inhibits kinesin-1's initial microtubule-stimulated ADP release step, while a region of the tail roughly 15 residues N-terminal to this sequence binds to microtubules (2, 5). If these two activities occurred simultaneously, kinesin-1 could pause in a state that is tightly bound to microtubules but inhibited in its ATPase activity and thus movement. Consistent with this idea, pauses have been observed in processive runs by single molecules of full-length but not truncated kinesin-1 (4). While regulation primarily prevents the heads from productively engaging with microtubules, it is intriguing to suggest that a second regulatory mechanism of the kinesin-1 tail may affect its movement on microtubules by enabling it to pause its enzymatic activity but remain microtubule-bound.

In this work, we show that a direct interaction occurs between the inhibitory QIAKPIRP sequence of the tail domain and the Switch I region in the head of kinesin-1 (residues 190–205). For kinesin motors and for small GTPases, Switch I plays a critical role in nucleotide binding and/or release (11–14). Thus, a Switch I–tail interaction is consistent with the known kinetic mechanism of tail-mediated regulation (2) and is analogous to the mechanisms by which GDP dissociation inhibitor proteins (GDIs) inhibit small GTPases[1] (10, 15). Our results also show that the tail can, at least in principle, bind to the heads and microtubule at the same time. This may create a paused state for kinesin-1 that can be modulated by other factors for additional regulation of motor activity.

Author contributions: K.A.D. and S.E.R. designed research; K.A.D., C.V.S., P.D.B., and C.R.C. performed research; K.H.D. contributed new reagents/analytic tools; K.A.D., C.V.S., C.R.C., and S.E.R. analyzed data; and K.A.D., C.V.S., C.R.C., and S.E.R. wrote the paper.

The authors declare no conflict of interest.

Data deposition: The cryo-EM map reported in this paper has been deposited into the Electron Microscopy Database (EMBD), no. EMD-5011.

§To whom correspondence should be addressed. E-mail: srice@northwestern.edu.

[1]Stock MF, Hackney DD, 48th Annual Biophysical Society Meeting, February 14–18, 2004, Baltimore, MD.

This article contains supporting information online at www.pnas.org/cgi/content/full/0803575105/DCSupplemental.

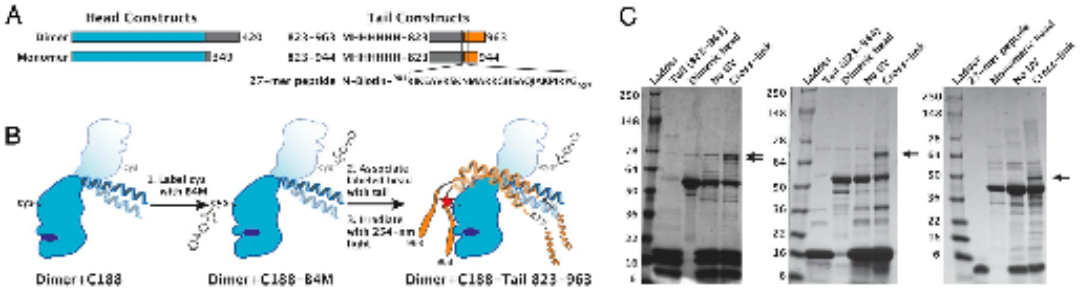


**Fig. 1.** Photocross-linking of kinesin-1 head and tail domains. (A) Head and tail constructs. Head residues are cyan, coiled-coil residues gray, and predicted globular tail residues are orange (17). Cysteine-light monomeric and dimeric head constructs have been described (19, 24). Dimeric tail constructs contain N-terminal 6x-histidine tags and residues 823–963 or 823–944. The 27-mer tail peptide (residues 901–927 with an N-terminal biotin tag) corresponds to the bracketed region of the dimeric tail constructs and is shown with the conserved QIAKPIRP underlined. (B) Photocross-linking scheme. Heads and tails are colored as in A with blue outlining on the neck coiled-coil and orange outlining on the predicted tail coiled-coil. The head in the foreground is positioned as if it were docked on a microtubule with the plus end up, the same orientation as the head in Fig. 3A. Cys-188 and bound ADP (blue ellipse) are shown. After conjugation to the maleimide moiety of the B4M (Center), heads were associated with tails, then irradiated to initiate photocross-linking (see Methods). A red star marks the cross-linked site (Right). Dimeric heads and tails are shown, but cross-linking was observed at position 188 using any combination of the head and tail constructs shown in A. We cannot determine whether one or both heads of a kinesin-1 dimer interact with the dimeric tail. This diagram model is consistent with our observed 50% cross-linking efficiencies (see Methods). An interaction between the neck coiled-coil and tail coiled-coil is shown, based on previous studies (4, 9). (C) SDS/PAGE gels (4–20%) showing photocross-linking. For the photo cross-linking experiment shown in the left gel, the heads contained Cys 188 and the G234A mutation, whereas in the others, the heads contain only the Cys 188 mutation. The tail constructs used for these experiments are indicated on each gel. Lanes for all gels are as follows: SeeBlue Plus2 Prestained Standard (Invitrogen), tail, head Cys 188, head tail before UV exposure, head tail after 5-min UV exposure. Bands marked with arrows contained both head and tail sequences, as verified by MALDI-MS.

## Results and Discussion

**Specific Association and Photocross-Linking of Kinesin-1 Heads and Tails.** We hypothesized that kinesin-1 regulation occurs through a direct interaction of the enzymatically active head with the C-terminal tail. To identify head–tail interactions, we combined separate truncated head and tail constructs (Fig. 1A) and allowed them to associate in trans. We used either monomeric or dimeric untagged human kinesin-1 heads having all reactive cysteines removed (referred to as cysteine-light). Truncated dimeric tail constructs consisted of either residues 823–963 or 823–944 with an N-terminal 6x-histidine tag. A monomeric N-terminally biotinylated 27-mer peptide containing the critical QIAKPIRP sequence of the tail was also used.

To demonstrate that kinesin-1 heads and tails associate, we performed a co-elution experiment (Fig. S2). We combined dimeric heads with dimeric tails containing residues 823–944. We flowed the combined heads and tails over TALON resin, which binds the 6x-histidine tag on the tails. After extensive washing, we performed sequential elutions using 10 and 100 M 27-mer tail peptide, followed by an imidazole elution. Kinesin-1 heads did not bind to TALON resin (Fig. S2A), but heads that were associated with tails were retained on the column. Because binding of heads to tails is relatively weak, some heads are visible in washes. Additional heads eluted after the addition of the 27-mer peptide, and the remaining heads and tails coeluted from the TALON resin after addition of imidazole (Fig. S2B). This result suggests that dimeric heads and tails interact, and the 27-mer tail peptide competes at least partially for the same binding site on the heads as the dimeric tail construct.

To test whether the head–tail interaction is specific, we added single reactive cysteines back to known locations on the monomeric or dimeric heads and photocross-linked them using benzophenone-4-maleimide (B4M), as described in Fig. 1B. We labeled the added cysteine with the maleimide moiety of the photocross-linker B4M, then combined heads and tails under conditions that allow them to associate (see Methods). We next irradiated the combined B4M heads and tails with 254-nm UV light, which initiates cross-linking of the benzophenone moiety to carbon-hydrogen bonds within 9 Å (16) (Fig. 1B). Formation of a head–tail cross-link indicates the tail may interact with the head near the position of the added cysteine. The collective results of several experiments suggest that cross-linking is specific. Head–head cross-links were not observed in any of our experiments, and efficient head–tail cross-linking was observed only for cysteines at certain locations in the head. In particular, cross-links were formed between tail proteins and cysteines added back to heads at positions 188 in the 3 helix (Fig. 1C) and positions 193 and 197 in Switch I (data not shown). In contrast, head–tail cross-links were not detected by using heads containing single cysteines in the neck linker region at positions 328, 330, or 333 (data not shown; see Fig. 3 and Movie S1 for cysteine locations).

We performed the B4M photocross-linking experiments as described above using either monomeric or dimeric head constructs containing Cys 188, in combination with each of the tail constructs shown in Fig. 1A. SDS/PAGE gels of all of these photocross-linking reactions revealed similar results. A sharp band appears on the gel with an apparent molecular weight equal to head and tail combined (Fig. 1C). The experiment using dimeric heads and tails containing residues 823–963 (left gel) shows two cross-linked products that differ in size by about 1.5 kDa. Both products (indicated by the double arrows) were excised and analyzed separately by mass spectrometry, and both contained peptides from both the head and tail. Therefore, we conclude that the smaller of these two products is due to cross-linking of the observed proteolytic product of this tail fragment. The size of this product is consistent with proteolysis occurring between residues 944 and 963. Previous experiments have shown that proteolysis of the kinesin-1 tail between residues 944 and 963 is common, and that residues C-terminal to 944 are not necessary for tail-mediated regulation of the heads' ATPase activity (2). Thus, we used either the tail construct containing residues 823–944 or the 27-mer tail peptide for all subsequent experiments of this study. Tail proteolysis is substantially reduced in the tail construct containing residues 823–944 (Fig. 1C, center gel), and completely eliminated in the 27-mer tail peptide (Fig. 1C, right gel), both of which still cross-link efficiently to heads containing Cys 188.

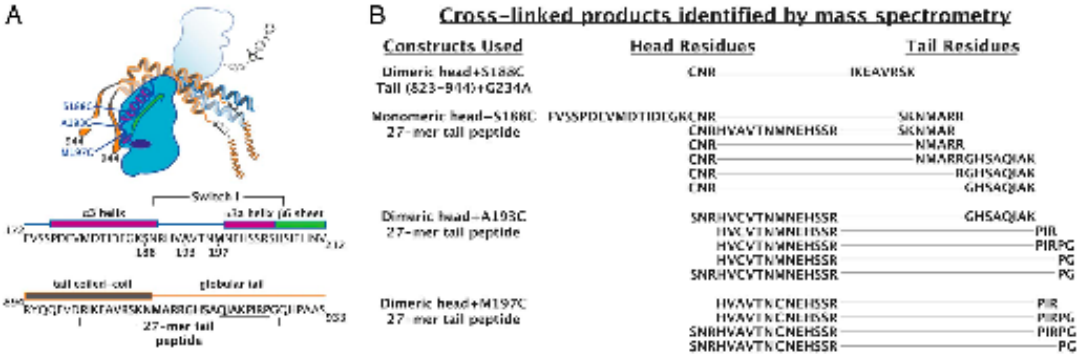


**Fig. 2.** Mass spectrometry analysis of cross-linked products. (*A*) Diagram model and partial sequences of kinesin-1 head and tail. Coloring and relative positions of head and tail elements are as in Fig. 1*B*, except that positions of cysteine mutations used for cross-linking (S188C, A193C, and M197C) in the head are indicated, 3/Switch I are in purple, and the 6 sheet immediately after Switch I is in green. Below, sequences of head (residues 172–212) and tail (residues 894–933) near the identified B4M cross-links are shown. Residues 188, 193, and 197 of the head sequence are in bold, Switch I residues are bracketed, and the kinesin superfamily conserved SSRSH sequence in Switch I is underlined. The predicted break between the tail coiled-coil and globular tail is shown in the tail sequence (17). The 27-mer peptide sequence is bracketed, and the conserved regulatory QIAKPIRP sequence is underlined. (*B*) Cross-linked products of heads and tails identified by MALDI-MS. The cys mutation in the head and the constructs used for B4M photocross-linking reactions are identified in the left column. Specific head-tail cross-links found in each reaction are shown in the two right columns, with a line connecting the head and tail peptide fragments found within each cross-linked product.

That monomeric heads cross-link efficiently to the 27-mer tail peptide (Fig. 1*C*, right gel) indicates the monomeric kinesin-1 head and 27-mer tail peptide can associate directly, albeit weakly, despite the fact that they lack the majority of the interacting neck and tail coiled-coil residues that stabilize kinesin-1's folded conformation (Fig. S1). This result is consistent with previous data indicating that short peptides containing the QIAKPIRP sequence have regulatory activity, and residues C-terminal to 944 are not necessary for the tail to bind to the head (2, 5, 10).

**Identification of Head–Tail Cross-Linked Products by MALDI-MS.** To identify the exact locations on the tail that cross-linked to the head, we excised cross-linked head tail bands from Coomassie-stained gels from the above experiments (Fig. 1*C*), digested with trypsin and analyzed the resulting peptides by MALDI-MS. Fig. 2*A* shows a diagram model of a cross-linked product of a kinesin-1 head and tail, with sequences corresponding to cross-linked regions in the head and tail below. The break between the coiled-coil tail and globular tail is shown to occur at residue 910, as predicted by the COILS program (17).

Fig. 2*B* summarizes the results of several B4M cross-linking experiments analyzed by MALDI-MS. Head and tail constructs used for each cross-linking experiment are shown on the left. Cross-linked, trypsinized peptides identified by MALDI-MS that contained both head and tail sequences are indicated for each reaction on the right, joined by a line. For each of these products, the position of the cross-link on the head is at the added cysteine residue, and the position on the tail is within the peptide sequence displayed. The sequence of the cross-linked product of the dimeric head G234A S188C and the dimeric tail containing residues 823–944 was confirmed by sequencing using tandem mass spectrometry as described in ref. 18. All other cross-linked products occurred in "families," that is, several similar masses were identified that result from slight variations in the tryptic digest pattern. Families of cross-linked products are grouped together in Fig. 2*B*. The existence of these families serves as positive identification of a cross-link (18).

Monomeric and dimeric head constructs containing Cys 188 cross-linked to similar locations in the 27-mer tail peptide and the dimeric tail construct. These data show that our head and tail constructs can associate specifically, regardless of whether the interaction of the neck coiled-coil and tail coiled-coil is intact. The locations of the single cysteine addbacks at residues 188, 193, and 197 on the kinesin-1 structure roughly form a line on the side of kinesin-1 leading from 3 (Cys 188) into Switch I (Cys 193 and 197) (Fig. 2*A*). The cross-links follow a pattern such that the region of the tail that cross-links to Cys 188 is immediately N-terminal to the Cys 193 and Cys 197 cross-links. Notably, Cys 193 and Cys 197 in Switch I cross-link directly to the conserved QIAKPIRP sequence of the tail. Because Switch I controls the rate of microtubule-stimulated ADP release by kinesin motors (14), an interaction of the QIAKPIRP sequence with Switch I is consistent with the fact that the sequence inhibits microtubule-stimulated ADP release approximately 80-fold (2).

**Visualization of Head–Tail Interactions by CryoEM.** To gain a detailed structural picture of the regulatory head–tail interaction, we performed cryoEM on microtubules decorated with head–tail products that were first photocross-linked at Cys 188 as before, then enriched using TALON affinity purification (see Methods). Although this material is enriched for the cross-linked product, some non-cross-linked material was present. For these experiments, we used G234A, a head mutant that binds tightly to microtubules regardless of nucleotide state (19). The cross-linked product of monomeric G234A heads and the tail protein containing residues 823–944 binds tightly to microtubules in the presence of ADP. We expect that the G234A mutation enables the heads to remain tightly bound to the microtubule while the tail prevents ADP release. It is possible that the Switch I–tail contact with wild-type kinesin-1 is primarily formed in solution, but by using the G234A mutant, we have imaged the interaction of the head and tail using cryoEM on microtubules.

In our 8-Å cryoEM map, shown in Fig. 3, density for tubulin and kinesin-1 closely resembles that reported for the 8-Å nucleotide-free kinesin-1–microtubule complex (11). Considerable additional density corresponds to the cross-linked tail (yellow density in Fig. 3). The tail appears as an elongated density parallel to the microtubule axis and makes simultaneous contacts with the kinesin-1 head (Fig. 3*A*) and the microtubule (Fig.

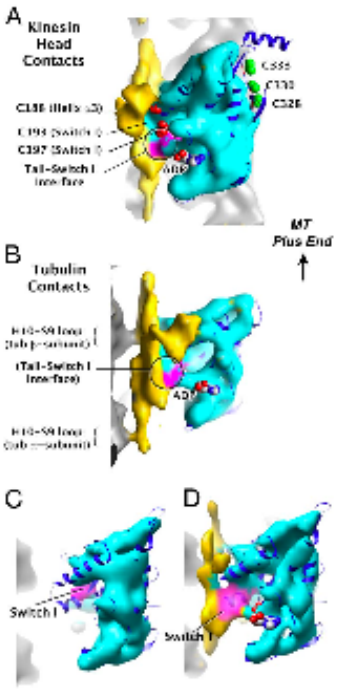


**Fig. 3.** CryoEM map of cross-linked head and tail bound to microtubules at 8-Å resolution. (A) View from outside the microtubule, with the plus end pointing up. Cyan head density, magenta Switch I density, white microtubule density, and yellow tail density were rendered by using the "Color Zone" function of University of California, San Francisco (UCSF) Chimera (27), by coloring the isosurface based on proximity to fitted crystal structures of tubulin and kinesin-1 (11). Atomic models of bovine tubulin (21) and human kinesin-1 (20) (dark blue ribbon) were fit into map density using the real-space docking function "Fit Model in Map" from UCSF Chimera. Sites for photocross-linking experiments are rendered in colored van-derWaals (VDW) spheres, where red indicates that specific cross-links were found, and green indicates they were not. ADP is rendered in VDW spheres. The head–tail contact at Switch I, where a magenta–yellow boundary occurs on the isosurface, is circled. (B) Side view, similar to A but rotated 90° about the vertical axis, with tail–microtubule contacts visible. (C) Reconstruction of nucleotide-free kinesin-1 bound to microtubules, from ref. 11. View, rendering, and color scheme are matched to A and B, and view orientation is intermediate between those of A and B. Switch I is out of density in this structure, as it is for several others at this resolution. (D) Kinesin-1 head–tail reconstruction with the same orientation, view, rendering, and color scheme. Switch I from the x-ray crystal structure (PDB ID code 1mkj) is within the cryoEM density in this reconstruction, consistent with the tail holding Switch I in a "solution-like" state. See text for discussion.

3B). Although we cannot deduce the precise structure of the tail from this map, direct and specific head–tail contacts are readily apparent. These are described in detail below.

To identify specific residues involved in tail interactions with the head and the microtubule, we fitted the crystal structures of monomeric human kinesin-1 (20) and bovine tubulin (21) into our map. Residue 188 is within 5 Å of the tail density, consistent with the fact that the heads and tails used for this cryoEM reconstruction were cross-linked together by B4M at this location. The most significant contact between the head and tail in our map encloses residues 193 and 197 in Switch I (Fig. 3A, magenta). That residues 188, 193, and 197 all appear within or very near the tail density in our cryoEM map is consistent with the specific cross-linking of the tail to these residues, shown in Fig. 2. Also consistent with our photocross-linking data, locations that did not cross-link to the tail (328, 330, and 333) appear on the opposite side of the kinesin-1 head from the tail density in our cryoEM map (Fig. 3A, Movie S1). Looking at two adjacent kinesin-1 head–tail complexes in this 8-Å reconstruction, a distinct gap can be seen between the side of a kinesin-1 head where residues 328, 330, and 333 are located, and the tail corresponding to the adjacent head (Fig. S3). Thus, we conclude that the tail interacts with the side of the kinesin-1 head near Switch I, and it does not interact with the side of the head near the neck linker.

The most prominent contact made by the tail in our map is with Switch I of the head. This is an extensive interaction, because it is maintained even if the cryoEM reconstruction is rendered at isocontour levels where no other head–tail and head–microtubule interactions are evident (Movie S1). To demonstrate that this tail–Switch I contact is specific, we produced an asymmetric microtubule density map by reconstructing our data without averaging the 13 protofilaments together (Fig. S4).

Although the asymmetric map shown in Fig. S4 is of lower resolution compared with our fully averaged 8-Å map (16 Å; see Methods), it preserves the specific geometry of the 13-protofilament microtubule, including the seam. The 40-Å offset of and tubulin subunits at the seam disrupts the usual position of the heads immediately to the right side of the seam relative to tubulin subunits immediately to the left side of the seam. Therefore, if the Switch I–tail contact simply reflected a convenient crevice in the kinesin-1–microtubule interface for the tail to dock into, it would be absent at the microtubule seam, because the crevice formed by the kinesin-1 heads to the right of the seam and tubulin subunits to the left of the seam is different from everywhere else on the microtubule (Fig. S4A). However, the asymmetric reconstruction shows that the Switch I–tail contact is clearly preserved and appears strong for tails lying along the seam (Fig. S4C). This would be seen only for a specific contact between the tail and Switch I.

**The Tail Induces the Head to Adopt a Conformation with High ADP Affinity.** The presence of the tail in our cryoEM reconstruction confers unique structural features to the head that are consistent with the tail's regulatory function. Fig. 3C shows the microtubule-bound nucleotide-free kinesin-1 structure (11) for comparison to our tail-bound structure (Fig. 3D). The entire Switch I element from the x-ray crystal structure of ADP-bound kinesin-1 [1mkj, dark blue (20)] fits into the electron density assigned to Switch I in our cryoEM reconstruction of the head–tail complex on microtubules (Fig. 3D, magenta). This is in stark contrast to the cryoEM reconstruction of nucleotide-free kinesin-1 without bound tail (Fig. 3C), in which the majority of the Switch I element from the x-ray crystal structure is well outside the cryoEM density. Indeed, the Switch I conformations seen in x-ray crystal structures of ADP-bound kinesin-1 (20, 22) are different from those found in cryoEM reconstructions of kinesin-1-microtubule complexes in various nucleotide states (ref. 11; C.V.S. and K.H.D., unpublished data). These data are consistent with the hypothesis that Switch I moves when kinesin-1 binds to microtubules. By analogy to the known movement of Switch I in myosin motors upon actin activation, the movement of Switch I may weaken kinesin-1's ADP affinity, allowing for microtubule-stimulated ADP release (14). Conversely, because the conformation of Switch I found in x-ray crystal structures of ADP-bound kinesin-1 fit into Switch I density in our cryoEM reconstruction of the tail-bound kinesin-1–microtubule complex (Fig. 3D), we hypothesize that the tail inhibits ADP release by binding to Switch I and locking the head into a "solution-like" conformation with very high ADP affinity.

**A "Paused" State for Kinesin-1 on Microtubules.** In our map, the tail makes simultaneous contacts with the microtubule and Switch I. Through these two contacts, the tail could potentially pause the head on the microtubule, so it would be bound through the microtubule–tail contact while the QIAKPIRP sequence of the tail simultaneously shuts down the head by interacting with Switch I. Tail–microtubule contacts are observable between the tail and both the and tubulin subunits in the H10/S9 loop (Fig. 3B). The region of the tail that contacts -tubulin is near the Cys 188 cross-link (Fig. 2, approximately residues 913–915), consistent with previous data showing that residues 901–911 of the tail have microtubule-binding activity (2). Residues 907–916 of the tail also constitute a portion of the binding site for the Fez-1 protein that activates cargo transport (23). Our hypothesized "paused state" appears to contradict the main function of tail-mediated regulation, which is to prevent kinesin-1 from binding to microtubules. However, the C-terminal residues that were not present in our truncated dimeric tail construct, the Fez-1 protein, or other factors, may reversibly mask the tail–microtubule interaction. This would enable regulatory partners of kinesin-1 to fully control its motile properties by inducing transitions between its regulated state in solution, our hypothesized paused state on microtubules, and the actively moving state on microtubules.

**Switch I Is a Common Regulatory Target for Kinesin-1 and Small GTPases.** Kinesins and small GTPases share a common core structure and mechanism by which nucleotide binding and hydrolysis result in enzyme activation. It is therefore intriguing that the interaction of the conserved QIAKPIRP sequence in the kinesin-1 tail with Switch I is analogous to the manner in which several small GTPases are regulated. In light of the structural, enzymatic, and now regulatory, similarities between small GTPases and kinesin-1 it is tempting to suggest that targeting Switch I may be a common means of regulation for other members of the kinesin superfamily.

## Methods

**Constructs Used (Fig. 1 *A*).** Untagged cysteine-light monomeric and dimeric head constructs of human kinesin-1 heavy chain were received from R. Vale (University of California, San Francisco). These constructs were expressed and purified as described (24). Tail constructs were created by PCR by using a full-length human kinesin-1 clone from R. Vale and purified by using TALON resin (Clontech). Full details on cloning and purification of tail constructs are described SI Text. The 27-mer tail peptide (residues 901–927 with an N-terminal biotin tag) was purchased from GenScript. The biotin tag was not used for any specific purpose in this study.

**Photocross-linking with B4M.** Heads were dialyzed into labeling buffer (25 mM Hepes, pH 7.5; 100 mM NaCl; 2 mM $MgCl_2$; 1 mM EGTA; 200 M Tris(2-carboxyethyl) phosphine hydrochloride, 50 M ADP) at 4°C. A 5-fold molar excess of B4M (Invitrogen) was added to 1–2 mg/ml head and reacted for 12 h in the dark. The reaction was quenched with 25 mM 3-mercaptoethanol( ) and excess label removed by repeated spin concentration in centrifugal filter devices (Millipore) into binding buffer (50 mM K-acetate; 10 mM Tris-acetate, pH 7.0; 4 mM $MgSO_4$; 20 mM imidazole; 5 mM ME; 40 M ADP) plus 300 mM NaCl. Approximately 90% of kinesin-1 heads reacted with B4M under these conditions, as measured by 5,5 -dithiobis 2-nitrobenzoic acid (Pierce) assay. TALON-purified tails were added to yield an approximate ratio of five tails:one head. The combined proteins were dialyzed into binding buffer for 3 h, spun 10 min at 355,000 g to remove any aggregates, then irradiated for 5 min with 254-nm UV light. Approximately 25% of monomeric heads or 35% of dimeric heads cross-linked to tails or the 27-mer peptide.

**Mass Spectrometry Analysis of Photocross-Linked Products.** Sample preparation and trypsin digestion procedures for mass spectrometry and mass spectral data analysis were essentially as described (18). Some of the digests were applied to a C18 PepMap 100 column (Dionex) and chromatographed using a gradient from 2% acetonitrile, 0.1% formic acid, to 80% acetonitrile, 0.08% formic acid on an UltiMate 3000 Nano LC System (Dionex) attached to a Probot microfraction collector (LC Packings) spotting sample directly to a MALDI plate in 7 mg/ml -cyano-4-hydroxy-cinnamic acid supplemented with 2% (wt/wt) ammonium citrate in 75% acetonitrile. Internal standards were insulin B-chain and angiotensin 1–7 clip. The sequence of the dimeric head G234A S188C cross-linked to the tail construct containing residues 823–944 was confirmed by tandem mass spectrometry as described (18).

**Protein Preparation, Grid Preparation, and Data Analysis for CryoEM.** Photocross-linked protein was batch bound to TALON resin (Clontech) for 1 h at 4°C. Resin was washed with TALON buffer (50 mM phosphate buffer, pH 7.0; 20 mM imidazole; 2 mM $MgCl_2$; 5 mM ME; 40 M ADP) plus 300 mM NaCl, eluted with TALON buffer plus 300 mM NaCl plus 500 mM imidazole, and spin-concentrated as described above. This step enriched the cross-linked product 3-fold, so that 65% of heads were cross-linked to tails. Protein was dialyzed for 1.5 h each into EM buffer (2.5 mM Pipes, pH 6.8; 2 mM $MgCl_2$; 1 mM EGTA; 5 mM ME; 40 M ADP) plus 10 mM NaCl plus 10 mM imidazole, then EM buffer plus 5 mM NaCl plus 5 mM imidazole, and shipped overnight on ice for cryoEM. Microtubules were prepared as described (11) but with no added kinesin-1 or apyrase; after the final ultracentrifuge step, the microtubules were resuspended in a final volume of 7.5 l in a buffer of 25 mM Pipes, pH 6.8; 25 mM KCl; 1 mM EGTA; 1 mM $MgCl_2$. For each specimen, 0.4 l of microtubules was added to 3 l of distilled water and applied to a nonglow-discharged homemade holey carbon grid. After wicking away the excess fluid with filter paper, 2 l of head–tail cross-linked product was applied; after 60 sec of incubation, the grid was blotted and plunge-frozen in liquid ethane. Data collection and image processing were performed as described in ref. 11, using the nucleotide-free kinesin–1-microtubule complex of that work as an initial reference. Approximately 400,000 particles were incorporated into the final dataset. Six cycles of reference matching and volume reconstruction were carried out as described (11), yielding a nominal resolution of 8 Å as reported by the program RMEASURE (25), in agreement with Fourier Shell Correlation comparisons using two independent sets of particles (26).

**ACKNOWLEDGMENTS.** We thank R. Vale for constructs; M. Seeger, S. McBrayer, M. Wallace, D. Quilici, and R. Woolsey for assistance; Park Packing Company for supplying material for tubulin preparation; and the COBRE Proteomics core facility supported by COBRE Grant 1P20RR018751. K.A.D. is supported by National Institutes of Health Grant T32 GM008382, S.E.R. is supported by National Institutes of Health Grant 5 R01 GM072656-02, and C.R.C. by National Institutes of Health Grant 5 R01 AR040917-18. C.V.S. and K.H.D. are supported by National Institutes of Health Grants GM46033 and GM51487 and by the U.S. Department of Energy under contract no. DE-AC02-05CH11231. The mass spectral work was performed at the Nevada Proteomics Center at the University of Nevada, Reno, funded by National Institutes of Health Grant P20 RR-0164-05 from the Nevada IDeA Network of Biomedical Research Excellence (INBRE) Program of the National Center for Research Resources.

1. Cai D, Hoppe AD, Swanson JA, Verhey KJ (2007) Kinesin-1 structural organization and conformational changes revealed by FRET stoichiometry in live cells. J Cell Biol 176:51–63.
2. Hackney DD, Stock MF (2000) Kinesin's IAK tail domain inhibits initial microtubule-stimulated ADP release. Nat Cell Biol 2:257–260.
3. Verhey KJ, et al. (1998) Light Chain-dependent Regulation of Kinesin's Interaction with Microtubules. J Cell Biol 143:1053–1066.
4. Friedman DS, Vale RD (1999) Single-molecule analysis of kinesin motility reveals regulation by the cargo-binding tail domain. Nat Cell Biol 1:293–297.
5. Stock MF, et al. (1999) Formation of the compact confomer of kinesin requires a COOH-terminal heavy chain domain and inhibits microtubule-stimulated ATPase activity. J Biol Chem 274:14617–14623.
6. Bathe F, et al. (2005) The complex interplay between the neck and hinge domains in kinesin-1 dimerization and motor activity. Mol Biol Cell 16:3529–3537.
7. Hackney DD, Levitt JD, Suhan J (1992) Kinesin undergoes a 9S to 6S conformational transition. J Biol Chem 267:8696–8701.
8. Hisanaga S, et al. (1989) The molecular structure of adrenal medulla kinesin. Cell Motil Cytoskeleton 12:264–272.
9. Seiler S, et al. (2000) Cargo binding and regulatory sites in the tail of fungal conventional kinesin. Nat Cell Biol 2:333–338.
10. Yonekura H, et al. (2006) Mechanism of tail-mediated inhibition of kinesin activities studied using synthetic peptides. Biochem Biophys Res Commun 343:420–427.
11. Sindelar CV, Downing KH (2007) The beginning of kinesin's force-generating cycle visualized at 9-A resolution. J Cell Biol 177:377–385.
12. Himmel DM, et al. (2002) Crystallographic findings on the internally uncoupled and near-rigor states of myosin: Further insights into the mechanics of the motor. Proc Natl Acad Sci USA 99:12645–12650.
13. Willard FS, Kimple RJ, Siderovski DP (2004) Return of the GDI: The GoLoco motif in cell division. Annu Rev Biochem 73:925–951.
14. Kull FJ, Endow SA (2002) Kinesin: Switch I and II and the motor mechanism. J Cell Sci 115:15–23.

15. Kimple RJ, Kimple ME, Betts L, Sondek J, Siderovski DP (2002) Structural determinants for GoLoco-induced inhibition of nucleotide release by G alpha subunits. Nature 416:878–881.
16. Dorman G, Prestwich GD (1994) Benzophenone photophores in biochemistry. Biochemistry 33:5661–5673.
17. Lupas A, Van Dyke M, Stock J (1991) Predicting coiled coils from protein sequences. Science 252:1162–1164.
18. Salzameda B, Facemyer KC, Beck BW, Cremo CR (2006) The N-terminal lobes of both regulatory light chains interact with the tail domain in the 10S-inhibited conformation of smooth muscle myosin. J Biol Chem 281:38801–38811.
19. Rice S, et al. (1999) A structural change in the kinesin motor protein that drives motility. Nature 402:778–783.
20. Sindelar CV, et al. (2002) Two conformations in the human kinesin power stroke defined by X-ray crystallography and EPR spectroscopy. Nat Struct Biol 9:844–848.
21. Lowe J, Li H, Downing KH, Nogales E (2001) Refined structure of alpha beta-tubulin at 3.5 A resolution. J Mol Biol 313:1045–1057.
22. Sack S, et al. (1997) X-ray structure of motor and neck domains from rat brain kinesin. Biochemistry 36:16155–16165.
23. Blasius TL, Cai D, Jih GT, Toret CP, Verhey KJ (2007) Two binding partners cooperate to activate the molecular motor Kinesin-1. J Cell Biol 176:11–17.
24. Naber N, et al. (2003) EPR spectroscopy shows a microtubule-dependent conformational change in the kinesin Switch 1 domain. Biophys J 84:3190–3196.
25. Sousa D, Grigorieff N (2007) Ab initio resolution measurement for single particle structures. J Struct Biol 157:201–210.
26. van Heel M (1986) Similarity measures between images. Ultramicroscopy 21:95–100.
27. Pettersen EF, et al. (2004) UCSF chimera–A visualization system for exploratory research and analysis. J Comput Chem 25:1605–1612.

# Supporting Information

Dietrich et al. 10.1073/pnas.0803575105

## SI Text

**Cloning and Purification of Tail Constructs.** Tail constructs were created by PCR. The forward primer introduced a unique EcoRI site, followed by an N-terminal methionine and a 6xhistidine tag before residue 823. The reverse primer for the tail construct containing residues 823–963 introduced a unique XhoI site after the stop codon. The reverse primer for the tail construct containing residues 823–944 introduced a stop codon after residue 944 followed by a unique XhoI site. These constructs were cloned into a pET17B vector that was modified to remove an N-terminal T7 tag (Novagen). All constructs were verified by DNA sequencing. Tail proteins in the modified pET17B vector were grown in BL21(DE3)RP cells in the presence of 50 g/ml carbenicillin and 34 g/ml chloramphenicol. Tail proteins were induced by addition of 0.1 mM IPTG overnight at 24°C. Bacteria were resuspended in 50 mM phosphate buffer pH 8.0, 300 mM NaCl, 20 mM Imidazole, 5 mM ME and 10% glycerol, supplemented with the following protease inhibitors: 500 M PMSF, 1 M E-64, and 1 g/ml each pepstatin A, aprotinin, and leupeptin. Cells were lysed with a French press, and tail proteins were batch bound to TALON resin (Clontech) for 1 hour at 4°C with rotation. Resin was then poured into a 5-ml disposable column and washed with 30 column volumes, using buffer containing 50 mM phosphate buffer pH 7.0, 1 M NaCl, 20 mM imidazole, 5 mM ME. The resin was then washed with 20 column volumes of buffer consisting of 50 mM phosphate buffer pH 7.0, 300 mM NaCl, 20 mM imidazole, and 5 mM ME. Tail protein was eluted with 50 mM phosphate buffer pH 7.0, 300 mM NaCl, 500 mM Imidazole, and 5 mM ME. Twenty percent sucrose was added and protein was spun 10 min at 355,000 g to remove any aggregates and frozen in liquid nitrogen.

**Binding of Heads and Head–Tail Complexes to TALON Resin.** Purified dimeric heads with single cysteine addbacks at position 188 (2 mg/ml) were either dialyzed alone or after being combined with purified tails (823–944), (1.5 mg/ml) for three hours into binding buffer (50 mM K-Acetate, 10 mM Tris-Acetate pH 7.0, 4 mM $MgSO_4$, 20 mM Imidazole pH 7.0, 5 mM ME, 40 M ADP) 50 mM NaCl 0.05% Tween-20. Protein was spun 10 min, at 355,000 g to remove any aggregates, and then batch-bound to TALON resin (Clontech) equilibrated in the same buffer for one hour at 4°C with rotation. Resin was then poured into a Handee centrifuge column (Pierce) and flow-through was collected. Resin was then washed 8 times with 10 column volumes of the same buffer for a total of 80 column volumes, and eluted 5 times with 5 column volumes of binding buffer 350 mM NaCl 500 mM Imidazole 0.05% Tween. Experiments in which heads were eluted from tails bound to TALON using the tail peptide were conducted in the same way, except that after the extensive wash step, 5 column volumes of 10 M 27-mer tail peptide in the same buffer were added, eluted after 10 min of incubation, followed by 5 column volumes of 100 M tail peptide, eluted after 10 min of incubation. These peptide elutions were followed by two final elutions in 5 volumes of binding buffer 350 mM NaCl 500 mM imidazole 0.05% Tween.

**Asymmetric Reconstruction of Kinesin-1 Head–Tail Complex on Microtubules.** Preparation of proteins and grids for cryo-EM is as described in Methods for the fully averaged, 8 Å reconstruction. For this asymmetric reconstruction, no protofilament averaging was implemented. The resulting structure had 13 unique tubulin-kinesin-1 complexes corresponding to the positions of kinesin-1 heads on each of the 13 microtubule protofilaments. In this case, the reported resolution by either RMEASURE or the Fourier Shell Correlation method was 16 Å.

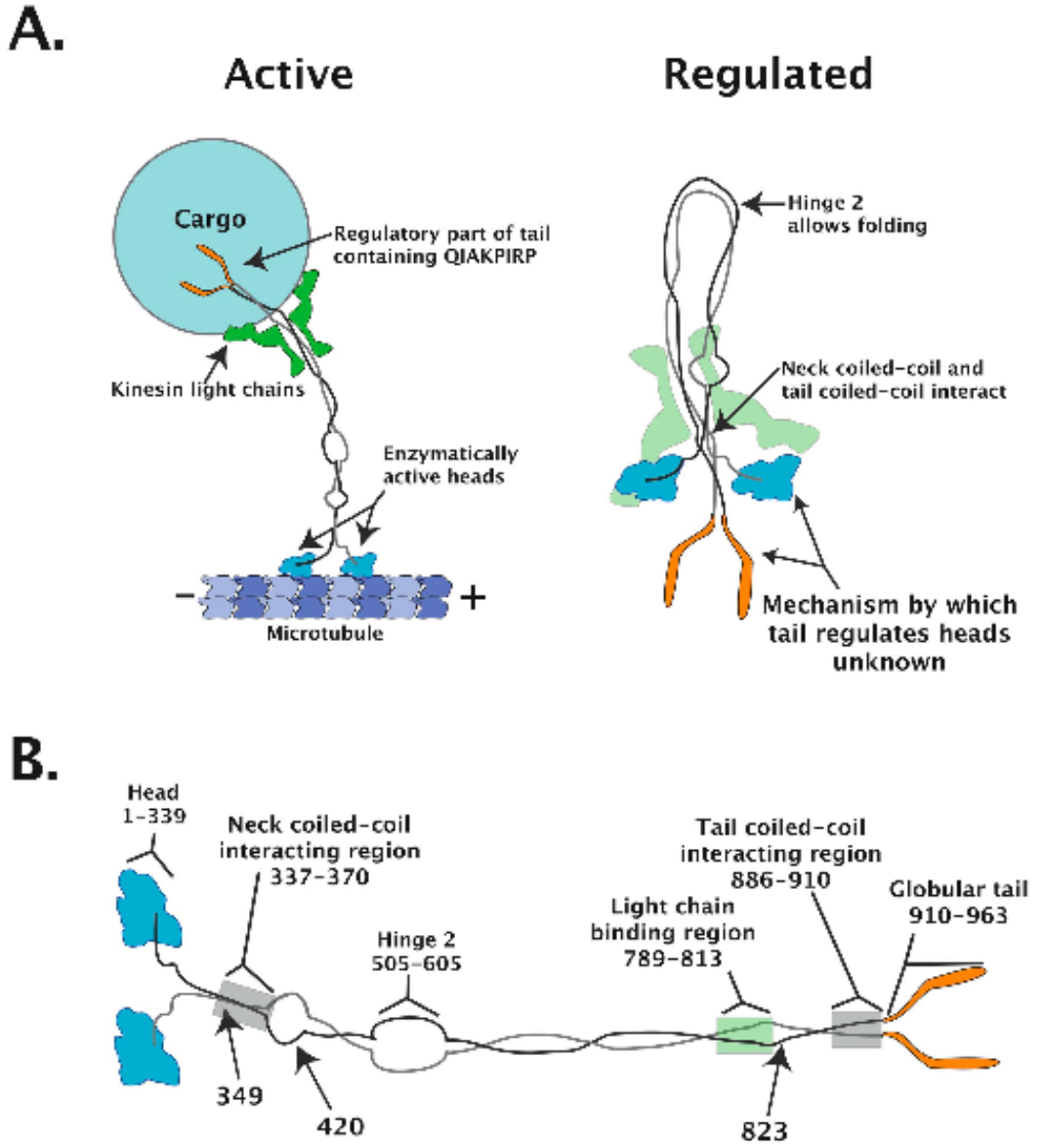


**Fig. S1.** Description of kinesin-1 regulation. Color scheme is as in Fig. 1A for kinesin-1 heavy chains, and kinesin-1 light chains and/or the light chain-binding region of the heavy chain are shown in green. (A) Model of active kinesin-1 carrying cargo along a microtubule and regulated kinesin-1 in solution. (B) Model of kinesin-1 heavy chain showing regions of head, stalk, and tail involved in tail-mediated regulation.

A. Dimeric kinesin-1 heads in the absence of dimeric tails

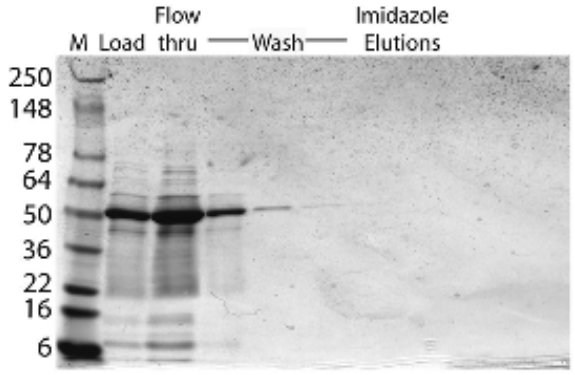


B. Dimeric kinesin-1 heads in the presence of dimeric tails with peptide elution

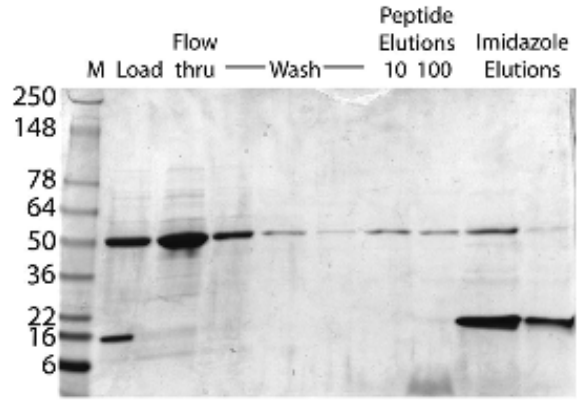


**Fig. S2.** Binding of dimeric head and tail constructs to TALON resin and elution with tail peptide. See Fig. 1 A for construct details, methods for experimental details. We mixed roughly 1:2 dimeric heads and tails containing residues 823–944 under conditions in which they associate, then batch-bound the mixture to TALON resin (Clontech), which specifically binds polyhistidine tags. (A) 4–20% SDS/PAGE gel showing that dimeric heads do not bind to TALON resin in the absence of tails. Lanes are as follows: SeeBlue Plus2 Prestained Standard, 5 l of the heads loaded onto resin, 20 l of the column flow-through, 20 l of the first wash, 20 l of the second wash, 30 l of the 8th wash, 30 l of the first imidazole elution, 30 l of the second imidazole elution. (B) Similar gel showing binding of head-tail complexes to TALON resin. Some heads eluted when 10 or 100 M of the 27-mer tail peptide was added in the same buffer. The remainder of the heads co-eluted with tails, demonstrating that they associate directly and that the 27-mer tail peptide competes with the dimeric tail construct for binding to heads. Lanes are as follows: SeeBlue Plus2 Prestained Standard, 5 l of the mixture of heads and tails loaded onto resin, 20 l of the column flow-through, 20 l of the first wash, 20 l of the second wash, 30 l of the 8th wash, 30 l of the 10 M peptide elution, 30 l of the 100 M peptide elution, 30 l of the first imidazole elution, 30 l of the second imidazole elution.

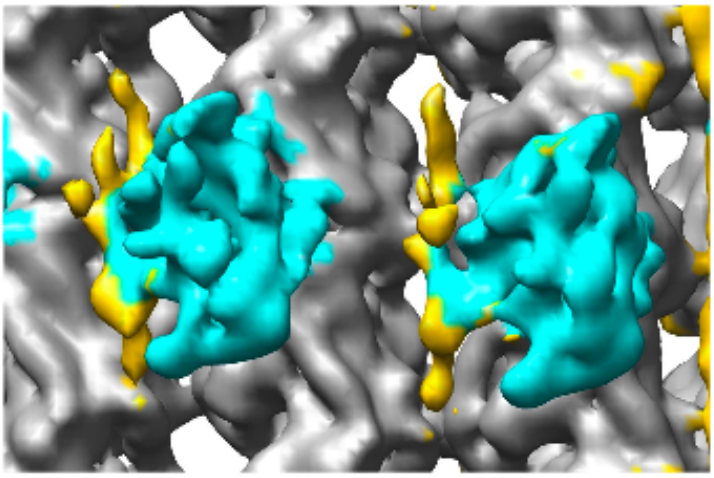

**Fig. S3.** Reconstruction of head-tail complex showing tail contacting the head near Switch I and not near the neck linker. Cryo-EM reconstruction was performed as described in Methods. Coloring and kinesin position are as in Fig. 3. The tail makes a contact with the left side of the kinesin head near Switch I, and there is a visible gap between the right side of the kinesin head near the neck linker and any tail density in the reconstruction.

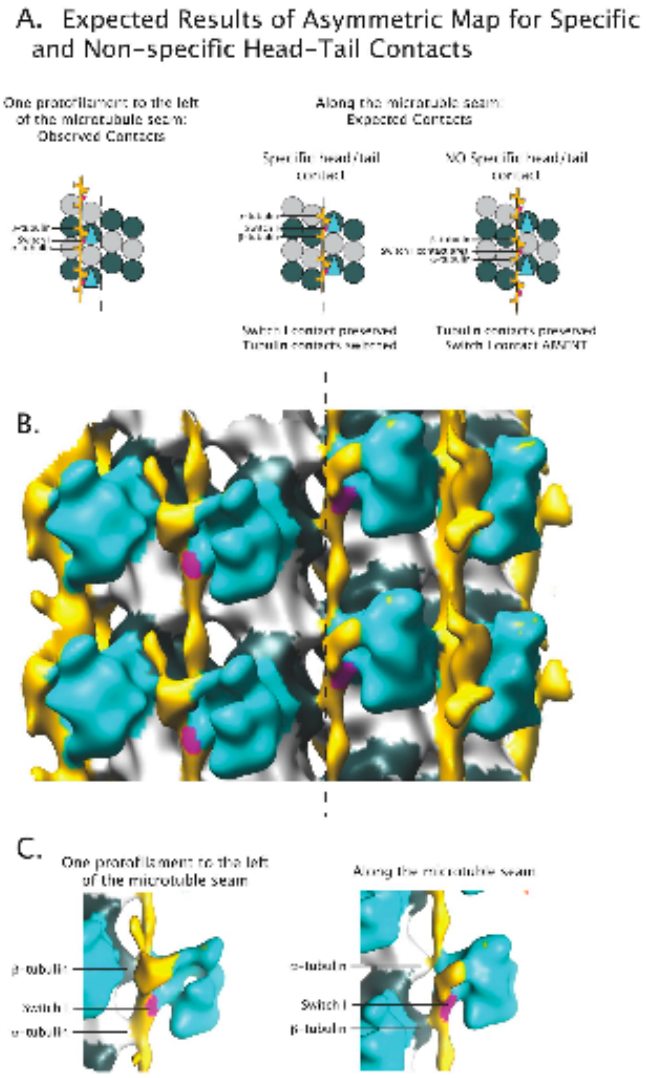


**Fig. S4.** Asymmetric 13-protofilament microtubule map of kinesin-1 head-tail complex showing specific Switch I/Tail contact at the microtubule seam. (A) Diagram models showing expected geometry of specific vs. nonspecific Switch I-tail contacts for tails at the microtubule seam versus elsewhere. Coloring is as in Fig. 3. Microtubule plus end is up. To the left of the microtubule seam as with elsewhere on the microtubule (Left), the observed contacts from top to bottom are between the tail and -tubulin, then Switch I, then -tubulin. On the microtubule seam, the expected contacts depend on whether the tail-Switch I contact is specific or not because of the unique 40-Å shift in the lateral contacts between tubulin monomers at the seam. If the tail/Switch I contact is specific, then it will be preserved, occurring between the tail at the seam and the kinesin-1 head to the right side of the seam, at the expense of - and -tubulin contacts with the tail (Center). These tubulin contacts will be switched so that -tubulin occurs at the top (where -tubulin was in the Left), the preserved Switch I/tail contact is in the center, and the -tubulin-tail contact occurs at the bottom. If the Switch I/tail contact is nonspecific, tubulin/tail contacts will be preserved at the seam while the Switch I/tail contact with the head to the right will be absent (Right). This is expected because the position of the heads on the right of the seam is shifted by 40 Å. (B) Section of an asymmetric map, colored as in A, microtubule plus end is up. The Switch I/tail contact is magenta, and the microtubule seam is denoted with a dashed line. (C) Side view (as in Fig. 3B) of kinesin-1 head/tail complexes located one protofilament to the left of the seam (Left) and at the seam (Right). To the left of the seam, contacts are as expected in the Left of (A) above. At the seam, the Switch I/tail contact is preserved while tubulin/tail contacts are switched, as expected for a specific Switch I/tail contact.

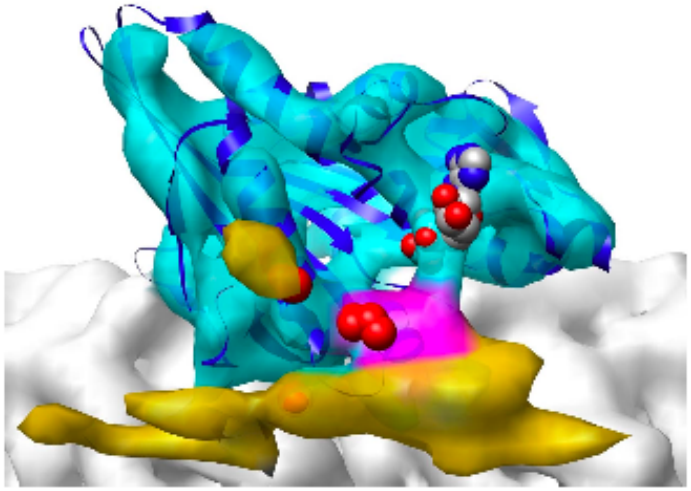

**Movie 1.** 3D animated view of the kinesin-1–tail complex. Rendering and color scheme are the same as in Fig. 3.

Movie S1 (MOV).

## Other Supporting Information Files

# Chapter III

## The Kinesin-1 Tail Conformationally Restricts the Nucleotide Pocket

**Foreword**

In Chapter II of this thesis, we demonstrated by photochemical cross-linking and cryo-electron microscopy (cryo-EM) that the regulatory QIAKPIRP sequence of the kinesin-1 tail directly interacts with the motor domain in the vicinity of the Switch I element, near the nucleotide pocket (84). Kinetic data show that the tail inhibits both intrinsic and microtubule-stimulated ADP release from kinesin-1 (62, 64). A critical lysine residue (K922) in the conserved QIAKPIRP motif of the tail is absolutely required for inhibition (61, 62). The mechanism by which the tail, specifically the critical K922 residue, inhibits ADP release is unknown.

Within the conserved motor core are various "Switch" elements, including Switch I and Switch II, as well as the P-loop. These motifs are sequence conserved and intimately involved in nucleotide binding and release. In the motor domain Switch I, together with Switch II, form a γ-phosphate sensing mechanism that is structurally conserved in the nucleotide pockets of kinesins, myosins, and G-proteins (21, 68, 69,70). Switch I undergoes a conformational change upon binding to microtubules in which the element "closes" onto the nucleotide pocket, promoting the hydrolysis of ATP. In contrast, our cryo-EM reconstruction of a head-tail interaction on microtubules reveals that the tail maintains Switch I in an "open" conformation, in which it is distal to the nucleotide. This state is associated with a high affinity for bound ADP in the nucleotide pocket, and is thus consistent with the tail's role in inhibiting both basal and microtubule-stimulated ADP release from the motor domain. Since kinesins and G-proteins share multiple structural elements, it has been suggested that they may also be regulated in a similar fashion (64, 84).

In order to investigate whether the kinesin-1 tail may be acting in a similar fashion to the guanine nucleotide dissociation inhibitors, or GDIs, of G-proteins, we have used electron paramagnetic resonance and fluorescence spectroscopy to further analyze the interaction between the kinesin-1 head and the regulatory tail domain. We found using spin-labeled nucleotides that the tail causes a conformational restriction of the nucleotide pocket that is distinct from the "closing" of Switch I seen upon microtubule binding. This restriction is not dependent on the identity of the bound nucleotide or the regulatory K922 residue. Additionally, the combined data reveal that the inhibitory mechanism of the tail does not involve stabilization of the $Mg^{2+}$ ion or simple steric hindrance of nucleotide ejection. Together, the data suggests that the head-tail interaction serves as a scaffold to position K922 to exert its inhibitory effect. While the exact role the K922 residue is playing remains unknown, it is possible that this lysine residue is interacting with the nucleotide α/β-phosphates in a manner analogous to the arginine finger regulators of some GTPases (71). Work on this project has been a collaboration with Yao Wong, co-author of the manuscript submitted to the *Biophysical Journal* (114), and Roger Cooke's lab at UCSF.

## Section I: Introduction and Experimental Design

### Introduction

The kinesin-1 motor protein transports cargo towards the microtubule plus-ends. In cells, the motor is regulated to prevent futile ATP expenditure and mislocalization at MT plus ends. Regulated kinesin-1 adopts a folded conformation in which the C-terminal regulatory tail domains directly interact with and inhibit both the intrinsic and MT-stimulated ADP release from the N-terminal motor domain (50, 51, 62, 64). Found within the conserved regulatory

QIAKPIRP motif of the tail, a critical lysine residue (K922) is absolutely required for inhibition (61, 62). The mechanism by which the tail, specifically the critical K922 residue, inhibits ADP release is unknown.

We have recently demonstrated by photochemical cross-linking and cryo-electron microscopy (cryo-EM) that the regulatory QIAKPIRP sequence of the tail interacts in the vicinity of the Switch I element of the head, near the kinesin-1 nucleotide pocket (84). Switch I, together with Switch II, form a γ-phosphate sensing mechanism that is structurally conserved in the nucleotide pockets of kinesin, myosin, and G-protein family members (21, 68, 69, 70). Regions surrounding the nucleotide pocket of kinesin-1 undergo a conformational change upon binding to MTs, which was observed as a restriction of the mobility of electron paramagnetic resonance (EPR) probes attached to the ribose oxygens of ADP or other diphosphate nucleotides on both kinesin-1 and the kinesin family member ncd (79, 85). This is thought to correspond to a "closing" of Switch I that promotes the hydrolysis of ATP when the motor binds microtubules. A salt bridge between Switch I and Switch II forms in order to stabilize this "closed" (proximal to the nucleotide) state. In contrast, our cryo-EM structure of the kinesin-1 tail protein (residues 823-944) complexed with the head on MTs shows an "open" (distal to the nucleotide) Switch I conformation (84). This "open" conformation is seen in all solution-state x-ray crystal structures of the motor domain to date, and is associated with a strong ADP-binding state (17, 18). The ability of the tail to hold the motor domain in an "open" Switch I conformation is consistent with the tail's role in preventing MT-stimulated ADP release.

Kinesin family members and G-proteins share multiple structural elements, including their core structures, regions that translate changes in the nucleotide pocket to the moving parts (referred to as the "relay helix" in myosin), as well as the moving parts of the molecule that

undergo conformational changes dependent on the nucleotide state, mainly the neck linker region in kinesin. Also contained in the conserved core are the "Switch" elements: Switch I, Switch II, and the P-loop, that are both sequenced conserved and structurally align (see Figure 15B). A good review written by Ron Vale on the structural similarities between the motor proteins kinesin and myosin and the G-protein superfamily can be found in J Cell Biol. (1996) 135(2):291-302.

Release of bound GDP from the nucleotide pocket of G-proteins is inhibited by binding partners called guanine nucleotide dissociation inhibitors, or GDIs. Three main classes of GDI proteins exist. Each of these classes act to inhibit the release of bound GDP from the nucleotide pocket by a variety of means, including structural interactions with the Switch elements and direct and indirect interactions with the bound nucleotide or essential magnesium ion. RhoGDIs and RabGDIs are two non-homologous GDI classes that act similarly to inhibit GDP release. Both classes can interact with and force specific conformations of the Switch I/Switch II γ-phosphate sensors that are incompatible with nucleotide ejection. These GDIs can also stabilize the $Mg^{2+}$ ion in the nucleotide pocket. Release of the $Mg^{2+}$ ion is followed by rapid release of bound nucleotide; therefore stabilization of the $Mg^{2+}$ ion in the pocket allows a bound nucleotide to be retained (86, 87, 88). The third major class of GDIs, known as GoLoco proteins, inhibits GDP release by positioning a critical arginine finger to stabilize the α/β-phosphates of a bound nucleotide (69, 71).

Experimental Design

Since kinesins and G-proteins share multiple structural elements and enzymatic cycles, it has been suggested that these protein families may also be regulated in a similar fashion (64, 84).

Based on the homology between kinesins and G-proteins, a kinesin-1 head-tail interaction could position the critical K922 tail residue to inhibit ADP release by one or more of these mechanisms, through direct or indirect interactions with the γ-phosphate sensors, $Mg^{2+}$ ion, α/β-phosphates, ribose oxygens or coordinating water molecules. Our work on this project is to determine how the kinesin-1 tail, specifically the regulatory K922 residue, is acting to inhibit the release of ADP. Through the use of spin-labeled nucleotide probes and fluorescence nucleotide release assays we sought to determine if the tail is acting by any of these mechanisms commonly used by GDIs to inhibit nucleotide release in G-proteins.

Unlike myosins and G-proteins, the kinesin-1 nucleotide pocket is found on the surface of the protein and is highly exposed to the aqueous environment (17, 89, 90, 91). Because the tail binds in the vicinity of Switch I and the exposed nucleotide pocket, we also considered a scenario where the tail might simply sterically block ADP release from the nucleotide pocket. Finally, we could not discount the possibility that the role of the critical K922 is purely structural and not enzymatic; it may be strictly required for the proper interaction of the tails with the heads so that other elements can inhibit nucleotide release.

Previous Electron Paramagnetic Resonance (EPR) spectroscopy experiments on kinesin-1 with spin-labeled nucleotides showed that MT binding induces the Switch I element of the kinesin-1 nucleotide pocket to "close" into the pocket (85), and these results were later corroborated by high-resolution cryo-EM structures (21, 85 see also Figure 6D in Chapter II). We sought to use the same EPR probes on kinesin-1 heads in the presence of truncated tails added *in trans* to assess whether the tail, like MTs, induces conformational changes in the kinesin-1 nucleotide pocket. We also utilized EPR to explore the role of this tail-induced restriction in kinesin-1's regulatory mechanism using triphosphate analogs and single point

mutations in either the head or tail domain. In conjunction with EPR, fluorescence spectroscopy experiments were performed using Mant-ADP to assess the tail's ability to retain bound ADP in the presence of excess EDTA, an indicator of the tail's ability to stabilize the bound $Mg^{2+}$ ion. The combined data support a mechanism for tail-mediated inhibition in which tail residues form interactions in and around the nucleotide pocket, acting as structural supports for head-tail interactions that are not directly involved in inhibition. The supporting residues position K922 to act as the sole inhibitory agent. While the mechanism by which the K922 residue acts to inhibit nucleotide release remains in question, it is possible that this lysine acts in a similar manner as an arginine finger, forming interactions with the α/β-phosphates of the nucleotide, resulting in the further stabilization of bound ADP. Additional experiments will need to be performed in order to fully understand the mechanism in which the regulatory lysine is acting to inhibit the release of ADP from the motor domain.

## Section II: Material and Methods

### Head and Tail constructs

Untagged cysteine-light monomeric (K349) and dimeric (K420) head constructs of human kinesin-1 heavy chain, as well as the point mutant G234A, were received from R. Vale (University of California, San Francisco). These constructs were expressed and purified as described in Chapter 1I of this thesis and reference (79). Tail944, containing residues 823-944 of the kinesin-1 heavy chain tail domain with a N-terminal 6x-histidine tag, was expressed and purified as described in Chapter II and reference (84). The regulatory lysine found in the conserved QIAKPIRP regulatory motif of the tail, K922, was mutated to alanine, resulting in the loss of the tail's inhibition of nucleotide release. This K922A tail mutant was generated using a

Quikchange II site-directed mutagenesis kit (Stratagene). The primers used were 5'-GCATTCTGCACAGATTGCTGCGCCTAT TCGTCCCGGGC-3' and its complementary sequence. The construct was verified by DNA sequencing. See Figure 9A for constructs. Frozen purified protein in 20% (w/v) sucrose was then shipped to Drs. Nariman Naber and Roger Cooke at UCSF for EPR experiments.

Kinesin-1 labeling with nucleotide spin labels

Monomeric K349CLM or dimeric K420CLM heads were dialyzed for 3 hours into Labeling Buffer containing 40 mM MOPS pH 7.0, 100 mM NaCl, 2 mM $MgCl_2$, and 1 mM EGTA. Protein was then spin concentrated to roughly 200 $\mu$M and mixed with 2′,3′-SLATP or SSL-NANTP at a ~1:1 molar ratio (See Figure 9C for structures). These spin-labeled probes have a single nitroxide group at the indicated positions. In labeling reactions with the 2′,3′-SLATP probe, the protein-label mixture was incubated for 1 hour and unbound probe was removed with the use of a micro bio-spin 30 column (Bio-Rad, Hercules, CA, Product #732-6250) equilibrated with binding buffer + 300 mM NaCl. An EPR spectrum was then recorded to ensure unbound probe had been removed from the sample. For SSL-NANTP labeling, the protein-label mixture was incubated with 0.1 mg/ml myokinase overnight to facilitate the exchange of the spin probe into kinesin-1. Unbound probe was removed with the use of spin column as above and an EPR spectrum was recorded.

Preparation of spin-labeled kinesin-1 heads and tails for EPR

Tail944 and TailK922A solutions were thawed and given a hard spin to remove protein precipitation. The proteins were then concentrated using a Centricon 10,000 mwco spin

concentrator (Millipore Corporation, Billerica, MA) and buffer exchanged several times into a buffer containing 25 mM HEPES pH 7.0, 100 mM NaCl, 2 mM $MgCl_2$, and 1 mM EGTA. The final concentration of the tail protein was adjusted to ~250 $\mu$M. Additional NaCl was added to labeled kinesin-1 heads to bring the salt concentration to 300 mM NaCl to ensure against tail precipitation due to low ionic strength. A four-fold molar excess of tail was added to a solution of spin-labeled heads. The resulting mixture was dialyzed overnight into Binding Buffer (25 mM HEPES pH 7.0, 50 mM NaCl, 2 mM $MgCl_2$, 1 mM EGTA). The EPR spectrum of the resulting solution was then recorded.

For the $AlF_4$ experiments, solutions of 2 mM $AlCl_3$ and 10 mM NaF were freshly added to the kinesin-1—Tail mixture after dialysis, before the EPR spectrum was recorded.

The time course of nucleotide release experiments using spin-labeled nucleotides was performed by adding 10 mM ADP to the spin-labeled-kinesin-1 head-tail solution containing 20μM head and therefore spin-labeled probe. The mixture was rapidly mixed by pipetting, then inserted into a 25 $\mu$l capillary and placed in the EPR cavity for time measurements within roughly 30 seconds of ADP addition.

EPR spectroscopic measurements

EPR data was collected in collaboration with Drs. Nariman Naber and Roger Cooke at UCSF with the help of either myself or Dr. Sarah Rice. EPR measurements were performed with a Bruker EMX EPR spectrometer from Bruker Instruments, Inc. (Billerica, MA). First derivative, X-band spectra were recorded in a high sensitivity microwave cavity using 50 sec, 100 Gauss wide magnetic field sweeps. The instrument settings were as follows: microwave power, 25 mW; time constant, 164 ms; frequency, 9.83 GHz; modulation, 1 Gauss at a frequency

of 100 kHz. Each spectrum used in data analysis is an average of 5-50 sweeps from an individual experimental preparation. For nucleotide release experiments, 11 second scans were taken at a 25 Gauss field sweep that detects the high-field peak of the free probe in the EPR spectrum and these were fit to a single exponential function. All experiments were performed at room temperature.

Mant-ADP release assays

Fluorescence spectroscopy analysis of the release of mant-ADP from the dimeric kinesin-1 head construct K420 in a variety of experimental conditions was performed by Yao Wong, co-author of this manuscript. Mant-ADP was a kind gift from Dr. Christine Cremo at the University of Nevada School of Medicine in Reno. 15-20 $\mu$M dimeric K420 heads were thawed and incubated with 100 $\mu$M Mant-ADP for 12-60 hours at 4°C to allow exchange into the nucleotide pocket. Unbound nucleotide was removed by batch binding and elution from phosphocellulose resin (Whatman P11 resin). Mant-ADP-bound K420 heads and tail proteins were dialyzed separately into Experiment Buffer (20 mM HEPES pH 7.2, 30 mM potassium acetate, 20 mM imidazole, 2 mM $MgCl_2$, 0.1 mM EGTA, 5 mM βME) before fluorescence experiments. Protein concentrations were determined and adjusted to 6 $\mu$M heads and 15 $\mu$M tails for all experiments. Data was collected on a TimeMaster fluorescence lifetime spectrometer (PTI Photon Technology International, Birmingham, NJ), exciting the sample at 360 nm and measuring emission at 450 nm. For the standard nucleotide release experiments, 280 $\mu$M ATP was used to initiate Mant-ADP release. For $Mg^{2+}$ release experiments, a mixture of 7 mM EDTA + 280 $\mu$M ATP was used to initiate the reaction. All experiments were performed at room temperature.

**Figure 9. EPR probes and kinesin-1 constructs**

A. Monomeric K349 and dimeric K420 head constructs, and the Tail944 tail construct are shown below a schematic of the full-length kinesin-1 heavy chain homodimer. Head residues are tan, coiled-coil residues gray, predicted globular tail residues are black. These constructs have been previously described (84).

B. Close-up view of the kinesin-1 nucleotide pocket (from PDB 1bg2) showing the positions of the bound nucleotide and components of the nucleotide pocket. Switch I (in red), Switch II (cyan), and P-loop (orange) motifs of the motor are shown. The G234 residue in Switch II is depicted in spacefill representation. The ribose oxygens (where the 2′,3′-SLATP nitroxide spin label is attached) of the bound ADP and the $Mg^{2+}$ ion are indicated.

C. Chemical structures of the nucleotide analogs are shown. 2′,3′-SLATP is derived from ATP via ribose modifications. SSL-NANTP is derived from a substituted phenylring-amino-ethylspacer-triphosphate structure.

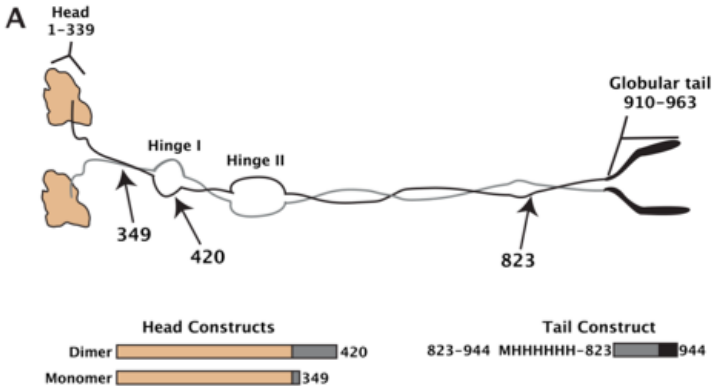
A
Head
1-339
Hinge I
Hinge II
Globular tail
910-963
349
420
823
Head Constructs
Dimer
420
Monomer
349
Tail Construct
823-944 MHHHHHH-823
944

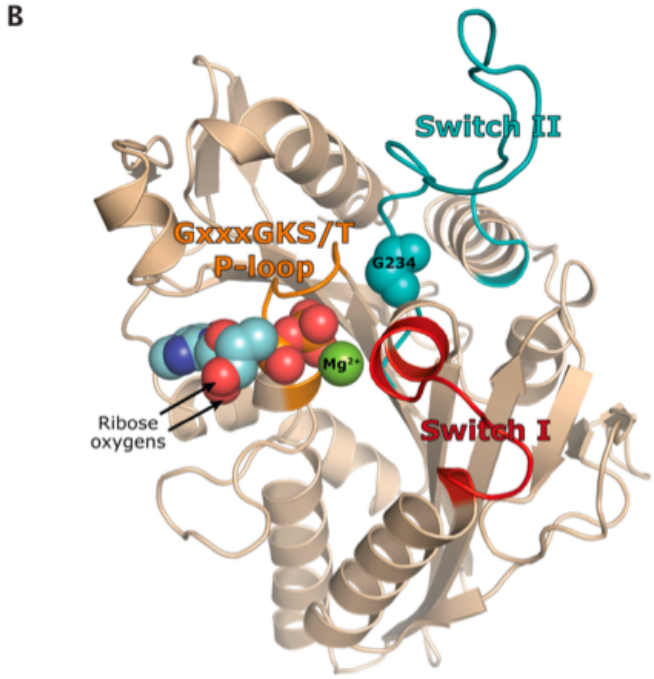
B
Switch II
GxxxGKS/T
P-loop
G234
Mg2+
Ribose
oxygens
Switch I

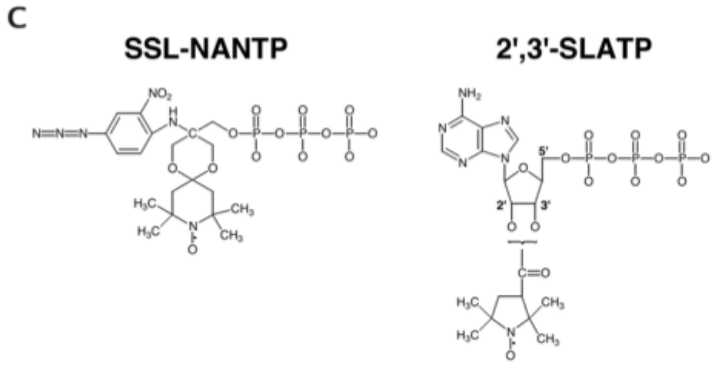
C
SSL-NANTP
2',3'-SLATP

**Section III: Experimental Results and Discussion**

The kinesin-1 tail restricts the mobility of EPR probes in the nucleotide pocket

To assess whether the tail domain of the kinesin-1 heavy chain could induce conformational changes in the nucleotide pocket of the motor domain we turned to a technique previously used to look at conformational changes in kinesin-1 upon microtubule binding. As mentioned above, EPR spectroscopy experiments with spin-labeled nucleotides were able to show that microtubule binding causes a conformational change in the nucleotide pocket that could be modeled as a "closing" of Switch I (85). Additional high-resolution cryo-EM structures were able to validate this model (21, 85). The conformational changes were observed as a restriction of the mobility of the spin-labeled nucleotide probes 2′,3′-SLATP and SSL-NANTP, shown in Figure 9C. This restriction was seen as a broadening of the EPR spectrum that correlates with decreased rotational mobility of the nitroxide on the probe. This restriction of the probes mobility is due to additional protein contacts made with the probe or steric hindrance by the nearby protein structure. Previous cross-linking and cryo-EM results, presented in Chapter II, indicated that the tail was directly interacting with the motor domain in the Switch I region of the protein, placing the regulatory QIAKPIRP motif directly in Switch I and very near the nucleotide pocket (84). We therefore sought to use these same spin-labeled nucleotide probes to look at how the binding of the kinesin-1 tail domain to the head changes the conformation of the nucleotide pocket.

For these experiments we exchanged the 2′,3′-SLATP or SSL-NANTP spin-labeled nucleotide probes into the nucleotide pockets of truncated kinesin-1 monomeric or dimeric heads (residues 1-349, designated K349, or residues 1-420, designated K420; Figure 9A). The EPR spectrum was then taken in the absence and presence of the kinesin-1 tail fragment (residues

823-944, designated Tail944; Figure 9A). As synthesized, the 2′,3′-SLATP and SSL-NANTP spin-labeled probes are triphosphate analogs, however, due to the intrinsic ATPase activity of the kinesin-1 motor domain, the nucleotide analogs were hydrolyzed into their diphosphate forms in the period before measurements were taken.

At the protein concentrations used for our EPR measurements, ~20 $\mu$M labeled heads and ~80 $\mu$M tails as assayed by Bradford reagent, we expected all the heads to be tail-bound as the concentrations are in large excess of the reported $K_d$ (<0.1$\mu$M) for a head-tail interaction (64).

As expected, the 2′,3′-SLADP and SSL-NANDP spin-labeled probes were exchanged into the nucleotide pocket of kinesin-1, as determined by the loss of the sharp free-probe peak in the EPR spectrum and the emergence of a low-field peak and high-field dip corresponding to restriction of the probes mobility due to protein binding.

We observed that both EPR probes demonstrated reduced mobility in the presence of Tail944 added *in trans*, indicating a tail-induced conformational restriction of the nucleotide pocket (Figure 10). The splitting between the low-field peak and high-field dip of the immobilized components of 2′,3′-SLADP-bound K349 in the absence of tail is 43.31±0.10 Gauss, consistent with previous results (85). In the presence of Tail944, the splitting increases to 45.63±0.13 Gauss. These values correspond to a decrease in probe mobility, from a full cone angle of 130.4° for heads alone to 125° in the tail-bound state. With SSL-NANDP-bound K349, the splittings change from 60.30±0.07 Gauss (70° cone angle) to 63.15±0.10 Gauss (61.7° cone angle) after addition of Tail944. SSL-NANDP spectra exhibit larger splittings than 2′,3′-SLADP spectra because the SSL-NANDP spin label ring is attached to both the 2’ and 3’ ribose oxygens and the probe is deeper inside the nucleotide pocket than the spin label ring on the ribose of 2′,3′-SLADP (85).

The observation that a decrease in mobility occurs with two different nucleotide analogs that place probes at different positions in the nucleotide site shows that the changes in mobility that we see upon tail binding are not due to a simple local change in structure, but rather reflect a more global change. Thus, the tail appears to cause a restriction of the area around the nucleotide pocket. We next sought to explore the role of this tail-induced restriction in kinesin-1's regulatory mechanism.

The tail-induced conformational restriction is distinct from the changes observed upon microtubule binding

Similarly to the experiments performed in reference 85, we collected spectra on kinesin-1 bound to microtubules using both the 2′,3′-SLADP and SSL-NANDP spin-labeled probes. The spectra of both 2′,3′-SLADP and SSL-NANDP exhibit a free component in the presence of microtubules, reflecting kinesin-1's weak affinity for these probes when it is microtubule-bound (92). Nevertheless, at the high protein concentrations used in our experiments, we were able to observe immobilized spectral components corresponding to microtubule-bound heads containing spin-labeled nucleotides.

As expected, both the binding of the tail and microtubules causes a restriction of the nucleotide pocket with both of our spin-labeled probes. While the spectra are similar, a direct comparison of the microtubule-bound spectra and the tail-bound spectra reveals that tail and microtubule binding restrict the nucleotide pocket in different ways.

The splitting of the immobilized components of 2′,3′-SLADP-bound K349 or K420 in the presence of Tail944 is 45.63±0.13 Gauss (125° cone angle), which differs significantly from that of microtubule-bound K349 (47.9 Gauss, 118.8° cone angle; Figure 10). The difference is more

prominent in K349 containing the SSL-NANDP probe, which has a splitting of 63.15±0.10 Gauss (61.7° cone angle) in the presence of Tail944 and 67.0 Gauss (46° cone angle) in the presence of microtubules. It is also worth noting that the EPR signal of the free peak (P2; Figure 10) is much smaller when the tail is bound to K349 than in the K349-MT complex, because the tail acts to inhibit nucleotide release into solution. The data demonstrate that tail binding does indeed cause a restriction of the nucleotide pocket. However, the tail-induced restriction is clearly different from the conformational changes observed when kinesin-1 interacts with microtubules. This was not unexpected, as our cryo-EM reconstruction of the head-tail complex on microtubules clearly showed Switch I in an "open" conformation, more akin to solution x-ray crystal structures of the motor domain complexed with ADP.

**Figure 10. Kinesin-1 tails induce a conformational change in the nucleotide pocket that differs from the conformational restriction that occurs upon microtubule binding**

Spectra of 2′,3′-SLADP -bound kinesin-1 are shown in the absence of tail (*cyan*), in the presence of tail (*black*), and in the presence of MTs (*red*). Spectra of SSL-NANDP are not shown due to a very large spectral component corresponding to free probe. Arrows and dashed lines mark the EPR spectral splittings of kinesin-1 heads bound to the nucleotide spin probe in the presence of tails. The splittings between the low field peak (*P1*) and high field dip (*P5*) of the immobilized components, and full cone angles corresponding to these splittings are shown below the spectra. With 2′,3′-SLADP, the difference in tail-induced and microtubule-induced restriction of probe mobility is small but significant. The differences are made more obvious with the SSL-NANDP spin-labeled probe.

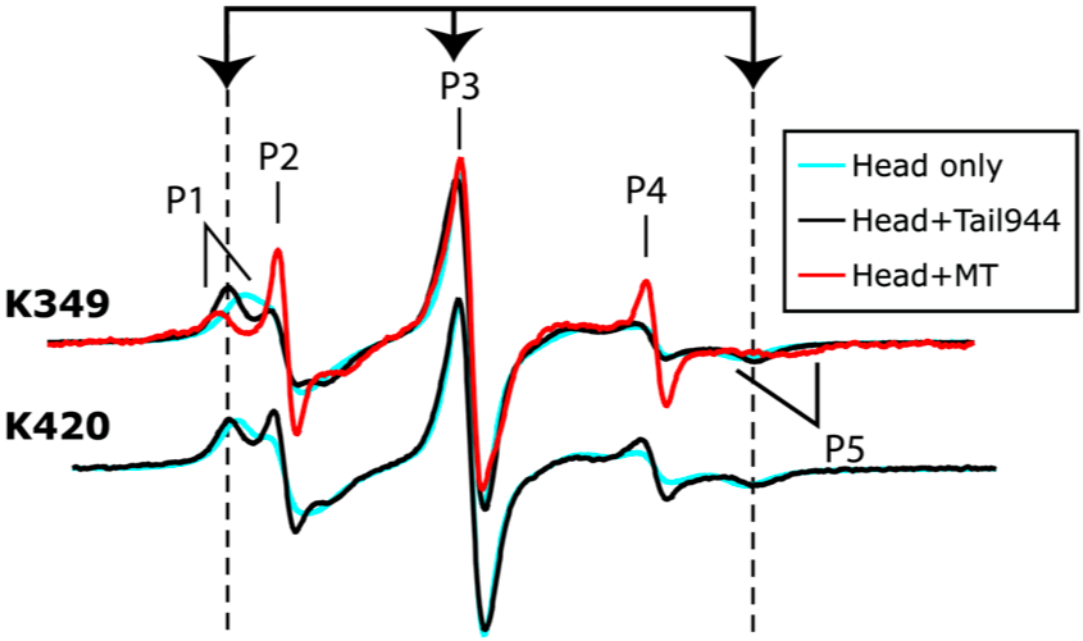


| | Splitting (Gauss) | | | Cone angle (°) | | |
|---|---|---|---|---|---|---|
| | Head Alone | +Tail944 | +MT | Head Alone | +Tail944 | +MT |
| **2',3'-SLADP** | | | | | | |
| K349 | 43.3±0.1 | 45.6±0.1 | 47.9±0.3 | 133.2 | 124.8 | 117.3 |
| K420 | 43.9±0.1 | 45.7±0.2 | N.D. | 130.9 | 124.5 | N.D. |
| **SSLNANDP** | | | | | | |
| K349 | 60.3±0.1 | 63.2±0.1 | 67.0±0.3 | 77.2 | 65.1 | 44.9 |

Tail-induced conformational restrictions do not specifically require ADP in the kinesin-1 nucleotide pocket

As mentioned above, GDIs may target and interact with the Switch I/Switch II γ-phosphate sensing mechanism that forms part of the nucleotide pocket in a cognate G-protein (86, 87). Whereas GDI proteins seem to bind with nearly equal affinity to G-proteins in both the GDP and GTP-bound states (93), tail-head interactions in myosin V appear to be dependent on nucleotide state; conformational changes in the myosin γ-phosphate sensors seem to affect the ability of the myosin tail to bind to the head. Thus, tail-induced inhibition of actin binding is observed more prominently when ADP is bound in the nucleotide pocket, rather than ATP (94).

To determine whether the kinesin-1 head-tail interaction was more akin to regulatory interactions in G-proteins or myosin V, we tested whether the nature of the bound nucleotide affected interactions between the kinesin-1 head and tail. As mentioned in Chapter II, the cross-linking reaction between K420CLM S188C and tail protein seemed to be independent of nucleotide state, as reactions with either bound ADP or the triphosphate analog AMPPNP were equally efficient at cross-linking heads and tails at position S188C. However, mass spectrometry analysis was not done on the cross-linked head-tail sample in AMPPNP, therefore it remained unknown whether the nature of the bound nucleotide had an effect on the way the head and tail were interacting. To validate this finding and further investigate the effect the presence of the γ-phosphate may have on the head-tail interaction we turned to the use of EPR. As our spin-labeled 2′,3′-SLADP probe could directly assay conformational changes occurring around the nucleotide pocket we used this probe or 2′,3′-SLADP •$AlF_4$, an ATP analog (95) to not only look at whether the tail is able to bind to the head in both the diphosphate and triphosphate states, but how the presence of the triphosphate affected the conformational restriction seen due to tail

binding. As expected, similar to our cross-linking results, the tail was able to bind to the head under either nucleotide state, as assayed by immobilization of the bound probe upon the addition of tail protein in the sample. Interestingly, upon further inspection of the EPR spectra, we found that the tail-induced immobilization of the 2′,3′-SLADP spin labeled probe bound to K349 was identical in the absence and presence of $AlF_4$, indicating that the nature of the nucleotide does not affect how the head and tail are interacting (Figure 11).

In a complementary experiment, we also used a G234A point mutant of K349. The G234A mutation (Figure 9B) results in a motor that cannot form the Switch I/Switch II salt bridge that serves as kinesin-1's γ-phosphate sensor (24). G234A kinesin-1 is catalytically incompetent and unable to hydrolyze ATP, so a 2′,3′-SLATP exchanged into its nucleotide pocket remains in a triphosphate state. EPR spectra of K349 G234A containing bound 2′,3′-SLATP showed the same spectral shift as wild-type K349 containing the hydrolyzed 2′,3′-SLADP probe in the presence of the Tail944 protein (Figure 11).

It is not truly known whether the $AlF_4$ ion is bound in the nucleotide pocket, as the aluminum fluoride was added to the sample after the association of the head and tail. It is possible that the tail blocks the ability of the $AlF_4$ ion to enter and bind tightly in the nucleotide pocket. Further, it is unknown whether aluminum fluoride acts as a triphosphate or transition state analog (115). However, the cross-linking data with AMPPNP and the EPR data with both the $AlF_4$ ion and the G234A Switch II mutation that is unable to hydrolyze ATP all indicate that the interaction between the head and the tail is not dependent on the nucleotide state. Whether there is a structural difference between these two species remains unknown, as the EPR probe is placed off the ribose ring, far from the γ-phosphate. This distance may be too great to measure slight conformational changes occurring at the far end of the nucleotide pocket around the γ-

phosphate. In addition to the non-ideal location of the probe, the observed lack of structural changes upon the presence of the third phosphate may be due to the inability of the $AlF_4$ ion to enter the nucleotide pocket, or the G234A mutation. As far as our data can tell, the interaction of the head and tail does not change relative to the absence or presence of the γ-phosphate, however we will have to await structural confirmation to be sure.

Together, the EPR data in conjunction with the cross-linking experiments suggest that the head-tail interaction can occur independently of an intact γ-phosphate sensing mechanism, and regardless of the presence or absence of the nucleotide γ-phosphate. This behavior is similar to the G-protein—GDI interaction, in that a GDI protein, like the kinesin-1 tail, can bind to its partner G-protein with equal affinity in either nucleotide states. While this data does not show that the kinesin-1 tail and GDI proteins have the same regulatory mechanism, it does effectively rule out an inhibitory mechanism which involves the tail targeting the γ-phosphate sensors as has been proposed for myosin V.

**Figure 11. The tail-induced conformational change occurs independent of nucleotide state**

Spectra of kinesin-1 bound to 2′,3′-SLADP or 2′,3′-SLATP are shown in the absence of tail (*cyan*), in the presence of tail (*black*), and in the presence of tail and 2 mM $AlCl_3$ + 10 mM NaF (*pink*). EPR spectral splittings are indicated as in Figure 10. G234A kinesin-1 does not hydrolyze ATP, so the probe in the nucleotide pocket remains 2′,3′-SLATP (not 2′,3′-SLADP). 2 mM $AlCl_3$ + 10 mM NaF induces an ADP•$AlF_4$ triphosphate mimic state. The tail-bound spectral splittings are identical in the absence and presence of $AlF_4$ or the G234A mutation, indicating that the tail-induced conformational restriction can occur with ADP or ATP in the pocket.

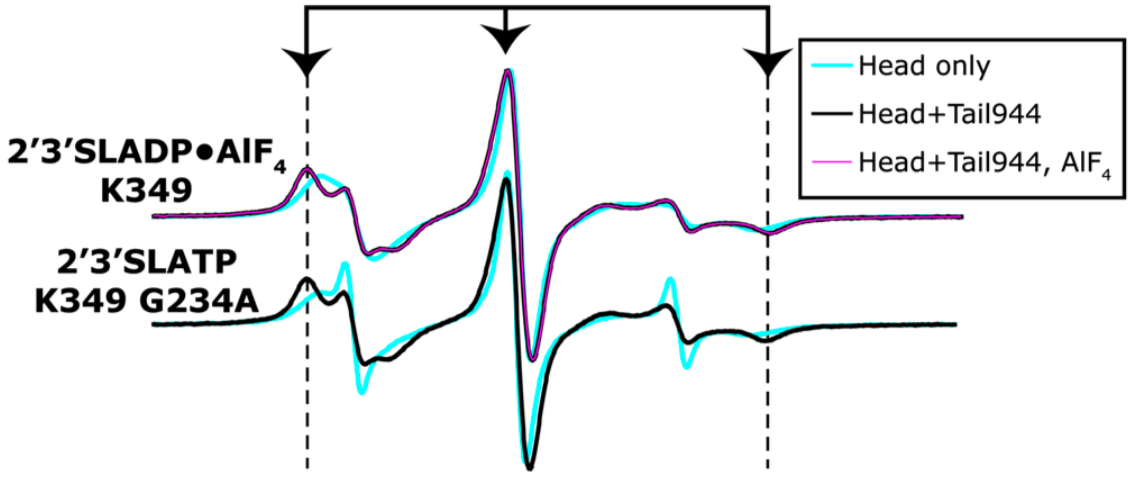


| | Splitting (Gauss) | | Cone angle (°) | |
|---|---|---|---|---|
| | Head Alone | +Tail944 | Head Alone | +Tail944 |
| **2',3'-SLADP•$AlF_4$** K349 | 43.1±0.3 | 45.8±0.3 | 134.0 | 124.2 |
| **2',3'-SLATP** K349 G234A | 42.3±0.3 | 45.4±0.3 | 137.2 | 125.6 |

The tail-Induced conformational restriction of the nucleotide pocket does not stabilize $Mg^{2+}$

Similarly to G-proteins, a $Mg^{2+}$ ion in the nucleotide pocket of kinesin-1 plays an integral role in the enzymatic cycles of these protein families. This $Mg^{2+}$ ion is required for tight binding of adenosine nucleotides to kinesin motors, and chelation or removal of the $Mg^{2+}$ ion efficiently strips away the bound nucleotide (96). Not surprisingly, this $Mg^{2+}$ ion is a target for some guanine nucleotide exchange factors (GEFs) that remove bound GDP from G-proteins by disrupting $Mg^{2+}$ binding (97). On the opposite end of the spectrum, members of the RhoGDI and RabGDI families have been shown to exert their regulatory effect through stabilization of the $Mg^{2+}$ ion in the nucleotide pocket, allowing a bound nucleotide to be retained (86, 87, 88). We therefore wanted to investigate the possibility that the tail was acting in a similar manner to these GDI family members, and could stabilize a bound adenosine nucleotide by coordinating $Mg^{2+}$ in the nucleotide pocket. These experiments were designed are carried out by Yao Wong using fluorescence spectroscopy.

Mant-ADP, a fluorescent nucleotide analog that has a characteristic emission peak at 450 nm when bound to protein, was used for these experiments. After allowing for the Mant-ADP to exchange into the nucleotide pocket and removal of unbound fluorescent nucleotide the rate of Mant-ADP release from the dimeric K420 head was measured using excess EDTA to chelate $Mg^{2+}$ out of the nucleotide pocket in the presence or absence of the Tail944 protein. As the tail protein is mixed with the Mant-ADP labeled head prior to the addition of EDTA, it is expected that if the tail is acting to stabilize the $Mg^{2+}$ ion through either direct or indirect interactions, that the rate of nucleotide release in the presence of the tail will be slower compared to the head alone. Our data shows that Tail944 only marginally affected EDTA-induced removal of the $Mg^{2+}$ ion (release rate of $0.0724 \pm 0.0058\ s^{-1}$ for K420 alone vs. $0.0507 \pm 0.0053\ s^{-1}$ for K420 in the

presence of Tail944; Figure 12). This trend is consistent with results reported by Hackney and Stock showing that the tail only weakly inhibits sequential release of $Mg^{2+}$ followed by ADP (64). They concluded that the observed difference in rates could be attributed to strong tail-induced inhibition of non-sequential Mg•ADP release occurring simultaneously. From this, we determine that the tail does not bind either directly or indirectly to stabilize $Mg^{2+}$ in the nucleotide pocket. However, the possibility exists that the tail could inhibit specific MT-induced mechanisms for triggering $Mg^{2+}$ release, as our experiments did not assess MT-stimulated $Mg^{2+}$ release explicitly.

**Figure 12. The tail does not inhibit release of $Mg^{2+}$ from the nucleotide pocket**

EDTA chelation of $Mg^{2+}$ ions was monitored via a Mant-ADP release assay measuring the fluorescence intensity of the sample, exciting at 360 nm and measuring the emission at 450 nm. Removal of $Mg^{2+}$ from the nucleotide pocket is followed sequentially by rapid release of bound nucleotide. Traces are with the dimeric head K420 alone and K420 associated with Tail944, as labeled. Smooth lines are first-order fits to the traces. Rates and standard deviations are shown below the curves (n=5 for both samples). The rates of Mant-ADP release from EDTA-treated K420 were only marginally different in the absence and presence of Tail944.

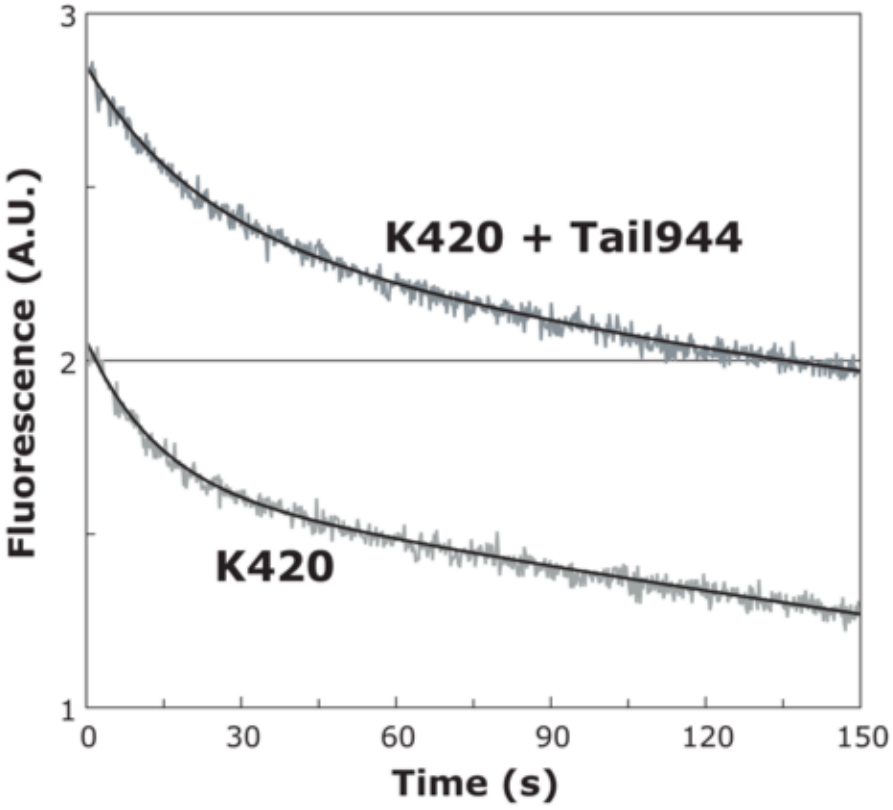


| | Rate ($s^{-1}$) |
|---|---|
| **K420** | 0.0724 ± 0.0058 |
| **K420 + Tail944** | 0.0507 ± 0.0053 |

The K922 residue is critical for inhibition but not required for tail-induced conformational restriction of the nucleotide pocket

Using EPR spectroscopy we have demonstrated that the tail induces a distinct conformational change around the nucleotide pocket that restricts the mobility of spin-labeled nucleotide probe. However, the head-tail inhibitory interaction does not appear to involve the $Mg^{2+}$ ion or the kinesin-1 γ-phosphate sensing mechanism. We next sought to examine whether the K922 residue plays a role in the formation of this head-tail interaction. Several results by other groups have identified the conserved tail K922 residue in the QIAKPIRP sequence motif as being absolutely critical for kinesin-1 regulation (61, 62). The reason why this lysine 922 residue is critical to regulation remains unknown. It is possible that this K922 residue acts as a structural lynchpin that is required for the proper interaction of the tails with the heads to inhibit ADP release by a steric blocking mechanism, rather than acting by itself in an inhibitory fashion. In order to test this we created a single point mutation, lysine 922 to alanine (K922A), in our Tail944 construct. If this residue is key to the tail's ability to properly interact with the motor domain, we expect that this K922A mutation would disrupt the proper binding of the tails to Switch I and the nucleotide pocket of the motor domain, and thus the characteristic conformational restriction of the nucleotide pocket by the interacting tail would not be observed. Alternatively, other elements in the tail may interact with the head to properly position K922 for inhibition by binding to the nucleotide or coordinating nucleotide-sensing elements into a tightly-bound configuration. If this is the case, we expect that a K922A mutation would abolish regulation without having a significant effect on the tail-bound structure.

To distinguish between these two possible roles of the K922 residue in inhibition, discussed above, we tested whether the characteristic conformational restriction of the nucleotide

pocket occurs in the presence of the tail with the K922A point mutation. We measured static EPR spectra of monomeric K349 and dimeric K420 head proteins containing 2′,3′-SLADP or SSL-NANDP in the presence of wild-type Tail944 and the TailK922A mutant. Analysis of the EPR spectra reveals that TailK922A induces an identical restriction of both EPR probes as wild-type Tail944 (Figure 13). Additionally, we measured the rates of 2′,3′-SLADP release using excess ADP from K420 in the presence of Tail944 or TailK922A. The dimeric K420 head alone released the spin-labeled 2′,3′-SLADP probe at a rate of 0.031±0.008 $s^{-1}$. In the presence of the wild-type Tail944, the release rate was slowed to 0.015±0.002 $s^{-1}$. While we found that the Tail944 protein inhibited the rate of nucleotide release in solution, our point mutation TailK922A did not (release rate of 0.033±0.003 $s^{-1}$), despite the identical restriction of EPR probe motility (Figure 14, bottom). Variability in the EPR rates of spin-labeled probe release were observed and are most likely due to mixing irregularities and the low time resolution of the EPR measurements. We confirmed our results in an independent assay by measuring K420 Mant-ADP release rates in the presence of Tail944 or TailK922A (Figure 14). While the observed rates of nucleotide release are faster with the spin-labeled nucleotides than the fluorescence data with Mant-ADP, most likely stemming from the affinity of kinesin-1 for these modified nucleotides, it is quite clear that the wild-type Tail944 is able to hold the bound nucleotide in the pocket, while the K922A point mutation is completely deficient in this ability. These data reinforce the fact that the K922 residue is critical for inhibition, but surprisingly it does not participate in the tail-head interaction that causes a conformational restriction of the nucleotide pocket. As a corollary, we conclude that restriction of the nucleotide pocket alone does not inhibit ADP release. Therefore, the tails do not appear to prevent nucleotide release via a steric blocking mechanism.

The unique placing of the spin-labeled nitroxide on the ribose oxygens of the 2′,3′-SLADP EPR probe also allows us to assess whether residue K922 is acting either directly or indirectly to stabilize the bound nucleotide through interactions with the ribose oxygens. While the chemical nature of the probe does remove key chemical groups from the ribose ring, no difference was observable between the wild-type and K922A tail constructs. This suggests that the tail is also not exerting its inhibitory effect through stabilizing interactions with the ribose oxygens.

The combined data lead us to believe that the tail-induced conformational restriction that we observe in the nucleotide pocket may be a stabilizing interaction between the tail and the head, that is directly involved in the tail's regulatory function. This is the first evidence of a stabilizing interaction between the kinesin-1 tail and the nucleotide pocket in the head. It is possible that the tail-induced restriction of the nucleotide pocket serves to increase the binding affinity of the kinesin-1 head and tail and serve as a scaffold to specifically position the inhibitory K922 residue to inhibit nucleotide release.

**Figure 13. K922A tails induce similar structural changes as wild-type tails**

Spectra of 2′,3′-SLADP -bound kinesin-1 are shown in the presence of Tail944 (*black*), and in the presence of TailK922A (*orange*). Only the 22′,3′-SLADP spectra are shown because of the large free component in SSL-NANDP spectra. EPR spectral splittings are indicated as in Figure 10. The 2′,3′-SLADP and SSL-NANDP splittings of monomeric (K349) and dimeric (K420) head spectra are the same with Tail944 or TailK922A. The Tail944 and TailK922A spectra are hard to distinguish because they are almost perfectly superimposed on each other.

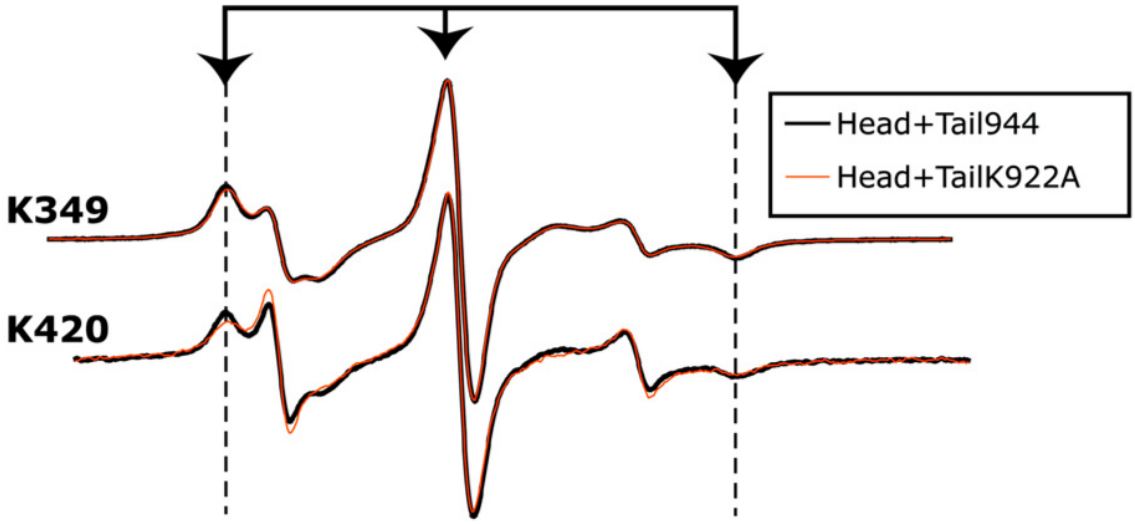


| | Splitting (Gauss) | | Cone angle (°) | |
|---|---|---|---|---|
| | +Tail944 | +Tail K922A | +Tail944 | +Tail K922A |
| **2′,3′-SLADP** | | | | |
| K349 | 45.6±0.1 | 45.3±0.1 | 124.8 | 125.8 |
| K420 | 45.7±0.2 | 45.7±0.1 | 124.6 | 124.6 |
| **SSLNANDP** | | | | |
| K349 | 63.2±0.1 | 62.9±0.2 | 65.1 | 66.3 |

**Figure 14. Wild-type tails inhibit nucleotide release, whereas K922A tails have no effect**

Mant-ADP release curves are shown for dimeric K420, K420 +Tail944 and K420 +TailK922A as labeled. Smooth lines are first-order fits to the traces. Means and standard deviations for calculated rates are tabulated for Mant-ADP (n=4-8) and 2′,3′-SLADP (n=3-5). The values for Mant-ADP release are consistent with published data on basal ADP release rates from kinesin-1 heads (39). The 2′,3′-SLADP data measured by EPR are different due to the lower affinity of kinesin-1 for the spin-labeled nucleotides. Nevertheless, both experiments demonstrate that the K922A Tail-944 is completely deficient at inhibiting nucleotide release from K420.

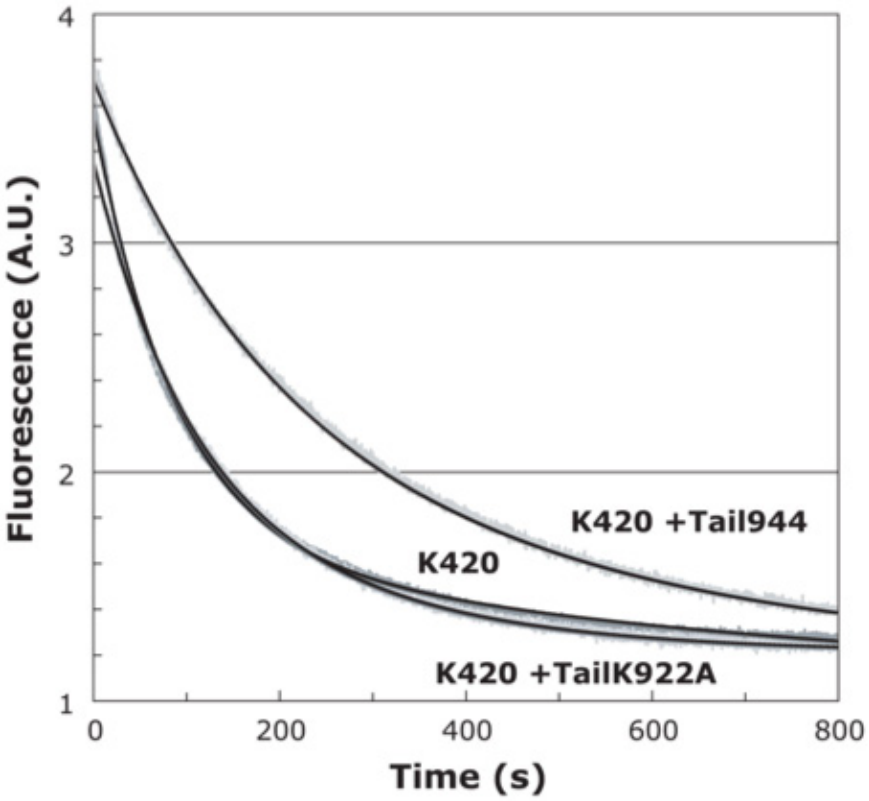


| Nucleotide | Rate ($s^{-1}$) K420 Alone | K420 + Tail944 | K420 + TailK922A |
|---|---|---|---|
| Mant-ADP | 0.0108 ±0.0008 | 0.0048 ±0.0013 | 0.0093 ±0.0021 |
| 2'3'-SLADP | 0.0310 ±0.0078 | 0.0148 ±0.0024 | 0.0326 ±0.0029 |

Discussion

In our combined work on this project, we have shown that the kinesin-1 tail induces a conformational restriction around the nucleotide pocket of the motor domain. This restriction may be due to conformational changes of the nucleotide pocket residues induced by the interaction of the tail with the kinesin-1 head, or from the tail itself. The tail-induced restriction of the pocket is not caused by the "closing" of Switch I that is seen when kinesin-1 binds microtubules, as the EPR spectra in the presence of tail protein is quite different than that seen upon microtubule binding. Rather, it appears that the tail forms stabilizing interactions with the nucleotide pocket and holds Switch I in a more solution-like conformation seen in our cryo-EM structure (84, see Chapter II for discussion). Inhibition does not appear to involve stabilization of the bound $Mg^{2+}$ ion, interactions with the ribose oxygens, or the γ-phosphate sensing mechanism of the motor. As our regulatory-deficient K922A mutant showed identical restriction of the nucleotide pocket compared to the inhibitory wild-type tail, inhibition does not seem to be through a simple steric mechanism blocking nucleotide release. Together this data suggests that the observed conformation of Switch I could be a side effect of the tail binding around the nucleotide pocket, and not a strict requirement for inhibition, however additional work would be required to confirm this. One possible experiment would be to repeat the cross-linking and cryo-EM reconstruction using the TailK922A mutant to show that this mutant, although completely deficient at holding ADP in the nucleotide pocket, induces the same Switch I "open" conformation seen in our previous structure.

As the spin label on 2′,3′-SLADP is directly attached to the 2′/3′ ribose oxygens, it serves as a direct sensor for interactions that might involve them. Since the TailK922A fragment restricts the mobility of our EPR probes exactly like wild-type Tail944, we rule out the

possibility that K922 interacts directly or indirectly with the ribose oxygens of the bound nucleotide. Because TailK922A, while inducing the same conformational restriction of the nucleotide pocket, is incapable of inhibiting nucleotide release, this also tells us that the tail does not block nucleotide exit by a steric hindrance mechanism. However, the data to date remain consistent with a possible interaction of the K922 residue in the vicinity of the α/β-phosphates. Such an interaction would not necessarily hinder the mobility of 2′,3′-SLADP or SSL-NANDP probes, as the spin labels are somewhat distal to the phosphates. The observed mobility shifts are likely stabilizing interactions between the tail and head to position K922, which while critical to the tail's activity, is not itself required for the tail to bind to the nucleotide site. Additional experiments would be necessary to further investigate the possible role that residue K922 may have in stabilizing bound ADP through interactions with the α/β-phosphates of the nucleotide.

Two points of comparison from G-protein/GDI interactions lead us to a possible model for kinesin-1 tail inhibition. First, affinity studies of G-proteins have shown that the β-phosphate-P loop interaction to be the most important element for tight binding of nucleotide (97). The P-loop contains a lysine that is invariant in both the G-protein and ATPase motor protein families. In crystal structures of G-proteins complexed with their cognate GEFs, the P-loop lysine which formerly contacted negative charges on the α/β-phosphates in crystal structures of uncomplexed G-proteins, is rotated away to interact with acidic residues either on the G-protein or a glutamic acid finger on the GEF (97). Motor proteins, including kinesin-1, are thought to have analogous interactions, as an invariant glutamic acid analogous to Glu62 of Ras (highly conserved in G-proteins) is found in an identical position in the Switch II region of motor proteins, where it might be necessary for stabilizing the nucleotide-free state. Microtubules act as a nucleotide exchange factor for kinesins and likely force the P-loop lysine (K91 in kinesin-1)

away from the nucleotide phosphates to interact with the invariant glutamic acid. Confirmation of this conformational change is difficult however, as the need for microtubule filaments prohibit the use of x-ray crystallography.

In addition to analogous mechanisms of action between the NTPases and GEFs for G-proteins and kinesins, in which a critical P-loop lysine contact with the α/β-phosphates is broken by conformational changes induced by the binding of the cognate GEF, allowing for nucleotide release, there are similarities between kinesin-1 tail regulation and the regulation of G-proteins by the GoLoco class of GDIs. The GoLoco class of GDIs have been shown to inhibit GDP release by inserting an "arginine finger" into the nucleotide binding site to additionally coordinate the α/β-phosphate in conjunction with the P-loop lysine (69, 71). This additional coordination of the nucleotide increases the binding affinity and results in the inhibition of GDP release. Interestingly, a R516A mutation of the critical arginine in the RGS14 GDI of $G_{\alpha i}$ results in a tenfold reduction in GDI activity, while an R516F mutation completely abrogates activity (71). However, neither of these regulatory mutations decreases the ability of the GDI to complex with its partner G-protein. Our experiments have shown that this is exactly the same phenomenon observed between the kinesin-1 head and tail. Mutation of K922 to alanine (K922A) completely abrogates the ability of the tail to inhibit ADP release, however, this mutation seems to have no effect on the ability of the kinesin-1 tail to bind and interact with the motor domain, as evidenced by the identical restriction of the nucleotide pocket seen with EPR probes. Furthermore, when the crystal structures of the GoLoco-G-protein complex and kinesin-1 are aligned using the conserved P-loop (GxxGxGKS/T) and Switch II (DxxG) motifs, we see that the inhibitory GoLoco peptide is positioned in the same area we predict the kinesin-1 tail to be based on our previous crosslinking and cryo-EM data (Figure 15A-E). In the superimposed

structure, the critical GoLoco arginine is perfectly positioned to coordinate the α/β-phosphates of kinesin-1's bound ADP.

The analogous Switch mechanisms of G-proteins and kinesins, as well as the regulatory similarities between the GoLoco family of GDIs and the kinesin-1 tail discussed above have allowed us to postulate a mechanism in which the kinesin-1 tail may be acting to inhibit nucleotide release from the motor domain. We propose a model wherein the tail regulatory K922 residue may act as a GoLoco-like "lysine finger" to bolster or completely substitute for the conserved P-loop lysine by interacting directly with the nucleotide α/β-phosphates. The additional contacts with the bound nucleotide would stabilize ADP in the nucleotide pocket as well as potentially allowing for ADP to remain in the nucleotide pocket while the motor is bound to microtubules. As our EPR probes are situated closer to the ribose ring, they may not be close enough to detect the presence of the stabilizing interaction between the α/β-phosphates and the K922 residue, which would explain why the interaction between the head and both our wild-type and K922A tail fragments look identical by EPR. This proposed mechanism would also explain our observed lack of dependence on the nucleotide γ-phosphate. In this scenario, when the P-loop lysine interaction with the α/β-phosphates is disrupted by microtubule binding or occurs spontaneously in solution for basal ATPase activity, the tail K922 residue can successfully substitute for the lost P-loop interaction and keep the nucleotide in the pocket by the K922-phosphate interactions coupled with the tail-head stabilizing interactions. While there exists no direct evidence for this mechanism, the striking similarities between the kinesin-1 tail and the GoLoco family of GDI proteins are impossible to ignore. As this mechanism will be hard to test directly without a spin-labeled probe situated to observe structural changes surrounding the α/β-phosphates we must await a complete structural view of the kinesin-1 head-tail complex to verify

our proposed model for inhibition of nucleotide release. Mark Seeger is currently attempting to crystallize the kinesin-1 motor domain with an inhibitory tail peptide. Until then, our working model of kinesin-1 auto-regulation of the motor domain's ATPase activity by the tail domain remains open for scrutiny, however, the existing data and the structural and mechanistic similarities with G-protein—GDI interactions suggest that the tail may be interacting with the α/β-phosphates of the bound ADP.

**Figure 15. A possible role of the tail K922 residue in kinesin-1 inhibition**

A. Structure of the RGS14 GDI GoLoco region complexed to the Ras-like domain of $G_{\alpha i1}$ (PDB 1kjy) (71). The RGS14 GoLoco region that contains the critical regulatory arginine finger is shown in purple. Switch I and Switch II in $G_{\alpha i1}$ are indicated in red and cyan, respectively.

B. The RGS14 GoLoco motif superimposed onto the kinesin-1 crystal structure (PDB 1bg2) (17). The structures were aligned using the P-loop (GxxGxGKS/T) and Switch II (DxxG) motifs that are conserved between G-proteins and motor proteins. Switch I and Switch II are indicated as above. The kinesin-1 tail interacts with Switch I in approximately the same area that RGS14 is positioned in the structure, as shown by chemical crosslinking (84). In a manner analogous to RGS14 and $G_{\alpha i1}$, scaffolding interactions could position residue K922 of the tail to coordinate the nucleotide $\alpha/\beta$-phosphates as a lysine “finger”.

C. The same superposition as B, but without $G_{\alpha i1}$ visible for clarity.

D. Close-up of the nucleotide pocket of $G_{\alpha i1}$ showing the bound nucleotide and the regulatory arginine of RGS14 in the same orientation as A.

E. Close-up of the kinesin-1 nucleotide pocket showing the bound ADP and the superimposed RGS14 regulatory arginine. The orientation is identical to B.

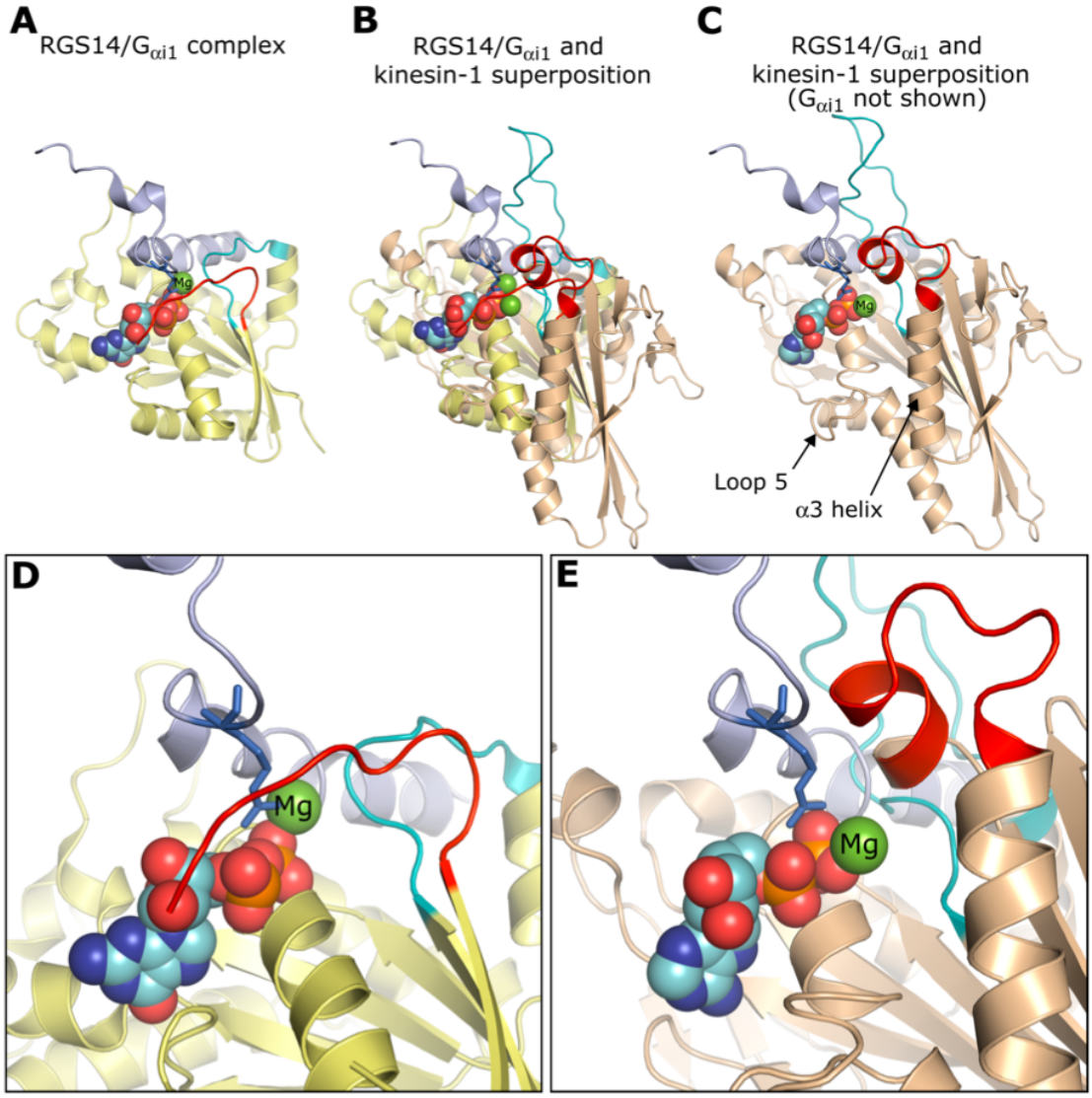
A
RGS14/Gαi1 complex
B
RGS14/Gαi1 and
kinesin-1 superposition
C
RGS14/Gαi1 and
kinesin-1 superposition
(Gαi1 not shown)
Mg
Loop 5
α3 helix
D
Mg
E
Mg

**Conclusions**

In this project, we use EPR spectroscopy to show that the kinesin-1 tail causes a conformational change around the nucleotide pocket that restricts the mobility of spin-labeled nucleotides. While the EPR spectra of kinesin-1 heads bound to tails is similar to the spectra of kinesin-1 bound to MTs, the tail-induced restriction of probe motility is significantly different from the steric interaction that is caused by MT-induced "closing" of Switch I. Importantly, using single point mutations in either the head or the tail, we found that the conformational restriction around the nucleotide occurs regardless of the phosphate state of the bound nucleotide or whether the Switch I/Switch II γ-phosphate sensor is intact, and surprisingly, independently of the regulatory K922 residue. These findings suggest that the tail is not inhibiting nucleotide release by a simple steric mechanism. Fluorescence spectroscopy experiments in the presence of excess EDTA found that the tail does not act to inhibit ADP release through stabilization of the bound $Mg^{2+}$ ion. Additionally, although both techniques revealed that the regulatory K922 residue is necessary to inhibit the intrinsic release of ADP, spin labels positioned on or near the ribose oxygens of the nucleotide were unable to detect conformational differences between the wild-type and K922A mutant tail constructs, suggesting that the regulatory lysine residue is not interacting directly or indirectly with the ribose oxygens to inhibit nucleotide release. These data support a mechanism for tail-mediated inhibition in which tail residues form interactions in and around the nucleotide pocket, acting as structural supports for head-tail interactions that are not directly involved in inhibition. These supporting residues position the K922 residue to act as the sole inhibitory agent. While the mechanism by which the K922 residue acts to inhibit nucleotide release remains in question, it is possible that this lysine acts in a similar manner as an arginine finger in the GoLoco family of GDI proteins, forming interactions with the α/β-phosphates of

the nucleotide, resulting in the further stabilization of bound ADP and therefore inhibition of the enzymatic cycle of the kinesin-1 molecular motor protein. We thus await for the crystal structure of the head-tail interaction to be determined in order to fully understand the mechanistic details behind the tail-mediated regulation of the kinesin-1 motor domain.

# Chapter IV

## Conclusions

**Prior results**

How does the kinesin-1 tail auto-regulate the motor domain?

When the present work on this project began, the kinesin-1 tail was obviously critical for regulation of the motor domain, but it was not clear as to the mechanism by which the tail inhibited the enzyme's catalytic activity. The importance of the tail for kinesin-1 inhibition was shown by multiple means. First, purified full-length kinesin did not exhibit the necessary enzymatic and motile abilities to facilitate the observed rates of *in vivo* cargo transport or *in vitro* motility (55, 56, 57). Truncated kinesin motor domains, on the other hand, possessed the kinetic characteristics required for the observed rates of organelle transport *in vivo* (58). This disparity in the kinetics allowed for the speculation that kinesin purified from natural sources was trapped in an inhibited state (36, 50, 56). This biochemical data combined with evidence from electron microscopy and hydrodynamic sedimentation assays that at physiological ionic strength the kinesin-1 heavy chain existed in a compact conformation in which the N and C-termini of the protein are in close proximity (50, 51, 52, 53, 54) suggested a possible explanation for the difference between the observed behavior of full-length kinesin and that necessary to support intracellular motion. It was therefore postulated that the tail of the kinesin heavy chain was in some way inhibiting the microtubule-stimulated ATPase activity of the motor, and that this inhibition was relieved when kinesin was absorbed onto glass surfaces or beads, which mimic cargo binding (59). This idea coupled with observations from cell fractionation and immunolocalization studies indicating that a majority of kinesin-1 in cells is neither bound to microtubules or cargo, but is rather in a soluble, cytoplasmic form (5, 31, 48, 49), gave physiological relevance to kinesin-1 regulation, as cells required a mechanism that keeps

kinesin-1 in an inactive, non-microtubule-bound state until it is needed to transport cargo (31, 50).

Mutagenesis studies confirmed the importance of the tail domain for motor regulation. Deletion of the flexible Hinge II region of the stalk was found to restore enzymatic activity and single molecule motility to the motor by prohibiting the formation of the compact conformation (59, 60, 61). Importantly, the ability of the molecule to adopt a folded conformation also was shown to have *in vivo* consequences, as the deletion of Hinge II displayed an unregulated phenotype in Neurospora, in which kinesin accumulated at the microtubule plus-ends located at the hyphae tips (61). As the inability to form the compact conformation keeps the N-terminal motor domain and the C-terminal tail domain at opposite ends of the molecule, an interaction between these two domains was thought to be the cause of inhibition of the motor domain. Through studies involving truncation from the C-terminus, *in trans* association assays, and genetic yeast two-hybrid screening, an interaction between the neck coiled-coil of the motor domain and the tail coiled-coil was found (54, 65). Interestingly, the ability to form the compact conformation and inhibition could be uncoupled, revealing the importance of a sequence conserved regulatory motif in the tail domain, the QIAKPIRP motif. C-terminal truncations that removed this sequence prevented inhibition, but did not influence the ability of the molecule to fold until further deletions were made (54, 62). These results imply that the ability of the full-length molecule to form the compact conformation is necessary, but not sufficient for inhibition of ATPase activity, and that the QIAKPIRP sequence is fundamental to regulation. The inhibitory nature of the tail was further confirmed using sets of short tail peptides (63). These experiments found that peptides containing the QIAKPIRP sequence motif were able to significantly inhibit the microtubule-stimulated ATPase activity of the motor as well as reduce

microtubule motility in a gliding assay. Within this regulatory sequence, lysine 922 (Drosophila numbering) was found to absolutely essential for regulation. Mutation of this residue to either alanine or glutamic acid completely abolished regulation both *in vivo* and *in vitro* (61, Yao Wong personal communication, see Chapter III). Kinetic assays revealed that the tail inhibited the first microtubule-stimulated ADP release step in the enzymatic cycle of the motor, and did not inhibit subsequent stepping (62). Consistent with the ability of the tail to inhibit the microtubule-stimulated ADP release activity of the motor, it was also shown to have an effect on motor movement. Single molecule fluorescence assays demonstrated that full-length kinesin had a 90-99% decrease in the frequency of motility events (59). The molecule was able to move processively once it became bound to a microtubule, but this movement was discontinuous with pauses and then bursts of unidirectional motion (59). Little more regarding kinesin regulation was known prior to this work. Since this work started it has been shown that the tail is able to inhibit both the basal and microtubule-stimulated release of ADP from the motor domain (62, 64, 114, Chapter III), most likely through stabilization of the bound ADP.

## The present work

### Understanding the mechanism of tail-mediated inhibition of ADP release

While the importance of the tail domain, specifically the QIAKPIRP motif, in kinesin regulation was clear, the mechanism by which the tail acted to inhibit the motor domain remained unknown. It was puzzling that the only interaction found between these two domains was an interaction between the coiled-coil regions. Not only was the essential lysine of the QIAKPIRP motif of the tail C-terminal to this region, but an interaction with the neck coiled-coil to shut down the motor's enzymatic activity did not seem likely to be inhibitory, as mutations,

deletions, and stabilization of this region have no effect on the motors kinetic ability (66, 67). We therefore proposed that this known interaction was in fact a stabilizing interaction that allowed for a second direct interaction to occur between the head and tail domain, specifically the QIAKPIRP motif. Understanding the mechanism by which the tail is acting to inhibit ADP release was best approached using a variety of biophysical methods to first determine the interacting regions between the two domains, and then analyze how the tail was able to inhibit enzymatic activity through this interaction. This work has answered several questions about kinesin regulation. We have shown that there is indeed a direct interaction between the head and tail domains of kinesin-1. Specifically, the regulatory QIAKPIRP motif of the tail interacts with the enzymatically critical Switch I region of the motor domain. Additionally, a cryo-EM reconstruction of the head-tail interaction indicates that kinesin-1 may also be regulated while bound to microtubules through a nucleotide-independent interaction between the tail and tubulin. Using EPR and fluorescence assays, several mechanisms for how the critical inhibitory lysine K922 acts to inhibit ADP release were refuted, and the existing data is consistent with an arginine finger mechanism similar to that used in G-protein regulators.

The QIAKPIRP sequence of the tail interacts directly with Switch I of the motor domain

The use of photochemical cross-linking and MALDI mass spectrometry described in Chapter II came together to show that a direct interaction between the head and tail domains does in fact occur. *In trans* photochemical cross-linking experiments using head constructs labeled on engineered single cysteine add-backs with the photo-activatable crosslinker benzophenone-4-maleimide and tail proteins showed that the kinesin-1 head and tail domain are able to associate in a specific manner, even in the absence of the stabilizing coiled-coil interaction. The

combination of the photochemical cross-linking technique with mass spectrometry allowed for us to map the interaction surface between the head and tail domain. Interestingly, these techniques showed that the regulatory QIAKPIRP motif of tail interacts with the Switch I region of the motor domain (Chapter II, Figure 5). As Switch I is integral in kinesin's enzymatic cycle and positioned adjacent to the nucleotide pocket, the tail interacting with this region of the motor allowed for speculation as to the mechanism of inhibition. The positioning of key regions of the tail on the opposite face of the motor as the microtubule-binding domain indicates that the tail does not act by directly blocking microtubule binding. Instead, the mechanism appears to instead be due to stabilization of the bound ADP.

Cryo-EM reveals that the tail hold Switch I in a "solution-like" conformation and contacts Switch I and the microtubule simultaneously

A cryo-EM reconstruction of a cross-linked head-tail complex confirmed that the tail does not directly compete with microtubule binding, as the head-tail complex was able to bind tightly to microtubules with the help of a Switch II mutant, G234A, that uncouples microtubule binding from the phosphate state of the nucleotide. This sub-8 Å structure clearly shows that the tail interacts with the Switch I region and nucleotide pocket. Not only does the tail directly interact with Switch I, it also holds Switch I in a solution-like conformation, in which the affinity for ADP is high. This conformation of Switch I had never before been seen for microtubule-bound motors. The ability of the tail to hold Switch I "open" in a high ADP-affinity state is thus consistent with the tail's role in inhibiting both basal and microtubule-stimulated ADP release from the motor domain. Surprisingly, this cryo-EM structure also revealed that the tail could simultaneously interact with both the nucleotide pocket and the microtubule. This visualization

suggests that there may be a state within the cell in which kinesin can remain inhibited through the interaction of the QIAKPIRP motif of the tail with Switch I to stabilize bound ADP, yet be microtubule-bound through additional interactions between a N-terminal region of the tail with tubulin. This "parked" state for kinesin-1 would allow for fine-tuning of the motors movement, as this pool of kinesin would be poised for transport and subject to additional levels of motor regulation (Chapter II, Figure 7).

Kinesin-1 regulation bears a striking resemblance to the way G-proteins are regulated by GDIs

The photochemical cross-linking and cryo-EM data suggested that the tail was interacting directly with Switch I and the nucleotide pocket to inhibit the release of bound ADP. Since kinesins and G-proteins share multiple structural elements, it has been suggested by us and others that these two protein superfamilies may also be regulated in a similar fashion (64, 84). The release of bound GDP from G-proteins is inhibited by regulatory binding partners called guanine nucleotide dissociation inhibitors (GDIs) that act through a variety of means to inhibit nucleotide release through interactions with Switch I or the nucleotide pocket. Based on the homology between kinesins and G-proteins, a kinesin-1 head-tail interaction could position the critical K922 tail residue to inhibit ADP release by one or more of these mechanisms, through direct or indirect interactions with the γ-phosphate sensors, $Mg^{2+}$ ion, α/β-phosphates, ribose oxygens or coordinating water molecules. We sought to determine how the kinesin-1 tail, specifically the regulatory K922 residue, is acting to inhibit the release of ADP. Through the use of EPR with spin-labeled nucleotide probes and fluorescence nucleotide release assays we sought to determine if the tail is acting by any of these mechanisms commonly used by GDIs to inhibit nucleotide release in G-proteins and to further analyze the interaction between the kinesin-1 head

and the regulatory tail domain.

The kinesin-1 tail causes a conformational restriction of the nucleotide pocket that is distinct from the "closing" of Switch I seen upon microtubule binding but not dependent on the K922 residue

EPR studies using the 2′,3′-SLADP and SSL-NANDP spin-labeled probes revealed that the nucleotide pocket of the motor domain is conformationally restricted upon interaction of the regulatory tail domain with the head. Importantly, comparison of the EPR spectra revealed that this restriction was different than that seen when the motor binds to microtubules (Chapter III, Figure 10). Therefore, consistent with the cryo-EM reconstruction, the tail is not acting to "close" Switch I. Interestingly, while we found using fluorescent Mant-ADP release assays that mutation of lysine 922 (K922A) in the QIAKPIRP motif of the tail resulted in a complex that was no longer able to inhibit the basal release of ADP, the EPR spectra was identical to the wild-type tail (Chapter III, Figures 13, 14). Together these data suggest that although the K922 residue is critical for the tail's ability to retain ADP in the nucleotide pocket, it is not required for the head-tail interaction.

Understanding the mechanism of K922 inhibition of ADP release

We tested multiple mechanisms by which known GDI regulators inhibit GDP release in G-proteins using our wild-type and K922A mutant tails. The ability of both the wild-type and regulatory mutant K922A tail to produce identical EPR spectras indicate that the tail is not inhibiting ADP release by a simple steric blocking mechanism. Additionally, the lysine is not acting through stabilization of the ribose oxygens, as the location of the spin-label on the probes

is a direct readout of this region. Analysis of EPR spectra on catalytically incompetent motor domains (which are bound to the triphosphate spin label) or the presence of $AlF_4$ (a triphosphate analog) found that the tail's ability to restrict the nucleotide pocket is not dependent on the identity of the bound nucleotide; The aforementioned conformational restriction of the nucleotide pocket was identical for the diphosphate and triphosphate forms of the motor domain (Chapter III, Figure 11). Fluorescence assays using Mant-ADP found that the tail does not stabilize bound ADP through stabilization of the $Mg^{2+}$ ion in the nucleotide pocket, as EDTA could efficiently remove the ion and thus nucleotide, equally in both the presence and absence of the tail (Chapter II, Figure 4). The combined EPR and fluorescence data lead us to believe that the tail-induced conformational restriction that we observe in the nucleotide pocket may be a stabilizing interaction between the head and the tail that is directly involved in the tail's regulatory function. This is the first evidence of a stabilizing interaction between the kinesin-1 tail and the nucleotide pocket in the head. It is possible that the tail-induced restriction of the nucleotide pocket serves to increase the binding affinity of the kinesin-1 head and tail and serve as a scaffold to specifically position the inhibitory K922 residue to inhibit nucleotide release. While the exact mechanism of tail-mediated inhibition remains elusive, the data to date remain consistent with a possible interaction of the K922 residue in the vicinity of the α/β-phosphates. Additional experiments would be necessary to further investigate the possible role that residue K922 may have in stabilizing bound ADP through interactions with the α/β-phosphates of the nucleotide.

**Future experiments**

Solution structure of the head-tail interaction

A solution state x-ray crystal structure of the head-tail complex would be a significant step towards understanding how the tail acts to inhibit nucleotide release from the motor domain. As it is now thought that the tail exerts its regulatory effect mainly in the solution state of the molecule, crystallography would provide the ideal means towards fully understanding the tail's mechanism. This feat would allow for a direct observation of not only the regulatory K922 residue's interactions, but would be a better picture of how the tail interacts with the motor domain, potentially allowing for the design of both kinesin-based inhibitors and activators. This structure could provide verification to our hypothesis that the K922 residue interacts with the α and/or β-phosphates of the bound nucleotide to stabilize it in the nucleotide pocket, or instead could reveal how the tail is truly acting. As the crystal structure of the motor domain is solved, this structure should be able to be used for molecular replacement to determine the phases, and would provide the ideal model for comparison as to how the tail structurally influences the motor domain. The ability of the 27-mer tail peptide to associate specifically with the head provides an ideal complex for crystallography that would make cross-linking unnecessary for product formation, however, it has been shown that efficient cross-linking between residue S188C in the motor domain and an engineered cysteine in the tail is possible (Mark Seeger, personal communication), providing a different construct for crystallization if the affinity between the head and tail peptide is not strong enough to produce crystals of the head-tail interaction. This prospect is being followed-up by Mark Seeger and will hopefully result in a better understanding of how the regulatory tail is interacting with the motor domain to inhibit nucleotide release.

The relevance of the "parked" state for kinesin-1 on microtubules

The visualization of the kinesin-1 tail bound simultaneously to both the Switch I region of the nucleotide pocket and the microtubule is intriguing. A second, nucleotide-independent microtubule-binding site in the kinesin-1 tail has been proposed by others (62, 63), however the physiological relevance for this mostly electrostatic interaction remains unknown. While no *in vivo* data on this state exists to date, single molecule motility assays have shown that full-length motors exhibit discontinuous motion while remaining microtubule-bound (59), suggesting that the tail can indeed inhibit enzymatic activity and simultaneously keep kinesin bound to the microtubule. Identification of the interacting regions between the tail and tubulin is underway in our lab by Mark Seeger, who is using similar photocross-linking and mass spectrometry techniques with single cysteine add-backs on the tail domain to map the tail-tubulin interaction. Also, the role additional proteins may play in fine-tuning this regulatory mechanism is being examined.

OSM-3: is an intramolecular interaction involving Switch I a common regulatory mechanism for kinesin family members?

In light of our finding that the kinesin-1 tail interacts with Switch I to inhibit nucleotide release, the regulatory similarities between the kinesin and G-protein superfamilies became intriguing, as these families also exhibit strong structural and enzymatic homology. The tail domain exhibits a strong resemblance to the GoLoco family of GDIs, as these proteins also act to inhibit GDP release from G-proteins through interactions with Switch I. Additionally, the data to date suggest that the tail may be acting in the same regulatory manner as some classes of these molecules. These similarities bring into question whether other kinesin family members are

regulated through similar interactions between the Switch I region of their motor domain and elements in their tail domain (discussed more thoroughly in Appendix II). OSM-3, a Kinesin-2 family member exhibits many of the biochemical signatures of kinesin-1, including regulation through its C-terminal tail domain (108). Additional sequence similarity between the conserved regulatory QIAKPIRP motif of the kinesin-1 tail with a seemingly similar sequence at the extreme C-terminus of OSM-3 further substantiate this hypothesis. Therefore, we initiated photochemical cross-linking studies similar to those used to determine the kinesin-1—tail interaction using comparable cysteines in the context of the full-length OSM-3 molecule. While we were unable to successfully cross-link the head and tail domain of OSM-3 together using the benzophenone-4-malaimide crosslinker attached to the equivalent of residue S188C in the kinesin-1 motor domain, the feasibility of an analogous regulatory mechanism remains, as many technical difficulties and factors need to be addressed before conclusions can be drawn. As OSM-3 is easy to express and purify, these experimental details should be easily dealt with. It is very possible that OSM3 is indeed regulated by it's tail domain in a manner similar to kinesin-1, and photochemical cross-linking experiments identical to those used successfully to determine the head-tail interaction in kinesin-1 (discussed in Chapter II) should be able to tease this out.

**References**

1. Howard J, Hudspeth AJ, Vale RD (1989) Movement of microtubules by single kinesin molecules. *Nature* 342, 154-8.

2. Block SM, Goldstein LS, Schnapp BJ (1990) Bead movement by single kinesin molecules studied with optical tweezers. *Nature* 348, 348-52.

3. Vale RD, Funatsu T, Pierce DW, Romberg L, Harada Y, Yanagida T (1996) Direct observation of single kinesin molecules moving along microtubules. *Nature* 380(6573):451-3.

4. Svoboda K, Schmidt CF, Schnapp BJ, Block SM (1993) Direct observation of kinesin stepping by optical trapping interferometry. *Nature* 365, 721-7.

5. Vale RD, Reese TS, Sheetz MP (1985) Identification of a novel force-generating protein, kinesin, involved in microtubule-based motility. *Cell* 42, 39-50.

6. Adio S, Reth J, Bathe F, Woehlke G (2006) Review: regulation mechanisms of Kinesin-1. *J Muscle Res Cell Motil* 27, 153-60.

7. Bloom GS, Endow SA (1995) Motor proteins 1: kinesins. *Protein Profile 2*, 1105-71.

8. Sharp DJ, McDonald KL, Brown HM, Matthies HJ, Walczak C, Vale RD, Mitchison TJ, Scholey JM (1999) The bipolar kinesin, KLP61F, cross-links microtubules within interpolar microtubule bundles of Drosophila embryonic mitotic spindles. *J Cell Biol* 144(1):125-38.

9. Desai A, Verma S, Mitchison TJ, Walczak CE (1999) Kin I kinesins are microtubule-destabilizing enzymes. *Cell* 96, 69-78.

10. Hirokawa N, Takemura R (2004) Molecular motors in neuronal development, intracellular transport and diseases. *Curr Opin Neurobiol* 14, 564-73.

11. Yildiz A, Selvin PR (2005) Kinesin: walking, crawling or sliding along? *Trends Cell Biol* 15, 112-20.

12. Miki H, Setou M, Kaneshiro K, Hirokawa N (2001) All kinesin superfamily protein, KIF, genes in mouse and human. *Proc Natl Acad Sci U S A* 98, 7004-11.

13. Vale RD (2003) The molecular motor toolbox for intracellular transport. *Cell* 112, 467-80.

14. Hirokawa N, Takemura R (2003) Biochemical and molecular characterization of diseases linked to motor proteins. *Trends Biochem Sci* 28, 558-65.

15. Seog DH, Lee DH, Lee SK (2004) Molecular motor proteins of the kinesin superfamily proteins (KIFs): structure, cargo and disease. *J Korean Med Sci* 19, 1-7.

16. Vale RD, Fletterick RJ (1997) The design plan of kinesin motors. *Annu Rev Cell Dev Biol* 13:745-77.

17. Kull FJ, Sablin EP, Lau R, Fletterick RJ, Vale RD (1996) Crystal structure of the kinesin motor domain reveals a structural similarity to myosin. *Nature* 380, 550-5.

18. Kozielski F, Sack S, Marx A, Thormählen M, Schönbrunn E, Biou V, Thompson A, Mandelkow EM, Mandelkow E (1997) The crystal structure of dimeric kinesin and implications for microtubule-dependent motility. *Cell* 91(7):985-94.

19. Sablin EP, Kull FJ, Cooke R, Vale RD, Fletterick RJ (1996) Crystal structure of the motor domain of the kinesin-related motor ncd. *Nature* 380, 555-9.

20. Hirose K, Amos LA (2007) High-resolution structural analysis of the kinesin-microtubule complex by electron cryo-microscopy. *Methods Mol Biol* 392:213-30.

21. Sindelar CV, Downing KH (2007) The beginning of kinesin's force-generating cycle visualized at 9-A resolution. *J Cell Biol* 177(3):377-85.

22. Hirose K, Löwe J, Alonso M, Cross RA, Amos LA (1999) 3D electron microscopy of the interaction of kinesin with tubulin. *Cell Struct Funct* 24(5):277-84.

23. Mandelkow E, Hoenger A (1999) Structures of kinesin and kinesin-microtubule interactions. *Curr Opin Cell Biol* 11(1):34-44.

24. Rice S, Lin AW, Safer D, Hart CL, Naber N, Carragher BO, Cain SM, Pechatnikova E, Wilson-Kubalek EM, Whittaker M, Pate E, Cooke R, Taylor EW, Milligan RA, Vale RD (1999) A structural change in the kinesin motor protein that drives motility. *Nature* 402(6763):778-84.

25. Case RB, Rice SE, Hart CL, Ly B, Vale RD (2000) Role of the kinesin neck linker and catalytic core in microtubule-based motility. *Curr Biol* 10, 157-60.

26. Case RB, Pierce DW, Hom-Booher N, Hart CL, Vale RD (1997) The directional preference of kinesin motors is specified by an element outside of the motor catalytic domain. *Cell* 90, 959-66.

27. Henningsen U, Schliwa M (1997) Reversal in the direction of movement of a molecular motor. *Nature* 389, 93-6.

28. Lakamper S, Meyhofer E (2006) Back on track - On the role of the microtubule for kinesin motility and cellular function. *J Muscle Res Cell Motil* 27, 161-71.

29. Kirchner J, Woehlke G, Schliwa M (1999) Universal and unique features of kinesin motors: insights from a comparison of fungal and animal conventional kinesins. *Biol Chem* 380, 915-21.

30. Kirchner J, Seiler S, Fuchs S, Schliwa M (1999) Functional anatomy of the kinesin molecule in vivo. *Embo J* 18, 4404-13.

31. Verhey KJ, Lizotte DL, Abramson T, Barenboim L, Schnapp BJ, Rapoport TA (1998) Light chain-dependent regulation of Kinesin's interaction with microtubules. *J Cell Biol* 143(4):1053-66.

32. Cai D, Verhey KJ, Meyhöfer E (2007) Tracking single Kinesin molecules in the cytoplasm of mammalian cells. *Biophys J* 92(12):4137-44.

33. Cai D, Hoppe AD, Swanson JA, Verhey KJ (2007) Kinesin-1 structural organization and conformational changes revealed by FRET stoichiometry in live cells. *J Cell Biol* 176(1):51-63.

34. Verhey KJ, Rapoport TA (2001) Kinesin carries the signal. *Trends Biochem Sci* 26, 545-50.

35. Hackney DD (1994) Evidence for alternating head catalysis by kinesin during microtubule-stimulated ATP hydrolysis. *Proc Natl Acad Sci U S A* 91, 6865-9.

36. Sadhu A, Taylor EW (1992) A kinetic study of the kinesin ATPase. *J Biol Chem* 267, 11352-9.

37. Hackney DD (1988) Kinesin ATPase: rate-limiting ADP release. *Proc Natl Acad Sci U S A* 85, 6314-8.

38. Cross RA (2004) The kinetic mechanism of kinesin. *Trends Biochem Sci* 29, 301-9.

39. Ma YZ, Taylor EW (1997) Kinetic mechanism of a monomeric kinesin construct. *J Biol Chem* 272, 717-23.

40. Berliner E, Young EC, Anderson K, Mahtani HK, Gelles J (1995) Failure of a single-headed kinesin to track parallel to microtubule protofilaments. *Nature* 373, 718-21.

41. Hancock WO, Howard J (1998) Processivity of the motor protein kinesin requires two heads. *J Cell Biol* 140, 1395-405.

42. Hackney DD (1995) Highly processive microtubule-stimulated ATP hydrolysis by dimeric kinesin head domains. *Nature* 377, 448-50.

43. Lockhart A, Cross RA, McKillop DF (1995) ADP release is the rate-limiting step of the MT activated ATPase of non-claret disjunctional and kinesin. *FEBS Lett* 368, 531-5.

44. Schief WR, Howard J (2001) Conformational changes during kinesin motility. *Curr Opin Cell Biol* 13, 19-28.

45. Schnitzer MJ, Block SM (1997) Kinesin hydrolyses one ATP per 8-nm step. *Nature* 388, 386-90.

46. Hua W, Young EC, Fleming ML, Gelles J (1997) Coupling of kinesin steps to ATP hydrolysis. *Nature* 388, 390-3.

47. Yildiz A, Tomishige M, Vale RD, Selvin PR (2004) Kinesin walks hand-over-hand. *Science* 303, 676-8.

48. Niclas J, Navone F, Hom-Booher N, Vale RD (1994) Cloning and localization of a conventional kinesin motor expressed exclusively in neurons. *Neuron* 12, 1059-72.

49. Hollenbeck PJ (1989) The distribution, abundance and subcellular localization of kinesin. *J Cell Biol* 108, 2335-42.

50. Hackney DD, Levitt JD, Suhan J (1992) Kinesin undergoes a 9 S to 6 S conformational transition. *J Biol Chem* 267, 8696-701.

51. Hisanaga S, Murofushi H, Okuhara K, Sato R, Masuda Y, Sakai H, Hirokawa N (1989) The molecular structure of adrenal medulla kinesin. *Cell Motil Cytoskeleton* 12(4):264-72.

52. Hirokawa N, Pfister KK, Yorifuji H, Wagner MC, Brady ST, Bloom GS (1989) Submolecular domains of bovine brain kinesin identified by electron microscopy and monoclonal antibody decoration. *Cell* 56(5):867-78.

53. Amos LA (1987) Kinesin from pig brain studied by electron microscopy. *J Cell Sci* 87 (Pt 1), 105-11.

54. Stock MF, Guerrero J, Cobb B, Eggers CT, Huang TG, Li X, Hackney DD (1999) Formation of the compact confomer of kinesin requires a COOH-terminal heavy chain domain and inhibits microtubule-stimulated ATPase activity. *J Biol Chem* 274(21):14617-23.

55. Kuznetsov SA, Vaisberg YA, Rothwell SW, Murphy DB, Gelfand VI (1989) Isolation of a 45-kDa fragment from the kinesin heavy chain with enhanced ATPase and microtubule-binding activities. *J Biol Chem* 264, 589-95.

56. Hackney DD, Levitt JD, Wagner DD (1991) Characterization of alpha 2 beta 2 and alpha 2 forms of kinesin. *Biochem Biophys Res Commun* 174, 810-5.

57. Saxton WM, Porter ME, Cohn SA, Scholey JM, Raff EC, McIntosh JR (1988) Drosophila kinesin: characterization of microtubule motility and ATPase. *Proc Natl Acad Sci U S A* 85(4):1109-13.

58. Huang TG, Hackney DD (1994) Drosophila kinesin minimal motor domain expressed in Escherichia coli. Purification and kinetic characterization. *J Biol Chem* 269, 16493-501.

59. Friedman DS, Vale RD (1999) Single-molecule analysis of kinesin motility reveals regulation by the cargo-binding tail domain. *Nat Cell Biol* 1, 293-7.

60. Coy DL, Hancock WO, Wagenbach M, Howard J (1999) Kinesin's tail domain is an inhibitory regulator of the motor domain. *Nat Cell Biol* 1, 288-92.

61. Seiler S, Kirchner J, Horn C, Kallipolitou A, Woehlke G, Schliwa M (2000) Cargo binding and regulatory sites in the tail of fungal conventional kinesin. *Nat Cell Biol* 2(6):333-8.

62. Hackney DD, Stock MF (2000) Kinesin's IAK tail domain inhibits initial microtubule-stimulated ADP release. *Nat Cell Biol* 2, 257-60.

63. Yonekura H, Nomura A, Ozawa H, Tatsu Y, Yumoto N, Uyeda TQ (2006) Mechanism of tail-mediated inhibition of kinesin activities studied using synthetic peptides. *Biochem Biophys Res Commun* 343(2): 420-7.

64. Hackney DD, Stock MF (2008) Kinesin tail domains and Mg2+ directly inhibit release of ADP from head domains in the absence of microtubules. *Biochemistry* 47(29):7770-8.

65. Bathe F, Hahlen K, Dombi R, Driller L, Schliwa M, Woehlke G (2005) The complex interplay between the neck and hinge domains in kinesin-1 dimerization and motor activity. *Mol Biol Cell* 16(8):3529-37.

66. Romberg L, Pierce DW, Vale RD (1998) Role of the kinesin neck region in processive microtubule-based motility. *J Cell Biol* 140, 1407-16.

67. Tomishige M, Vale RD (2000) Controlling kinesin by reversible disulfide cross-linking. Identifying the motility-producing conformational change. *J Cell Biol* 151, 1081-92.

68. Himmel DM, Gourinath S, Reshetnikova L, Shen Y, Szent-Györgyi AG, Cohen C (2002) Crystallographic findings on the internally uncoupled and near-rigor states of myosin: Further insights into the mechanics of the motor. *Proc Natl Acad Sci USA* 99:12645–12650.

69. Willard FS, Kimple RJ, Siderovski DP (2004) Return of the GDI: The GoLoco motif in cell division. *Annu Rev Biochem* 73:925–951.

70. Kull FJ, Endow SA (2002) Kinesin: Switch I and II and the motor mechanism. *J Cell Sci* 115:15–23.

71. Kimple RJ, Kimple ME, Betts L, Sondek J, Siderovski DP (2002) Structural determinants for GoLoco-induced inhibition of nucleotide release by G alpha subunits. *Nature* 416:878–881.

72. Rice, SE (2001) A structural change in the neck region of kinesin motors drives unidirectional motility. Thesis UCSF

73. Lupas A, Van Dyke M, Stock J (1991) Predicting coiled coils from protein sequences. *Science* 252:1162–1164.

74. Salzameda B, Facemyer KC, Beck BW, Cremo CR (2006) The N-terminal lobes of both regulatory light chains interact with the tail domain in the 10 S-inhibited conformation of smooth muscle myosin. *J Biol Chem* 281:38801–38811.

75. Sindelar CV, Budny MJ, Rice S, Naber N, Fletterick R, Cooke R (2002) Two conformations in the human kinesin power stroke defined by X-ray crystallography and EPR spectroscopy. *Nat Struct Biol* 9:844–848.

76. Lowe J, Li H, Downing KH, Nogales E (2001) Refined structure of alpha beta-tubulin at 3.5 A resolution. *J Mol Biol* 313:1045–1057.

77. Sack S, Müller J, Marx A, Thormählen M, Mandelkow EM, Brady ST, Mandelkow E (1997) X-ray structure of motor and neck domains from rat brain kinesin. *Biochemistry* 36:16155–16165.

78. Blasius TL, Cai D, Jih GT, Toret CP, Verhey KJ (2007) Two binding partners cooperate to activate the molecular motor Kinesin-1. *J Cell Biol* 176:11–17.

79. Naber N, Rice S, Matuska M, Vale RD, Cooke R, Pate E (2003) EPR spectroscopy shows a microtubule-dependent conformational change in the kinesin Switch 1 domain. *Biophys J* 84:3190–3196.

80. Pettersen EF, Goddard TD, Huang CC, Couch GS, Greenblatt DM, Meng EC, Ferrin TE (2004) UCSF chimera–A visualization system for exploratory research and analysis. *J Comput Chem* 25:1605–1612.

81. Burmeister Getz E, Xiao M, Chakrabarty T, Cooke R, Selvin PR (1999) A comparison between the sulfhydryl reductants tris(2-carboxyethyl)phosphine and dithiothreitol for use in protein biochemistry. *Anal Biochem* 273(1):73-80.

82. Sousa D, Grigorieff N (2007) *Ab initio* resolution measurement for single particle structures. *J Struct Biol* 157:201–210.

83. van Heel M (1986) Similarity measures between images. *Ultramicroscopy* 21:95–100.

84. Dietrich KA, Sindelar CV, Brewer PD, Downing KH, Cremo CR, Rice SE (2008) The kinesin-1 motor protein is regulated by a direct interaction of its head and tail. *Proc Natl Acad Sci U S A*. 105(26):8938-43.

85. Naber N, Minehardt TJ, Rice S, Chen X, Grammer J, Matuska M, Vale RD, Kollman PA, Car R, Yount RG, Cooke R, Pate E (2003) Closing of the nucleotide pocket of kinesin-family motors upon binding to microtubules. *Science* 300(5620):798-801.

86. Scheffzek K, Stephan I, Jensen ON, Illenberger D, Gierschik P (2000) The Rac-RhoGDI complex and the structural basis for the regulation of Rho proteins by RhoGDI. *Nat Struct Biol* 122-6.

87. Hoffman GR, Nassar N, Cerione RA (2000) Structure of the Rho family GTP-binding protein Cdc42 in complex with the multifunctional regulator RhoGDI. *Cell* 100(3):345-56.

88. Rak A, Pylypenko O, Durek T, Watzke A, Kushnir S, Brunsveld L, Waldmann H, Goody RS, Alexandrov K (2003) Structure of Rab GDP-dissociation inhibitor in complex with prenylated YPT1 GTPase. *Science* 302(5645):646-50.

89. Rosenfeld SS, Correia JJ, Xing J, Rener B, Cheung HC (1996) Structural studies of kinesin-nucleotide intermediates. *J Biol Chem* 271(47):30212-21.

90. Noel JP, Hamm HE, Sigler PB (1993) The 2.2 A crystal structure of transducin-alpha complexed with GTP gamma S. *Nature* 366(6456):654-63.

91. Ford B, Skowronek K, Boykevisch D, Bar-Sagi D, Nassar N (2005) Structure of the G60A mutant of Ras: implications for the dominant negative effect. *J Biol Chem* 280:25697-25705.

92. Ma YZ, Taylor EW (1997) Interacting head mechanism of microtubule-kinesin ATPase. *J Biol Chem* 272:724-730.

93. Olofsson B (1999) Rho guanine dissociation inhibitors: pivotal molecules in cellular signalling. *Cell Signal* 11(8):545-54.

94. Olivares AO, Chang W, Mooseker MS, Hackney DD, De La Cruz EM (2006) The tail domain of myosin Va modulates actin binding to one head. *J Biol Chem* 281(42):31326-36.

95. Müller J, Marx A, Sack S, Song YH, Mandelkow E (1999) The structure of the nucleotide-binding site of kinesin. *Biol Chem* 380(7-8):981-92.

96. Shimizu T, Sablin E, Vale RD, Fletterick R, Pechatnikova E, Taylor EW (1995) Expression, purification, ATPase properties, and microtubule-binding properties of the ncd motor domain. *Biochemistry* 34(40):13259-66.

97. Vetter IR, Wittinghofer A (2001) The guanine nucleotide-binding switch in three dimensions. *Science* 294(5545):1299-304.

98. Stock MF, Hackney DD (2001) Expression of kinesin in Escherichia coli. *Methods Mol Biol* 164:43-8.

99. Skinner RH, Bradley S, Brown AL, Johnson NJ, Rhodes S, Stammers DK, Lowe PN (1991) Use of the Glu-Glu-Phe C-terminal epitope for rapid purification of the catalytic domain of normal and mutant ras GTPase-activating proteins. *J Biol Chem* 266(22):14163-6.

100. Yamaguchi M, Sanbuissho A, Yamamoto S, Tangkawattana P, Sako T, Motoyoshi S, Oba T (1995) DNase I interaction on muscle Z-line. *J Muscle Res Cell Motil* 16(2):123-9.

101. DeBonis S, Simorre JP, Crevel I, Lebeau L, Skoufias DA, Blangy A, Ebel C, Gans P, Cross R, Hackney DD, Wade RH, Kozielski F (2003) Interaction of the mitotic inhibitor monastrol with human kinesin Eg5. *Biochemistry* 42:338-49.

102. Yan Y, Sardana V, Xu B, Homnick C, Halczenko W, Buser CA, Schaber M, Hartman GD, Huber HE, Kuo LC (2004) Inhibition of a mitotic motor protein: where, how, and conformational consequences. *J Mol Biol* 335:547-54.

103. Brier S, Lemaire D, DeBonis S, Kozielski F, Forest E (2006) Use of hydrogen/deuterium exchange mass spectrometry and mutagenesis as a tool to identify the binding region of inhibitors targeting the human mitotic kinesin Eg5. *Rapid Commun Mass Spectrom* 20:456-62.

104. Cochran JC, Gilbert SP (2005) ATPase mechanism of Eg5 in the absence of microtubules: insight into microtubule activation and allosteric inhibition by monastrol. *Biochemistry* 44:16633-48.

105. Turner J, Anderson R, Guo J, Beraud C, Fletterick R, Sakowicz R (2001) Crystal structure of the mitotic spindle kinesin Eg5 reveals a novel conformation of the neck-linker. *J Biol Chem* 276:25496-502.

106. Maliga Z, Kapoor TM, Mitchison TJ (2002) Evidence that monastrol is an allosteric inhibitor of the mitotic kinesin Eg5. *Chem Biol* 9:989-96.

107. Ou G, Blacque OE, Snow JJ, Leroux MR, Scholey JM (2005) Functional coordination of intraflagellar transport motors. *Nature* 436(7050):583-7.

108. Imanishi M, Endres NF, Gennerich A, Vale RD (2006) Autoinhibition regulates the motility of the C. elegans intraflagellar transport motor OSM-3. *J Cell Biol* 174(7):931-7.

109. Vale RD, Goldstein LS (1990) One motor, many tails: an expanding repertoire of force-generating enzymes. *Cell* 60(6):883-5.

110. Tabish M, Siddiqui ZK, Nishikawa K, Siddiqui SS (1995) Exclusive expression of C. elegans osm-3 kinesin gene in chemosensory neurons open to the external environment. *J Mol Biol* 247(3):377-89.

111. Snow JJ, Ou G, Gunnarson AL, Walker MR, Zhou HM, Brust-Mascher I, Scholey JM (2004) Two anterograde intraflagellar transport motors cooperate to build sensory cilia on C. elegans neurons. *Nat Cell Biol* 6(11):1109-13.

112. Higgins D, Thompson J, Gibson T, Thompson JD. Higgins DG, Gibson TJ (1994) CLUSTAL W: improving the sensitivity of progressive multiple sequence alignment through sequence weighting, position-specific gap penalties and weight matrix choice. *Nucleic Acids Research* 22: 4673-4680.

113. Ingold AL, Cohn SA, Scholey JM (1988) Inhibition of kinesin-driven microtubule motility by monoclonal antibodies to kinesin heavy chains. *J Cell Biol* 107(6 Pt 2):2657-67.

114. Wong YL, Dietrich KA, Naber N, Cooke R, Rice SE. Kinesin's tail Restricts its ATP Pocket. Manuscript submitted, *Biophys J*.

115. Focia PJ, Gawronski-Salerno J, Coon JS 5th, Freymann DM (2006) Structure of a GDP:AlF4 complex of the SRP GTPases Ffh and FtsY, and identification of a peripheral nucleotide interaction site. *J Mol Biol* 360(3):631-43.

# Appendix I

## Progress on the purification and salt-dependent conformational changes of the full-length drosophila kinesin-1 heavy chain

**Foreword**

Our original experiments designed to determine how the kinesin-1 motor protein is auto-regulated revolved around the use of the full-length protein. We reasoned that the known interaction between the neck coiled-coil of the motor domain and the tail coiled-coil is not inhibitory, but is instead a stabilizing interaction that allows for an unknown direct interaction between the N-terminal motor domain of the protein and the inhibitory region of C-terminal tail domain. Experiments to study regulation using the full-length molecule necessitated the ability to express and purify the protein in its unproteolyzed form. Historically, not much is known about kinesin-1 auto-regulation, as the full-length molecule has been difficult to work with; not only is the protein poorly expressed, but it also suffers from large amounts of proteolysis, specifically from the C-terminus. As regulation depends on the extreme C-terminal region, even small amounts of proteolysis from this end result in motors that are no longer inhibited. Thus, contamination of a full-length kinesin-1 protein preparation with even small amounts of these proteolyzed species make studying regulation of the molecule very difficult, especially for kinetic assays, as an unregulated motor has very robust activity that will overshadow the effects of regulation. Similarly to other labs, we also had difficulty expressing and purifying the full-length kinesin-1 motor protein. However, after much work, significant progress was made on a purification scheme resulting in our ability to obtain full-length drosophila kinesin-1 with relatively very little contamination. Unfortunately, expression levels limit the amount of protein that we can obtain and the protein by itself is difficult to work with. These challenges can be overcome, but will require significant work and patience. Section I begins with a short introduction to previous efforts on purifying full-length kinesin-1. I will then discuss the development of a better scheme for the purification of the full-length kinesin-1 heavy chain as

well as additional lessons learned while working with the protein. Finally, in Section II, I will touch on the salt-dependent conformational changes that have been observed for the kinesin-1 heavy chain, and discuss our efforts to recapitulate these conformational changes with hydrodynamic studies done in our lab.

## Section I: Development of a purification scheme for the full-length kinesin-1 heavy chain

### Introduction

The full-length kinesin-1 heavy chain has proven itself very difficult to work with for a large number of investigators. Shorter constructs of the motor domain of the protein are readily expressed in *E. coli* and can be purified quite easily both using affinity tags or in their untagged native state. However, longer constructs containing significant portions of the stalk or tail domains, including the full-length molecule, are not expressed well in bacteria. Additionally, a majority of this expressed protein aggregates into insoluble inclusion bodies within the cells. The necessity of an untagged kinesin-1 heavy chain results in a significantly more demanding purification scheme, especially for the full-length protein. The original purification scheme, described in more detail below, relies both on ion exchange chromatography and gel filtration, as well as protein precipitation using ammonium sulfate (98). It exploits the binding properties of the head domains to charged medias, as well as salt-dependent conformational changes within the full-length molecule and solubility characteristics of longer constructs.

Kinesin-1 head domains have been shown to bind quite strongly to the cationic exchanger phosphocellulose (PC), despite the absence of a large net positive charge for the protein at neutral pH. It is believed that the interaction is due to the microtubule-binding surface of kinesin-1, as the outside surface of the microtubule, like the resin, is highly negatively charged

(98). PC media thus provides a very good initial purification step for any construct that contains the motor domain. The resin is easy to work with and the strong binding characteristics of kinesin-1 allows for the removal of significant amounts of contaminating proteins. Kinesin-1 head constructs can be eluted with buffer containing moderate amounts of salt (~450 mM NaCl), although longer constructs may have slightly different elution characteristics that can be determined experimentally.

Longer kinesin constructs containing the C-terminal region of the stalk precipitate at low concentrations of ammonium sulfate (98). This characteristic provides a means of both purifying the full-length protein from contaminating *E. coli* proteins, many of which remain soluble at low concentrations of ammonium sulfate, as well as concentrating the protein sample. Full-length kinesin-1 readily precipitates upon the addition of 36% (w/v) ammonium sulfate to the sample. This precipitate can be collected by centrifugation and resuspended in a minimal amount of buffer, concentrating the sample.

The highly asymmetrical shape of the extended full-length molecule under high ionic strength makes gel filtration chromatography an ideal purification step for full-length kinesin-1, as the desired protein will migrate ahead of contaminating *E. coli* proteins (98). The purification power of this step is limited by the resolution of the gel filtration column, which is greatly affected by the sample injection volume. Thus this technique is a logical step after protein precipitation by ammonium sulfate. Not only can the precipitate be resuspended in a minimal volume, but also the use of a high ionic strength buffer for gel filtration eliminates concerns regarding residual ammonium sulfate. This contamination may be problematic for use with other chromatographic techniques that require binding of the molecule at low ionic strength, but will not affect this procedure.

Constructs containing the kinesin-1 head domain also bind well to positively charged surfaces, allowing for anion exchange chromatography to be used in the purification scheme. This step requires dilution or dialysis of the full-length kinesin-1 peak from the gel filtration column, as the salt concentration must be reduced in order for proper binding of the protein to the column. Bound kinesin-1 will elute from the anion exchange column in roughly 150 mM NaCl.

The combination of the cationic exchanger phosphocellulose and an anionic exchanger such as media containing diethylaminoethyl (DEAE) or quaternary ammonium (Q) groups is sufficient for purification of isolated motor domains. However, the longer kinesin-1 constructs are not as easily purified by these means alone, due to the low ratio of kinesin-1 to contaminating *E. coli* proteins, and thus requires the additional ammonium sulfate precipitation and gel filtration steps to achieve a sufficient level of purity. The protocol as described is time consuming and the resultant yield of full-length protein is quite low. Additionally, the preparation suffers greatly from protein proteolysis. This proteolysis occurs from the C-terminus of the protein and is very problematic for studying regulation; even small deletions from the C-terminal tail domain result in a motor that no longer has regulatory ability. These contaminants must be removed from the full-length protein preparation if one wishes to study regulation, as even small amounts of unregulated protein will skew experiments.

Experimental Objective

My thesis project centered upon determining the mechanism in which the kinesin-1 heavy chain is auto-regulated. In order to study how regulation works in the context of the whole molecule we set out to purify the full-length protein. As alluded to above, this is not a trivial

matter and required significant work in order to produce enough protein suitable for use in experiments testing regulation.

The full-length human and drosophila kinesin-1 heavy chains have been shown to be regulated molecular motor proteins. These proteins not only suffer from expression problems in *E. coli*, but they are also heavily subjected to proteolysis during purification that results in the loss of motor regulation. Thus it is essential for us to purify the full-length, unproteolyzed protein from fragments that contain even slight amounts of proteolysis. Therefore, the main objective of my work was to develop a purification scheme to separate the full-length regulated protein from the proteolyzed fragments that are no longer capable of regulation.

## Constructs

### *Untagged Constructs*

One of our major concerns with designing constructs for the full-length regulation project was that we could not confidently engineer a tag at either the amino or carboxy terminus of the protein without the potential for interference with regulation. Some data suggests that even a 6x-histidine tag located at the N-terminus effected how the motor was being regulated (59), so ideally we wanted to try to work with the untagged version of this protein. Both the human and drosophila kinesin-1 heavy chains have been shown to have regulated enzymatic activity that centers around a critical region of their C-terminal tail domain, the QIAKPIRP sequence motif, and the ability of the molecule to fold over on itself through a flexible hinge region (Hinge II). Truncated motor domains of these proteins are well characterized and full-length constructs are available. Thus we selected these proteins for use in the full-regulation project.

The full-length regulation project initially started using the human kinesin-1 construct our lab had previously been working to purify. This construct, referred to as K963, contains all 963 amino acids of the ubiquitous human kinesin-1 heavy chain (KIF5B) protein in a pET17b vector and is untagged. Before my work on this project, Kari Barlan, a research technician in the lab, had created a cysteine-light version of this protein (K963CLM), built off a K560CLM construct kindly given to us by R. Vale. This construct has all surface cysteine residues mutated to either serine or alanine depending on their structural environment, and seems to behave identically to the wild-type protein.

In addition to using the human K963 constructs we also received from David Hackney at Carnegie Mellon both the full-length drosophila kinesin-1 heavy chain (DKH975), which contains all 975 amino acids of the protein, and a slightly truncated construct, DKH960, which contains residues 1-960. These constructs are untagged and in a pGEX-2T vector. Importantly, they have been shown to be regulated in *in vitro* microtubule-stimulated ATPase assays (54), and a majority of the knowledge regarding kinesin-1 auto-regulation has come from these constructs.

*Tagged Constructs*

Two additional tagged constructs were made in the attempt at purifying solely the full-length molecule. First, we constructed a K963CLM construct that would be amenable to DNA digestion and ligation into a vector containing a 6x-histidine tag. This involved mutating the unique XhoI enzyme cut site out of the K963CLM construct, followed by mutation of the stop codon to a XhoI site. This allowed for ligation into a vector that places a 6x-histidine tag on the C-terminus of the protein, followed by a stop codon. The position of the histidine affinity tag on the C-terminus of the protein would allow for easy purification of only the unproteolyzed protein

using resins containing either nickel or cobalt ions. This construct was never tested, and would most likely exhibit some defects in regulation due to position of the purification tag.

We also made a second construct that contained a smaller tag on the protein's C-terminus. This tag contains only three amino acids, Glu-Glu-Phe. YL1/2, a tubulin antibody, recognizes this sequence of amino acids only when it is found on the extreme C-terminus of the protein (99). The plan was to create this construct in the full-length background, and then selectively purify unproteolyzed full-length DKH975 using a YL1/2 antibody column. This small tag may not interfere as much with regulation and be worth trying if other purification strategies cannot perform well enough for downstream applications. This DKH975-YL1/2 construct was made and sequence verified, but was never tested for expression or purification. This may be a viable option for attaining full-length kinesin heavy chains without the concomitant expression of the kinesin light chains, which has found both stabilize the heavy chain, almost eliminate proteolysis, and allow for the purification of the complex using a 6x-histidine tag found on the light chains (Yao Wong personal communication).

*Constructs testing regulation*

One additional construct, a DKH975 loop deletion mutant (DKH975LD), was made in the DKH975 background to directly test regulation. This construct contains full-length drosophila kinesin-1 heavy chain in which we deleted loop 5 (residues 104-112) in the motor domain, creating an unbroken helix $\alpha 2$. This loop-deletion mutant contained an NcoI restriction site in the mutation, providing a useful screening tool for success of the mutagenesis reaction. The rationale for this mutant is described in more detail in Section II below.

Expression of full-length kinesin-1 constructs

Upon receiving and verifying the untagged full-length constructs, I began trying to purify this difficult protein. Protein expression was the first hurdle that needed to be overcome. As mentioned in the introduction, full-length kinesin-1 does not express particularly well in *E. coli*. Additionally, what little protein that is expressed aggregates within the bacteria and is found in insoluble inclusion bodies within the cells. This is especially the case if the induction of protein expression takes place at 37°C. It has been shown by others that reducing the temperature during induction can result in an overall greater yield of soluble protein, as the protein does not aggregate as readily at lower temperatures (98). We therefore sought to determine the ideal induction conditions for our system.

I found that long induction times and elevated temperature were not desirable for the expression of our protein. While these conditions did increase the total amount of expressed protein, a significant amount of this protein is not usable, as the protein did indeed aggregate into inclusion bodies that are insoluble upon cell lysis. Two types of media, LB (Luria-Bertani) and low-salt TPM (see expression protocol for media components), were tested under a variety of growth temperatures and induction times. We even tested the use of Novagen's Overnight Express AutoInduction media (Novagen (EMB Chemicals, Merck KgaA), Darmstadt, Germany), a system that allows for very high cell density and little care, as the culture auto-induces itself upon depletion of necessary components of the media. Overall we found that decreased induction temperatures and short to moderate induction times gave the best overall yield of soluble, unproteolyzed protein. Specifically, 6 L of low-salt TPM media was supplemented with a 20% glucose solution and antibiotics. These flasks were inoculated with overnight cultures, and allowed to grow at 37°C until the optical density of the culture reached between 0.6 and 1.0.

Cells were then transferred to a refrigerated shaker set at 4°C and allowed to cool for 30 minutes. IPTG was then added at a concentration of 50 μM to induce protein expression for 3.5-6 hours at 20-22°C.

The above optimized expression conditions did not result in an abundance of soluble protein, and therefore other alternatives were considered. Options included purifying protein found in the inclusion bodies under denaturing conditions, as well as turning to a baculovirus expression system using insect cells. Neither of these options seemed truly feasible for this project. We decided against purifying precipitated kinesin-1 from inclusion bodies mostly because of concerns we had for working with denatured protein. Our protein is quite large and refolding the protein into not only a single species, but also the physiological structure may be quite difficult, and not something we have experience with in our lab. We would also need to assure that refolded structure was regulated in the same manner as kinesin-1 purified by other methods. Kinetic activity of the motor may also be compromised upon aggregation within the cells or the denaturing conditions used to purify the insoluble protein. Furthermore previous attempts at purifying kinesin-1 heads from inclusion bodies resulted in enzymatically inactive protein (Sarah Rice and Peter Chien, unpublished observation). The use of a baculovirus expression system employing insect cells was also considered, as the amount of usable soluble protein is our biggest problem. Traditionally, this system can allow for the better expression of difficult proteins. However, the construction of these constructs can take months to prepare and our lab was not equipped to take on this challenge so early in the project. All in all, we decided to use the traditional expression system described above, as it was sufficient enough for our immediate purposes.

Purification using established protocols

*Purification of K963CLM*

Once expression conditions to maximize the amount of soluble, full-length K963CLM were optimized, we set out to do what so many other labs had tried and couldn't achieve; the purification of unproteolyzed, full-length, enzymatically active kinesin-1 without the use of purification tags. We started this process using the established protocol in the lab.

After induction, pelleted cells were resuspended in K963CLM Lysis Buffer containing 20 mM MOPS pH 7.0, 2 mM $MgCl_2$, 1 mM EGTA, 100 mM NaCl, 100 μM ADP, and 1 mM DTT supplemented with protease inhibitors (500 μM PMSF, 1 μM E-64, 10 μg/ml Leupeptin, and 1 μg/ml each of Pepstatin A and Aprotinin). The cell paste was then frozen in liquid nitrogen to aid in lysis as well as long-term storage at -80°C. Cells were then thawed and lysed using a French Press, and lysate was subject to a 100,000 x g spin to pellet insoluble species. This high-speed spin leaves only soluble proteins in the supernatant, and any aggregated protein found in inclusion bodies will be pelleted.

As outlined in the introduction, the first purification step in the procedure is a phosphocellulose (PC) column (P11 resin, Whatman Inc. (GE Healthcare), Florham Park, NJ). The high speed supernatant is loaded onto a 30-ml activated PC column and washed with buffer containing 100 mM NaCl. Bound protein is then eluted with a linear gradient of 100-700 mM salt. K963CLM was present in all protein fractions collected therefore all fractions were pooled. The eluted protein was then subject to a selective ammonium sulfate precipitation, using 36% $(NH_4)_2SO_4$ for 30 minutes at 4°C. K963CLM should precipitate at this concentration of ammonium sulfate, whereas a majority of the contaminating *E. coli* proteins remain soluble. Following centrifugation to pellet the precipitated K963CLM, the pellet was resuspended in a

low-salt buffer containing 20% sucrose for further purification using an Uno-Q anion exchange column (Bio-Rad, Hercules, CA). Resolubilized protein was loaded onto the Q column and washed with buffer containing 100 mM NaCl. A linear gradient was then run to elute bound protein; K963CLM should elute from the anion exchange column at roughly 250 mM NaCl.

Analysis of the end product off the Q column required the use of additional techniques, as K963CLM could not be seen on a Coomassie-stained SDS-PAGE gel, whereas other contaminating proteins were clearly visible. However, the eluted K963CLM protein was easily detected by western blotting using the Suk4 antibody. Suk4 is a very specific monoclonal antibody to the motor domain of the kinesin-1 heavy chain that detects both human and drosophila constructs, with little cross-reactivity (113). Overall, we found that not only was our protein contaminated and not very abundant, as it was undetectable by Coomassie staining, but western blotting revealed that it also suffered from variable degrees of proteolysis (Figure 16).

Thus, the purification scheme as such was not ideal for producing protein for use in studying regulation. Not only were we unable to get decent amounts of protein to work with, but we also suffered from large amounts of degradation that are not separable from the full-length protein using these purification techniques.

Additional attempts at obtaining larger amounts of soluble, full-length K963CLM were not fruitful. The protein was quickly found in insoluble inclusion bodies upon induction of expression in *E. coli*, and the levels of proteolysis were unpredictable between protein preparations. Due to our problems with the human construct, that many other labs had also experienced, we turned to the full-length drosophila constructs that had been characterized by David Hackney. These regulated drosophila kinesin-1 constructs are thought to be easier to

express and purify in an unproteolyzed form, and thus may allow for the purification of the full-length regulated molecule.

*Purification of DKH975*

I next set out to purify the DKH975 construct we had received using David Hackney's protocol from his original regulation work. The published protocol for these constructs is similar to the one used above for K963CLM, however, it includes an added gel filtration step in the purification scheme (54). It was possible that both the nature of the proteins and the added purification step would be key in isolating full-length kinesin-1. Studies using DKH960 were not tried, and would most likely behave similarly to DKH975.

As in the K963CLM protocol, the first step involved binding soluble protein to a PC column equilibrated in 100 mM NaCl. After elution using a linear gradient the pooled protein is subject to selective precipitation using 36% ammonium sulfate. Again, DKH975 should precipitate at this concentration of ammonium sulfate, while contaminating *E. coli* proteins remain soluble. The next step in this scheme is the addition of a gel filtration column run under high salt. As mentioned in the introduction, gel filtration should result in considerable purification of the protein, as the extended conformation formed under high ionic strength will have a much faster mobility through the column, thus eluting before a vast majority of contaminants. The pellet from the ammonium sulfate precipitation was therefore dissolved in a minimal amount of buffer, as the injection volume of the column is limited, spun to remove any remaining insoluble particles, and injected onto the S200 gel filtration column. Fractions containing DKH975 were identified using western blotting and pooled. At this point the salt concentration of the sample must be reduced before use in the fourth and final step, the Q ion

exchange column. This reduction in the ionic strength can be done through either dialysis or dilution. I found that dilution of the sample is favorable for these constructs, as an overnight dialysis step results in significant loss of protein through precipitation. The Uno-Q column was then run as above and the elution fractions analyzed for total protein using Coomassie staining, and DKH975 using western blotting with Suk4 (Figure 17).

Overall, this published protocol gave promising results. Not only did the purification scheme result in a much cleaner final sample, as many of the contaminating proteins were eliminated as assayed by Coomassie staining (Figure 17A), but also the amounts of full-length DKH975 were increased compared to the proteolysis products (Figure 17B). The better performance of this purification was almost certainly due to the addition of the gel filtration step in the protocol. However, despite the promising results, this purification scheme was unpredictable and still suffered greatly from our two biggest concerns: yield and proteolysis. Individual batches varied greatly in the amount of proteolysis seen (see Figure 17B, 18A) and selective precipitation of DKH975 in ammonium sulfate was not dependable. In addition, the length of the prep, particularly the gel filtration step, and sample dilution into a low salt buffer for use on the anion exchange column, proved problematic in keeping the protein soluble. Additionally, having to locate the fractions containing DKH975 added time to the prep, as not only gels, but also western blots frequently needed to be run to ensure that major contaminants were not pooled with DKH975.

**Figure 16. Purification of K963CLM**

Western blot of the final Uno-Q1 anion exchange column used to purify K963CLM, using the monoclonal Suk4 antibody to the kinesin-1 motor domain. Lanes are as follows: molecular weight ladder (cannot be seen), Uno-Q1 Elution fractions #25-33. Although not detectable by Coomassie-staining, full-length K963CLM is clearly visible in the Uno-Q1 Elution fractions #26-33 by western blotting (uppermost band) however shows significant levels of proteolysis. These proteolysis products were not separated from the full-length protein using the initial purification scheme for K963CLM.

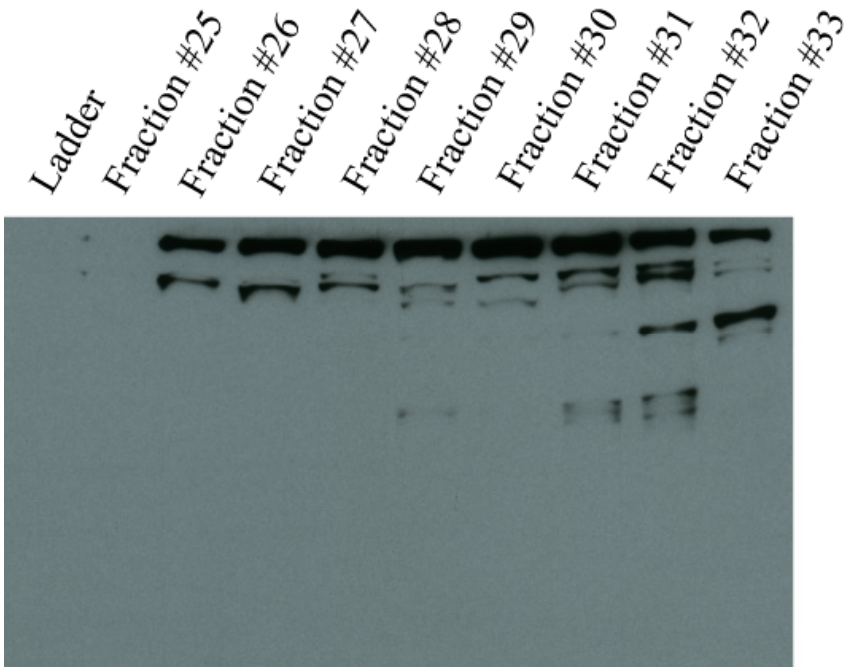
Ladder
Fraction #25
Fraction #26
Fraction #27
Fraction #28
Fraction #29
Fraction #30
Fraction #31
Fraction #32
Fraction #33

**Figure 17. DKH975 Protein Purification**

A. A coommassie-stained SDS-PAGE gel of eluting fractions from the final Uno-Q1 anion exchange column. Lanes are as follows: Invitrogen BenchMark Prestained Protein Ladder with molecular weights at left, protein pooled from S200 gel filtration column, flow-through fractions 1-4 from the Uno-Q1, 1$^{st}$ Peak in Uno-Q1 Elution Fractions #6F-4E, 2$^{nd}$ Peak in Elution Fractions #4D-6D. Relatively few contaminating proteins elute from the Uno-Q1 column, although little full-length DKH975 is detectable (upper-most band, ~110kDa, in 2$^{nd}$ peak).

B. Western blot of the same gel using the Suk4 monoclonal antibody. Full-length DKH975 can be seen in the S200 protein pool and elutes from the Uno-Q1 column only in the 2$^{nd}$ protein peak (three rightmost lanes). Proteolysis products co-elute with this band. Proteolysis levels seen for the purifications were varied, see Figure 18A for another example.

A.

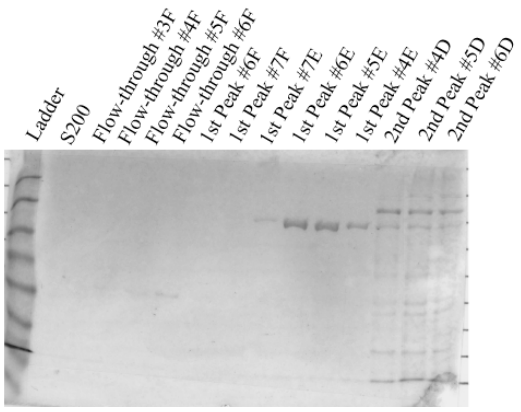
Ladder
S200
Flow-through #3F
Flow-through #4F
Flow-through #5F
Flow-through #6F
1st Peak #6F
1st Peak #7F
1st Peak #7E
1st Peak #6E
1st Peak #5E
1st Peak #4E
2nd Peak #4D
2nd Peak #5D
2nd Peak #6D
kDa
181.8
115.5
82.2
64.2
48.8
37.1

B.

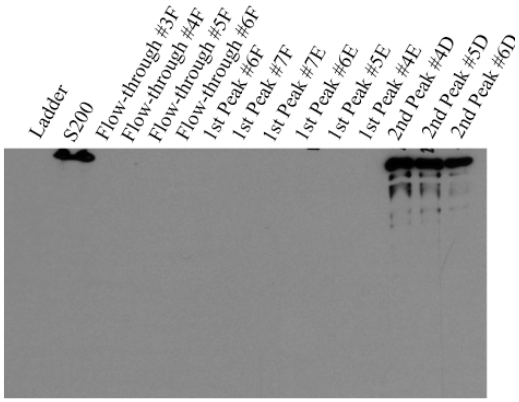
Ladder
S200
Flow-through #3F
Flow-through #4F
Flow-through #5F
Flow-through #6F
1st Peak #6F
1st Peak #7F
1st Peak #7E
1st Peak #6E
1st Peak #5E
1st Peak #4E
2nd Peak #4D
2nd Peak #5D
2nd Peak #6D

Development of a better purification scheme for full-length DKH975

We investigated a myriad of ways in which to clean up our full-length DKH975 protein purification. We first sought to limit the amount of proteolysis that was seen in the preparation by supplementing our cell lysis with additional protease inhibitors, including a commercially available cocktail. We also tried to employ the use of a microtubule bind and release assay to separate the full-length protein from unregulated proteolysis products. Finally, we further investigated a variety of chromatographic techniques, including ion exchange, gel filtration, and hydrophobic interaction chromatography (HIC). The results are detailed below, and our findings allowed for the creation of an improved purification scheme for isolating the full-length protein without contamination from unregulated proteolysis products, detailed at the end of this section.

*Limiting proteolysis*

As our end goal was to be able to test full-length DKH975 for inhibition in various assays, it still was a concern that we were seeing a significant amount of DKH975 proteolysis in our protein preparation. The amount of proteolysis varied between preps and our current purification scheme adapted from reference 54 was unable to isolate the full-length protein from the smaller proteolysis fragments. We therefore attempted to limit the amount of proteolysis in the sample. I found many factors that contributed to the proteolysis, however none of the solutions resulted in the complete inhibition of protein degradation.

Proteolysis of DKH975 was reduced when protein was expressed at lower temperatures for shorter periods of time. I found the ideal conditions to be induction for 3.5 hours at 20°C after the cells were chilled at 4°C for thirty minutes prior to the addition of IPTG. One factor that needs to be considered regarding protein expression is the total amount of soluble DKH975

compared to degraded products. A robust purification that is capable of isolating the full-length protein would allow for the longer 6-hour induction, which results in more soluble DKH975 and ultimately a higher yield of purified protein.

Additionally, I found that the use of DNase I to aid in cell lysis was also contributing to proteolysis. Protein proteases have been shown to contaminate some preparations of DNase I (100). We found that eliminating DNase I from the cell lysis procedure decreased the amount of proteolysis that we were seeing without any effect on the efficiency of cell lysis. I would therefore suggest foregoing the addition of DNase I for any protein in which degradation is a problem unless cell lysis is greatly affected. If this were the case, I would ensure the use of appropriate concentrations of protease inhibitors for all of the major protease classes and limit the use of DNase I as necessary.

Other major factors affecting the level of proteolysis were temperature and the length of the preparation, particularly the early stages. I found that degradation was reduced if steps prior to the ammonium sulfate precipitation were performed as quickly as possible. This includes the cell lysis step using the French Press. I recommend that this step be performed as quickly as possible at 4°C, including the thawing of cell paste, which occurs rapidly upon their addition to the cold French Pressure cell. The use of chilled glassware is helpful for maintaining the reduced temperature necessary to limit the enzymatic activity of the proteases during the high-speed spin and loading of the PC column. Many of the contaminating proteases are likely to be removed with the use of the PC column, however I found that proteolysis does continue throughout the prep, suggesting that at least some protease contamination remains through a majority of the purification steps.

After determining various technical factors within our procedure that allowed for the reduction, but not elimination, of proteolysis, we next turned to the use of additional protease inhibitors to further limit degradation. Our previous homemade protease inhibitor mix contained 500 μM PMSF, 10 μg/ml Leupeptin, and 1 μg/ml of Pepstatin A and Aprotinin. In practice, the protease inhibitor concentrations were at least double, as I found adding the protease inhibitors both upon the initial cell resuspension in lysis buffer and after the first pass through the French Press decreased the amount of proteolysis seen. These protease inhibitors cover a wide range of protease classes, as PMSF and Aprotinin are inhibitors of serine proteases, Leupeptin is a reversible competitive inhibitor of both serine and cysteine proteases, and Pepstatin A is a reversible aspartic protease inhibitor. I found that using a fresh solution of PMSF helped to limit some of the proteolysis, and some variability between the production lots for this chemical exist.

We first added an additional cysteine protease inhibitor to our homemade cocktail: E-64. E-64 is an irreversible inhibitor of cysteine proteases, and its addition seemed to mildly help our proteolysis issues. However, significant proteolysis still remained. We next explored the use of commercially available protease inhibitor cocktails. One consideration in using commercial inhibitor mixes is that many of them contain EDTA. EDTA is a very effective protease inhibitor towards metal-dependent proteases, as it chelates metal ions in solution that are required in the proteases active site, rendering the proteases inactive. However, EDTA cannot be used as a protease inhibitor with kinesin-1, as it also chelates the $Mg^{2+}$ ion from the nucleotide pocket. Loss of the $Mg^{2+}$ ion causes rapid release of the bound nucleotide. Nucleotide-free kinesin-1 is not stable in solution and will quickly precipitate as well as become deactivated over time. Vendors are increasingly realizing the need for EDTA-free protease inhibitor cocktails, as this

chemical component also cannot be used to purify histidine-tagged proteins using nickel or cobalt resin as the metals are stripped from the resin. We thus chose to try the Roche Complete mini EDTA-free protease inhibitor tablets (Roche Diagnostics, Indianapolis, IN) in our purification of DKH975. Unfortunately, we found no difference in the amount of degradation seen compared to our revised homemade protease inhibitor cocktail containing E-64.

Having tried a variety of options to reduce the amount of proteolysis present in our purification, including expression conditions, technique, and additional classes of protease inhibitors, we still had a significant problem that needed to be worked around. The amount of proteolysis seen, while reduced, is still problematic, and necessitates the further development of a protein purification scheme capable of separating the full-length protein from the degradation products.

*Microtubule bind and release*

Various methods were initially tried to both concentrate and clean up the full-length K963CLM and DKH975 proteins from irrelevant contaminants and proteolyzed kinesin. One such experiment tried was a microtubule (MT) bind and release experiment. This experiment exploits the kinesin-1 heavy chains ability to bind to microtubules under some conditions, including the triphosphate nucleotide analog AMPPNP, and be released under conditions of saturating ATP. The binding of kinesin to microtubules allows for removal of irrelevant protein contaminants, while the release step, in theory, should be able to separate full-length kinesin-1 from proteolysis products containing an exposed second microtubule-binding site.

Much work has been done on kinesin-1's enzymatic cycle, and it has been established that the full-length motor binds strongly to microtubules in a triphosphate-bound state (62).

Therefore the kinesin-1 heavy chain will bind to microtubule filaments when the non-hydrolyzable ATP analog AMPPNP is bound in its nucleotide pocket. This tight binding will allow for MT-bound kinesin to be pelleted through a 60% glycerol cushion, while proteins that are unable to bind to microtubules remain in the supernatant above the cushion. This step should provide for both the concentration of kinesin-1 in the sample, as the microtubule pellet is quite small compared to the volume of the staring solution, as well as significant purification of kinesin-1 from contaminating *E. coli* proteins that will be unable to bind microtubules.

The binding step of this experiment must be performed with salt concentrations less than about 50 mM NaCl in order for kinesin to bind tightly to microtubule filaments. Our full-length kinesin-1 samples are in roughly 250 mM NaCl upon elution from the Q ion exchange column and therefore need to be diluted 4-fold in BRB80 buffer to drop the salt concentration. Microtubules were polymerized using purified porcine tubulin as per our established protocol. Taxol was added to the kinesin sample for microtubule stabilization at a final concentration of 50 μM, and 10 μM microtubules, 2 mM AMPPNP, and 2 mM $MgCl_2$ were added. Lastly, 1 unit/ml of apyrase was used to rid the sample of excess ATP and ADP from the purification step, leaving AMPPNP as the sole nucleotide. The reaction was then incubated for 15 minutes at room temperature. Kinesin should bind tightly to microtubules when bound to AMPPNP under these conditions and will pellet with microtubule filaments. The kinesin-microtubule mixture was then spun over a 60% glycerol cushion at 80,000 rpm for 20 minutes at room temperature in a TLA110 rotor and the resulting supernatant above the cushion was removed for later analysis of unbound protein. Microtubule-bound kinesin will now be found in the pellet, whereas proteins unable to bind to MTs are in the supernatant.

The next step of the experiment is the release step. Normally kinesin-1 will be released from the microtubule when excess ATP is added to the solution (62). The addition of hydrolyzable ATP allows for kinesin-1 to continue its enzymatic cycle. After hydrolysis of ATP, inorganic phosphate is released and the resultant ADP-bound motor has a low affinity for microtubules and the head will detach from the filament. This is the case for both isolated motor domains and full-length K963CLM or DKH975. However, it has been shown that proteolysis from the C-terminus of the protein uncovers a second, nucleotide independent microtubule-binding site in the tail domain. Fusion products containing residues 883-937 of the kinesin-1 heavy chain in drosophila bind tightly to microtubules and truncation of DKH975 to DKH937 produces the same effect (62). As this is a nucleotide independent site, these proteolysis products should remain tightly bound to the microtubule under conditions of excess ATP, whereas the full-length protein will be released.

The microtubule pellet from part one of the experiment was then resuspended in release buffer containing BRB80 + 200 mM KCl, 5 mM ATP, 5 mM $MgCl_2$, and 50 μM Taxol. The resuspended pellet was allowed to incubate at room temperature for 5 minutes before given a hard spin at 80,000 rpm for 15 minutes at room temperature. The supernatant and pellet are then separated for analysis. In theory, full-length kinesin-1 should be released from the microtubule under these conditions and be found in the supernatant, while some of the proteolysis products will remain microtubule-bound through their second microtubule-binding site uncovered by degradation.

Unfortunately, these experiments were done early on in the project and suffered from low initial protein levels as well as problems with concentrating the protein found in the supernatants for visualization, and difficulties with our western transfer techniques. Additionally, initial

results suggested that a majority of both the full-length protein and the proteolysis products were remaining bound to the microtubule upon the addition of excess ATP. Overall, a microtubule bind and release step may still be a viable option for either concentrating and further purifying the full-length protein, however, the assay will require significant work and resources before its usefulness can be determined.

*Chromatography Techniques*

As we required a way to separate full-length protein from active proteolysis products we looked into various chromatographic techniques for separating the full-length protein from the proteolysis products present in our purification. We tested the separation ability of a variety of techniques, including anion exchange chromatography, gel filtration, and hydrophobic interaction chromatography. Considerations for success of these techniques hinged both on feasibility and resolution of the full-length protein from proteolyzed fragments. Two of these techniques, gel filtration and hydrophobic interactions, proved particularly promising for our applications, allowing for the development of a new purification scheme for kinesin-1 detailed below.

*1) Ion Exchange Chromatography*

We first investigated the use of ion exchange columns to separate the full-length protein from the various proteolysis products. The use of ion exchange columns necessitates the sample to be in a low salt condition to allow for protein binding. Ideally, the salt concentration needs to be reduced to 50-100 mM NaCl. A variety of anion exchange columns with different functional groups were tested, including a strong exchanging quaternary ammonium (Q) column and

weaker diethylaminoethyl (DEAE) column. None of the columns tested showed much separation in the species we were interested in. Given the lack of resolution and the demands on reducing the ionic strength to allow for binding of the protein we next tested the use of gel filtration chromatography.

*2) Gel Filtration Chromatography*

Previous use of a S200 gel filtration column (Amersham Biosciences (GE Healthcare), Piscataway, NJ) in the published purification of DKH975 (54) that is detailed above proved to be a valuable technique for the separation of kinesin-1 from a large majority of contaminating *E. coli* proteins. We next wanted to test this techniques ability at separating the full-length protein from the smaller degradation products.

Separation of proteins using a gel filtration column relies on the size and shape of the molecule. Larger molecular weight proteins or molecules with an extended rather than globular conformation cannot penetrate as many of the pores in the gel filtration media. Smaller or more compact proteins must therefore travel an effectively longer distance through the column, and therefore elute from the column later than larger proteins or those with extended rod-like conformations. This conformational and size dependence on the elution of proteins from the column may therefore provide a means for us to separate the larger DKH975 from shorter contaminants.

DKH975 partially purified using PC resin was injected onto a smaller Super6 gel filtration column (Amersham Biosciences (GE Healthcare), Piscataway, NJ) under both high salt (500 mM NaCl) and low salt (50 mM NaCl) conditions. Partially purified protein was used in order to maximize the amount of DKH975 in the sample, as protein detection was a concern in

analyzing runs of the gel filtration columns. Not only is the sample injection volume limited (500 µl for the Super6 column), but eluting protein is also sufficiently diluted. We found that under the high-salt conditions we were able to get decent separation between the extended full-length DKH975 and some of the shorter proteolysis fragments (Figure 20A). However, some overlap remained and determination of fractions containing full-length protein versus the proteolysis products required the use of western blotting, thus greatly increasing the length of this purification step.

Although very promising as a purification tool, the use of a gel filtration step in the purification protocol will be difficult, as scale-up will be problematic. This technique will require a concentrated protein sample, as the injection volume is limited (12 ml for our largest column, the S200) and also plays a significant role in the resolution of the column. A smaller injection volume equates to more distinct elution bands, allowing us to better separate the extended full-length protein from slightly shorter proteolysis products. Concentration of the protein sample will be tough as DKH975 is particularly prone to precipitation under high total protein concentrations, limiting the use of spin concentrators. The elution volume off the PC column is typically about 70 ml of pooled protein. This volume may be lessoned by either the use of a high salt concentration rather than a linear gradient, or by batch elution from loose media with high salt. Further reduction will likely be necessary and these concentrated elutions may suffer from protein solubility problems. This precipitation also occurs upon resolubilization of the pellet formed upon ammonium sulfate precipitation of DKH975, resulting in a significant loss of protein. Ideally, as we will be trying to investigate the structure of the full-length protein, I would like to shy away from techniques that require the precipitation of the protein, and therefore am not keen on including an ammonium sulfate precipitation step in the purification.

Thus, how sample concentration will be achieved for injection onto a gel filtration column is a major point of consideration.

Gel filtration under high salt conditions is also not an ideal step for downstream applications, as it will require further sample manipulation. Not only does the gel filtration column significantly dilute the sample, possibly requiring concentration, but also the column must be run under high salt conditions to promote the extended conformation, in which the protein is not regulated. The salt concentration must therefore be significantly dropped after the gel filtration step for downstream assays or for further purification using other chromatographic methods, such as ion exchange.

We unfortunately ran into problems dropping the salt concentration of our protein sample. Dialysis of protein pooled after elution from the PC column into a low salt MgM buffer (20 mM MOPS pH 7.0, 80 mM NaCl, 2 mM $MgCl_2$, 1 mM EGTA, 1 mM DTT, and 100 μM ADP) results in the almost immediate precipitation of DKH975 and its proteolysis products. Interestingly, at least in one dialysis trial, we seem to get selective precipitation of the larger proteolysis products, while less than half of the full-length protein and a much smaller proteolysis product remain soluble (Figure 18A). This may be useful for purifying full-length DKH975 from some of the longer proteolysis products, but may also be nonselective and problematic. Not only is the precipitation of specific proteins inconsistent, but it also results in a significant loss of full-length protein as well, and additional protein may precipitate over time in the lower salt conditions even if dialysis is stopped. The precipitation was most likely due to the low ionic strength of the buffer, as well as the high total protein concentration of the sample. Dialysis into buffers containing additional NaCl (50 mM) did not alleviate the problem. Additional options for desalting and/or concentrating the protein still remain untested, including

the use of spin concentrators to buffer exchange into lower salt conditions, as well as the use of G25 resin. However, given the requirements for both loading the gel filtration column and manipulation of the sample afterwards, we sought to explore other chromatographic techniques for separating our protein. We thus turned to the use of hydrophobic interaction chromatography columns, or HIC.

*3) Hydrophobic Interaction Chromatography*

Hydrophobic interaction chromatography is an increasingly popular technique that relies on hydrophobic interactions between the protein's surface and the uncharged ligand attached to the column media. It has frequently been used for the separation of pure native protein from proteolysis products as the interaction is sensitive enough to be influenced by non-polar groups normally buried in the tertiary structure of a protein but are exposed following protein damage by such things a protease cleavage. These features make this chromatography technique a powerful addition in the purification of proteins with similar characteristics.

Hydrophobic columns are also an ideal addition to a purification scheme, as they are complementary to gel filtration and ion exchange chromatography, and require little sample manipulation when used either before or after other purification techniques. Hydrophobic columns are run using a reverse salt gradient, meaning that protein is bound under high salt conditions and eluted with decreasing ionic strength. This allows the column to be easily used at any point in a purification scheme as no desalting or concentration of the sample is necessary. The only sample manipulation that may be required is the addition of salt or a change of pH. This chromatography technique was thus perfect for our applications, as we could use this column after virtually any step, including the PC or Q ion exchange columns, ammonium sulfate

precipitation, or gel filtration under high ionic strength. Additionally, as the protein elutes as a concentrated sample under conditions of low ionic strength, it could then be used immediately for either kinetic assays or additional purification steps.

A variety of hydrophobic interaction media are available for use in protein purification. Amersham has a Hydrophobic Interaction Chromatography (HIC) selection kit that contains columns of seven HIC media with different hydrophobic characteristics, testing both functional groups and substitution levels (Amersham, GE Healthcare, Piscataway, NJ Product #28-4110-07). This kit allows for the rapid screening of the different chromatographic medias at a low cost to best determine which media is appropriate for your use. We used this selection kit as a starting point for evaluating HIC as a possible purification technique for the separation of full-length and proteolyzed DKH975.

As the binding strength of proteins to the HIC media increases with increasing salt, the HIC selection manual suggests starting with 1.5 M (19.8%) ammonium sulfate in the buffer of your choice for screening proteins with unknown binding characteristics. Our protein, in theory, should remain soluble at this concentration of ammonium sulfate, as 36% (2.72 M) ammonium sulfate is used to precipitate kinesin-1 from solution. Unfortunately, we found that a significant amount of protein from our sample precipitated at 1.5 M ammonium sulfate, necessitating a reduction in the ammonium sulfate concentration. Interestingly, it seemed that shorter proteolysis fragments were selectively precipitating from the protein sample at 750 mM ammonium sulfate, while a majority of the full-length protein remained soluble (Figure 18B). A small number of major kinesin-1 bands are detectable by western blotting after this precipitation. The most prominent band is the full-length DKH975, while lesser amounts of both some slightly smaller proteolysis products and a band roughly the size of the motor domain can be seen.

Although the amount of selective precipitation was variable, the addition of ammonium sulfate did provided us an additional level of purification by removing many of the proteolyzed contaminants in a simple step.

Further reduction of the ammonium sulfate concentration did not decrease the amount of full-length kinesin-1 precipitation; this thus may represent protein precipitating prior to this step and not due to the addition of ammonium sulfate. I have found that giving protein solutions a hard spin at 100,000 x g for 10 minutes at various steps reduces the total amount of protein precipitation seen in samples. This is likely due to the removal of protein precipitates that act as nucleators for further precipitation. I therefore recommend adding a short, hard spin whenever total protein concentration is high, or the ionic strength of the sample is low, to minimize unwanted precipitation.

Upon finding a high ionic strength condition in which our protein is soluble we then tested the columns included in the HIC selection kit for both their ability to bind and elute DKH975, as well as the separation between the full-length protein and remaining proteolysis contaminants. Analysis by western blotting revealed that while we were still losing a significant amount of protein upon addition of ammonium sulfate, the selective precipitation of at least some of the smaller fragments remained. The trial runs of the HIC columns were promising. Full-length protein bound in varying degrees to all media tested. Some columns were found to elute the protein very late in the gradient, at very low ionic strength, while others started eluting the bound protein within the gradient itself.

Multiple factors were considered in determining which of the columns was the most promising purification technique for further optimization. We looked at whether a significant amount of the full-length DKH975 bound to the column under our conditions, or if it was instead

present in the flow through and wash steps. Also considered was the salt concentration required to elute the full-length protein, as too low of an ionic strength may result in significant loss of protein as much of it may remain bound to column, or may present problems with protein solubility. A major consideration was the resolution of the column for separating the full-length DKH975 from the shorter proteolysis products still present in the sample.

All things considered, the Phenyl HP media seemed very promising as a purification technique for DKH975 (Figure 19A). This media gave selective elution during the reverse linear gradient of the shortest proteolysis fragment calculated using conductivity readings at about 536-315 mM ammonium sulfate, while the longer fragment and full-length protein do not elute until later in the gradient, at about 244-64 mM ammonium sulfate. We attempted to exploit these elution characteristics using various ammonium sulfate concentrations to bind or wash the Phenyl HP column in an attempt to better separate full-length protein from the proteolysis products. We predicted that the shortest fragment would be unable to bind to the media at 250 mM ammonium sulfate, while the full-length protein would still be able to be retained. As predicted, the smallest fragment was found in the column flow-through, but so was a significant amount of full-length protein. Slight increases in the ionic strength of the sample may allow for stronger binding of DKH975 without proteolytic contamination, however, this was not tested. Step elutions were also examined to clean up the elution profile, however while we could again remove the smallest contaminant, overlap during the elution still remained between the full-length protein and the longer proteolysis product.

As hydrophobic interaction chromatography using the Phenyl HP media was a promising purification step for DKH975 we sought a higher resolution phenyl column in an attempt to better separate the full-length protein from the overlapping proteolytic fragments. We opted to

try using the Source15PHE media (Amersham, GE Healthcare, Piscataway, NJ) that we could pack into a column ourselves. The initial test of this column, similar to the Phenyl HP, gave us good separation of the full-length DKH975 from the shortest fragments, but overlap with the longer fragments remained (Figure 19B). Additional runs using a step wash at 40% (300 mM) ammonium sulfate followed by a linear elution gradient removed the shortest product, however did nothing for the overlap between full-length and a slightly shorter protein fragment. Hydrophobic interaction chromatography remains a viable option for purifying unproteolyzed DKH975, but will requires additional work to determine the ideal wash steps and elution gradients to separate out the full-length protein from the longer proteolysis fragments. I would also suggest varying the pH of the buffer as this may allow for differential binding of the full-length protein from the overlapping degradation products and subsequent isolation of DKH975.

*Purification Scheme to Isolate Full-length DKH975*

Overall, the hydrophobic interaction chromatography technique, especially using the Phenyl HP and Source15PHE columns, is a promising additional purification step for isolating full-length DKH975. Combined with other steps, it will be a powerful addition as well as a useful tool. Our experiences with different purification techniques have allowed us to propose a better purification scheme for separating the full-length DKH975 from unregulated proteolysis products. This scheme is not meant as a final working purification scheme, as it has not been tested in its entirety as some steps need further optimization, however this outline will provide a strong starting point for a researcher who wishes to purify the unproteolyzed kinesin-1 heavy chain. Below I lay out an ideal purification scheme with suggestions on steps that need further work to fully realize the potential of the purification. I feel that a complete purification scheme

will not be too hard to obtain, as we have determined individual conditions for the columns, and have not yet fully realized the combinatorial power of the columns. This is due to technical difficulties with the sample as well as the decision to go about my thesis project in a different way, no longer necessitating the full-length protein.

An ideal purification scheme based on my experiences with this project would combine some of the previously used techniques, such as the PC and gel filtration columns, with new options explored within my project. Additionally, we avoid the previously used precipitation of DKH975 using ammonium sulfate, which was inconsistent and may have been problematic from a structural and enzymatic point of view. As this purification has never been tested in its entirety, one may find some of the suggestions unnecessary, as prior steps may remove the contaminants being considered.

The first step of the purification consists of the original cation exchange step using phosphocellulose (PC) media. DKH975 binds strongly to this column and elutes within a linear gradient of increasing salt. As DKH975 is found in all of the eluting protein fractions and thus no separation from other bound proteins is obtained, I would suggest the use of a high-salt step elution instead of the linear gradient. The step elution would be advantageous as it decreases the sample volume if the higher salt concentration is not an issue. Alternatively, one could perform a batch elution under high salt to further minimize the sample volume. The higher salt conditions should also better maintain the solubility of DKH975, although I would recommend giving the sample a quick high-speed spin to remove any precipitates that do form due to the high protein concentration.

I would next suggest the use of a gel filtration column run under high salt conditions. This step takes advantage of the ability of the full-length molecule to adopt an extended

conformation under high ionic strength and allows for significant purification from contaminating *E. coli* proteins. It is also a powerful purification technique that allows for the separation of DKH975 from the shorter proteolysis fragments present in the sample. In order to run this column, the eluted protein from the PC column would need to be concentrated for injection onto the column. This concentration step will still need to be worked out, as keeping DKH975 soluble under high protein concentrations has been problematic. The volume reduction in the PC elution step will help, as will performing the concentration under high salt conditions and giving the protein a short high-speed spin directly after both the PC elution and concentration steps to remove any unseen precipitation that could act as a nucleator for further precipitation. Alternatively, multiple runs on the gel filtration column could be performed and full-length protein pooled at the end, however this would be time consuming and the ability to easily detect the full-length protein would need to be considered. Small injection volumes, which increase the resolution of the column, and careful selection of protein fractions may provide all of the actual purification needed for the preparation, as both the *E. coli* proteins and unregulated proteolysis fragments could be resolved from the full-length DKH975. I would highly suggest the use of at least a Coomassie-stained SDS-PAGE gel for fraction selection, if not a western blot to limit the amount of proteolysis products pooled with DKH975, as the column resolution may not be large. Although the gel filtration step provides significant and possibly sufficient purification, the conditions under which the column is run are not ideal for downstream applications. I therefore would still recommend the use of the Phenyl hydrophobic column described below, as it will not only concentrate the sample, but elutes bound protein under conditions amenable to downstream applications.

The last purification step that I would recommend in the purification scheme is the use of a Source15PHE phenyl hydrophobic column. As mentioned above, this column is ideal after a gel filtration step performed under high salt condition, as little manipulation of the sample is necessary. This step also allows for additional purification from proteolysis products if they are still present after the gel filtration step as well as concentration of the purified protein and placement into buffer conditions that are ideal for a wide variety of downstream applications. 750 mM ammonium sulfate would be added to protein fractions containing DKH975 from the gel filtration column and the sample would be given a hard spin to remove precipitation, selective to proteolyzed protein, thus cleaning up the sample slightly. DKH975 will bind to the phenyl column under these conditions. A step wash at 300 mM ammonium sulfate will remove some proteolysis fragments, if they are still present, while a further reverse linear elution gradient to 0% ammonium sulfate elutes full-length DKH975. Additional work on the elution profile of this column may be necessary if the gel filtration step does not sufficiently remove these products, however proper fraction selection in both these steps should allow for the isolation of pure DKH975.

Overall, I believe that this revised purification scheme that both eliminates the use of an ammonium sulfate precipitation step and takes advantage of hydrophobic interaction chromatography will result in the complete purification of unproteolyzed DKH975 with little additional work necessary for optimization. This purification scheme has the power to isolate DKH975 and results in concentration of the protein under conditions ideal for downstream applications. The biggest challenges that must be faced to fully utilize this procedure will be in concentrating the protein prior to gel filtration and picking protein fractions in a timely manner. I do recommend working as fast as possible through the purification, which will both help limit

protein precipitation and proteolysis. Additionally, occasional high-speed spins will remove precipitation nucleators, and storage in 20% sucrose should maintain enzymatic activity and protein solubility after freezing. Another high-speed spin is recommended upon thawing the purified protein, as I have found small amounts of additional protein will precipitate after freezing. Combining what we have learned regarding ideal conditions for DKH975 expression, the use of protease inhibitors, and various purification techniques we have now developed a working protocol for the purification of DKH975, resulting in protein amenable for use in a variety of other applications testing regulation.

**Figure 18. Potential Selective Precipitation of Proteolysis products by Dialysis and Ammonium Sulfate Addition**

A. Western blot using Suk4 showing the selective precipitation of proteolysis products upon a 1 hour dialysis into low-salt conditions. Lanes are as follows: DKH975 protein pooled from the PC column before dialysis, protein remaining in the supernatant after dialysis, protein found in pellet (not quantitative). A significant amount of DKH975 is left remaining in the supernatant after the short dialysis, however this may be due to higher overall starting concentration of this protein rather than selective precipitation of other species.

B. Western blot showing the selective precipitation of proteolysis products upon the addition of various amounts of ammonium sulfate to DKH975 protein pooled from the PC column. Significant amounts of full-length DKH975 remain soluble in the presence of 1.0 M ammonium sulfate or less, while a majority of the shorter proteolysis fragments are found in the pellet. Further decreasing the ammonium sulfate concentration did not result in additional solubility of DKH975, thus this precipitation may be due to unstable protein regardless to the addition of precipitants. Varying levels of proteolysis between preparations can be seen: compare to Figures 17B, 18A.

A.

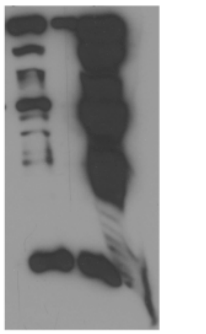
PC Pooled
Dialysis Sup
Dialysis Pellet

B.

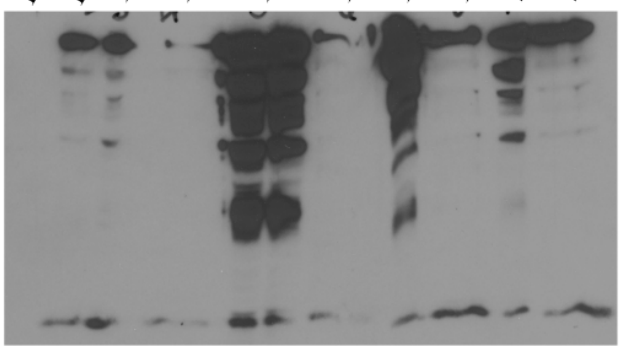
Ladder
DKH975
1.5 M Pellet
1.5 M Sup
1.25 M Pellet
1.25 M Sup
1 M Pellet
1 M Sup
750 mM Pellet
750 mM Sup

**Figure 19. Hydrophobic Interaction Chromatography on DKH975**

A. Western blot of a Phenyl HP column run showing selective elution of proteolysis products at a higher concentration of ammonium sulfate compared to the full-length protein, which elutes towards the end of the linear gradient (Elution fractions 18-23). Lanes are as follows: Ladder, DKH975, Supernatant after addition of 750 mM ammonium sulfate to protein pooled from the PC column, Phenyl HP column flow-through, Wash, Elution fractions #1-10 from the reverse linear gradient, DKH975, Ladder, Elution fractions #11-23.

B. Western blot of a Source15PHE column run again showing later elution of the full-length protein during the reverse linear gradient. Some overlap with longer proteolysis products remains.

A.

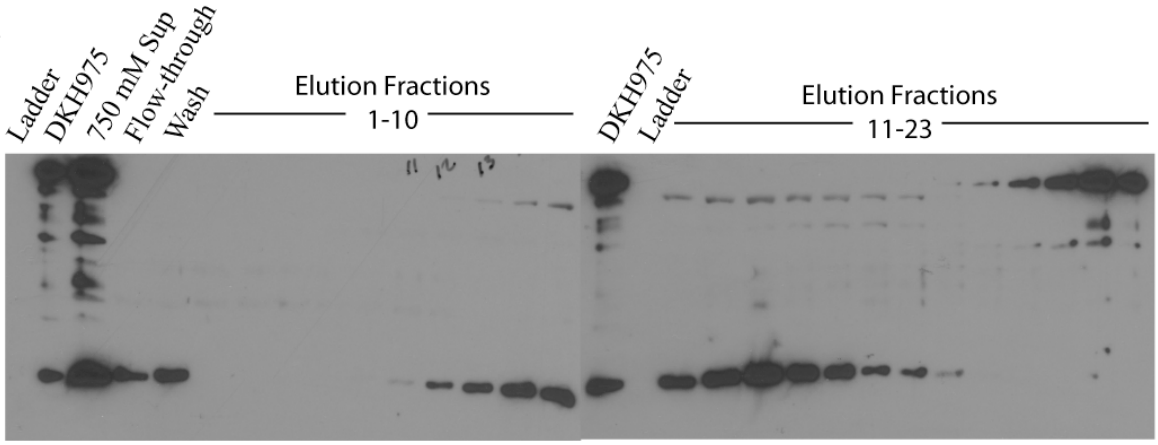
Ladder
DKH975
750 mM Sup
Flow-through
Wash
Elution Fractions
1-10
DKH975
Ladder
Elution Fractions
11-23

B.

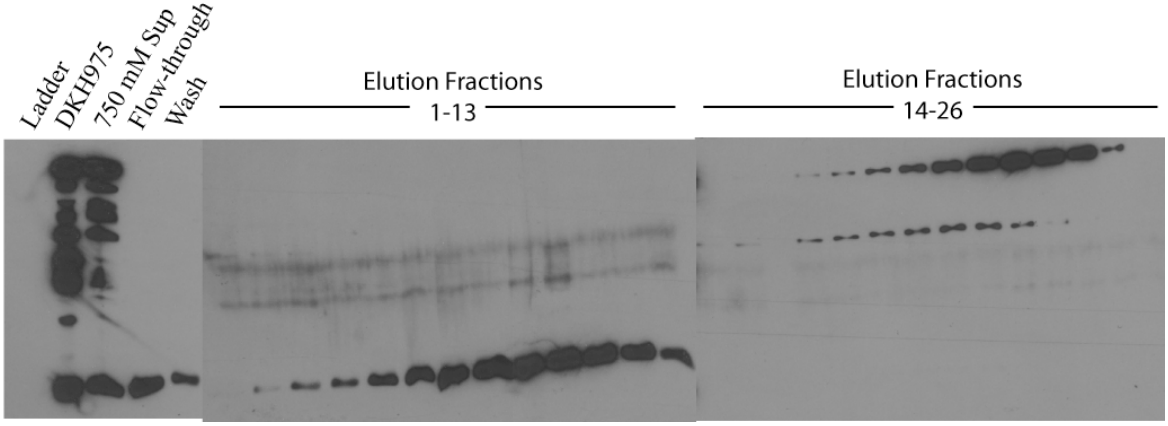
Ladder
DKH975
750 mM Sup
Flow-through
Wash
Elution Fractions
1-13
Elution Fractions
14-26

Technical Challenges and Additional Considerations for working with full-length kinesin-1

Many technical challenges presented themselves throughout the life of this project, thus hampering our efforts at performing experiments aimed at studying how the kinesin-1 heavy chain is auto-regulated. Many of these problems have been worked through, lessons have been learned, and are now no longer limiting factors. Despite finding a purification scheme that will work at purifying DKH975, many difficulties in the full-length regulation project still remain. These problems will need to be addressed in order for regulation studies of the full-length molecule to be feasible. Below are brief descriptions of some of the problems that we have run into with this project, along with either solutions or suggestions for dealing with them that will be useful to future researchers working with the kinesin-1 heavy chain. I also discuss additional considerations for the project that may impact future experiments.

First of all, it is very hard to get appreciable amounts of protein with which to do experiments. This is further complicated by considerable loss of protein throughout the purification due to protein precipitation. As a result, protein detection was a significant problem in our experiments. Low expression levels coupled with dilute samples necessitated the use of western blotting techniques to visualize our protein, as levels were too low to analyze experiments using Coomassie-stained gels. The consistent transfer of high molecular weight proteins to nitrocellulose for western blotting presented a problem for our lab, however we found the use of a heated western transfer protocol to be very helpful in this matter as well as a considerable time saver. Additionally, the protein concentration of many of the samples was so low that it was necessary to precipitate the protein for detection. Not only was this time-consuming, but also presented it's own challenges. We found that using trichloroacetic acid, or TCA, to precipitate full-length protein was not ideal. High molecular weight proteins did not

seem to precipitate fully with this method, and the resulting pellet is very high in salt, creating problems for running the samples on SDS-PAGE. Additionally, I found that samples that were precipitated with TCA did not transfer well to nitrocellulose for western blotting. The problems we experienced with TCA precipitation were greatly alleviated by using acetone to precipitate our proteins instead. Acetone precipitates gave far better recovery of protein in the sample and were more amenable to SDS-PAGE as well as transferring to nitrocellulose compared to TCA precipitates.

The necessity to precipitate our samples for visualization created additional problems as well. Not all of our experimental conditions were amenable to protein precipitation. High concentrations of salts, such as ammonium sulfate, complicated matters, as the salt would also precipitate upon the addition of acetone to the sample. Also the presence of either sucrose or glycerol in the sample did not allow for the pelleting of the precipitates, as the pellet could not be spun through the higher density solution. Experiments run under these conditions therefore required us to use large amounts of our protein samples in order to visualize what is happening to our protein throughout the procedure. Unfortunately, some of these experiments, such as the sucrose gradient centrifugation discussed in Section II, were limited in the amount of starting sample we were able to load, and therefore were inconclusive due to the lack of protein detection.

Protein solubility was also a driving factor. DKH975 does not seem to be very stable, especially under conditions of low ionic strength or high total protein concentration. I found that giving the protein sample a quick high-speed spin (10 minutes at 100,000 rpm) after any sample manipulation was very effective at keeping a majority of the full-length protein soluble. This most likely is the result of removal of precipitation nucleators from the sample. I also suggest

keeping DKH975, especially when concentrated, in moderate salt (~200 mM NaCl) if possible and avoiding long dialysis times into a low salt buffer. However, in order to do kinetic assays studying regulation a concentrated stock of kinesin must be attainable if storage is to be under significant ionic strength. Kinesin-1 is regulated under relatively low-salt conditions (50 mM NaCl), therefore solutions must be of sufficient concentration for enzymatic detection after dilution to the correct ionic strength. Attempts at performing Malachite Green ATPase assays with DKH975 were unable to detect any enzymatic activity and most likely failed due to insufficient protein quantities.

A major concern within the project that I believe is a real possibility is the formation of kinesin-1 heterodimers, specifically a dimer containing one full-length heavy chain and one proteolyzed heavy chain. This may explain our difficulties in separating DKH975 from proteolysis products as well as inconsistencies in the salt-dependent conformational changes discussed in Section II. If this is truly the case, working with the full-length molecule to test regulation may prove impossible. Purification techniques will be unable to separate the full-length protein from proteolyzed protein within the dimer, and thus proteolysis must be eliminated by further examination of the expression and lysis conditions.

## Section II: Hydrodynamic studies of the salt-dependent conformational changes of the kinesin-1 heavy chain

### Introduction

The kinesin-1 heavy chain has been shown to undergo salt-dependent conformational changes by a variety of different techniques. Rotary shadowing electron microscopy (EM) was

the first visualization of the kinesin-1 motor protein (51). These images revealed that kinesin-1 underwent a conformational change dependent on the salt concentration in the solution. At high ionic strength, a majority of kinesin-1 existed in an extended conformation in which the coiled-coil stalk is a straight rod and the globular amino and carboxy termini are located at the ends of the molecule, far from each other in space. As the salt concentration was decreased, kinesin-1 started to fold-over onto itself by a break in the coiled-coil stalk at the Hinge II region. This compact conformation brought the motor and tail domains in close proximity. Importantly, this folded conformation was seen in a majority of the molecules at physiological ionic strength, suggesting that these conformational changes seen by EM are physiologically relevant in the cell. Additional hydrodynamic work using sucrose gradient centrifugation and gel filtration on both the kinesin-1 heterotetramer, containing bound light chains, and a homodimer of the heavy chains were able to verify these salt-dependent conformational changes. This direct hydrodynamic evidence for a transition from a 9.4S form for the heterotetramer containing bound light chains or a 6.7S form for the heavy chain homodimer at low ionic strength to a 6.5S or 5.1S extended form respectively at high ionic strength shows that this conformational change is independent of the presence of the kinesin-1 light chains and are an inherent property of the heavy chains themselves (50).

The combination of this structural data along with the observation that the kinesin-1 heavy chain is enzymatically inhibited by it's C-terminal tail domain at low ionic strength (62) allowed for speculation that the observed compact conformation of kinesin-1 is a regulatory conformation. Folding of the molecule brings the head and tail domains in close proximity, thus allowing for an interaction in the folded conformation that could regulate the motor domain. Multiple lines of evidence, including *in vitro* binding assays, single molecule motility, and

genetic yeast two-hybrid screening, pointed to an interaction between the neck coiled coil region of the motor domain and the tail coiled-coil region at the C terminus of the molecule (54, 59, 65). This interaction is therefore thought to occur while the molecule is in the observed compact conformation. How this relates to regulation was unknown and progress on this front is presented in Chapters II and III of this thesis. Below are our efforts at recapitulating the salt-dependent conformational changes seen for DKH975 as well as the testing of a DKH975 loop deletion mutant by gel filtration and sucrose gradient centrifugation. I also discuss technical challenges that we faced using these techniques.

## Salt-dependent Conformational Changes in DKH975 Using Gel Filtration

### *Experimental Objective*

During our work attempting to purify the unproteolyzed kinesin-1 molecule we wanted to test whether our protein exhibited characteristics indicative of regulation using published assays. The most straightforward experiment was to test whether our protein underwent the salt-dependent conformational changes discussed above using a gel filtration column. We reasoned that if we could not detect the formation of the compact and extended conformations for our protein, kinetic assays testing regulation would be problematic. The gel filtration assay could be done even with low concentrations of protein available, as well as with samples that contained proteolysis products, as the full-length DKH975 could be detected by western blotting. We thus set out to recapitulate the salt-dependent conformational changes seen for the kinesin-1 heavy chain using gel filtration chromatography and sucrose gradient centrifugation (described with the loop mutant below).

*Gel Filtration Experiments on DKH975*

After it was initially found that we could express a decent amount of full-length DKH975, the behavior of our protein under different ionic strengths was tested. Our goal was to determine whether DKH975 purified in our hands could undergo the same conformational changes that had previously been observed for the kinesin-1 heavy chain. We opted to use the Superose6 (Super6) gel filtration column (Amersham Biosciences (GE Healthcare), Piscataway, NJ), as it has a smaller bed volume and thus requires less protein and time then the much larger S200 column (Amersham Biosciences (GE Healthcare), Piscataway, NJ). The column was run under high and low salt conditions, 500 mM and 50 mM NaCl respectively, for both a set of molecular weight standard proteins to establish a standard curve, and DKH975. We found that DKH975 samples that had been through the entire published purification scheme was too dilute for our use, even when protein fractions were acetone precipitated and analyzed by western blotting. We thus performed these assays using DKH975 that had been purified only using phosphocellulose media. Both irrelevant proteins and large amounts of proteolysis products heavily contaminated these samples, however, full-length DKH975 can easily be detected by western blotting of the fractions after protein precipitation.

Results from the gel filtration experiments suggested that we were in fact able to induce salt-dependent conformational changes on the full-length protein. This was determined by plotting the $K_{av}$ of DKH975 eluting from the column under both condition versus the molecular weight of the dimer and comparing these positions relative to the standard curve determined using the molecular weight standard proteins. The protein standards are globular in shape and thus create a relatively straight line on the plot. Proteins that fall below this line appear larger to the gel filtration media than they are given their molecular weight and is indicative of more

extended, rod-like conformations of proteins. Proteins that lie above this line appear smaller than expected, indicating that they form a tighter, more compact structure.

Under high-salt conditions the full-length protein mostly eluded in the early fractions, indicating an extended conformation as it is running larger than its actual molecular weight. Most of the protein eluted in later protein fractions under the low-salt conditions, indicating that it was in a more compact conformation, running smaller than its actual molecular weight (Figure 20). In addition to the clear shift in the shape of the protein, we saw that we had an equilibrium between the extended and compact protein under both conditions, which was promising, as we did not expect to get 100% of the protein in one conformation or the other, only shift the equilibrium towards either the extended or compact conformation depending on the ionic strength of the solution. Importantly, this result was repeatable using protein from the same preparation that had been frozen in liquid nitrogen after the addition of 20% sucrose, allowing us to store protein for later use.

Initial concerns involving proteins "sticking" to the gel filtration media under the low ionic strength condition were addressed by the addition of 0.2% Tween-20, a non-ionic detergent, to the buffers. The presence of the detergent had no effect on the elution position of either the protein standards or DKH975 from the Super6 gel filtration column. However, the ability of the protein to adopt a "super compact" structure is alarming and suggests that nonspecific interactions between the media and protein are still taking place. Our initial results suggest that conformational changes within the protein are occurring, however further work would need to be done to confirm this observation.

DKH975 Loop Deletion Experiments: Is loop 5 involved in formation of the compact conformation?

*Experimental Rationale*

The neck coiled-coil and tail coiled-coil regions of the kinesin-1 heavy chain are known to interact under the low ionic strength conditions and we believe, act to stabilize the folded conformation so that an inhibitory interaction between the C-terminal tail and the motor domain directly can occur. Given what is known about the interacting surfaces of kinesin-1 together with the kinetic data, we believe that this known interaction between the coiled-coil regions is not inhibitory, but instead acts to stabilize kinesin-1 in a folded state. This folding brings together the motor domain and the C-terminal tail, and we believe, allows for a direct inhibitory interaction between the two (see Chapter II for a more detailed discussion). No evidence for this second, direct interaction between these two regions existed before my thesis work. The goal of my project was to determine the mechanism in which the regulatory tail acts to inhibit the motor's enzymatic activity. Key to this was determining the inhibitory interaction that occurred between these two domains.

Given the idea that two separate interactions between the motor and tail domains occur, we propose that there are three potential conformations of the kinesin-1 heavy chain, diagrammed in Figure 21A. The first is the extended conformation that we see under high ionic strength in the gel filtration assay (Figure 21A, *Left*). This conformation produces an enzymatically active and unregulated motor, as the regulatory C-terminal tail cannot interact with the N-terminal motor domain. This is thought to be the conformation adopted by the protein when it is bound to cargo and actively moving along microtubule filaments both *in vivo* and *in vitro*. The second conformation is the fully compact molecule that we see in gel filtration

experiments done under low ionic strength (Figure 21A, *Right*). In this conformation, the molecule is folded and stabilized by the neck coiled-coil-tail coiled-coil interaction, allowable by bending of the heavy chain at the flexible Hinge II region of the coiled-coil stalk. The stabilization of the folded conformation allows for the proposed inhibitory interaction between the tail and the motor domain to take place. These two interactions result in regulation of the kinesin-1 motor domain through inhibition of ADP release. The third, and yet unseen conformation of the kinesin-1 heavy chain is a folded conformation in which the neck coiled-coil and tail coiled-coil are interacting, but the inhibitory interaction involving the extreme C-terminus of the tail and the motor domain is absent (Figure 21A, *Center*). In this folded conformation, the motor would still be active, as the inhibitory interaction stabilizing bound ADP would not be present.

Mutations to either the motor or tail domains in areas that are involved in the inhibitory interaction would be expected to be unregulated molecules, as they would lose their interaction surface by decreased binding affinity or the mutation may remove critical residues involved in the regulatory mechanism. Mutations in the motor domain that resulted in unregulated molecules would most likely change the interaction surface on the motor domain so that the inhibitory part of the tail no longer had sufficient affinity to bind to the motor domain. Mutations to the tail domain would be slightly harder to assess on first look, as these mutations may either identify critical regions directly involved in inhibition, or may instead destabilize the inhibitory interaction by decreasing the affinity between the head and tail.

It may be possible to analyze head and tail mutants for regulation defects using our gel filtration assay. These mutations could be manifested in our gel filtration assay in two ways. Firstly, they could be seen as a shift in the equilibrium between the extended and compact

conformations. This shift in equilibrium could be determined by relative amounts of compact versus extended conformation seen at various salt concentrations. It would be expected that mutations that decreased the binding affinity of the inhibitory interaction would result in molecules that would more readily adopt the extended conformation at lower salt concentrations compared to the wild-type protein. However, this shift will most likely be overshadowed by the strong affinity between the neck coiled-coil and tail coiled-coil.

The second manifestation of unregulated mutants in a gel filtration assay is the emergence of the third conformation described above. This conformation is intermediate between the fully extended active molecule, and that of the inhibited compact conformation. Mutations that decreased the inhibitory binding affinity would still be expected to adopt the folded conformation through interactions between the coiled-coil regions of the neck and tail, but would not be able to fully adopt the fully compact conformation, as the inhibitory interaction cannot be made (Figure 21A, *Center*). The Super6 gel filtration column may provide us with the elution resolution that we require to determine the conformational differences between this folded, but uninhibited state (Figure 21A, *Center*), and the fully inhibited compact conformation (Figure 21A, *Right*). We therefore set out to investigate a region of the motor domain that the tail may be binding, loop 5.

Now that we had a conformational assay working for the full-length protein we wanted to investigate the role of loop 5 in the motor domain in the ability of the molecule to adopt the compact conformation. Loop 5 does not contain any sequence or length conservation within the kinesin superfamily, however it is a structurally conserved loop that breaks helix alpha 2 in all kinesin members. This loop, located 11 Å from the nucleotide pocket of kinesin, is the binding site for monastrol, a potent inhibitor of the mitotic kinesin Eg5 (Figure 21B). Monastrol targets

cell division by inhibiting the formation of the mitotic spindle through a specific interaction with Eg5. This interaction acts to allosterically inhibit both the basal and microtubule-stimulated release of ADP from the motor domain (101-106). It therefore was a logical start for investigating the mechanism of tail-mediated inhibition of the kinesin-1 motor domain, as the two inhibitors block the same step within the kinetic cycle of kinesin, and may work analogously. Therefore we first hypothesized that kinesin-1 was regulated allosterically by an interaction between the C-terminal tail and loop 5 in the motor domain. This interaction results in the stabilization of ADP in the nucleotide pocket and inhibition of the motor's enzymatic activity.

We would expect that if the C-terminal tail were binding to loop 5 to inhibit the motor domain's activity, that deletion of this loop would disrupt this interaction; resulting in a protein that is not able to fully adopt the compact conformation under the low-salt conditions compared to wild type. We therefore predict that the loop deletion mutant should be able to fold over onto itself into the folded conformation, as the neck coiled-coil, tail coiled-coil interaction is unaffected, but that the inhibitory interaction between the C-terminal tail and loop 5 in the motor domain cannot occur and the molecule will not be able to adopt the fully compacted conformation (Figure 21A, *Center*). In the gel filtration assay, this will result in a protein that elutes earlier, and thus less compact, than DKH975 in the low salt condition.

To test this hypothesis, we first created a full-length drosophila kinesin heavy chain in which we deleted loop 5 in the motor domain, creating an unbroken alpha 2 helix. This loop-deletion mutant contained an NcoI restriction site in the mutation, providing a useful screening tool for success of the mutagenesis reaction. After sequence verification and partial purification of expressed protein using the phosphocellulose column, we tested our mutant for its ability to

undergo the same salt-dependent conformational changes that we were able to induce for wild-type full-length kinesin-1, as assayed by gel filtration chromatography and sucrose gradient centrifugation.

*Gel Filtration Assays on the DKH975 loop deletion mutant*

We analyzed the conformation of the DKH975 loop deletion mutant using the Super6 gel filtration column under both the high salt and low salt conditions previously seen the induce conformational changes within DKH975 (see above). We found an identical shift in a salt-dependent fashion for both the wild-type DKH975 and the loop-deletion mutant (Figure 20C), with no difference in the elution profile. These results suggest that loop 5 is not necessary for the formation of the compact conformation, as no conformational differences between the wild-type and loop deletion mutant could be seen. However, it is possible that our gel filtration assay is not sensitive enough to separate out the slight conformational differences between the unregulated, but folded molecule (loop deletion mutant), and the fully compacted protein (wild-type DKH975). Overall, while we could not detect a conformational change upon deletion of the 5 loop of the motor domain, it cannot be ruled out that this loop plays a role in regulation. Further kinetic studies will need to be done to assess the microtubule-stimulated ATPase activities of the motor to determine if this mutant is no longer regulated.

*Sucrose Gradient Centrifugation*

As a confirmation of our gel filtration data, we also tried to recapitulate our results using sucrose gradient centrifugation, another technique routinely used to look at conformational changes in proteins under varying conditions. This technique presented several challenges to us,

mostly involving the amount of protein necessary for experimental analysis, and as thus the results were inconclusive due to inadequate detection of DKH975 and the loop deletion mutant after centrifugation.

The volume of protein sample layered on top of the sucrose gradient is limited and protein is diluted during the separation, thus a major consideration for this experiment was protein concentration. Protein purified only with phosphocellulose is ideal, as the amount of full-length protein in this sample is high compared to after additional purification steps. The use of a 5-20% sucrose gradient however, necessitates either use of the protein directly off the PC column or sample dilution, as protein is stored in a 20% sucrose solution for storage and will thus not fractionate correctly without a decrease in sucrose levels. Reduction of the sucrose concentration can be achieved by either a four-fold dilution or dialysis. In either case, the protein concentration is much reduced, as I have found that dialysis for sucrose removal greatly increases the sample volume. This dilution step also greatly exasperated the second concentration problem, which was the final concentration of our protein seen in the individual layers after the centrifugation. Precipitation of protein samples was almost impossible due to the high levels of sucrose in the fractions preventing the pelleting and thus recovery of the precipitate. These problems greatly hindered the functionality of this technique, rendering it useless without work concentrating the sample before the run.

This sucrose gradient centrifugation experiment was tried for both the DKH975 and DKH975 loop deletion proteins directly after purification from the PC column under both the high salt (500 mM NaCl) and low salt (50 mM NaCl) conditions previously used in gel filtration. Proteins were layered on top of a 5-20% sucrose gradient and spun in a SW41 swinging bucket rotor at 4°C for 13 hours. Catalase, ferritin, albumin, and ovalbumin were used as protein

standards for the runs. After collection of the various layers protein presence was analyzed by both coomassie staining and western blotting. Standard proteins were easily visible by staining with Coomassie-blue, and fractionated by their molecular weight as expected. However, we were never able to achieve the concentration of DKH975 or the loop deletion mutant necessary for visualization, even by western blotting with Suk4. Interestingly, we found that Suk4 cross-reacts with high concentrations of albumin. This should not present a problem, as the molecular weights of these two proteins are drastically different.

**Figure 20. Salt-Dependent Conformational Changes for DKH975 as assayed by Gel Filtration**

A. A western blot of a DKH975 elution profile from the Super6 gel filtration column under high salt conditions (500 mM NaCl). A majority of the full-length DKH975 elutes in the early protein fractions (left gel, peak at 11.75 ml), while the proteolysis products trail. Under both conditions there appears to be an equilibrium established between the extended and compact conformations.

B. Super6 gel filtration column run under low salt conditions (50 mM NaCl). A majority of the full-length protein elutes from the column much later at low ionic strength (right gel, peak at 18.5 ml). The gels show a clear shift in the location of the full-length protein elution peak dependent on the ionic strength of the solution.

C. Plot of $K_{av}$ versus the molecular weight (log scale) for molecular weight standard proteins, full-length DKH975, and the 5 loop deletion mutant, DKH975LD, under both high and low salt conditions. At high ionic strength (500 mM NaCl), DKH975 falls far below the standard curve, indicating it has adopted an extended conformation and appears much larger than it's real molecular weight. Under low ionic strength conditions (50 mM NaCl) DKH975 adopts a more compact conformation, appearing smaller than predicted as it lies much above the standard curve for globular proteins. The addition of Tween-20 to the buffers had no effect on the elution position of either DKH975 or the standard proteins, however, the elution of the protein far above the standards still

suggests some nonspecific interactions are occurring, as discussed in the text. Isolated motor domains (dimeric K420 and monomeric K349) do not show salt-dependent conformational changes and fall on the standard curve under both salt conditions. The DKH975LD mutant exhibits an identical conformational change as the wild-type DKH975 indicating that the loop 5 motif in the motor domain does not seem to have an effect on the ability of the full-length protein to adopt the compact conformation, suggesting that the C-terminal tail domain may not interact with this loop to adopt a fully compacted conformation.

A.

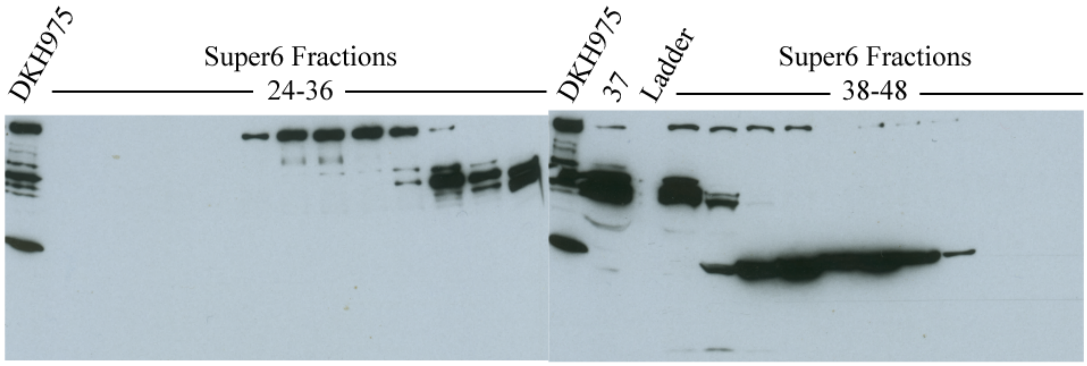
DKH975
Super6 Fractions
24-36
DKH975
37
Ladder
Super6 Fractions
38-48

B.

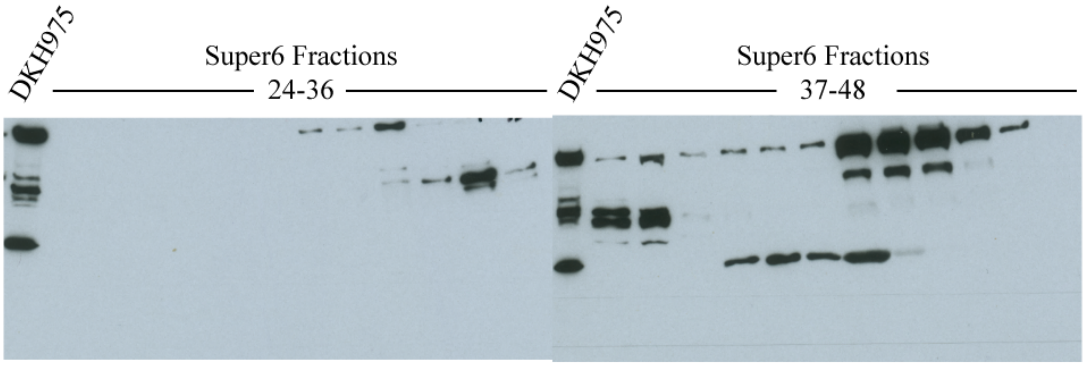
DKH975
Super6 Fractions
24-36
DKH975
Super6 Fractions
37-48

C.

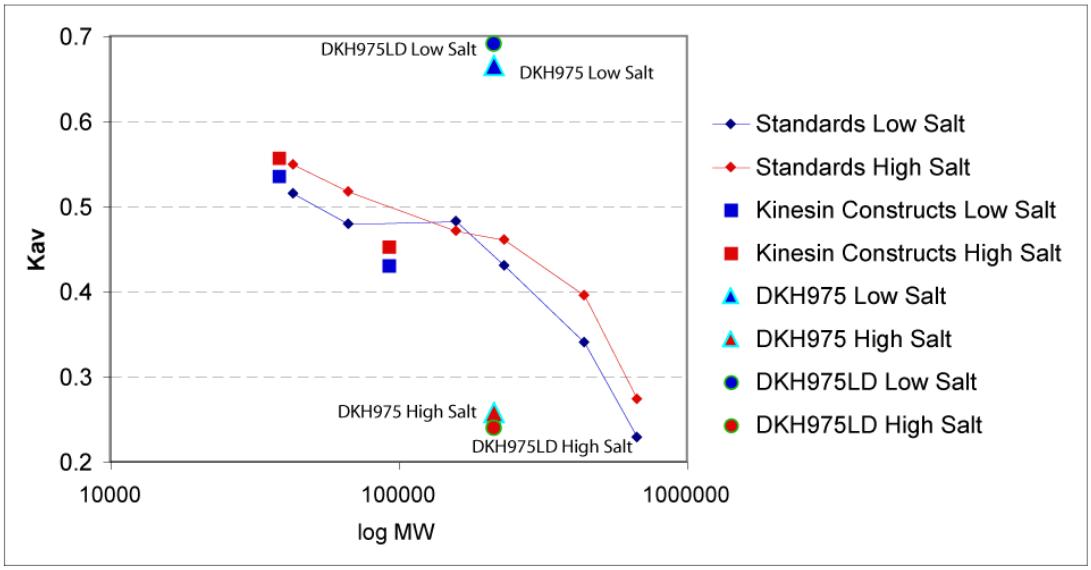
0.7
0.6
0.5
0.4
0.3
0.2
Kav
10000
100000
1000000
log MW
DKH975LD Low Salt
DKH975 Low Salt
DKH975 High Salt
DKH975LD High Salt
Standards Low Salt
Standards High Salt
Kinesin Constructs Low Salt
Kinesin Constructs High Salt
DKH975 Low Salt
DKH975 High Salt
DKH975LD Low Salt
DKH975LD High Salt

**Figure 21. Three possible conformations of DKH975, Location of Loop 5**

A. Diagram detailing the three conformational changes theoretically possible for full-length kinesin-1 heavy chain. The kinesin-1 motor domain is in cyan, the regulatory tail domain in orange, and the kinesin-1 light chains are in green. Under high ionic strength the molecule exists in the extended conformation (*Left*) in which the N and C termini are far from each other. As the ionic strength decreases the molecule is able to fold-over on itself through a flexible Hinge II region in the stalk coiled-coil (*Center*). This bending allows for an interaction between the neck coiled-coil and tail coiled-coil regions of the molecule, stabilizing the folded conformation. The motor domain is theoretically uninhibited, as the coiled-coil interaction between the neck and tail domains is not inhibitory. The third conformation is a fully inhibited motor, wherein the neck coiled-coil—tail coil-coil interaction stabilizes the compact conformation allowing for a direct inhibitory interaction between the kinesin-1 head and tail domains to occur.

B. Structure of the kinesin-1 motor domain (PDB 1mkj) detailing the location of the loop 5, shown in red. Positioning and coloring is similar to that of Figure 4A in Chapter II. The alpha 3/Switch I region is shown in magenta, with residue S188 shown in yellow spheres, β6 is in green, and bound ADP in blue. Loop 5 is deleted in the DKH975LD mutant, fusing the alpha 2 helix together so that it is continuous.

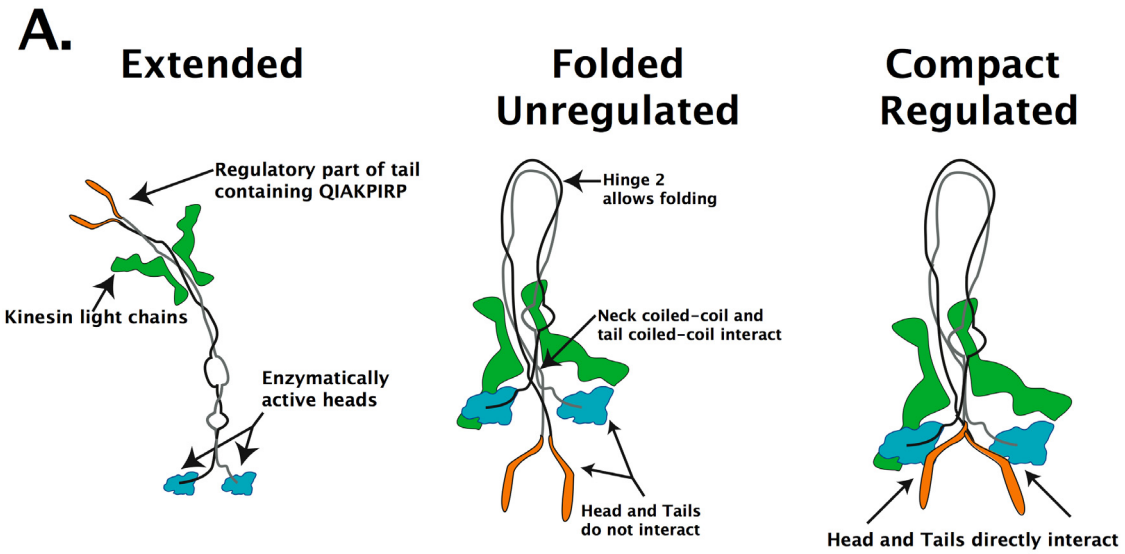
A.
Extended
Folded
Unregulated
Compact
Regulated
Regulatory part of tail
containing QIAKPIRP
Kinesin light chains
Enzymatically
active heads
Hinge 2
allows folding
Neck coiled-coil and
tail coiled-coil interact
Head and Tails
do not interact
Head and Tails directly interact

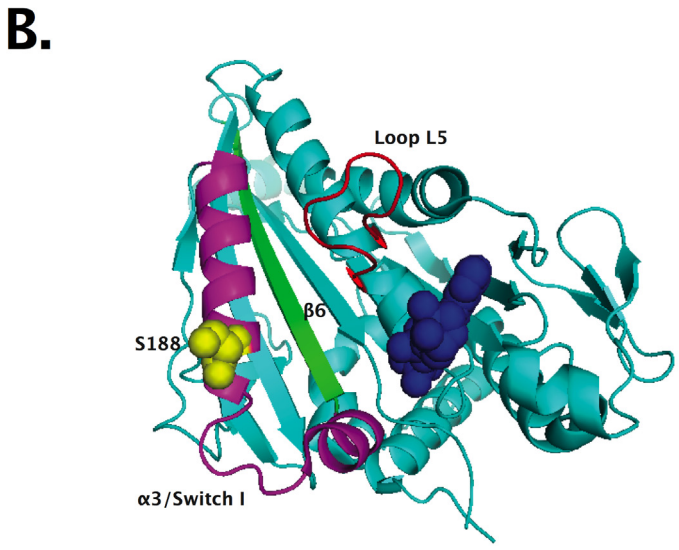
B.
Loop L5
β6
S188
α3/Switch I

Technical Difficulties

Our efforts to explore the conformational changes for both the full-length DKH975 and upon deletion of loop 5 were seriously hampered by problems regarding the amount of protein we could obtain and the variability in proteolysis of the full-length molecule. Many gel filtration runs were inconclusive, and sucrose gradient centrifugation was virtually impossible without gaining the ability to concentrate the protein prior to experimentation. Additionally, gel filtration experiments also lacked consistency, frequently resulting in broad peaks in the lower ionic strength conditions. This may be due to nonspecific interactions between the protein and the column under such low ionic strength, however, the addition of Tween-20 to the buffers did not ameliorate the situation. This broadening is quite possibly from the formation of heterodimers containing varying degrees of proteolysis, as the broadening was most often seen when larger amounts of proteolysis were seen in the sample. The formation of heterodimers would be extremely problematic for future purification schemes. For our regulation experiments we would require that none of the active proteolysis products contaminate our final protein product. However, if the heterodimers are formed, it will be very difficult to separate full-length protein. One would need to select for pure homodimers of the full-length kinesin-1 heavy chain, and thus take a huge loss in the amount of final product. This is not ideal, as the amount of protein produced is already a problem. These problems made determining whether a shift in the equilibrium between the extended and compact conformations nearly impossible. It may also be the case that the Super6 gel filtration column does not have the resolution necessary to separate the fully compact conformation from the folded conformation, and the broad peaks that we are occasionally observing are actually overlapping of the two distinct conformations. The use of the S200 gel filtration column would have the advantage of more separation between eluting

protein peaks, however, as the column is quite large, samples are extensively diluted upon elution requiring massive amounts of protein. This would exist as a problem to us, as we already precipitate our samples after the smaller Super6 column and still have difficulty seeing relevant bands, even by western blotting.

**Conclusions**

In order to study the mechanism of kinesin-1 heavy chain auto-regulation we first required purified full-length protein in large enough quantities and concentrations for downstream use. Similarly to other labs, we had difficulty expressing and purifying the full-length kinesin-1 motor protein. However, after much work, significant progress was made on the purification scheme resulting in our ability to obtain full-length drosophila kinesin-1 with relatively little contamination. Additionally, this protein underwent the expected salt-dependent conformational changes indicative of regulation. Unfortunately, expression levels limit the amount of protein that we can obtain and the protein by itself has proven difficult to work with. These challenges can be overcome, but will require significant work and patience; thus, we choose to approach the kinesin-1 regulation project from a different direction, working with the motor domain and tail domain *in trans* instead of within the context of the full-length molecule. This was a very fruitful turn in the project detailed in Chapter II in this thesis that allowed for the first evidence of a direct interaction between the motor and tail domains of the kinesin-1 heavy chain.

# Appendix II

## Progress on the intramolecular regulation of OSM-3, a Kinesin-2 family member: Does the OSM-3 tail domain interact with Switch I?

**Foreword**

After determining that kinesin-1 is regulated through a direct interaction between Switch I of the motor domain and the conserved regulatory QIAKPIRP motif in the C-terminal tail domain, and speculating that this may be a common mode of regulation among other kinesin and myosin family members, we sought to determine whether OSM-3, a Kinesin-2 family member from *Caenorhabditis elegans*, is regulated in a similar manner. This project proved to be slightly more difficult than originally thought, as we decided to work with full-length OSM-3 rather than work *in trans* as we did for kinesin-1. However, the project still remains promising, as most of the problems we encountered should be circumventable, dealing with technical issues such as labeling conditions and data analysis. However the project may require working *in trans* using OSM-3 motor and tail domains separately, or the construction of a cysteine-light construct similar to that used for kinesin-1. Regardless, the OSM-3 protein proved much easier to work with than full-length kinesin-1, and the crosslinking technique used to identify interacting regions worked well for us with kinesin-1, thus results may come very quickly once technical issues are solved. This appendix begins with an introduction to OSM-3, displaying its biochemical characteristics that led us to believe that it may be an easy target to show the generality of kinesin motor regulation. I then discuss the design of our experiments and initial results that we have obtained, as well as feasible future experiments and suggestions for the success of this project.

## Section I: Progress on characterizing the intramolecular interaction in OSM-3

### Introduction

Osmotic avoidance defective (OSM)-3 kinesin is a Kinesin-2 family member that is involved in intraflagellar transport (IFT) in the sensory neurons of *C. elegans*. OSM-3 works in concert with the heterotrimeric kinesin-II motor to assemble and maintain cilia by transporting IFT particles anterogradely from the base of the cilium to their sites of incorporation at the distal tip (107, 108). It has been shown that both motors cooperatively carry cargo along the middle segment of the cilia consisting of nine doublet microtubules, while OSM-3 alone carries cargo to the distal tip, consisting of nine singlet microtubules (108). A majority of research on this system had focused on how the heterotrimeric kinesin-II motor works, and thus OSM-3 is not well characterized.

Members of the Kinesin superfamily all contain a motor domain of 350-400 amino acids that contains both a nucleotide (adenosine triphosphate, ATP) and a microtubule (MT) binding site (109). Kinesin-1 and OSM-3. like all kinesin members, exhibit strong sequence conservation in this motor domain. Outside of this region very little sequence similarity exists, as these two motors belong to different classes in the kinesin superfamily that are thought to have diverged from each other very early in eukaryotic evolution (13). Examination of the domain architecture of these two molecules however, reveals additional structural similarities. Both proteins contain the sequence-conserved globular motor domain followed by a long coiled-coil stalk. This stalk is broken in two places by presumably flexible hinges. C-terminal to the coiled-coil stalk is a globular tail domain (110).

Recently research has been initiated to understand the OSM-3 motor, and in Imanishi et. al., the Vale lab set out to characterize the molecular properties of OSM-3 in vitro (108). In their

study they found that OSM-3 behaved remarkably similar to kinesin-1, exhibiting many of the same biochemical and hydrodynamic characteristics that had led to the conclusion that the kinesin-1 motor was regulated by an element in its C-terminus.

Biochemical assays on OSM-3 revealed that like kinesin-1, the full-length motor domain of OSM-3 does not exhibit the kinetic parameters necessary for its *in vivo* function. Initial microtubule gliding assays demonstrated that recombinant full-length OSM-3 was indeed a plus-end directed microtubule motor as expected, however the motor's velocity of movement (0.3 μm/s) was much lower than the rates measured for IFT transport by OSM-3 in distal cilia (1.3 μm/s). Additionally, microtubule-stimulated ATPase activity assays showed that the full-length OSM-3 motor exhibited low ATPase activity, with an ATP hydrolysis $k_{cat}$ of only 4 ATP/s/head (108). This rate was much lower than would be expected given the observed motor velocities in distal cilia (300-1300 nm/s), and assuming that like kinesin-1, the motor takes 8-nm steps per ATP hydrolyzed (4). Furthermore, using single-molecule fluorescence, full-length OSM-3 did not exhibit processive motion along the microtubule. This was surprising at first, given that many dimeric motors involved in long-range transport have been shown to be processive in vitro (108). Many of these assays were done under conditions that mimic cargo binding, and are thus activated motors. The lack of processive motion was previously seen for kinesin-1 when "cargo" was not attached (59), and is evidence that the full-length OSM-3 motor is in a regulated state under these assay conditions. In an effort to determine if the C-terminal tail domain was in fact inhibiting the processivity of OSM-3 Imanishi et. al did attempt single molecule fluorescence assays on a construct of OSM-3 that lacked the tail domain (containing residues 1-555). Unfortunately, this construct was found to be an unstable dimer at the low nanomolar concentrations used in that assay and further experiments to characterize the construct were not

attempted. Along these same lines, removal of the native C-terminal domain of OSM-3 (via attachment of the OSM-3 motor domain to the coiled-coil and tail of kinesin-1) fully activated the OSM-3 motor in microtubule-stimulated ATPase and microtubule-gliding assays to levels expected of the motor in its active state, and vice versa, as the kinesin-1 motor domain fused to the C-terminus of OSM-3 displayed the same kinetics. This indicated that like kinesin-1, an element located in the C-terminal domain of the protein was acting to inhibit the motor's kinetic activity, and relief of this interaction fully stimulated the motor.

In addition to the biochemical characteristics of the full-length OSM-3 motor, and further implicating a regulatory element located in the carboxy terminus of the protein, OSM-3 also exhibited salt-dependent hydrodynamic properties that centered on a flexible hinge in the coiled-coil stalk of the protein. Full-length OSM-3, like kinesin-1, adopted a compact conformation in low salt conditions (50 mM NaCl), and popped open into an extended conformation as the ionic strength was increased (500 mM –1 M NaCl) (108). The ability of OSM-3, like kinesin-1, to adopt this compact conformation was absolutely dependent on having a flexible hinge II region in the rigid coiled-coil stalk of the molecule. Deletion of hinge II and annealing of the coiled-coil abolished the ability of the molecule to fold, and a single point mutation of a conserved glycine (G444E) was sufficient for this effect. In addition to the hydrodynamic evidence that OSM-3 can adopt both a compact and extended conformation through folding around hinge II, it was also found that molecules that were unable to fold exhibited the kinetics expected of the activated motor. This included activation of microtubule-stimulated ATPase activity and processive movement in single-molecule TIRF assays. Interestingly, the G444E point mutation in hinge II is a naturally occurring allele found to exhibit chemosensory defects in *C. elegans* (111). These results together imply that this allele is a viable unregulated motor and that the

ability of OSM-3 to form the compact conformation is absolutely essential to the in vivo functioning of OSM-3.

Given the biochemical and conformational similarities between kinesin-1 and OSM-3, Imanishi et al. suggested that OSM-3 is regulated in a similar manner to kinesin-1, in that there is an element in the C-terminal tail domain that acts to inhibit the microtubule-stimulated ATPase activity of the motor, and that this inhibition requires the ability of the molecule to fold over onto itself into a compact conformation around hinge II in its coiled-coil stalk. Additionally, it seems that relief of this inhibition may be by similar means as well, as the binding of cargo to OSM-3 simulated by using beads, activated the motor, resulting in processivity and ATPase activity akin to that seen in the extended conformation.

Additional information regarding the interactions that occur within OSM-3 to inhibit the motor's microtubule-stimulated ATPase activity is limited. It is not presently known whether an interaction comparable to the neck coiled-coil—tail coiled-coil interaction in kinesin-1 exists, nor is there yet any functional regions in the tail domain that have been identified to be important for motor regulation. Interestingly, a sequence alignment of kinesin-1 and OSM-3 invites speculation that a QSAKRPPR sequence found at the extreme C-terminus of the OSM-3 tail (residues 685-692) may be a conserved regulatory motif akin to the QIAKPIRP sequence in the kinesin-1 tail. It is this motif of the tail that we found to interact directly with the Switch I region of the motor domain (84). Therefore the existence of a similar motif in the OSM-3 tail further corroborated the idea that OSM-3 was also regulated by an interaction of its C-terminal tail, specifically this motif, with Switch I of the motor domain. However, as there are not a large number of OSM-3 homologues it is difficult to assess the significance of this sequence similarity.

Full-length OSM-3 had proven to be a relatively easy protein for others to work with. The molecule expresses well in *E. coli*, is soluble, and can be purified using a 6x-histidine tag located on the C-terminus of the molecule. It seems that unlike kinesin-1, this histidine tag does not interfere with regulation, as these constructs exhibited inhibition by various biochemical tests, including microtubule-stimulated ATPase, microtubule-gliding, and single molecule motility assays. OSM-3 does not suffer the proteolysis problems that we experienced with full-length kinesin-1 (discussed in Appendix I), which is very important if the true regulatory element is located at the C-terminus. Overall, the similarities between how OSM-3 and kinesin-1 are regulated along with the ease of working with full-length OSM-3 protein makes OSM-3 the ideal candidate to test our theory that intramolecular interactions involving Switch I of the motor domain are a general mode of regulation among kinesin superfamily members.

Experimental Rationale

Due to our finding that the kinesin-1 motor is regulated through interactions with Switch I in the motor domain (84), and the knowledge that G-proteins, which share strong structural similarities to the motor domains of both the kinesin and myosin superfamilies, are also regulated through interactions with Switch I, it is intriguing to suggest that interactions with Switch I are a common strategy for regulation within the larger kinesin superfamily. We would like to postulate that other kinesin families may be regulated in an analogous way to kinesin-1, a Kinesin-5 family member; that an intramolecular interaction between a C-terminal regulatory motif and the Switch I region of the motor domain inhibits the microtubule-stimulated ATPase activity of the motor. Given the known data about the role of the Kinesin-2 family member OSM-3's C-terminus may play in modulating the motor domain's activity and the relative ease

of working with the full-length OSM-3 protein, we decided to pursue an approach similar to that undertaken with kinesin-1, specifically photochemical crosslinking using benzophenone-4-maleimide, a photoactivatable crosslinker that worked very well for us in determining the inhibitory interaction surface of kinesin-1. For kinesin-1 we really did not know where in the motor domain to start looking for interactions with the tail. Our research can be more focused here, as we are setting out to determine the generality of using Switch I for regulating kinetic activity and therefore our initial experiments will focus on the Switch I region of the motor domain.

Experimental Design

We designed our experiments using full-length OSM-3, as it has been shown by others to express well, was easy to purify, and lacked the proteolysis issues that hampered the full-length kinesin-1 experiments. The initial experimental set-up was to label the protein in it's extended conformation with benzophenone-4-maleimide (Invitrogen Corporation, Carlsbad, CA), then induce formation of the compact form and initiate crosslinking with irradiation with UV light. Cysteines in the motor domain that are located within 9 Å of the interaction surface with the C-terminus would covalently crosslink OSM-3 in the compact conformation. The crosslink retains OSM-3 in the compact conformation, even in high salt buffers that promote opening of the molecule into the extended conformation, or denaturing conditions.

For kinesin-1 we had used a cysteine-light motor domain that allowed us to site-specifically label our protein by adding a single cysteine point mutation at any location that we wished to probe for tail interaction. With OSM-3 we would have to first make this construct, ensure that the motor behaved as wild type in a variety of biochemical assays, and finally add a

cysteine back where desired. Instead of going through all this work we decided to leave in OSM-3's naturally occurring cysteines and simply add a cysteine point mutation near Switch I, a location we considered particularly promising for interacting with the C-terminal tail. This reduced the amount of cloning tremendously, and no longer required the development of kinetic assays for use with OSM-3.

Wild-type OSM-3 contains 6 native cysteines in its amino acid sequence, residues 11, 26, 133, 175, 181, and 303. An additional cysteine added using site-directed mutagenesis results in seven cysteines that could potentially be labeled and involved in crosslinking. In reality, the number of cysteines that are surface exposed and thus available for labeling is probably much smaller. Although we would no longer know at first glance exactly which cysteine is involved in crosslinking, it does not present a serious problem to us. The use of mass spectrometry after trypsin digestion or cleavage with cyanogen bromide is sensitive enough to determine not only which cysteine is cross-linked, but also the region of the C-terminus involved in the interaction within the compact conformation.

As a starting point for probing whether OSM-3 is regulated through an interaction with Switch I we decided to make a single cysteine point mutation corresponding to the S188C mutation that we made in kinesin-1. The S188C mutant provided us with a very good starting point in the kinesin-1 crosslinking project, and allowed us to show not only that Switch I interacts directly with the regulatory portion of the tail in kinesin-1, but the directionality of this interaction. This surface exposed residue is located at the end of the alpha 3 helix, near Switch I, and has been shown to label well in our hands with benzophenone-4-maleimide under mild labeling conditions. The OSM-3 and kinesin-1 motor domains have strong sequence similarity, and thus it is very likely that residues that align in the sequence analysis are spatially conserved,

especially those residues located within the structural core of the motor, rather than the more variable sequences found in loops. We can therefore predict that like residue S188 in kinesin-1, the aligned residue in OSM-3 will be surface exposed and in the position we desire to test for interactions with Switch I. Based on a CLUSTALW pairwise sequence alignment of the kinesin-1 and OSM-3 motor domains we found that residue 188 in kinesin-1 should correspond to asparagine N190 in OSM-3 (112). To try to ensure that we were adding a cysteine that would be located at the surface of the protein, we also made a point mutation at glycine G188 in OSM-3, in case the helix is positioned slightly different in this structure. Wild-type Osm-3 can now serve as a control for the crosslinking reaction. If crosslinking occurs only for the N190C construct we can be fairly sure that the crosslinking is through this cysteine. However, if crosslinking also occurs in the wild-type protein as well, it will be through a native cysteine. This would not be a negative result, as this crosslink may be interesting as well, but would help us to narrow down our results and guide the experiment.

## Materials and Methods

### Constructs

We obtained an OSM-3 clone from R. Vale at UCSF (original OSM-3 cDNA obtained from J. Scholey, UC Davis), in a pET-17b expression vector, which encodes amino acids 1-699 of *C. elegans* OSM-3 with a C-terminal 6x-histidine tag. The clone was sent to the Genomics Core Facility at Northwestern University for sequence verification using both the T7 promoter and T7 terminator sequencing primers. The single cysteine point mutations N190C and G188C were made in wild-type OSM-3 by Quikchange II mutagenesis (Stratagene, La Jolla, CA) following our standard site-directed mutagenesis protocol and verified by DNA sequencing.

Protein Expression and Purification

Expression studies based on published methods (26) were performed and indicated that our growth conditions in TPM media were able to produce significant amounts of soluble protein upon induction with 0.1 mM IPTG at 23°C overnight. However, the published protocol (26) for purifying this protein did not result in an abundance of OSM-3 over other contaminating proteins. Briefly, this protocol involved binding the histidine-tagged OSM-3 to Nickel-NTA resin (Invitrogen Corporation, Carlsbad, CA), washing with a phosphate buffer at pH 6.0, and after an imidazole elution, a Q ion exchange column. I then learned that many of the protocols for purifying histidine-tagged proteins from the Vale lab are not optimized for particular proteins, but are instead based off protocols for a histidine-tagged protein that contained a cloning error resulting in a 5x-histidine tag instead of the stronger binding 6x-tag (Sarah Rice, personal communication). This explains the use of the lower pH buffer during the Nickel-NTA wash step, as it is a less stringent condition, and thus the presence of a large number of contaminating proteins in the prep. Further attempts to purify OSM-3 using Nickel-NTA resin under more standard conditions (Wash buffer: 50 mM Hepes pH 7.0, 50 mM Imidazole, 500 mM NaCl, 4 mM $MgCl_2$, 1 mM EGTA, 5 mM βME, 10 μM ATP; Elution buffer: 50 mM Hepes pH 7.0, 500 mM NaCl, 350 mM Imidazole, 4 mM $MgCl_2$, 1 mM EGTA, 5 mM βME, 10 μM ATP) proved quite fruitful and resulted in relatively pure protein without the need for the additional ion exchange step in the purification (Figure 22).

**Figure 22. Coomassie-stained gel of purified wild-type OSM-3 and the N190C mutant before and after irradiation with UV light**

A Coosmassie-stained SDS-PAGE gel showing Ni-NTA-purified 6x-Histidine tagged OSM-3 and OSM-3 N190C. The protein was labeled with benzophenone-4-maleimide and the cross-linking reaction was attempted in the compact conformation induced by low ionic strength. No detectable bands thought to correspond to a successful cross-link are visible after irradiation of the sample with 254 nm UV light. The lanes are as follows: SeeBlue Plus2 molecular weight standard (Invitrogen Corporation, Carlsbad, CA), wild-type OSM-3 before irradiation, wild-type OSM-3 after a 5 minute irradiation, OSM-3 N190C before irradiation, OSM-3 N190C after a 5 minute irradiation. The molecular weight of the standards is indicated on the left in kDa. Significant precipitation can be seen in the UV-treated samples, however a successful cross-link is not detectable for either protein by comparison of the samples before and after irradiation.

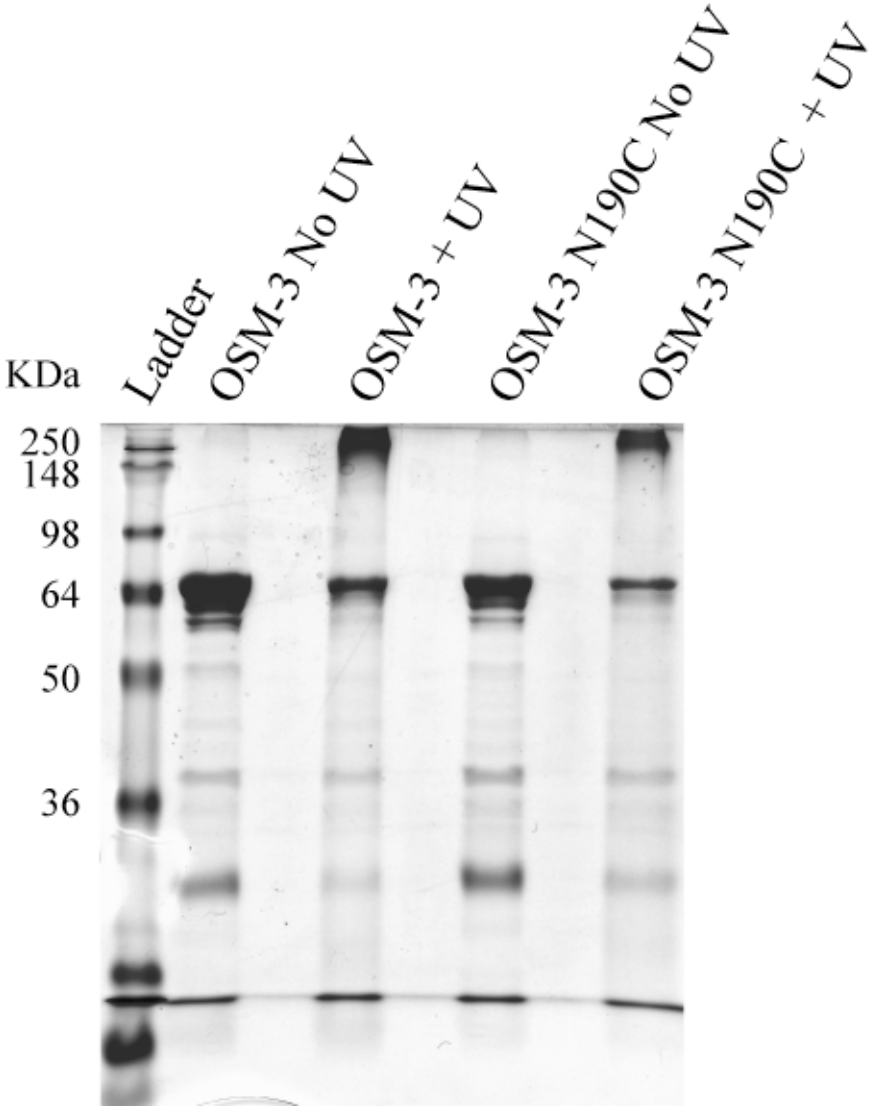
KDa
Ladder
OSM-3 No UV
OSM-3 + UV
OSM-3 N190C No UV
OSM-3 N190C + UV
250
148
98
64
50
36

Gel filtration to assay salt-dependent conformational changes

Once we were able to obtain pure protein we wanted to ensure that OSM-3 could undergo the published salt-dependent conformational changes under our conditions, as cysteines in critical interaction areas will label only when OSM-3 is in the extended conformation. Gel filtration experiments were performed using a Superose6 gel filtration column (Amersham Biosciences (GE Healthcare), Piscataway, NJ) on wild-type OSM-3 under conditions in which the protein has been published to be in an extended (500 mM NaCl) or compact (50 mM NaCl) conformation (108). After using the elution profile of blue dextran to determine the void volume of the column in the two different salt conditions, OSM-3 was injected onto the column and the elution volume was determined using Coomassie-stained gels of protein-containing fractions. OSM-3's $K_{av}$ was then calculated in each salt condition for data analysis (see appendix I for more detailed information about gel filtration experiments on the Super6 column). To determine if OSM-3 is undergoing a salt-dependent conformational change similar to kinesin-1s, I plotted the OSM-3 gel filtration data with the gel filtration data I had previously collected in similar buffer conditions for full-length drosophilia kinesin-1 heavy chain (DKH975) and other truncated kinesin constructs (Figure 23). Gel filtration molecular weight standards previously run with the DKH975 samples at both salt conditions are also shown in order to better visualize trends in protein elution that are based on salt concentration alone, not significant conformational changes. Plotting the log of the molecular weight (MW) versus the $K_{av}$ shows that OSM-3 seems to be undergoing the same conformational change as the kinesin-1 heavy chain. At low ionic strength OSM-3 is compact, as it lies above the line established for globular proteins, and appears smaller than expected given its molecular weight. As the ionic strength is increased to the high salt conditions OSM-3 adopts an extended conformation, falling below the line for globular proteins,

and now appears larger than it should. Although the difference is not as dramatic as that seen with DKH975, it is fairly conclusive that we are able to fold OSM-3 in a salt-dependent manner, and that the salt concentration in our labeling condition favors an extended conformation. The confirmation of the published salt-dependent conformational changes under our conditions should allow for both the labeling of cysteines in the extended conformation that are near the interaction surface of the motor domain with the C-terminus, and thus blocked for labeling in the compact conformation, as well as crosslinking the compact conformation by irradiating the sample with UV light in the low ionic strength conditions.

**Figure 23. Gel-filtration indicates that OSM-3 undergoes a salt-dependent conformational change**

Plot of the calculated $K_{av}$ versus the molecular weight (log scale) for OSM-3 under both high and low salt conditions (500 mM NaCl and 50 mM NaCl respectively). Molecular weight standard proteins and full-length drosophila kinesin-1 heavy chain (DKH975) under identical conditions are shown for comparison. At high ionic strength, OSM-3 falls below the standard curve, indicating it has adopted an extended conformation and appears larger than the real molecular weight of the homodimer. Under low ionic strength conditions OSM-3 adopts a more compact conformation, appearing smaller than predicted as it lies above the standard curve for globular proteins. The addition of Tween-20 to the buffers had no effect on the elution position of either DKH975 or the standard proteins. Isolated kinesin-1 motor domains (dimeric K420 and monomeric K349) do not show salt-dependent conformational changes and fall on the standard curve under both salt conditions. The location of OSM-3 below and above the globular standards in high and low salt respectively indicates that the protein is able to undergo a conformational change dependent on the ionic strength of the solution. While this conformational shift is not as extreme as that seen for the full-length kinesin-1 heavy chain (DKH975), the smaller difference between the two states was expected, as the coiled-coil region of OSM-3 is shorter than that of kinesin-1. The observed shift does not seem to be due to OSM-3 sticking to the column in the low salt condition, as the elution of OSM-3 trends in the opposite direction as the globular standards.

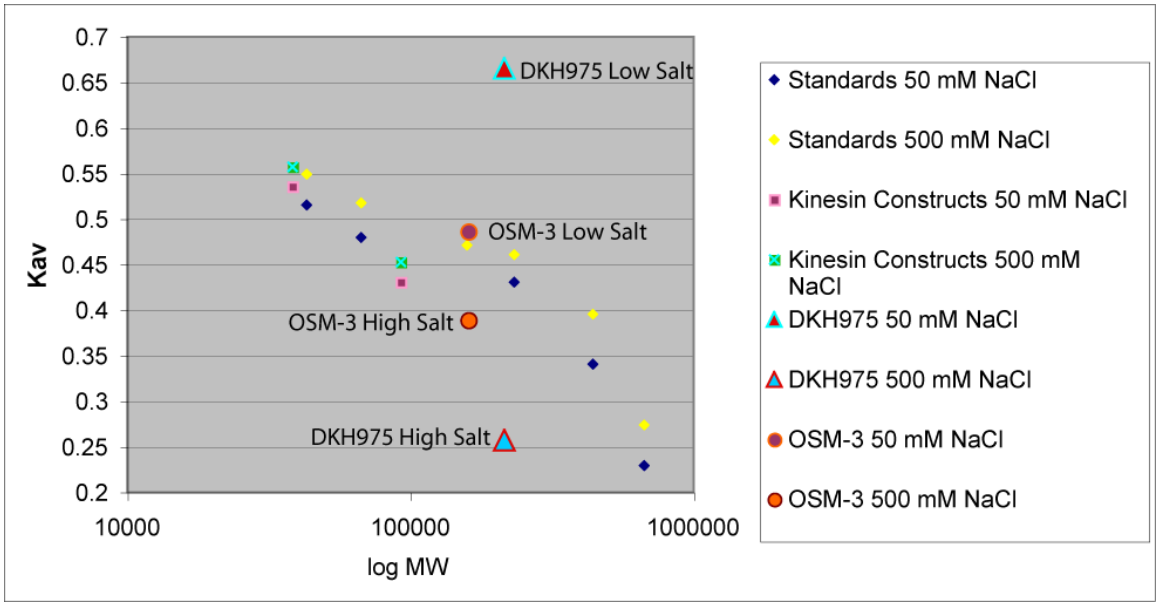
0.7
0.65
0.6
0.55
0.5
0.45
0.4
0.35
0.3
0.25
0.2
Kav
10000
100000
1000000
log MW
DKH975 Low Salt
OSM-3 Low Salt
OSM-3 High Salt
DKH975 High Salt
Standards 50 mM NaCl
Standards 500 mM NaCl
Kinesin Constructs 50 mM NaCl
Kinesin Constructs 500 mM NaCl
DKH975 50 mM NaCl
DKH975 500 mM NaCl
OSM-3 50 mM NaCl
OSM-3 500 mM NaCl

Labeling with B4M

Once we had determined conditions in which our protein is in the extended and compact state, we attempted to crosslink the compact conformation using both the native cysteines and our single engineered cysteine at the end of the alpha-3 helix (N190C). In order to label the extended conformation Nickel-NTA purified protein was first dialyzed into a high salt labeling buffer containing 25 mM Hepes pH 7.0, 500 mM NaCl, 2 mM $MgCl_2$, 1 mM EGTA, 200 μM TCEP, and 12.5 μM ATP. This buffer is essentially identical to that used in the gel filtration experiment under high salt conditions with the exception that the gel filtration buffer contained 25 mM PIPES pH 6.8 instead of Hepes at pH 7.0. This buffer change was made to facilitate the labeling reaction with the benzophenone-4-maleimide crosslinker, as maleimide groups are most reactive at a slightly higher pH in the range of 7.0-7.5 (72). We expect that a majority of OSM-3 remains in the extended conformation in this buffer, however the small change in pH may effect the folding and unfolding of the molecule. The moderate amount of sodium chloride used in our labeling buffer is also a point to consider. Large amounts of chloride salts (~1 M) can add to maleimides and render them unreactive (72). However, our labeling condition contains only 500 mM NaCl and is not expected to impede the labeling reaction greatly. In situations in which a high ionic strength is needed for the labeling reaction, and the concentration of chloride salts is too high, acetate salts are recommended, as they do not have the same side reaction with maleimides as the more commonly used chloride salts. See below for a discussion on concerns dealing with the labeling reaction.

Upon dialysis into the high salt labeling buffer, which induces the extended conformation and also acts to remove βME, a reagent incompatible with maleimide reactions, accessible cysteines were labeled using a 5-fold molar excess of benzophenone-4-maleimide per cysteine

using a 100 mM stock (dissolved in DMSO and stored at -20°C protected from light). The dye was slowly added to avoid precipitation of the protein due to the high local concentration of DMSO, mixed well, and the tube was wrapped in aluminum foil to protect the benzophenone moiety from light. The reaction was allowed to proceed overnight at 4°C and subsequently quenched by the addition of an excess of free sulfhydryl groups, here 25 mM βME. These were the only labeling conditions tried at this point, as the dye excess, reaction time and temperature were found to be ideal for labeling S188C (=N190C in OSM-3) in the kinesin-1 motor domain. However, the higher sodium chloride concentration in the OSM-3 reaction may require additional adjustment of the labeling conditions, as the kinesin-1 labeling buffer contained only 100 mM NaCl. See below for a detailed discussion on the labeling procedure.

After quenching the labeling reaction, excess label was removed by repeated spin concentration and buffer exchanged using 50,000 mwco spin concentrators (Millipore Corporation, Billerica, MA), and labeled protein was dialyzed for 3 hours into OSM-3 Low Salt Gel Filtration Buffer (25 mM PIPES pH 6.8, 50 mM NaCl, 2 mM $MgCl_2$, 1 mM EGTA, 5 mM βME, 40 μM ATP). The protein was relatively stable under these conditions as no visible precipitate was seen, although after removal from dialysis, the protein was spun for 10 minutes in a TLA110 rotor (Beckman Coulter, Inc., Fullerton, CA) at 100k rpm to remove any unseen aggregates or precipitated protein. In my experience I have found that even unseen protein aggregation or precipitation may act as a nucleation site for further protein precipitation, especially in low ionic strength conditions or increased temperature. It was therefore advantageous to give the protein a 100,000 x g spin at various points in the experiment to remove these nucleation sites. This was especially advisable before freezing the protein in liquid nitrogen, upon a fast thaw, after any dialysis or spin concentration step, or after any other

situation in which the proteins stability may be compromised, including increases in temperature or sitting on ice for large stretches of time. This technique has proven invaluable for working with the kinesin-1 tail domain, and was applicable to OSM-3, as previous experiments dialyzing OSM-3 into BRB25 with no added salt resulted in the almost complete precipitation of the protein, suggesting a propensity for instability in OSM-3.

Intramolecular cross-linking reaction

Following a hard spin of the labeled OSM-3 after dialysis into low salt, the protein was subject to irradiation with 254 nm UV light for 5 minutes at room temperature. The short wavelength UV light activates the benzophenone moiety and initiates the crosslinking reaction. Upon photoactivation, the benzophenone forms a covalent bond to any C-H group within the 9 Å reach of the crosslinker. If the C-terminus of OSM-3 is located within this distance of a cysteine labeled with the benzophenone-4-maleimide, a covalent bond will form, locking the protein in the compact conformation. Gel samples of both the non-irradiated and irradiated samples were run on a 15% SDS-PAGE gel and examined for the specific emergence of bands after irradiation.

Data analysis of the crosslinking reaction involved detecting a cross-linked band in either only the N190C OSM-3 sample, or both the wild-type and N190C OSM-3 samples. This analysis is harder then that used for crosslinking the kinesin-1 head to the tail *in trans*, as OSM-3 will be an intramolecular crosslink. We are therefore looking for a shift in the mobility of the protein on a denaturing gel, not the emergence of a band equal in molecular weight to the sum of our two constructs. Uncross-linked protein should be fully extended in the denaturing conditions of the SDS-PAGE gel and run at its expected apparent molecular weight, while a successfully cross-linked protein will not be fully denatured, as it is stuck in the compact conformation. This

shift in gel mobility may be detectable as the emergence of a band on the gel that is seen only in the irradiated sample, as well as a selective decrease in the intensity of the uncross-linked band in that sample. We reasoned that a gel shift to a lower apparent molecular weight would be seen for a cross-link, as it will remain in the compact conformation even under denaturing conditions and therefore run faster on the gel, appearing smaller than it really is. However, we do not know how much of a difference we should expect. A good guess is that it will run slightly faster than uncross-linked protein, as it will still be denatured, but will have the two ends linked. This may be seen as an unclear band in place of a sharp OSM-3 band, but this is further complicated if the motor domain cross-links to the other chain's tail in the homodimer. Overall, analysis of the gels showed no difference when non-irradiated and irradiated samples were compared for either the wild-type or mutant N190C OSM-3 constructs. A high molecular weight band could be seen after irradiation of both samples (Figure 22). While this may indicate the cross-linking of tetrameric protein, it is more likely precipitated protein that occurred after irradiation, as it did not fully enter the gel nor run as a clear band. The lack of a detectable crosslink could be due to a variety of reasons that are discussed in detail in Section II, and does not directly indicate that there is not an intramolecular interaction involving the Switch I region of OSM-3. All in all, the crosslinking experiments that we performed are inconclusive and problems with the experimental procedure should be addressed for project success.

## Section II: Discussion

### General comments about working with OSM-3

Although OSM-3 proved to express and purify well with only the use of Nickel-NTA resin, it still suffered some of the hallmarks of an unstable and misbehaving protein, and

therefore was not always the easiest to work with. I found that OSM-3 starts to precipitate quite strongly at very low ionic strength conditions (BRB25), and would recommend the use of at least 50 mM NaCl in the buffer. A combination of other salts of equal ionic strength could also be used. If solubility continues to be a problem I suggest including a small amount of imidazole in the buffer, as I have found histidine-tagged proteins are more stable at lower ionic strengths if a small amount of imidazole is present. If continued problems occur at low ionic strength it may be worthwhile to carefully repeat some of the gel filtration experiments with the addition of small amounts of salt. The gel filtration experiments as originally performed involved injection of 500 µl of purified OSM-3 in Nickel-NTA elution buffer (containing 350 mM Imidazole, 500 mM NaCl) directly onto the column equilibrated in the low ionic strength buffer. Therefore, the actual salt concentration of the sample may be higher than that of the buffer. I also noticed that upon irradiation at room temperature for only 5 minutes, precipitation of the sample did start to occur, even when the solution was being mixed while irradiated. This may not be problematic for our experiments as planned here, but should be considered if further purification of the cross-link is necessary for detection. The reaction mixture will most likely be better behaved if irradiation is performed at 4°C.

Technical Challenges

Various reasons could be possible for the lack of visible cross-linking of OSM-3 into its compact conformations under these experimental conditions. The project has not been rigorously tested, and therefore many of these possibilities actually have to do not with experimental design, but are more along the lines of potential technical challenges, especially when it comes to analyzing the data. Some of these difficulties are easy to test for, such as

labeling efficiency under different reaction conditions, and the results of these tests may offer simple solutions for experimental success. Other difficulties, especially with the data analysis, will need to be worked through, as our lab does not have expertise with some of the techniques that may be necessary for data analysis that I discuss below. In addition to highlighting areas of the experiment that I feel may be problematic and not quite worked out yet, I also provide additional opinions for the success of the project if it seems that the labeling and data analysis are not at fault for the lack of detectable crosslinking.

Technical problems that may be limiting our experimental results lie in two different arenas, those pertaining to labeling conditions and those dealing with the actual analysis of the crosslinking results. I will deal with the labeling reaction first, as this is a logical start and is easily testable.

Labeling Efficiency

The first problem to address is the possibility that the protein was never labeled very efficiently under our reaction conditions. To crosslink the inhibitory conformation of OSM-3 using benzophenone-4-maleimide, we first have to achieve conditions in which the benzophenone-4-maleimide labels the reactive cysteines that are of interest to us. In order to accomplish this, two conditions must be met: the reactive cysteines in OSM-3 must be accessible for labeling, and these labeling conditions need to be amenable for the maleimide reaction.

The first criterion is met by ensuring that we could get the extended conformation of OSM-3. This is necessary, as folding in the compact conformation would most likely mask any cysteine of interest. These cysteines would therefore not be labeled efficiently and the experiment would fail to crosslink the compact conformation. We were able to show using gel filtration that we

could get the extended conformation of OSM-3 in a high salt condition mimicked by our labeling buffer. The only buffer differences between the gel filtration experiment and our labeling are the identity of the buffer (PIPES vs Hepes), and the pH (6.8 vs. 7.0). While these buffer differences may have played a small effect on the equilibrium between the extended and compact conformations of OSM-3, I believe that sufficient amounts of the extended conformation existed for labeling using the benzophenone-4-maleimide.

The second criterion is maleimide reactivity under our labeling conditions. It is a legitimate concern that the conditions that we used are not very suitable for maleimide reactions, specifically that the chloride salt concentration may be too high. It has been found that large amounts of chloride salts (around 1 M) can add to maleimides and render them unreactive (Dan Safer, personal communication). Our labeling buffer contains half this amount (500 mM NaCl), but the chloride concentration may still be too high, and is reducing the amount of reactive probe.

There are two easy ways to ascertain whether we were actually labeling our protein under these conditions. I would suggest performing a 5,5'-dithiobis 2-nitrobenzoic acid (DTNB, Pierce, Thermo Scientific, Rockford, IL) assay to determine how many of our cysteines react with benzophenone-4-maleimide in our conditions for both the wild-type OSM-3 and the N190C construct. For S188C in kinesin-1, we were able to achieve 90% labeling efficiency with the benzophenone-4-maleimide as measured in this assay. Labeling efficiency can also be measured by labeling our protein with a fluorophore, like tetramethylrhodamine (TMR). By selecting a dye that has the same reactive chemistry as our crosslinker, here a maleimide, one can get a grip on how well the cysteines can be labeled with maleimide probes under our labeling conditions. Labeling with a fluorophore will allow for quantification of labeling efficiency using the

absorption coefficient of the dye under denaturing conditions. This can then be correlated with protein concentration, which can accurately be measured on a SDS-PAGE gel run with protein standards that have similar Coomassie binding properties to the sample protein. We have found that BSA standards work well for kinesin and will most likely be suitable for OSM-3. Dye spectra, and therefore absorption coefficients, can be affected by both the nature of the solvent and binding to protein. Denaturing the labeled protein in 6 M guanidine hydrochloride removes the effect that local protein environment may play on dye fluorescence, and the absorption coefficient of the dye alone in 6 M guanidine hydrochloride can be easily compared to the dye's published value in other solvents. Either the DTNB assay or fluorophore attachment will give a good measurement of how well OSM-3 is being labeled in the reaction conditions. However, the DTNB method has the advantage of actually measuring the labeling efficiency of the benzophenone-4-maleimide stock that you are using, which may be helpful in trouble-shooting other problems, such as inactivation of the probe, etc.

If it is found that OSM-3 is not being labeled very efficiently in our conditions various approaches may be taken to achieve better labeling. These include things such as adjusting the reaction conditions in terms of time and/or temperature, or making modifications to the labeling buffer, including attempting to lower the concentration of chloride salts, changing the chemical nature of salt used, or changing the buffer pH.

Adjusting the labeling reaction towards harsher reaction conditions, such as labeling at room temperature for 3 hours, may be beneficial in increasing our labeling efficiency under the same buffer conditions. This has been shown to work for getting hard-to-label cysteines in kinesin-1 motor domain constructs to label with maleimides (72). Increasing the temperature also increases the protein's structural dynamics. The higher temperature promotes more protein

breathing within the structure and may be useful in hitting probes that are slightly buried, as well as increasing the transitions between the extended and folded conformation. If our problem is insufficient amounts of extended protein, the temperature increase may help the labeling in this respect as well. One does need to consider that OSM-3 may not be stable for long periods of time at room temperature, as it has already proven to be temperamental in low salt conditions. However, the presence of large amounts of salts in the buffer may stabilize the protein for this period of time.

It is possible that the amount of sodium chloride present in our labeling buffer to induce the extended conformation is inhibiting the maleimide reaction by adding onto the maleimide moiety, resulting in an unreactive probe. We have two options in this respect. The first is to simply decrease the amount of sodium chloride salt in the reaction, the second is to change the chemical nature of the salt used to increase the ionic strength. High concentrations of acetate salts do not add onto maleimide groups as chlorides do and are thus suggested for use if maleimide labeling must be done under high ionic strength conditions (72). I would expect that OSM-3 would behave well in acetate salts as the use of acetate with the kinesin-1 tail constructs proved to be essential at stabilizing an otherwise very unstable protein under low ionic strength conditions. This may also be useful in stabilizing the compact conformation in low ionic strength conditions.

It is also possible to increase the labeling efficiency by increasing the pH of the reaction. Maleimide reactions are typically performed in a pH range of 7.0-7.5. This is an advantage of using maleimide probes, as the pH range is ideal for most proteins stability, as well as most likely mimics physiological conformations. As one increases the pH of the labeling reaction above pH 7.5, the labeling efficiency of maleimides increases. However, raising the pH above

pH 8.0 is not recommended as the maleimide moiety begins to form maleimic acid and is no longer reactive.

Regardless of the changes made in either buffer composition or pH, it will be necessary to ensure that the first labeling criterion is still met: OSM-3 is in the extended conformation. This can be tested using gel filtration to ensure that OSM-3 still adopts the extended conformation under the resultant buffer conditions.

Data Analysis

Once it is determined that the benzophenone-4-maleimide is efficiently labeling OSM-3 there are several other concerns that must be taken into consideration if the experiment is not working. The first is how the crosslinking data is analyzed. As designed, we are looking for a shift in gel mobility under denaturing conditions. In reality it may be that the difference in migration between a fully denatured (uncross-linked) OSM-3 is not drastically different than one that is denatured while cross-linked in the compact conformation. With no idea whether to expect a large or small change in mobility it is hard to optimize gel conditions for data analysis. The use of western blots is probably not the answer, as irradiated samples have been shown to contain a large number of reactive bands even when a very specific antibody (Suk4, a mAb towards the kinesin-1 motor domain) that detected a single band in the non-irradiated sample was used. One direction that could be taken is to digest the sample with trypsin or cyanogen bromide and analyzing the resultant peptides. We would be looking for a peptide molecular weight that was not found in the non-irradiated sample, as well as the loss of specific peptides in the irradiated sample. Another alternative would be to design a single specific enzyme cut site within the molecule, for example, at TEV protease site. Following irradiation and treatment with

the TEV protease, one could expect a band corresponding to full-length OSM-3 is successful crosslinking occurred, while two bands of lower molecular weight will be present in the control sample. One could also change the experimental design to ease in data analysis by creating separate head and tail constructs and adding them back together again *in trans*, in a manner similar to that used with kinesin-1 when full-length protein proved problem-some to deal with. The construction of these constructs may be much more difficult for OSM-3 though, as an OSM-3 construct that only contained residues 1-555 was an unstable dimer (108). However, these experiments were done at very low concentrations (low nanomolar range) and may be better well behaved at the concentrations needed for our studies. An additional problem comes about in that we do not have a good idea of what part of the OSM-3 C-terminus is involved in inhibition, making choosing a viable tail construct more difficult. However, the experiment would be identical to that used for kinesin-1 after constructs are made, and data analysis would be straightforward. I do not feel that the construction of a cysteine-light motor domain for OSM-3 is necessary, as mass spectrometry could be used to determine which cysteine(s) is involved in crosslinking to the tail.

Additional Considerations

Other potential concerns must be considered as well. The first is that the presence of the crosslinker attached to N190C or another cysteine near the interaction surface may inhibit formation of the compact conformation. In my opinion this is unlikely as we found in our work with kinesin-1 heads and tails *in trans* that the presence of the benzophenone attached to various locations in Switch I did not seem to significantly decrease the affinity of the interaction. In these experiments we were able to get significant cross-linkage with any cysteine in the Switch I

region, and this was true even using constructs that have a relatively low affinity for each other, specifically those that lacked the stabilizing interaction between the neck coiled-coil and the tail coiled-coil, as both these elements are absent in the K349 monomer and 27-mer tail peptide experiments. It therefore seems likely that OSM-3 should be able to overcome the small decreases in affinity due to the presence of the crosslinker. However, one should consider that we did mutate an asparagine to a cysteine. This mutation does create a little space for the crosslinker, as the cysteine residue is much smaller than the native asparagine, but may lower the affinity of the inhibitory interaction, as polar contacts through the asparagine are lost.

A very real possibility is that none of our labeled cysteines are in position to crosslink the compact conformation. To circumvent this one can start adding cysteines in other areas near Switch I of the OSM-3 motor domain. In the kinesin-1 regulation project we also had good luck crosslinking heads and tails using cysteines added back at residues 193 and 197 in Switch I of the motor domain. One thing to keep in mind however is that the project as designed is not about how OSM-3 is regulated, but is instead whether the mode of regulation seen in kinesin-1 is a common motif used among different kinesin family members. With the lack of additional clues as to how OSM-3 is regulated, an approach involving cysteine add-backs in other areas of the motor domain outside of Switch I could be akin to searching for a needle in a haystack. However, given the structural similarity in all kinesin motor domains whose structure has been determined so far, one could easily design mutants to strategically target surface and solvent-exposed locations in environments amenable to maleimide labeling. There are also additional regions of the motor, such as Switch II, that are logical places to start looking. The prospect of OSM-3 regulation not involving a direct interaction with Switch I is discussed in further detail below.

**Conclusions**

Overall, determining whether the Kinesin-2 family member OSM-3 is regulated through an interaction with Switch I in the motor domain, akin to the regulatory mechanism we found for kinesin-1, has proven not as simple as we thought. However, this project is in its infancy and at this stage most of our problems lie in technical difficulties involving the labeling reaction and data analysis. A lack of crosslinking with cysteines added in the Switch I region of OSM-3 after these problems have been worked out indicates that OSM-3 may be regulated in a different manner than that used in the kinesin-1 heavy chain. However, our crosslinking technique has proven to be a very powerful biophysical tool in determining protein interactions and given additional information regarding regions important for OSM-3 regulation, it may still prove useful in teasing out how OSM-3 regulation works.

The generality of regulation of kinesin motor proteins through changes in Switch I is still a plausible theory, even if a direct interaction involving Switch I of OSM-3 can not be found. Forced changes in Switch I may still be a common regulatory motif used by kinesin superfamily members. It may be the case that instead of a direct interaction between Switch I of OSM-3 and some element in it's C-terminus, the C-terminus is instead interacting with Switch II, or another region in the motor domain, and this allosteric interaction results in a conformational change that causes changes in Switch I that result in enzymatic inhibition of microtubule-stimulated ATPase activity.

Given the structural, mechanical and evolutionary similarities between G-proteins and the motor protein kinesin and myosin superfamilies, it seems very likely that general regulatory mechanisms will be found among the members. These proteins may have evolved slightly different means of regulation, all achieving the same result: effecting the conformation of Switch

I to modulate the motor's enzymatic activity. This theory remains to be tested, and OSM-3 is still an ideal candidate for finding a common theme in kinesin motor regulation that involves changes in Switch I.

# Kristen A. Dietrich

2020 N. Lincoln Park West #33C
Chicago, IL 60614
(773) 793-5515
k-dietrich@md.northwestern.edu

Northwestern University
Cell and Molecular Biology
Vassar Lab

## CURRENT POSITION:

**Postdoctoral Scholar** Northwestern University, Cell and Molecular Biology — November 2008
Laboratory of Dr. Robert Vassar

## EDUCATION:

**Ph.D** Cell and Molecular Biology, Northwestern University — October 2008
*Thesis Title:* The Kinesin-1 Motor Domain is Regulated by a Direct Interaction of its Head and Tail
*Thesis Advisor:* Sarah Rice

**B.A.** Environmental Science, Northwestern University — June 2003

## PUBLICATIONS:

• Wong YL, **Dietrich KA**, Naber N, Cooke R, Rice SE. Kinesin's Tail Restricts its ATP Pocket. *Manuscript submitted. Biophys J.*

• **Dietrich KA**, Sindelar CV, Brewer PD, Downing KH, Cremo CR, Rice SE. (2008). The Kinesin-1 Motor Protein is Regulated by a Direct Interaction of its Head and Tail. *PNAS*, 2008 Jul 1;105(26):8938-43.

• Sekulic N, **Dietrich KA,** Paarmann I, Ort S, Konrad M, Lavie A. (2007). Elucidation of the active conformation of the APS-kinase domain of human PAPS synthetase 1. *J. Mol Biol*. (2007), 367(2): 488-500.

• Sekulic N, **Dietrich K**, Paarmann I, Konrad M, Lavie A. (2005). Crystal Structure of Two Domains of Bifunctional Enzyme: Human PAPS Synthetase. *Acta Cryst*. A61, C195-C196.

## DISTINCTIONS:

Post Doctoral Fellowship, NIH Training Grant, Mechanisms of Aging and Dementia — November 2008-
Pre Doctoral Fellowship, NIH Training Grant, Molecular Biophysics — August 2006-August 2008
Invited Platform Speaker, 2008 Biophysical Society Annual Meeting — February 2008
Northwestern University Graduate School Travel Award — December 2007
Best Poster by a Graduate Student, Center for Drug Discovery and Chemical Biology Symposium, Northwestern University — October 2007
Graduated with Departmental Honors, Northwestern University — June 2003